UNIVERSITY OF OKLAHOMA

GRADUATE COLLEGE

CHARACTERIZATION
OF HOLLOW FIBER PROPERTIES
DURING THE MELT SPINNING PROCESS

A DISSERTATION

SUBMITTED TO THE GRADUATE FACULTY

In partial fulfillment of the requirements for the

degree of

DOCTOR OF PHILOSOPHY

By

Anne de Rovère

Norman, Oklahoma

2000

CHARACTERIZATION

OF HOLLOW FIBER PROPERTIES

DURING MELT SPINNING PROCESS

A DISSERTATION

APPROVED FOR THE SCHOOL OF CHEMICAL ENGINEERING

AND MATERIAL SCIENCE

BY

Robert L. Shambaugh

Lance Lobba

John Fagan

Edgar O'Rear

Dennis P. Wattley

Melissa Vaughn

ACKNOWLEDGEMENTS

I would like to take this opportunity to thank the following people:

Dr. R. L. Shambaugh, for his guidance and financial support for the past four years.

Dr. L. Lobban, Dr. M. Rieger, Dr. D. Glatzhofer, and Dr. E. O'Rear, for being members of my committee.

Dr. John Fagan, for being a member of my committee, and for his help and precious assistance with the LDV system.

Dr. L. L. Lee, for his help in Thermodynamics.

Dr. B. Grady, for teaching me Polymer Science and is guidance in the Fluids Rheology Lab.

Larry and Joel, for building the equipment essential to my research.

Chemical Engineering office staff – Rick, Donna, Terry, Cheryl, and Susan for their efficient work.

Ashwin and Jake, for being great colleagues and for creating the friendly atmosphere that made the lab such a fun place to work in.

Connie, for her assistance in developing experimental techniques and collecting data, and for her wonderful friendship.

Diana, Brandy, Jonathan, and Heath, for their assistance in collecting data.

Thor, Jeff, Katia, Matthieu, Aurélie, and Sonia, for their friendship and the endless memories.

My family, for their encouragement and support.

Axl, pour sa présence au cours des quatre dernières années.

TABLE OF CONTENTS

LIST OF ILLUSTRATIONS

LIST OF TABLES

ABSTRACT

Polypropylene hollow fibers were produced via the spunbonding process. Nitrogen gas was used as the lumen fluid. Individual fiber properties were tested, and web properties were also examined. In terms of compression-recovery and opacity, mats of hollow fibers are nearly identical to mats of solid fibers of the same outside diameter. In terms of individual fiber orientation, crystallinity, and strength, hollow fibers usually exhibit improved properties. On-line measurements showed that lumen fluid rate improves hollow fiber properties (orientation). Increased quenching rate may cause this difference. The fiber formation process was modeled with momentum, energy, and two continuity equations (one for the polymer, and one for the lumen fluid). The equations were solved numerically, and the results were compared to the on-line diameter data. Both Newtonian and viscoelastic constitutive equations were considered. The Newtonian model provided excellent fits to experimental outer diameters. Both experimental and predicted results show faster quenching, and thus higher orientation, on fibers processed using high nitrogen rates.

Substitution of hollow fibers for solid fibers would not only preserve the web properties (opacity and compression), but would actually improve the strength of each fiber. Hence, hollow fibers could be substituted for solid fibers in nonwoven webs. The final web would be lighter and cheaper that the same web made of solid fibers.

ON-LINE AND OFF-LINE CHARACTERIZATION OF HOLLOW FIBER PROPERTIES DURING THE MELT SPINNING PROCESS

CHAPTER 1

1. INTRODUCTION

1.1 NONWOVENS

Fiber formation, web formation and web consolidation generally are performed as a single unit operation in the manufacture of extruded nonwovens. Fiber formation consists of the extrusion of the polymer melt through a multiple holes spinneret. Web formation for spunbonding and meltblowing consists of collecting continuous filaments on moving screens to preferentially arrange them in layers of lofty and loosely held fiber networks called webs. The web consolidation phase interlocks webs by mechanical, chemical, solvent or thermal means [Narayanan et al., 1994]. The degree of consolidation, or bonding, is an essential factor in determining fabric strength, porosity, flexibility, softness, and density (thickness). In some fabric constructions, more than one bonding process may be used to achieve expected physical or chemical properties. In thermal bonding, heat and often pressure are used to weld fibers together in patterned bond sites. The heat is used to activate an

adhesive system, which can be the fiber itself or added binder fibers. In solvent bonding, fibers are partially dissolved to give them self-bonding properties. In chemical consolidation, a chemical agent is used to bond fibers together. Mechanical consolidation can be divided in several distinct techniques: needlepunching, stitchbonding, and hydroentangling. In needlepunching, fiber webs are interlocked by physically repositioning some of the fiber bundles from a horizontal to a vertical orientation. In stitchbonding, fiber webs are interlocked using knitting elements. In hydroentangling, individual fibers are repositioned in configurations that bring about frictional interlocking at the fiber level. The choice of technique for web consolidation is driven by economic and product properties considerations.

1.1.1 Spunbonding

The spunbond process transforms polymer directly from polymer pellets to fabric by extruding filaments, stretching them as bundles to develop molecular orientation, layering them on a moving screen in a random (or oriented) array, and finally bonding them using one of the techniques described earlier. The most common technique of spinning used for spunbonding is melt spinning. The solid polymer pellets are heated to lower viscosity levels and forced through small orifices into cool air where the polymer solidifies as continuous filament bundles [Ahmed, 1982]. The conveying screen is very often held under a vacuum. Because weaving (or knitting) is not used to form the mat, the mat is referred to as a nonwoven. The web height depends on the speed on the screen, the number of extrusion positions and the

polymer flowrate used. Figure 1.1 shows a typical spunbonding process in which a molten polymer is pressurized and forced through a fine capillary.

High speed spinning technology (speeds of ~ 6,000 m/min) presents benefits such as increased productivity, simplification of the process, reduction of energy and labor costs and reduction of the total production cost [Ziabicki and Kawai, 1985].

1.1.2 Melt blowing

Melt blowing is a single step process for converting resins into nonwoven, low denier, fibrous mat. The initial treatment of polymer pellets is identical between melt blowing and spunbonding: the resin in chip form is heated to liquid state and passes through the extrusion orifice [Shambaugh, 1988]. However, in the melt blowing process, the venturi is built right into the spinning die, and hot air is used in the die (versus cool air for spunbonding); see Figure 1.2. Since the gas is heated approximately to the spinneret temperature, the gas prevents polymer solidification at distances close to the melt blowing die [Ziabicki and Kawai, 1985]. The fast moving air streams exerts a tremendous drag force upon the molten stream. This drag force effectively stretches the molten polymer into a fine fiber, and solidifies it into a random array of discontinuous fibers. The rapidly moving fibers are collected on an open conveyor belt. Fibers can then be compressed between heated rolls to produce web consolidation.

Spinning speeds are quite high in both spunbonding and melt blowing processes: spunbonding is typically done at speeds of 2,000-4,000 m/min, while melt blowing is done at speeds of 2,000-30,000 m/min. The melt blowing process

produces extremely fine fibers that are very difficult to produce by the conventional spinning methods since no mechanical windup is fast enough to take up the fibers at speeds greater than 10,000 m/min. Thus, melt blown fibers can be orders of magnitude smaller than fibers produced by conventional melt spinning. The applications of melt blown fibers take advantage of the extreme fineness of these fibers: melt blown fibers make excellent filters, have high insulating value, and have high cover per unit length [Shambaugh, 1988]. Other uses for melt blown nonwovens include medical products, garment insulation, wipes, and oil absorbants. Worldwide, about $150x10^6$ kg/year of melt blown fabric is produced, and a similar amount of spunbonded material is made. Typical examples of these materials are Pall Corporation's cartridge filters, Kimberly-Clark's Spunguard® surgical gowns, and DuPont's Tyvek®. Tyvek® is used for computer diskette sleeves, house wrap, sterile packaging, high strength envelopes, and many other uses.

1.1.3 Polypropylene

Among the synthetic fibers, isotactic polypropylene is the most widely used polymer for spunbonded production [Mark et al., 1987]. It is one of the lightest textile fibers (density = 0.91) and consequently provides good economy in use. Because of its very good rheological characteristics, polypropylene is relatively easy to convert into a high quality fiber. Polypropylene actually dominates in many nonwoven markes such as absorbent product coverstock markets. It is the preferred fiber for most calender processes and is used extensively in through-air bonding as well.

Polypropylene fibers can be produced at different tenacity levels, appropriate for the different end uses.

1.2 HOLLOW FIBERS TECHNOLOGY

1.2.1 Hollow Fiber Applications

Presently, hollow fibers are used as membranes in the separations business. Water desalination (reverse osmosis) is the biggest single use, while use in hemodialysis (artificial kidneys) is also large. Uses in gas separation, microfiltration, and pervaporation are growing [Moch, 1991]. Typical hollow fibers have outside diameters of 20-250 microns and inner diameters of 2-50 microns [Maxwell et al., 1967]. Hollow fibers used in separations are difficult to make and are expensive (greater than $20/kg) compared with ordinary solid filaments (e.g., $2.50/kg for polypropylene fiber).

1.2.2 Hollow Fiber Spinning

Hollow fibers are prepared by spinning polymer or polymer solution through an annular die or spinneret. These three spinning methods can be used [Baum et al., 1976]: (1) wet spinning in which polymer solution is spun from the spinneret and into a liquid coagulation bath; a distance ("air gap") between the spinneret and coagulant is often used; (2) dry spinning in which the solvent in the polymer evaporates into a gas; no liquid bath is used; (3) melt spinning in which the polymer is cooled in air without evaporation of any plasticizer or other material. Wet spinning is by far the most common method for producing hollow fibers [Li et al., 1994]. Spinning speeds

are quite slow. For example, J.H. Kim et al. [1995] produced wet spun fibers at speeds of only 10-35 m/min (speeds of 3000-6000 m/min are common in the melt spinning of conventional solid fibers); these low speeds translate into high fiber cost. The structure of the fiber wall can be varied by controlling (a) the concentration of polymer in the feed solution, (b) the coagulant temperature, and (c) the coagulant concentration. Often the fiber wall is "asymmetric" with an outer skin of solid polymer supported by a thicker inner layer of porous material. The thin skin permits a high permeation rate, while the porous layer provides mechanical support. A number of researchers have described methods for controlling the formation of the fiber wall: see J.H. Kim et al. [1995], Doi and Hamanaka [1991], Miao et al. [1996], Li et al. [1994], and Kestring [1985].

When melt spinning is used to produce hollow filaments, the polymer may or may not be combined with a second component. For example, a polypropylene / soybean oil mixture can be melt spun into a hollow fiber; see J.J. Kim et al. [1995]. After spinning, the soybean oil can be leached from the fiber to create a porous membrane. If polypropylene is melt-spun without the soybean oil, the resulting fiber can be post-treated with several annealing and drawing steps. The result of this post-treatment will be the creation of pores in the fiber wall [J.J. Kim et al., 1994].

1.2.3 Hollow Fiber Spinnerets

Two types of spinneret can be used to manufacture hollow fibers. In both methods, the tubular structure is formed by delivering the spinning dope through a circular extrusion orifice wall [Moch, 1991]. One type (tube-in-orifice) uses an

annular die with a system of gas blowing into the inner core to form a hollow portion; the second type uses a segmented-arc design that induces an inflow of air (Figure 1.3). The *tube-in-orifice* design extrudes the polymer melt as an annular shape. A hollow tube or a hollow needle insert, centered within the annulus, permits the introduction of gas, liquid or suspended solids that will maintain the tubular shape. The *multiannular* design is an extension of the tube-in-orifice die; this design allows the production of multilayer fiber walls or encapsulated activated species in the composite hollow fiber. The *segmented-arc* design has a C-shaped orifice and no gas injection system. In a common configuration (see Figure 1.3), polymer from three C-shaped walls rapidly coalesces to complete the annular configuration. The air drawn through the gaps before the fiber becomes continuous prevents the walls from collapsing.

1.3 GLOSSARY OF NONWOVEN TERMS

Backing: A reinforcing material for the back layer of products such as carpet or wallpaper.

Binder: A material added during or after web formation that causes fibers to adhere to one another in webs; also used to describe material to adhere pigments, etc., to a surface.

Binder fiber: A fiber with a lower melting point than other matrix fiber or web elements that is activated through the application of heat.

Bonding: The process of joining fibers in a web to provide strength.

Calender: A machine consisting of two or more cylinders or rolls that can apply controlled and uniform pressure to a fabric or web as it goes through the nip.

Coverstock: Lightweight material used to cover absorbent cores in medical or hygienic products.

Denier. Unit of filament or fiber measurement of linear density based on the weight of a fiber per its unit length; unit varies within regions. In the U.S., denier is measured in grams of 9,000 m of material (the lower the number, the finer the fiber); this generally is expressed as denier per filament (dpf). Some countries outside the U.S. use the Tex system which equates the weight in grams of one kilometer of fiber.

Entanglement: Web bonding method that wraps or knots individual fibers into an integrated structure; can be done mechanically (needling) or hydraulically.

Extrusion: The method by which molten polymer is forced through an orifice to form a fiber, film, sheet, shape, etc.

Fiber: Unit of matter, synthetic or natural, characterized by a high ratio of length-to-width.

Filament: A fiber of an indefinite length.

Hydroentangling: The web bonding process using high-velocity water jets to wrap or knot individual fibers.

Industrial fabrics: Fabrics used in applications other than hygiene, apparel, medical, and home furnishings.

Meltblowing: A method of forming fabric from thermoplastic resins; the resin is melted, extruded, and blown with fast-moving air that stretches or attenuates the fibers, which are then condensed and collected.

Meltspinning: A method of passing melted, liquid polymer through spinnerets and coagulating the material in a cold air stream.

Needlepunching: A physical method of mechanically interlocking fiber webs by using barbed needles to reposition some of the fibers from a horizontal to a vertical orientation.

Nonwoven: A fabric consisting of an assembly of textile fibers (oriented in one direction or in a random manner) held together (1) by mechanical interlocking; (2) by fusing of thermoplastic fibers, or (3) by bonding with a rubber, starch, glue, casein, latex, or a cellulose derivative or synthetic resin.

Polymer: A high molecular weight, chemical chain formed by linking together molecular units called monomers; the structural material of many types of fibers; can be natural or synthetic.

Spinneret: Perforated plate through which polymer or solution is extruded to make fiber.

Spunbonding: The process of forming fabric by layering continuous filaments on a forming screen and bonding.

Staple fibers: Fibers cut to specific lengths; also refers to natural fibers produced with relatively short length.

Stitchbonding: The mechanical method of combining fiber webs by using a knitting stitch and a yarn or yarn-like fiber tuft.

Tensile strength: The greatest stress or load a material can bear without breaking.

Thermal bonding: The process of binding by applying heat to a web of thermoplastic fibers or a web impregnated with meltable powders or thermoplastic fibers.

Web. Preferentially arranged assembly or sheet of fibers.

1.4 REFERENCES

M. Ahmed, *Polypropylene Fibers – Science and Technology*, Elsevier Scientific Publishing Company, New York (1982).

B. Baum; W. Holley, Jr. and R.A. White, "Hollow fibers in reverse osmosis, dialysis, and ultrafiltration," in *Membrane Separation Processes*, P. Meares, Elsevier Scientific Publishing Company, New York, pp.187-227 (1976).

S. Doi and K. Hamanaka, "Pore size control technique in the spinning of polysulfone hollow fiber ultrafiltration membranes," *Desalination*, **80**, 167, 167-180 (1991).

R.E. Kesting, *Synthetic Polymeric Membranes- A Structural Perspective*, 2nd Ed., Wiley Intersciences, pp.10-15 (1985).

J.J. Kim; J.R. Hwang; U.Y. Kim; and S.S. Kim, "Operation parameters of melt spinning of polypropylene hollow fiber membranes," *Journal of Membrane Science*, **108**, 25-36 (1995).

J.J.Kim; T.S. Jang; Y.D. Kwong; U.Y. Kim; and S.S. Kim, "Structural study of microporous polypropylene hollow fiber membranes made by the melt-spinning and cold-stretching method," *Journal of Membrane Science*, **93**, 209-215 (1994).

J.H. Kim; Y.I. Park; J. Jegal; K.H. Lee, "The effects of spinning conditions on the structure formation and dimension of the hollow fiber membranes and their relationship with the permeability in dry-wet spinning technology", *Journal of Applied Polymer Science*, **57**, 1637-1644 (1995).

S.G. Li; G.H. Koops; M.H.V. Mulder; T. van den Boomgaard; and C.A. Smolders, "Wet spinning of integrally skinned hollow fiber membranes by a modified dual-bath coagulation method using a triple orifice spinneret," *Journal of Membrane Science*, **94**, p. 329 (1994).

H.F. Mark; M.M. Bikales; C.G. Overberger; G. Menges; J. Kroschuitz, editors. *Encyclopedia of Polymer Science and Engineering*, **10**, John Wiley & Sons, NY, pp. 227-239 (1987).

J.M. Maxwell; W.E. Moore; R.D. Rego, "Fluid separation process and Apparatus", U.S. Patent # 3,339,341, Sept. 5 (1967).

X. Miao; S. Sourirajan, and W.W.J. Lau, "Production of polyethersulfone hollow fiber ultrafiltration membranes. II. Effects of fiber extrusion pressure (EP) and PVP concentration in the spinning solution," *Separation Science and Technology*, **31** (3), 327 (1996).

I. Moch, "Hollow Fiber Membranes," *Encyclopedia of Chemical Technology*, **13**, 4th edition, Wiley, NewYork, p. 334 (1991).

V. Narayanan; N. Gosavi; K. Duckett, "Nonwoven Technology Primer", *Nonwoven Industries*, **25** (3), 50-58 (1994).

R.L. Shambaugh. "A macroscopic view of the melt blowing process for producing microfibers", *Industrial and Engineering Chemistry Research*, **27**, p. 2363 (1988).

A. Ziabicki and H. Kawai, editors. *High speed fiber spinning – Science and Engineering aspects*, John Wiley & Sons (1985).

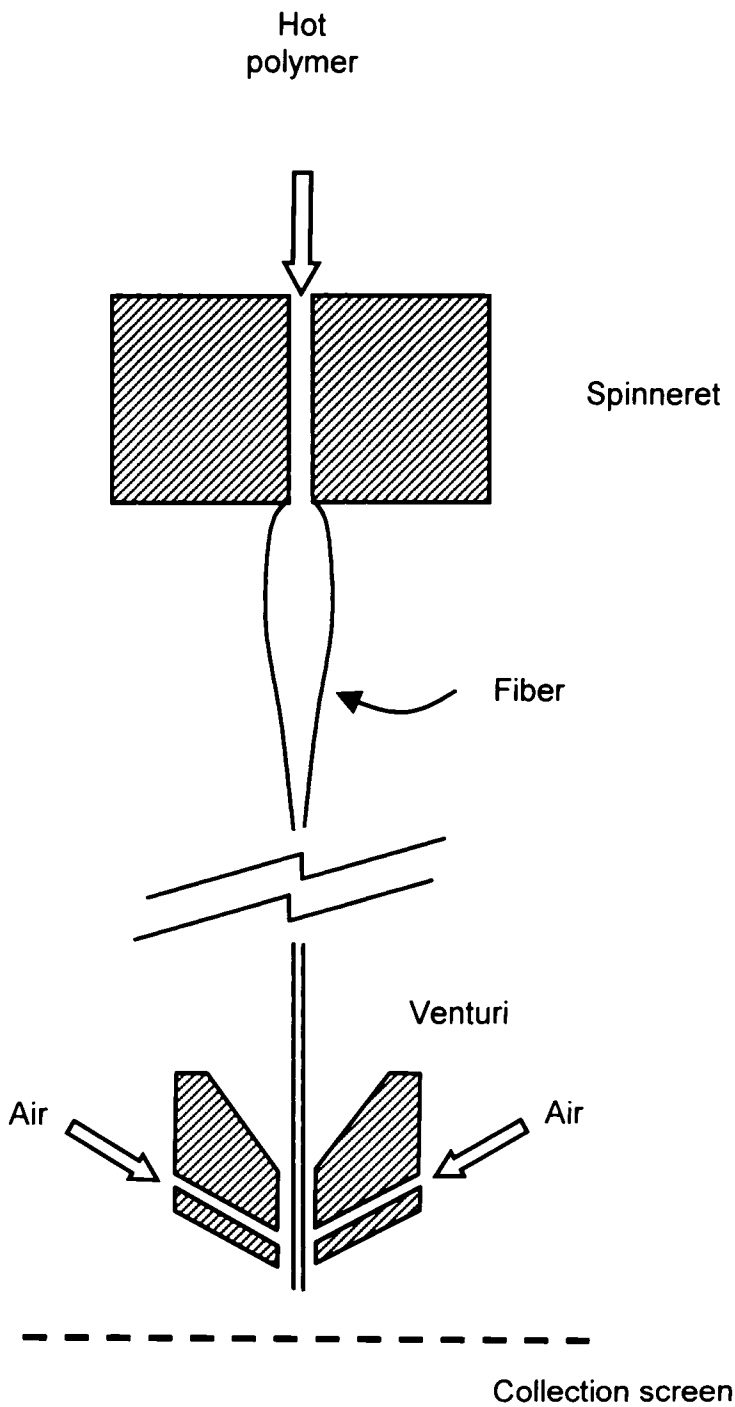

Figure 1.1: The Spunbonding Process.

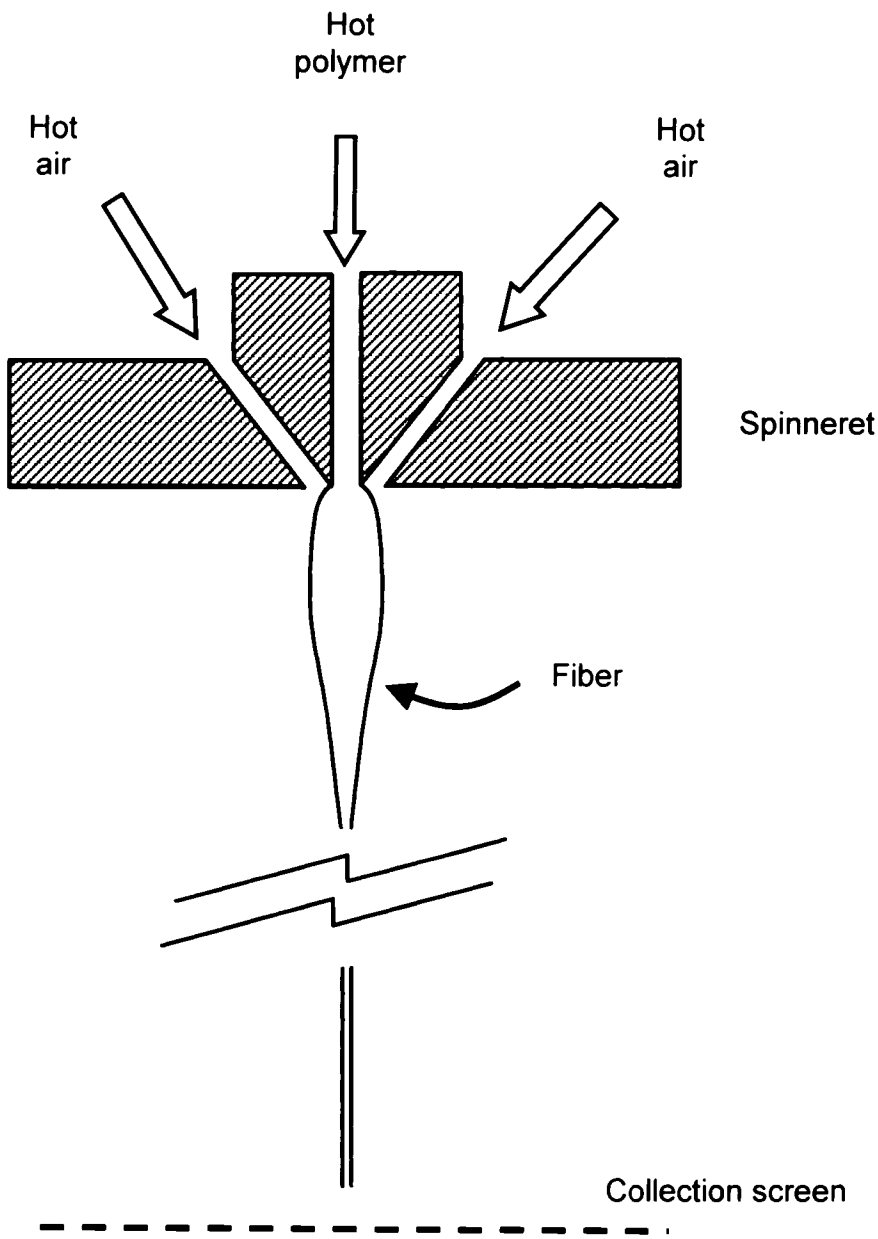

Figure 1.2: The Melt Blowing Process.

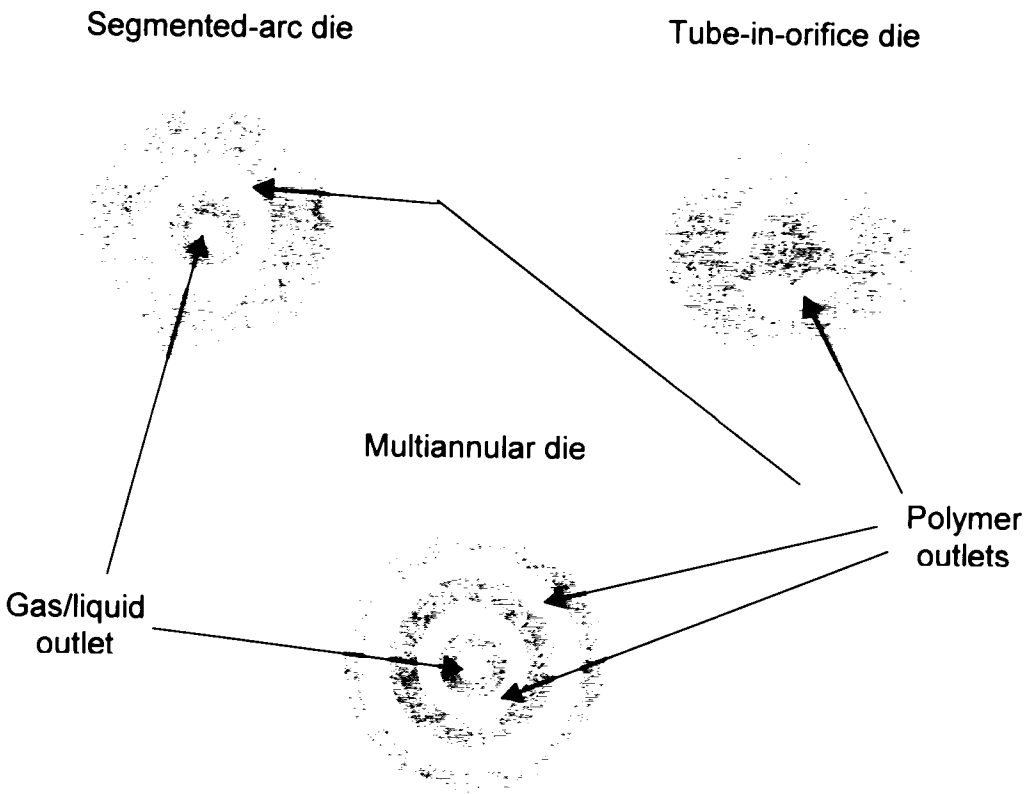

Figure 1.3: Hollow Fiber Spinnerets

CHAPTER 2

MELT-SPUN HOLLOW FIBERS FOR USE IN NONWOVEN STRUCTURES

(The content of this chapter has been submitted to a journal as: Anne de Rovere, R.L. Shambaugh. Melt Spun Hollow Fibers for Use in Nonwoven Structures, *Ind. & E.C. Research.*)

ABSTRACT

Polypropylene hollow fibers were produced via the spunbonding process. Nitrogen gas was used as the lumen fluid. The polypropylene continuity equation can be combined with the nitrogen continuity equation to give excellent predictions of inside diameter and outside diameter of the product fiber. Tests were developed to measure the compression-recovery behavior of hollow fiber mats (nonwoven structures) versus mats of solid fibers. Tests were also developed to measure the opacity of hollow fiber mats versus solid fiber mats. In terms of compression-recovery and opacity, mats of hollow fibers are nearly identical to mats of solid fibers of the same outside diameter.

2.1 INTRODUCTION

Nonwoven products can be used in hygiene or medical applications such as disposable diapers and disposable medical garments. They are also used in industrial applications (e.g., protective garments, filters, roof linings) and many more durable applications (e.g., carpet backings, insulation linings). Up to now, nearly all nonwoven techniques are used to produce solid fibers. This chapter describes the rapid production of hollow filaments via spunbonding (because of the similarities between melt blowing and spunbonding, many of the results presented herein also apply to melt blowing). Heretofore, hollow fibers have not been commonly produced via spunbonding. The commercially practical goal of this is to take a relatively low cost material (e.g., a spunbonded fabric) and impart higher value to this material by making the fibers hollow. Because hollow fibers are lighter than solid fibers of the same outer diameter, a nonwovens manufacturer could lower the basis weight of a fabric by using hollow filaments. In this case, the cost of the fabric would be reduced because of the reduction in polymer cost (i.e., less polymer is needed). Let us define fiber hollowness (h) as the hole area divided by the fiber total area:

$$h = \frac{ID^2}{OD^2} \tag{2.1}$$

where

ID = final (product) inside diameter

OD = final (product) outside diameter

Figure 2.1 shows the calculated effect of inner diameter on hollowness and fiber cross sectional area. The polymer cost is directly proportional to cross-sectional area. Also, cost is proportional to (1 – h).

Solid fibers could also be replaced by hollow fibers, while keeping the basis weight constant. The increased number of fibers could improve filtration properties, for example, without increasing the manufacturing price.

If solid filaments in nonwovens are replaced with hollow fibers, are the properties of the nonwovens changed ? This question is addressed in this chapter.

2.1.1 Use of the continuity equation in hollow fiber spinning

Figure 2.2 shows a diagram of the fiber spinline during the spunbonding process for hollow fibers. The d_2 is the outside diameter of the filament, while d_1 is the inside diameter of the filament. Both d_2 and d_1 vary along the spinline. Of course, at the fiber collection screen (see Figure 1.1), the values of d_2 and d_1 reach their final product diameters (OD and ID).

Since mass neither enters nor leaves the spinline during melt processing of fibers, then the mass at any point along the spinline is constant. For the polymer, the continuity equation (mass balance equation) for any z position along the spinline is:

$$m_p = \rho_p \pi \frac{\left(d_2^{\,2} - d_1^{\,2}\right)}{4} v_f \qquad (2.2)$$

where

m_p = polymer mass flowrate

ρ_p = polymer density

v_f = fiber velocity

d_1 = inside diameter

d_2 = outside diameter

For the core fluid (nitrogen), the mass balance equation is:

$$m_n = \rho_n \pi \frac{d_1^2}{4} v_f \tag{2.3}$$

where

m_n = nitrogen mass flowrate

ρ_n = nitrogen density

Implicit in equation 2.3 is the assumption that the nitrogen moves at the same velocity as the polymer. For typical core diameters (d_1 values) on the order of 40 microns, this is probably a very good assumption: gas boundary layers are generally greater than 40 microns in thickness. Of course, near the spinneret, the core diameter might be several hundred microns in diameter, but even here, the nitrogen is substantially dragged along with the polymer. The v_f is also a lot slower at positions near the spinneret.

2.1.2 Evaluation of nitrogen pressure inside the fiber

In order to use equation 2.3, information about the nitrogen density ρ_n along the spinline is needed. The ρ_n is a function of pressure and temperature. The pressure in the spinline is greater than the ambient atmospheric pressure. This difference can be calculated from the fundamental equation of capillarity which is [Adamson, 1967]:

$$\Delta P = \gamma (1/R_1 + 1/R_2) \tag{2.4}$$

where

ΔP = the pressure difference between two phases

R_1, R_2 = radii of curvature of the interface between the two phases

γ = surface energy

For a cylindrical fiber, one of the radii is infinite. Thus, the capillarity equation becomes:

$$\Delta P = \gamma (1/R) \tag{2.5}$$

Bicerano [1996] gives data for the surface energy of polypropylene and polyethylene at temperatures of 20-180°C. His data show that temperature has relatively little effect on γ. Based on Bicerano's data, it can be assumed that γ = 25 dyne/cm for the air-polypropylene interface and the nitrogen-polypropylene interface.

Because the hollow fiber has both an inner and outer surface, equation 2.5 must be applied twice. Let us assume an inner diameter (d_1) of 40 microns and an outer diameter (d_2) of 70 microns. Based on these dimensions, and assuming γ = 25 dyne/cm, the pressure of the core nitrogen is only 1964 Pa higher than the outside pressure. Based on an outside pressure of 1.01×10^5 Pa, the core pressure is 1.0296×10^5 Pa. Since this core pressure is only 1.9% higher than the outside pressure, and since the assumed fiber dimensions are typical of our minimum fiber sizes (the pressure difference would be even less for larger fiber dimensions), then it is safe to approximate the inner core pressure as atmospheric.

2.1.3 Use of continuity equations in hollow fiber spinning

Knowledge of the core pressure permits the determination of core density ρ_n (from tabulated or correlated data). The ρ_n is very useful. For example, if the injection rate of nitrogen (m_n) into a spinning system is known, and if the spinning speed (v_f) is known, then, from equation 2.3, the fiber inner diameter (d_1) can be predicted (for the collected product material). Furthermore, if the mass rate of polymer (m_p) is known, and if the polymer density (ρ_p) at room temperature is known (and it is for all common polymers), then equation 2.2 will allow the calculation of the fiber outer diameter (d_2).

The continuity equations can also be used in other ways. For example, if off-line measurements of d_1 and d_2 (ID and OD) are performed on the collected fibers, then equations 2.2 and 2.3 can be used to predict m_n and m_p.

When replacing solid filaments by hollow filaments, it is essential to compare the properties of a nonwoven material made of solid fibers and the properties of the same material made of hollow fibers. Specific properties have to be selected, depending on the application meant for the material. The goal of this paper is to compare a number of properties of hollow fibers versus solid fibers. The properties we selected are essential for most of the applications of nonwovens where hollow fibers could be substituted to solid fibers (mostly disposable material). Compression and opacity tests were performed to compare web properties.

2.2 EXPERIMENTAL EQUIPMENT

2.2.1 Melt spinning equipment

The experimental equipment used is shown in Figure 2.3. Polypropylene pellets were melted and pressurized in a Brabender screw extruder. The barrel had a 19.0 mm diameter, a 381 mm length, a 20:1 L/D ratio, and a 3:1 compression ratio. The extruder temperature was set at 225°C for all experiments. After exiting the extruder, the polymer was fed to a spin pack containing a modified Zenith pump which in turn fed the spinneret assembly. The polymer exited from an annular ring in the spinneret, and a center hole allowed nitrogen to be injected into the core of the polymer stream (see Figure 2.2). Two different spinnerets were used in spinning; the dimensions of these spinnerets are given in Table 2.1. For spinneret A, both the spinneret and the spin pack were set at 190°C; for spinneret B, both were set at 200°C. For spunbonding, the fibers were drawn with an air-powered venturi; the fibers were collected on an open screen. For conventional melt spinning, the venturi was replaced with a mechanical roll and the fibers were collected on the roll. The polymer used in our studies was 88 MFR Dypro® isotactic polypropylene donated by the Fina Company. This polypropylene has an M_w of 165,000 and an M_n of 41,500. Table 2.2 gives the experimental conditions used to produce fibers for off-line analysis. Outside diameters and inside diameters (for hollow fibers) were determined by first microtoming the samples and then measuring the diameters with a Nikon Labophot2-Pol Microscope at 100X magnification.

2.2.2 Experimental equipment for compression tests

For many end uses, nonwoven structures must be able to both resist compression and recover after compression. An INDA standard test [IST 120.4 (95)] is available for determining compression and recovery. This test, which is a pending ASTM test method, uses weights and plates to determine product properties. See Figure 2.4 for a diagram of the apparatus. In the INDA test, the nonwoven specimen is 200 mm by 200 mm, and a 7.26 kg weight is used. Because our spinning system is of small capacity, for our tests both the specimen size and the weight were scaled back to 25% of the INDA value. However, this scaling kept the pressure on the sample the same (1825 Pa). Thus, the results of our tests and the INDA tests are comparable.

Our apparatus consisted of the following pieces:

- The base plates were 150 mm x 150 mm x 6.4 mm (5.9 in x 5.9 in x 0.25 in) plywood plates covered with aluminum foil.
- The cover plates were 150 mm x 150 mm x 6.4 mm (5.9 in x 5.9 in x 0.25 in) plywood plates covered with aluminum foil. The weight of these plates was 106 ± 3 g (0.23 ± 0.007 lbs).
- The weights were 1.80 kg (3.96 lb) stainless steel cylinders with a 9.00 cm (3.54 in) diameter and a height of 3.61 cm (1.42 in).
- Ten cm (4 in) rulers were placed at the midpoints of the sides of each base and cover plate combination (i.e., there were four rulers per test assembly).

Four separate test assemblies (each similar to that shown in Figure 2.4) were constructed. These four assembles permitted simultaneous testing of four samples. Since a single specimen test takes 25 hours, this capability was quite useful for reducing experimental time.

Solid and hollow fibers were produced using the spinning apparatus described previously (see Figure 2.3). The fibers were collected by placing a hand-held metal screen below the venturi. This screen was constructed of 0.2 mm diameter aluminum wire; the screen was 6 mesh per cm by 8 mesh per cm (48 holes per cm^2). Fiber samples were collected for about 15 seconds while the screen was moved below the venturi. A number of these samples were carefully stacked on a 22 cm by 22 cm cutting board to produce a fiber mat (the number of samples used depended on the fiber hollowness, etc.). Next, 114 mm (4.49 in) diameter discs were cut from the mat with an X-ACTO knife. An aluminum tube was used as a cutting guide. This tube had an ID of 102 mm, and OD of 114 mm, a 54 mm length, and the tube had a sharpened lip on the end that was placed against the mat.

To obtain comparable results between compression tests of solid fiber webs, compression tests were performed on webs of 9.0 ± 0.1 g. Cut discs were stacked upon each other to produce this desired weight. The stacking took place on an electronic balance. For all discs, the final disc had a minimum thickness of 25 mm with the cover plate installed.

With a polypropylene density of 0.895 g/cm^3, the 9.0 g standard weight of solid fiber webs corresponds to a fiber volume of 10.05 cm^3. To compare solid

filaments with hollow filaments. this fiber volume was kept constant for all disc samples. Thus, the weight of hollow fiber in a nonwoven disc sample was:

$$w_h = \frac{OD^2 - ID^2}{OD^2} w_s \tag{2.6}$$

where

w_h = weight of hollow fiber

w_s = weight of solid fiber = 9.0 g

By keeping the fiber volume constant for the disc samples, the adverse effects (if any) of the presence of a hollow core could be quantified.

The disc samples were placed in the compression test apparatus, and a procedure very similar to that described in IST 120.4 (95) was followed. At the proscribed times, the height of the web was determined from the average of four measurements taken at the midpoint of each side of the cover plate. The heights were taken at the following times and conditions:

A = Initial height with cover plate on sample but no additional weight.

B = Height with weight added.

C = Height with weight added after ten minutes.

D = Height with weight removed after ten minutes.

E = Height with weight removed after 20 minutes.

F = Height with weight added after 20 minutes.

G = Height with weight added after 30 minutes.

H = Height with weight removed after 30 minutes.

I = Height with weight removed after 40 minutes.

J = Height with weight added after 40 minutes.

K = Height with weight added after 50 minutes.

L = Height with weight removed after 50 minutes.

M = Height with weight removed after 60 minutes.

N = Height with weight removed after 8 hours.

O = Height with weight added after 8 hours.

P = Height with weight added after 24 hours.

Q = Height with weight removed after 24 hours.

R = Height with weight removed after 25 hours.

As given in IST 120.4 (95), compression and recovery parameters are defined as follows:

$$\% \text{ Compression Resistance} = (C/A)x100\% \quad (2.7)$$

$$\% \text{ Elastic Loss} = \{(A-E)/A\}x100\% \quad (2.8)$$

$$\% \text{ Immediate Recovery} = (N/E)x100\% \quad (2.9)$$

$$\% \text{ Long Term Recovery} = (R/E)x100\% \quad (2.10)$$

The letters in the above equations refer to the heights taken during the alphabetized steps of the aforementioned procedure.

The test IST 120.4 (95) is suitable for highloft nonwovens. Highloft nonwovens have a low density fiber structure with (a) no more than 10% solids by volume, and (b) greater than 3 mm thickness. For both the solid and the hollow fibers, the disc samples that we prepared had thicknesses of at least 25 mm – so

criterium (b) was satisfied. To check if criterium (a) was satisfied, the volume density of polymer was measured for disc samples with all fiber diameters and types (solid or hollow) that were included in our experimental program. The results of these measurements are shown in Tables 2.3 and 2.4 (for all thickness measurements and density measurements, the cover plate, but not the weight, was placed on the nonwoven). Since the tables show a density range of 0.5 to 4%, all disc samples had densities well below the maximum of 10%. In particular, the hollow filaments had very low volume densities.

2.2.3 Experimental equipment for opacity tests

The cover of a fabric represents the fabric's ability to obscure or hide (see Hathorne, 1964). We developed an opacimeter to measure the cover of our nonwoven fabrics. Of interest to us is whether hollow fibers have as much opacity (cover) as solid fibers.

The body of our opacimeter was constructed from a cardboard mailing tube with a 5.5 cm OD and a 5.0 cm ID; see Figure 2.5. The upper section was 10.0 cm long, and the lower section was also 10.0 cm long. A 150 Watt Nikon MKII Fiber Optic Light provided the illumination. The end of the flexible fiber optic tube was placed at the top of the upper section of the opacimeter body. The top and bottom sections of the body were separated by a 2 cm gap. The nonwoven samples were placed on a clear polypropylene sheet (a transparency sheet), and then the samples were inserted into the gap. Only the sample's center (a 5.0 cm diameter circle) was illuminated during the measurements. However, to avoid edge effects each nonwoven

sample had substantially more area than the area of the illuminated center. A photocell was placed at the base of the lower tube section. The photocell had a diameter of 4.2 cm and was 0.5 cm thick. The photocell was part of a complete photometer (LX-101 lux meter from Lutron, Coopersburg, PA). The photometer had three ranges: 0 -1999 lux, 2000-19,999 lux, and 20,000-50,000 lux. The second range was used in our studies. The photometer supported the lower section of the opacimeter tube, while a ring stand and clamp held the upper section.

When using the opacimeter, a measurement of the intensity of light (I_o) was done with no sample inserted (only the polypropylene sheet). The intensity of the light source was adjusted until I_o equaled 8,000 lux. A nonwoven sample was then placed on the polypropylene sheet, and the intensity of light (I) that went through the sample was measured. The illuminated portion of the sample (a 5 cm diameter portion) was then cut out from the rest of the sample by using an X-ACTO knife. A sharpened stainless steel tube (5.0 cm outside diameter by 4.7 cm inside diameter) was used as a cutting guide. Samples weights ranged from 0.01 to 1 gram, and the sample weight was determined to within ± 0.1mg. After taking the opacity measurements, a small quantity of fibers was removed from the web. These fibers were microtomed to allow cross-sectional observation, and the fiber's OD and ID were determined with a micrometer eyepiece on a Nikon microscope at 100X magnification.

2.3 RESULTS AND DISCUSSION

2.3.1 Effect of operating parameters on fiber dimensions

In the melt spinning of hollow fibers, an additional dimension must be considered. This dimension is the fiber inside diameter, or (equivalently) the fiber wall thickness. To gain a better understanding of how hollow fibers are formed, the effects of experimental parameters on the fiber OD and ID were examined. Fibers were spun using hollow fiber spinneret B (see Table 2.1). Because analysis of individual fibers (rather than a fiber mat) was the goal, a windup roll was used instead of an air venturi (see Figure 1.1). The experimental parameters studied were polymer flowrate, fiber spinning speed, and nitrogen flowrate. The ranges of parameters studied are shown in Table 2.2.

Figure 2.6 shows the effect of nitrogen flowrate on OD, ID, and wall thickness for a polymer flowrate of 0.57 g/min and a fiber speed of 263 m/min. Increased nitrogen flowrate results in larger OD and larger ID. However, the wall thins as nitrogen rate increases. Results similar to Figure 2.6 were found for other combinations of polymer flowrates and fiber speeds. For the OD and ID measurements, each data point on Figure 2.6 is the average of three diameter measurements; the standard deviation of each point is about 2 μm. Also shown on Figure 2.6 are model estimates of OD, ID, and thickness. These estimates were based on continuity equations 2.2 and 2.3. Inputs to these equations were the polymer flowrate m_p (based on fiber samples collected and weighed over time), nitrogen flowrate m_n (based on the nitrogen flowmeter reading), and windup speed (based on a

digital tachometer reading of the windup roll speed). As an examination of Figure 2.6 shows, the model fits the data quite well. The goodness of fit lends credibility to the aforementioned assumptions relating to the development of the continuity equations and the capillarity equation.

The effect of nitrogen flowrate on the fiber cross-sectional area is shown in Figure 2.7, at the same take-up speed and polymer throughput as used in Figure 2.6. The cross-sectional area shows no variation, as expected.

Figure 2.8 shows the effect of nitrogen flowrate on outer diameter for three different fiber speeds. Also shown are the model predictions. The model does a very good job of predicting diameter behavior as a function of operating parameters. For the same conditions as for Figure 2.8, Figure 2.9 shows the effect of nitrogen flowrate on inner diameter. As before, the model equations do a very good job of predicting diameters. In Figure 2.9, the largest difference between the model and the data occurs for the high fiber speed (466 m/min). But even for this case, the model is not far off. Figure 2.10 shows how wall thickness is affected by nitrogen flowrate and fiber speed. The thinnest walls occur at the highest fiber speeds and the highest nitrogen flowrates. The model equations fit the data very well for Figure 2.10.

Figure 2.11 shows how the ratio ID/OD is affected by nitrogen flowrate. As was done for previous plots, the continuity equations (2.2 and 2.3) can be used to produce a model equation. This model equation is:

$$\frac{ID}{OD} = \left(\frac{m_n}{\frac{\rho_n}{m_p + m_n}} \right)^{0.5} \qquad (2.11)$$

What is interesting about this equation is that it is independent of fiber speed. And, indeed, the data follow this prediction: there is no dependence on fiber speed. The ratio ID/OD exceeds 0.9 for nitrogen flowrates above 3 ml/min. This corresponds to a mass ratio m_n / m_p above 0.0072. In other words, it takes relatively little gas to produce a large hole in the fiber. Figure 2.12 shows the effect of take-up speed on cross-sectional area. The cross-sectional area decreases for increasing speeds, to satisfy the continuity equation. Theoretically, each plot should be a flat line at a given speed. The variations that are observed are due to the error made when measuring the outer and inner diameters.

The effects of variable polymer flowrates are shown in Figures 2.13 to 2.17. Figure 2.13 shows the variation in outer diameter, while Figures 2.14, 2.15, 2.16 and 2.17 show the variations in, respectively, inner diameter, wall thickness, ID/OD, and cross-sectional area. The model equations are also included on these Figures.

The model equation for Figure 2.14 is:

$$ID = \left(\frac{4m_n}{\pi \rho_n v_f} \right)^{0.5} \qquad (2.12)$$

Note that ID is independent of m_p. This makes sense if you consider that m_n, not m_p, determines how much the fiber is "blown up". The m_p only affects the wall

thickness. Figure 2.15 shows how wall thickness is affected by m_p, while Figure 2.16 shows the variation of ID/OD. Unlike the situation in Figure 2.11, the model equation for ID/OD is not a single curve in Figure 2.16. Polymer flowrate does affect ID/OD. Figure 2.17 shows that the cross-sectional area increases with increasing polymer throughput.

Figure 2.18 shows actual photographs of cross-sections of hollow fibers produced in our laboratory. Figure 2.18a shows a thick-walled fiber with a hollowness of less than 1% (0.21%). Figure 2.18b shows a medium-walled fiber with a hollowness of 36%. Figure 2.18c shows a very thin-walled fiber with a hollowness of 69%. This fiber is mostly nitrogen! These three photographs illustrate the wide range of hollowness that is possible with the spinning equipment described herein.

2.3.2 Compression tests

Fibers were spun with hollow fiber spinneret A (see Table 2.1), and the fibers were collected on a screen below the air venturi (see Figure 1.1). Then, nonwoven discs were prepared as has just been described. Figure 2.19 shows typical results from two compression-recovery tests. The solid line represents the height of a disc sample from a 39 μm diameter solid fiber, while the dashed line represents the height of a disc sample from a hollow fiber with 38 μm OD and 21 μm ID. Both samples had an original thickness of about 32 mm. The letters on the solid line correspond to the height measurements (for the solid fiber) in the experimental procedure. Results for both fibers are similar.

Figure 2.20 shows the compression resistance and elastic loss for solid fibers with diameters ranging from 17 to 48.5 μm. Figure 2.21 shows immediate recovery and long term recovery for the same fibers. To estimate the reproducibility of the experimental measurements, eight replicate runs were made on samples of 32 μm fiber. From these tests, the average values and standard deviations were as follows: compression resistance: 39.16 ± 3.07, elastic loss: 35.18 ± 6.29, immediate recovery: 90.25 ± 3.97, long term recovery: 70.01 ± 4.09. The error bars on Figures 2.19 and 2.20 are based on these standard deviations.

From Figure 2.20, it appears that there is a slight loss of compression resistance as diameter increases. Also, elastic loss slightly increases. Perhaps the smaller fibers can integrate (function) together better than the larger fibers. In contrast, from Figure 2.21 it appears that immediate recovery is slightly better as fiber size increases. Long term recovery also appears to slightly increase as diameter increases. Now, immediate and long term recovery involve measurements taken later on in the compression-recovery test (see equations 2.7 to 2.10). Hence, the mat is more "tamped down" during these later measurements, and this may explain why solid fiber diameter increase has a different effect for immediate and long term recovery. Whatever, the four resistance and recovery parameters do not change all that much over the range of diameters that we tested.

Figure 2.22 shows compression resistance and elastic loss for hollow fibers as a function of hollowness (which was previously defined as $[ID/OD]^2$). Hollow fibers with three different OD values were used to produce this graph, and solid fiber data

are also included along the ordinate. It appears that there is a small decrease in compression resistance and a small increase in elastic loss as hollowness increases. Perhaps it is most interesting that there is in fact so little change, since a substantial part of the hollow fibers is air (the fibers with the greatest hollowness are 63% air).

Figure 2.23 shows immediate recovery and long term recovery for hollow fibers. It appears that neither parameter shows any significant change as hollowness increases. Both Figure 2.22 and Figure 2.23 imply that hollowness has little effect on compression-recovery properties. Thus, hollow fibers can be used to replace solid fibers in end uses where compression-recovery properties must be maintained.

2.3.3 Opacity tests

Solid Fibers

By analogy with the basic principles of light transmission and absorption (see Meyer-Arendt, 1984), transmission T is defined as $T = I/I_0$, while opacity OPA is defined as $OPA = -\log_{10}(I/I_0)$. In this paper, transmission and opacity refer to a complex process of reflection and refraction of light. Transmission and opacity do not refer to chemical absorption. Figure 2.24 shows the effect of fabric weight per area on transmission for solid fibers. A range of fiber sizes from 15 to 80 micron diameter is included in the figure. As expected, transmission decreases as weight per area increases. Figure 2.25 shows the effect of fabric weight per area on opacity for the same fibers. Obviously, since transmission increases as weight per area increases, then opacity decreases. Both figures show that diameter influences the transmission and opacity.

In order to fit the data of Figure 2.25, the following empirical equation was developed between opacity, sample surface area, and weight of solid fiber:

$$OPA = K \frac{w_s / s}{w_s / s + K'} \tag{2.13}$$

where OPA = opacity

w_s = weight of the solid fiber

s = sample surface area

K, K' = empirical constants.

The lines on Figure 2.25 are least squares fits of equation 2.13 to the data for the different diameter ranges. Interestingly, K~1 for all the diameter ranges.

Instead of using the weight of fiber per surface area (w_s / s), let us use projected area P_s, which is defined as:

$$P_s = L \cdot OD \tag{2.14}$$

where

L = total length of the fiber in the sample

OD = outer fiber diameter

If fiber crossovers are neglected, projected area P_s is a good quantitative measure of the fraction of a sheet which "covers" (obscures or hides). Figure 2.26 shows the data of Figure 2.25 replotted with projected area on the abscissa. As can be seen, all the data follow the same trend: the use of projected area has minimized the effect of fiber diameter (the projected area P_s is the fiber area contained in a disc of 5.0 cm diameter).

Analogous to equation 2.13, the following equation can be used to fit the data of Figure 2.26:

$$OPA = k\frac{w_s/s}{w_s/s + k'} \tag{2.15}$$

where

k, k' = empirical constants

The lines on Figure 2.26 are least squares fit of the data to equation 2.18. The data and the model fits are much more clustered together in Figure 2.26 than in Figure 2.25. Hence, projected area is a better parameter to use than weight/area.

Hollow Fibers

Hollow fibers of various OD's and ID's were produced with spinneret B. Our opacity meter was used to study mats of these fibers. Figure 2.27 shows the effect of weight per area on opacity for hollow fibers of various inner diameters. The effect of OD is the same as shown in Figure 2.25 for solid fibers: a smaller OD produces a higher opacity.

Figure 2.28 is a plot of opacity as a function of projected area for several ranges of fiber ID's. As was the case for correlating solid fiber data, projected area was selected as a better parameter to use than weight/area. As was also done for the solid fiber data, equation 2.15 was used to fit the various data sets on Figure 2.28. The figure illustrates that opacity is not effected by the presence of a hole in the fiber.

Fiber OD's of 40-50 microns are included in Figure 2.28. Figures 2.29 and 2.30 consider, respectively, fiber OD's of 50-60 and 60-70 microns. For Figure 2.29,

the mid-range ID's (24-29 microns) show opacity values which are a little bit higher than the values for the other ID's. For Figure 2.30, the opacity values are a little bit low for the largest ID range (45-55 microns). The k and k' values are similar for Figures 2.28 to 2.30.

In Figures 2.28 to 2.30, any particular data subset (a specific range of ID's and OD's) does not appear to diverge to any great extent from the overall data trend. To illustrate this more clearly, Figure 2.31 is an overall plot of opacity versus projected area for hollow fibers with ID's from 20-78 microns and OD's from 35-105 microns (Figure 2.31 includes all the data from Figures 2.28 to 2.30, plus additional data for fiber sizes beyond the range of Figures 2.28-2.30). Although there is some scatter, the hollow fiber data can be approximated by a single empirical curve. Also included on Figure 2.31 are data for solid fibers with about the same OD range as the hollow fibers. These data can also be approximated by a single empirical curve. What is most interesting is that the two empirical curves are nearly coincident. In other words, the presence of a hole in a fiber does not affect its opacity. So, as far as opacity is concerned, less polymer is required to achieve the same function.

2.4 CONCLUSION

In the production of polypropylene hollow fibers from the melt, the polymer and gas continuity equations can be used to predict the ID and OD of the product fiber.

The compression-recovery behavior of polypropylene hollow fibers is quite similar to that of solid polypropylene fibers.

The opacity behavior of hollow polypropylene fibers is nearly identical to that of solid polypropylene fibers.

For many nonwoven uses, hollow polypropylene fibers can be substituted for solid polypropylene fibers. When this substitution is made, the polymer cost savings can be substantial.

2.5 NOMENCLATURE

d_1 = filament inside diameter, μm
d_2 = filament outside diameter, μm
h = fiber hollowness
I = final light intensity, lux
I_o = initial light intensity, lux
ID = final product inside diameter, μm
k = empirical constant in equation 2.15
k' = empirical constant in equation 2.15, cm^2
K = empirical constant in equation 2.13, cm^2/g
K' = empirical constant in equation 2.13, g/cm^2
L = fiber length
m_n = nitrogen mass rate, g/min
m_p = polymer mass rate, g/min
OD = final product outer diameter, μm
OPA = fiber web opacity
P_s = projected area of solid filament, cm^2
ΔP = pressure difference between two phases, Pa
R_1, R_2 = radii of curvature of the interface between two phases, m
s = sample surface area, cm^2
T = transmission
v_f = fiber velocity, m/s
w_h = weight of hollow fiber, g
w_s = weight of solid fiber, g

Greek letters

γ = surface energy, N/m
ρ_p = polymer density, g/cm^3
ρ_n = nitrogen density, g/cm^3

Subscripts

f = fiber
n = nitrogen
p = polymer

2.6 REFERENCES

A.W. Adamson, *Physical Chemixtry of Surfaces*, 2nd edition, Interscience, New York, pp. 3-6 (1967).

J. Bicerano, *Prediction of Polymer properties*, 2nd edition, Marcel Dekker, New York, p. 195 (1996).

B.L. Hathorne, Woven Stretch and Textured Fibers, Interscience, New York, p. 57 (1967).

INDA IST 120.4, "Standard test method for determination of compression and recovery of highloft nonwoven fabrics at room temperature using weights and plates," Association of the Nonwoven Fabrics Industry, Cary, NC (1995).

J.R. Meyer-Arendt, *Introduction to classical and modern optics*, 2nd Ed., Prentice-Hall, p.481 (1984).

	Outer diameter of polymer annulus, mm (in)	Inner diameter of polymer annulus, mm (in)	Diameter of nitrogen capillary, mm (in)
Spinneret A	1.98 (0.078)	1.22 (0.048)	0.76 (0.030)
Spinneret B	7.01 (0.276)	3.78 (0.149)	1.00 (0.039)

Table 2.1: Dimensions of spinnerets used to produce hollow fibers.

PARAMETERS	VALUES
Polymer flowrate (g/min)	0.33, 0.57, and 1.13
Fiber speed (m/min)	150, 260 and 460
Nitrogen flowrate (ml/min)	0 to 4

Table 2.2: Experimental conditions used to produce fibers for off-line analysis.

Fiber Diameter (μm)	**V_{solid}/V_{sample} (%)**
17.0	3.07
21.0	3.07
24.5	2.73
32.0	3.07
39.0	3.07
48.0	3.40

Table 2.3: Percent solids in the nonwoven samples containing solid filaments.
V_{solid} = volume occupied by polymer;
V_{sample} = volume occupied by nonwoven sample.

OD (μm)	Hollowness (%)	V_{fiber}/V_{sample} (%)	V_{solid}/V_{sample} (%)
32	0	3.07	3.07
32	25	2.29	1.72
32	35.6	2.00	1.22
40	0	3.07	3.07
40	27	2.73	2.00
40	34	2.46	1.61
40	40	2.29	1.37
47	0	3.40	3.40
47	28	3.07	2.21
47	46	3.93	2.09
47	51	2.40	1.20
47	66	2.66	0.98

Table 2.4: Percent solids in the nonwoven samples containing hollow filaments.
V_{solid} = volume occupied by polymer;
V_{sample} = volume occupied by nonwoven;
V_{fiber} = volume occupied by fiber (i.e., polymer plus hollow core).

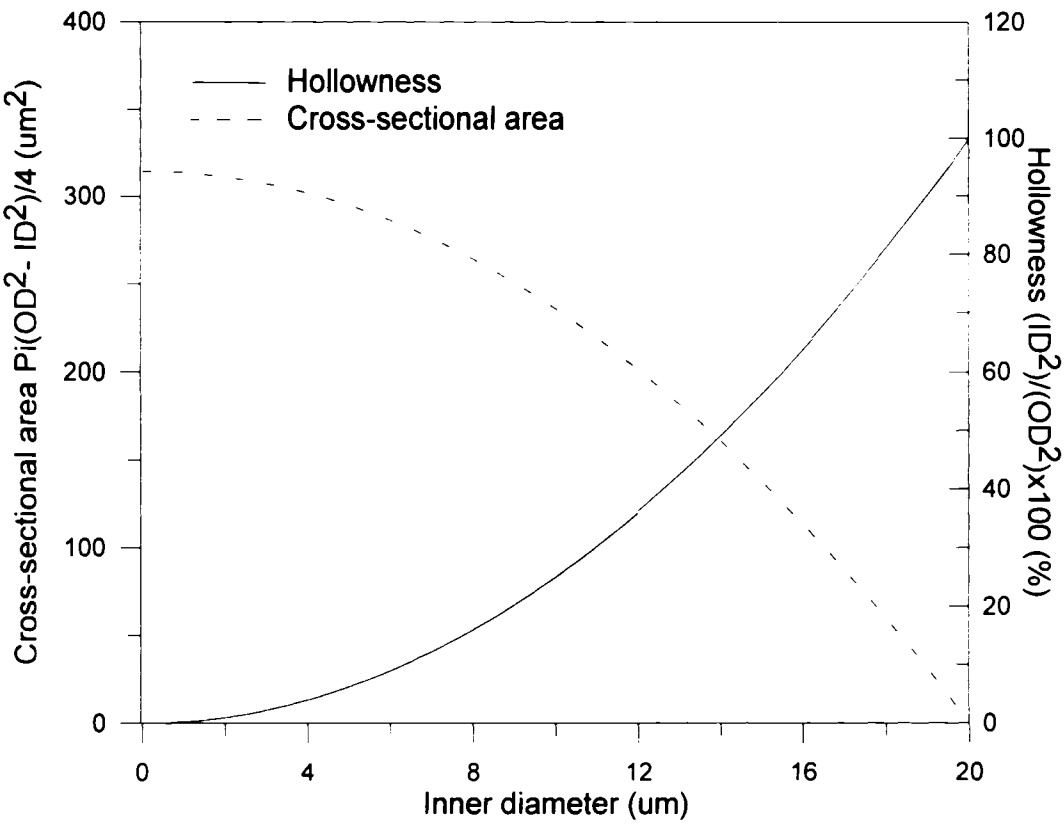

Figure 2.1: Effect of inner diameter on cross sectional area and hollowness ID^2/OD^2 with a constant OD = 20 μm (calculated results).

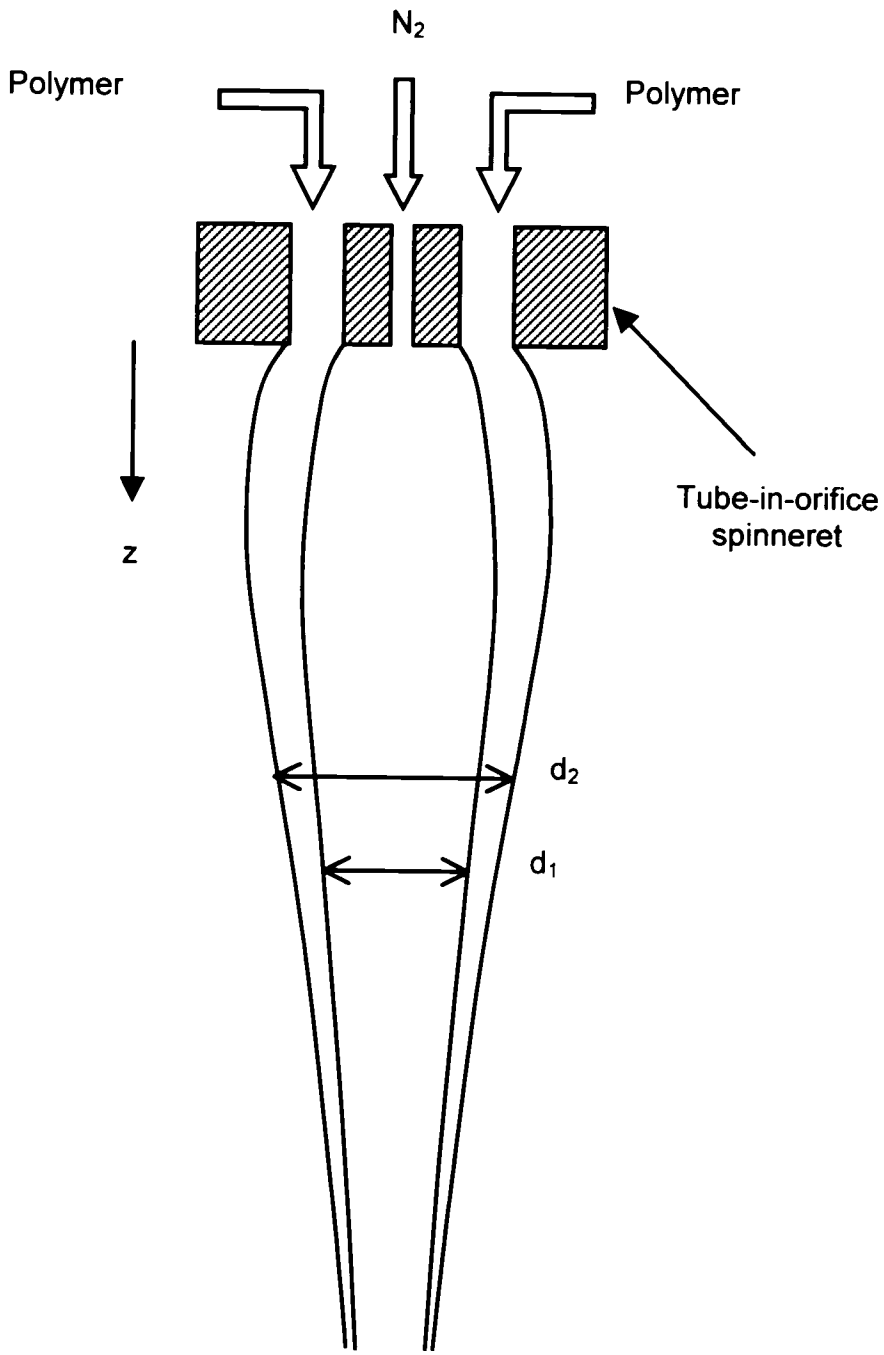

Figure 2.2: The fiber spinline during hollow fiber production.

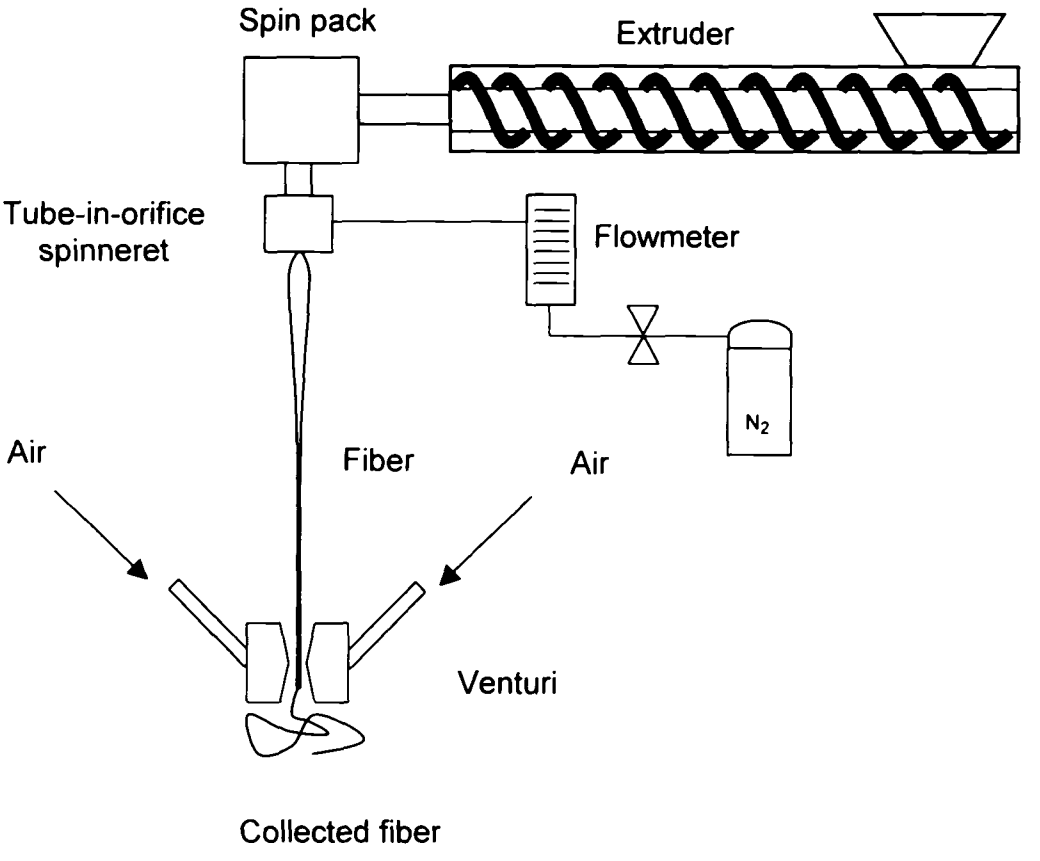

Figure 2.3: Hollow Fiber Melt Spinning.

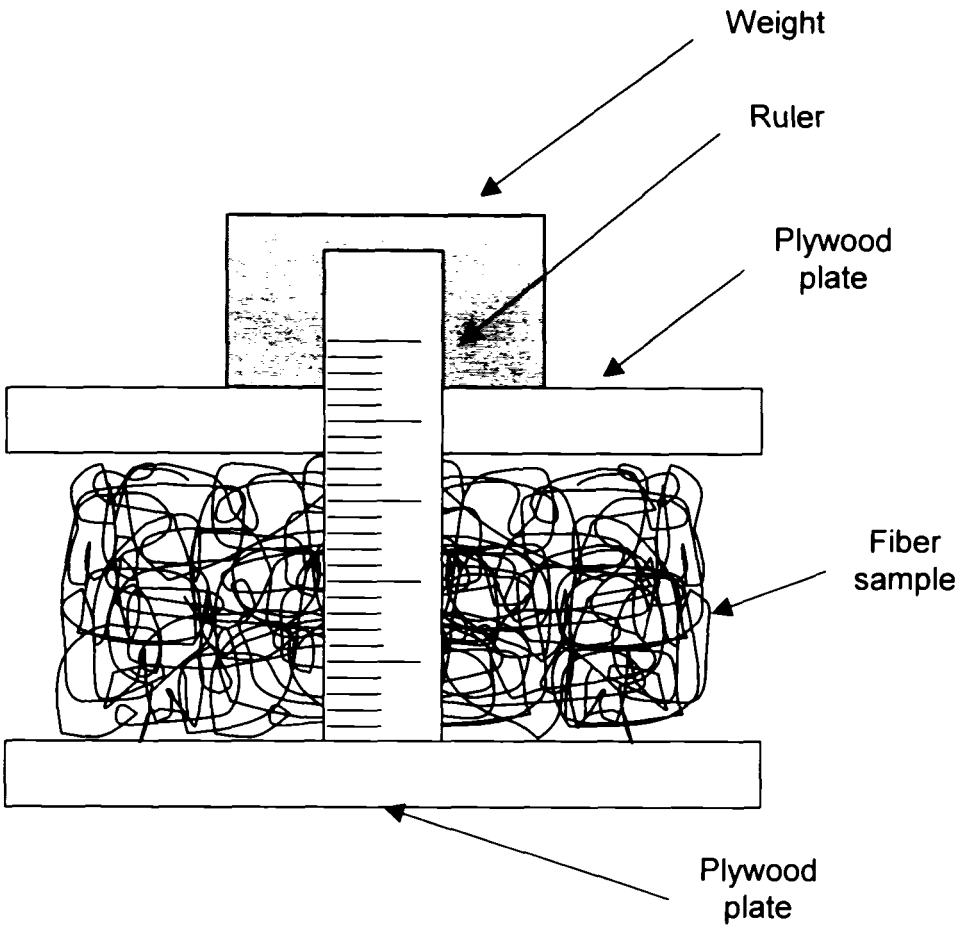

Figure 2.4: Compression – Recovery Apparatus.

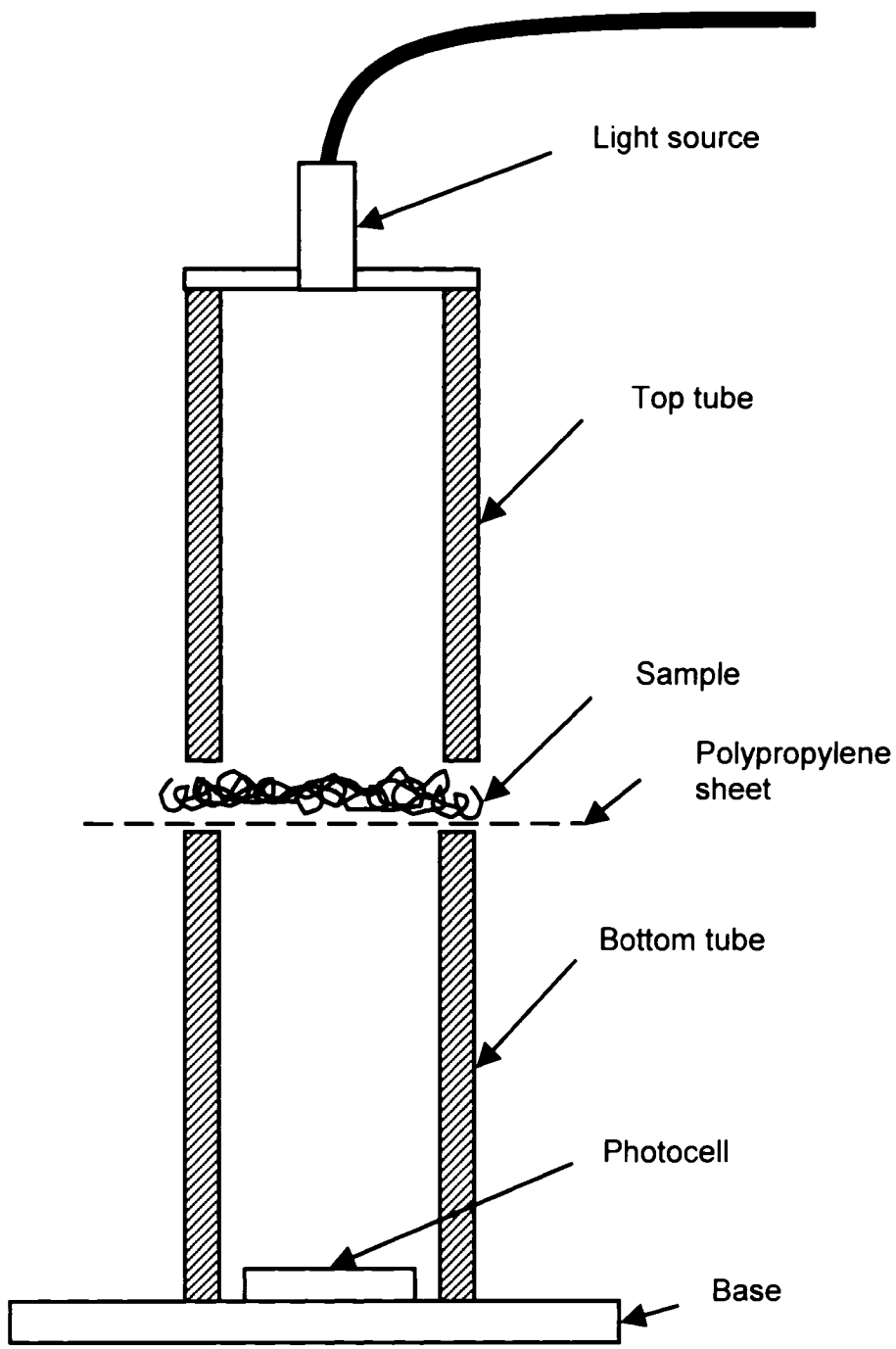

Figure 2.5: Cross-sectional view of opacity measurement device.

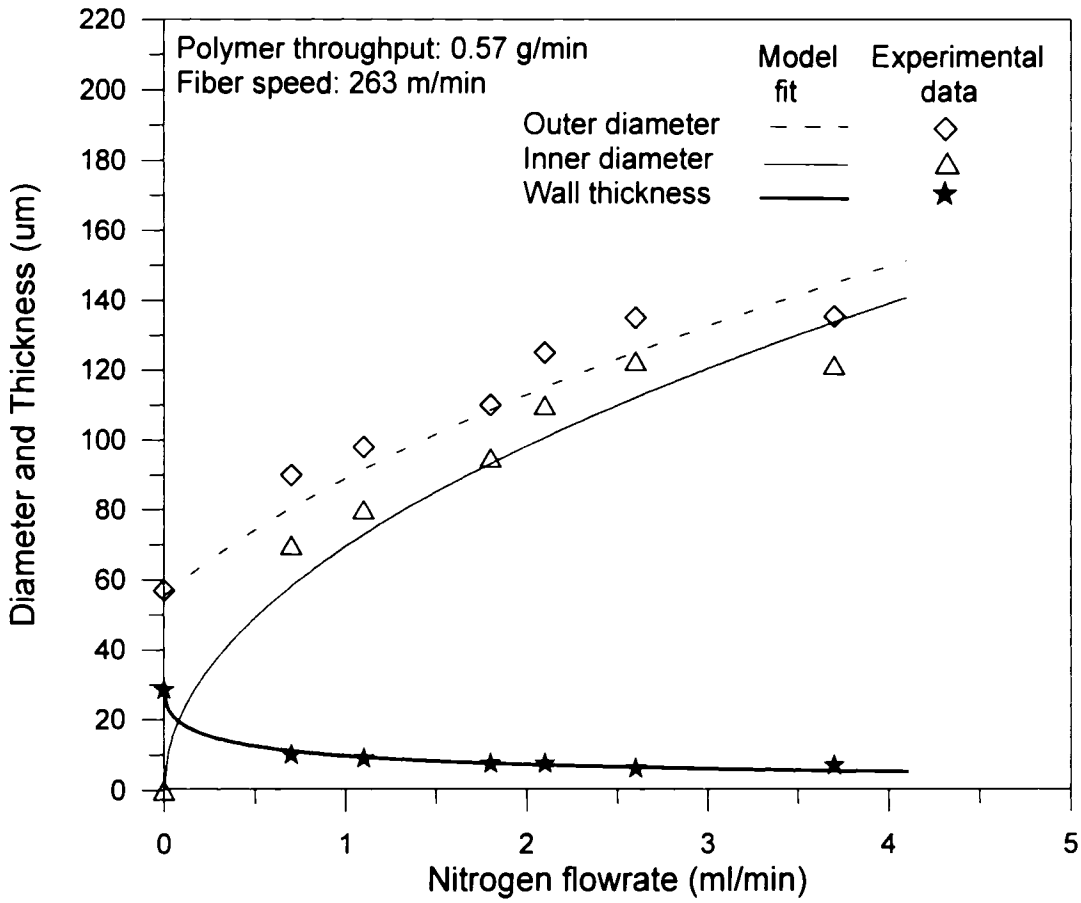

Figure 2.6: Effect of nitrogen flowrate on outer diameter, inner diameter and wall thickness.

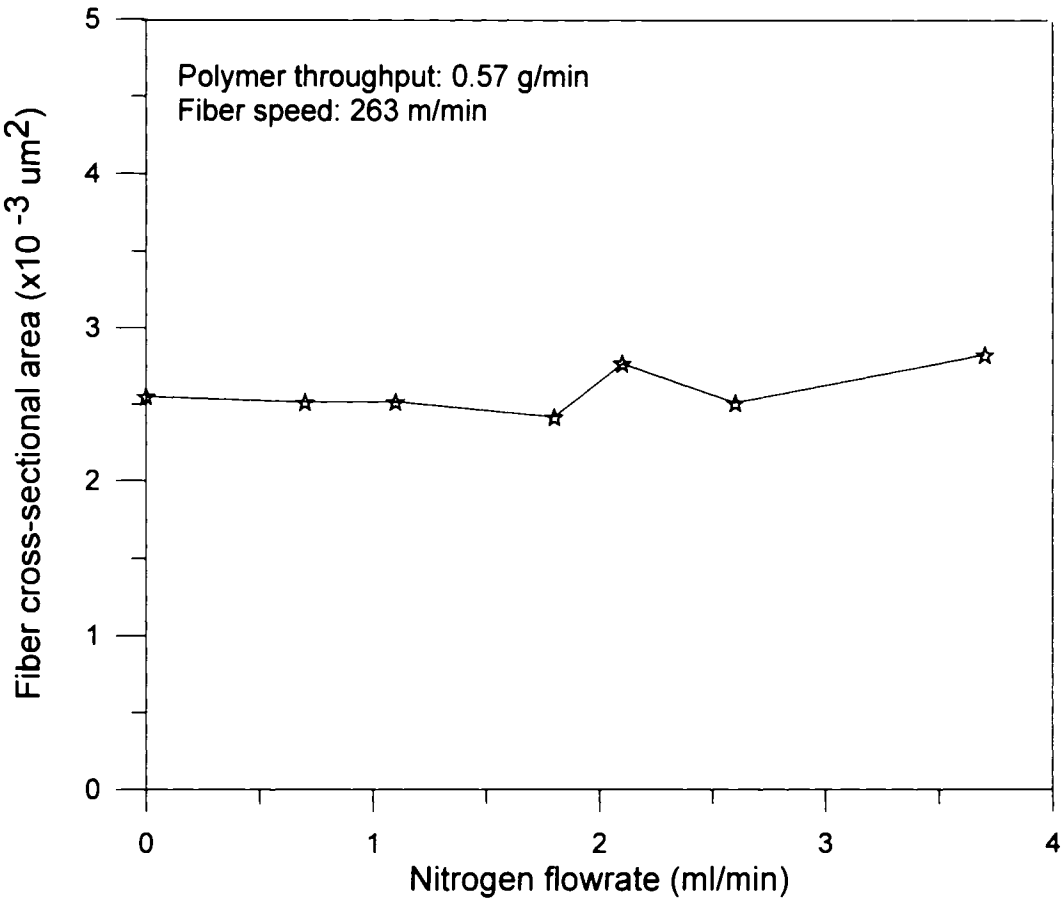

Figure 2.7: Effect of nitrogen flowrate on annular cross-sectional area.

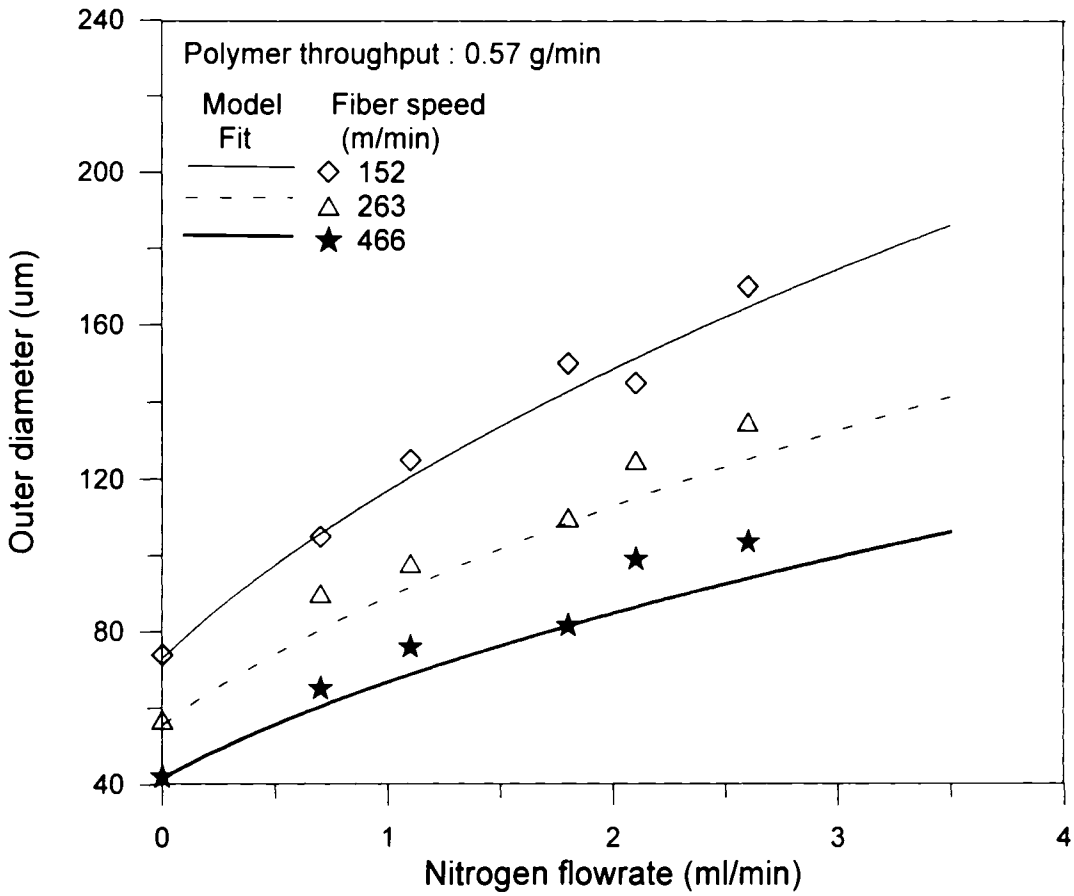

Figure 2.8: Effect of speed on outer diameter.

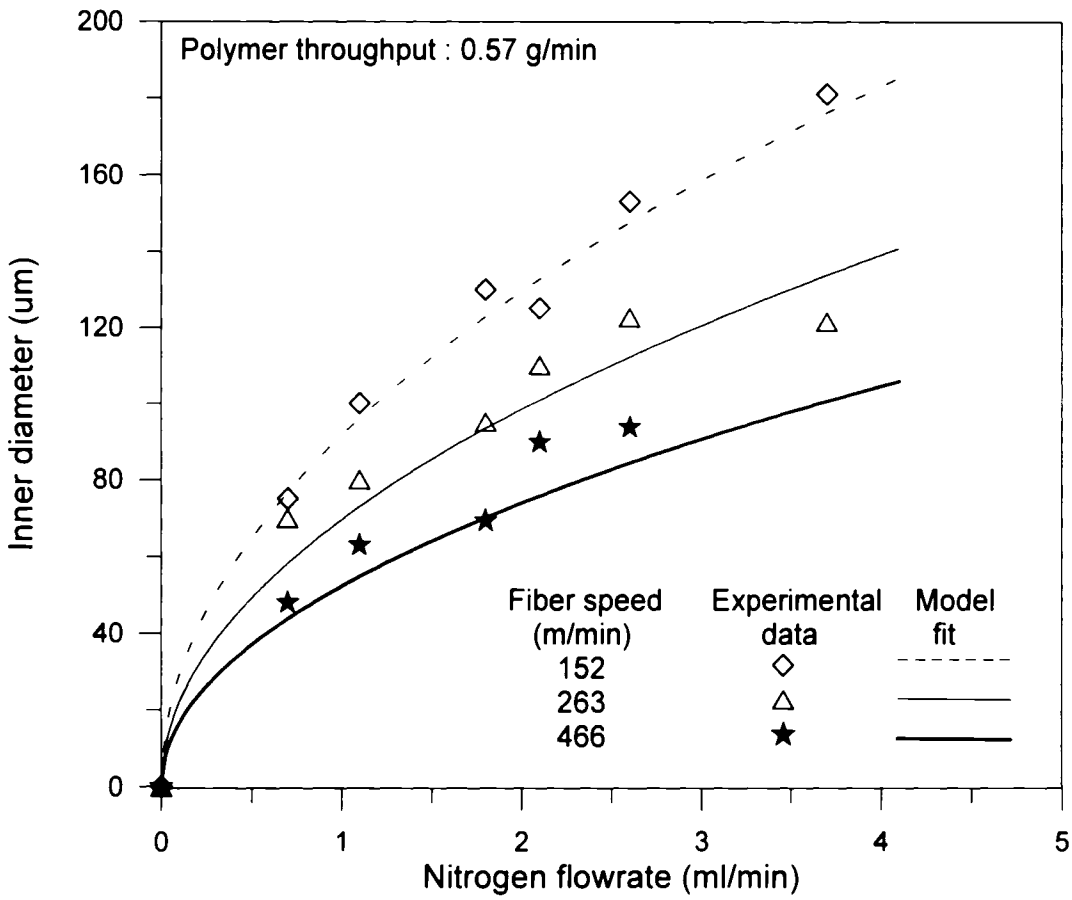

Figure 2.9: Effect of fiber speed on inner diameter.

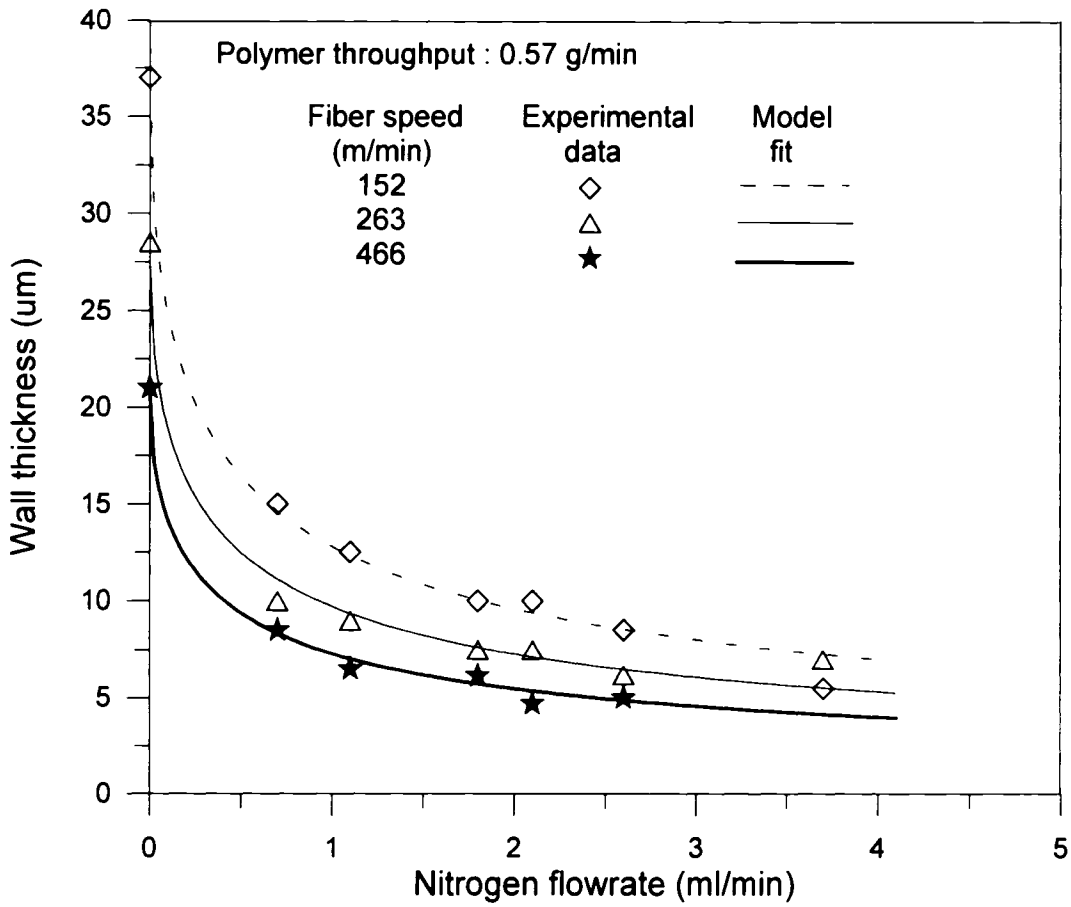

Figure 2.10: Effect of fiber speed on wall thickness.

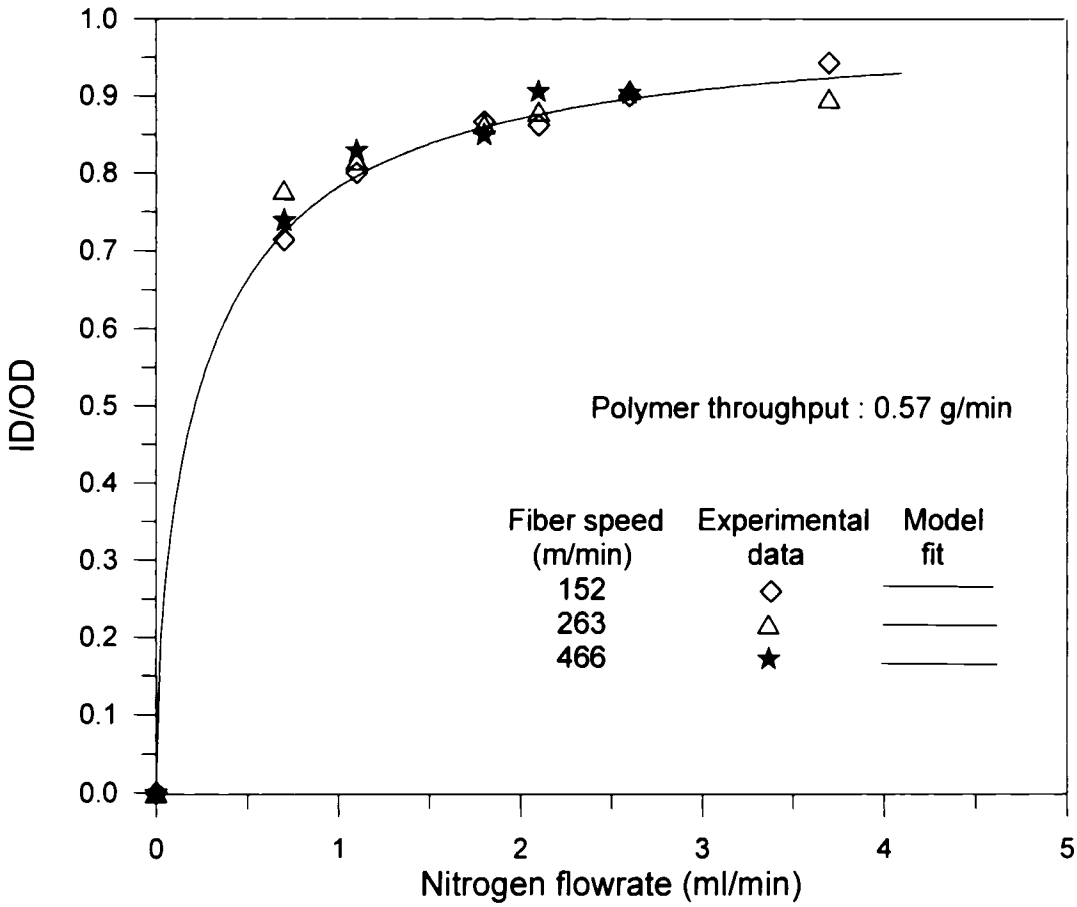

Figure 2.11: Effect of fiber speed on ratio of inner to outer diameter.

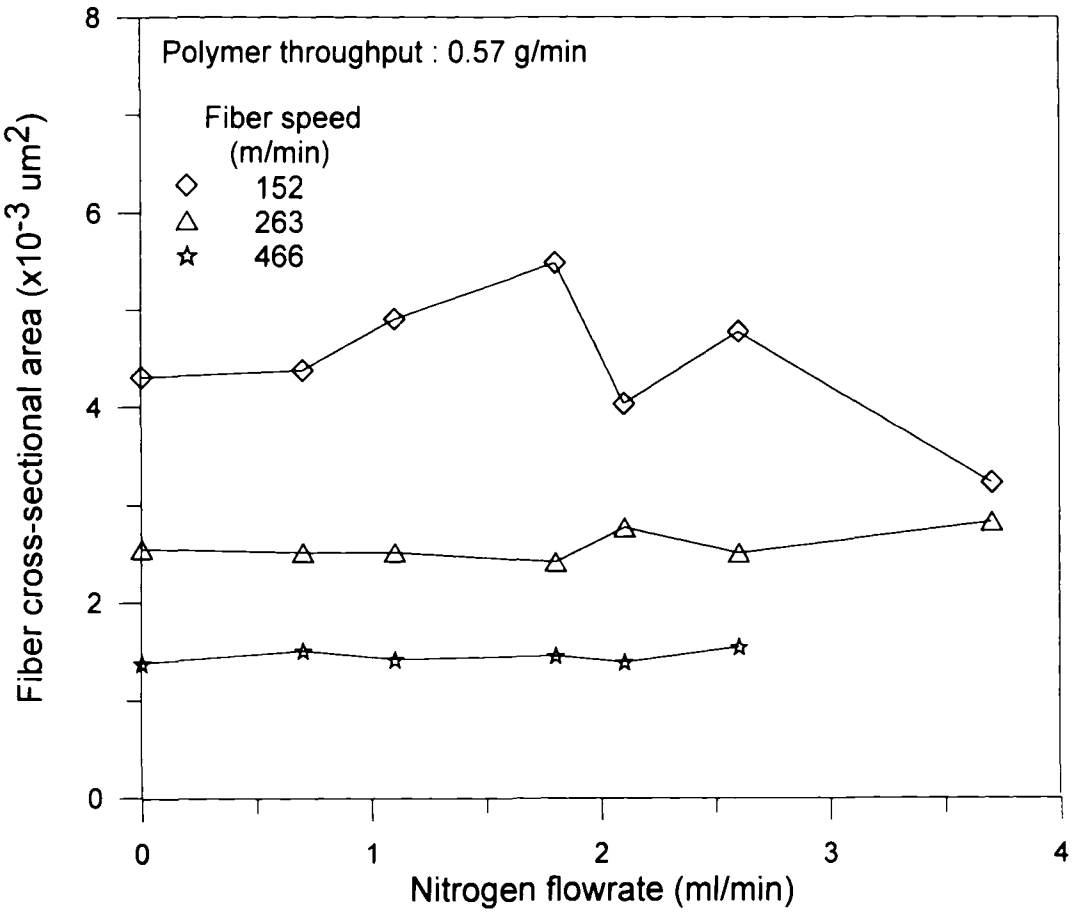

Figure 2.12: Effect of fiber speed on fiber cross-sectional area.

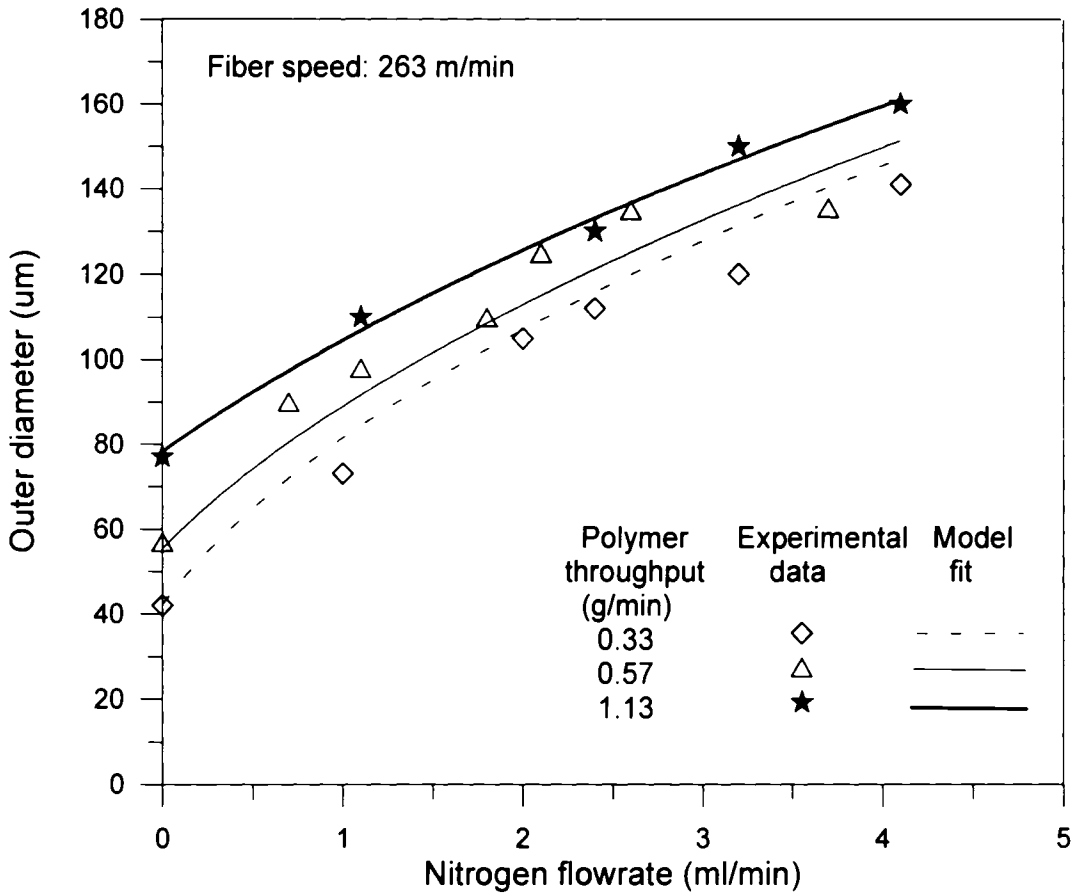

Figure 2.13: Effect of polymer throughput on outer diameter.

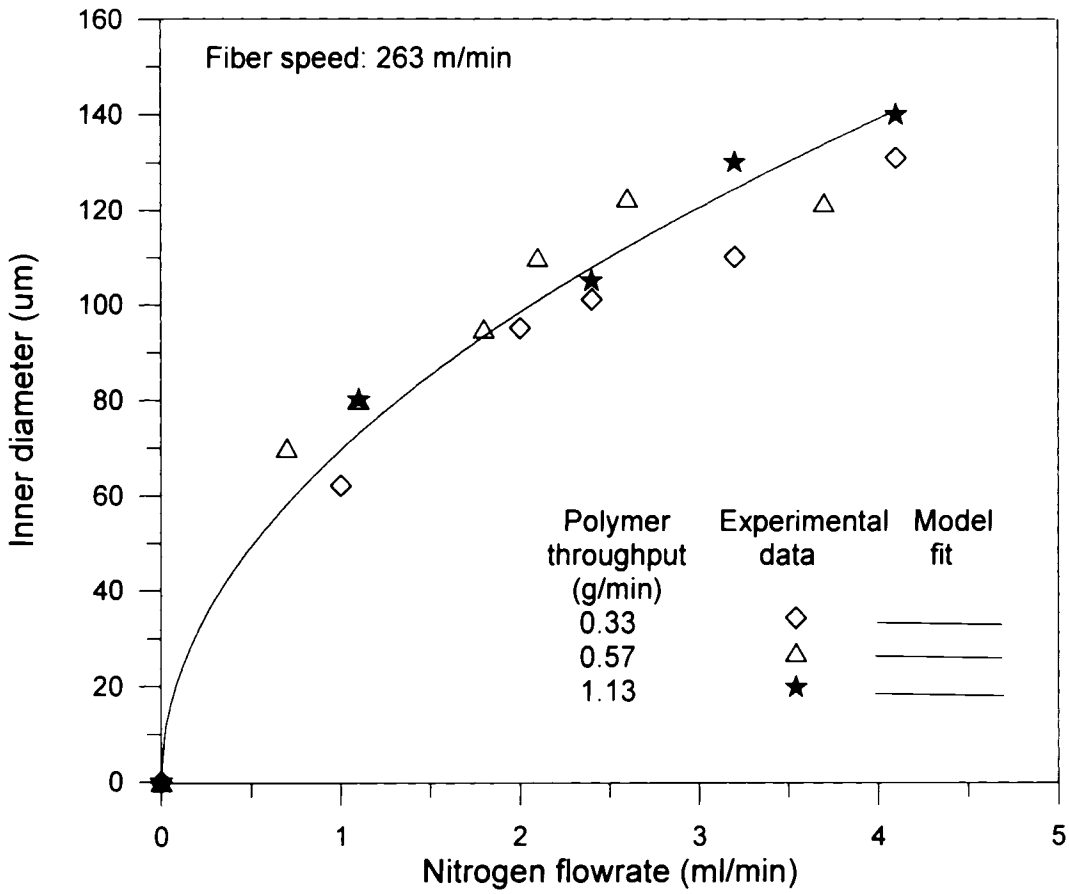

Figure 2.14: Effect of polymer throughput on inner diameter.

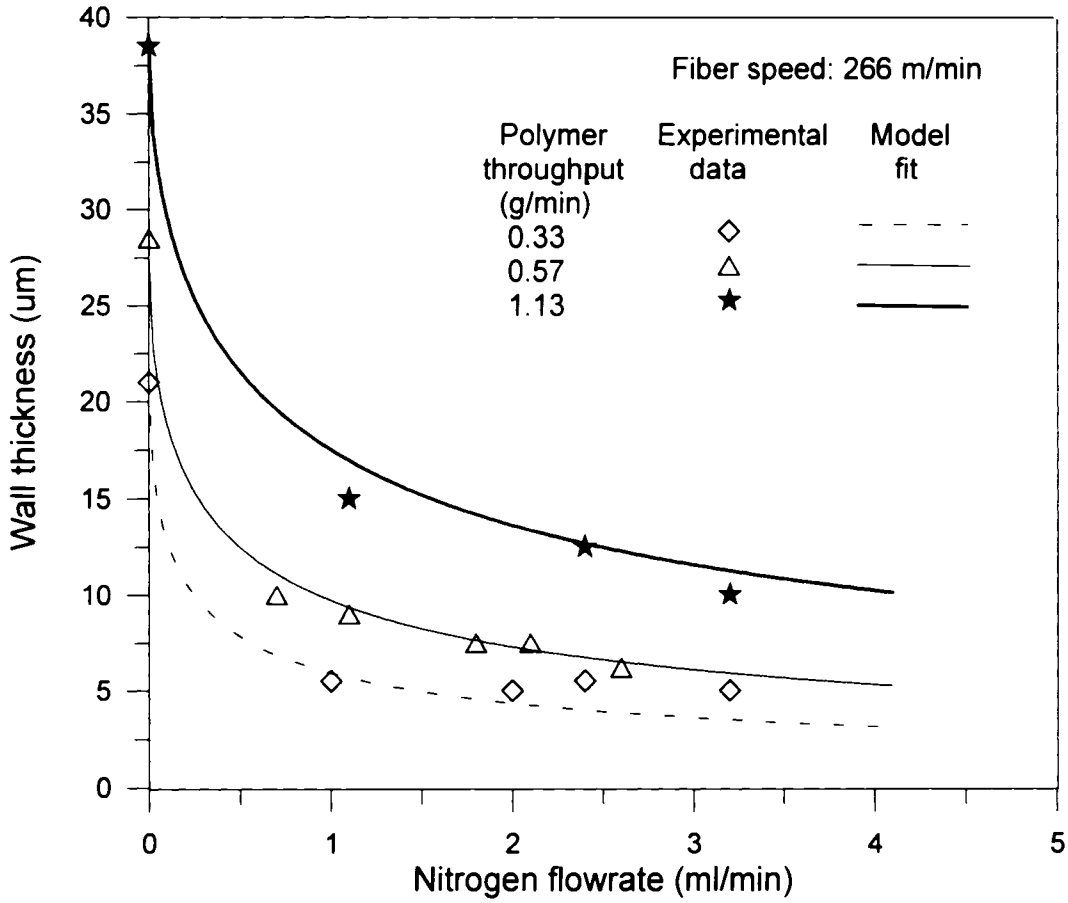

Figure 2.15: Effect of polymer throughput on wall thickness.

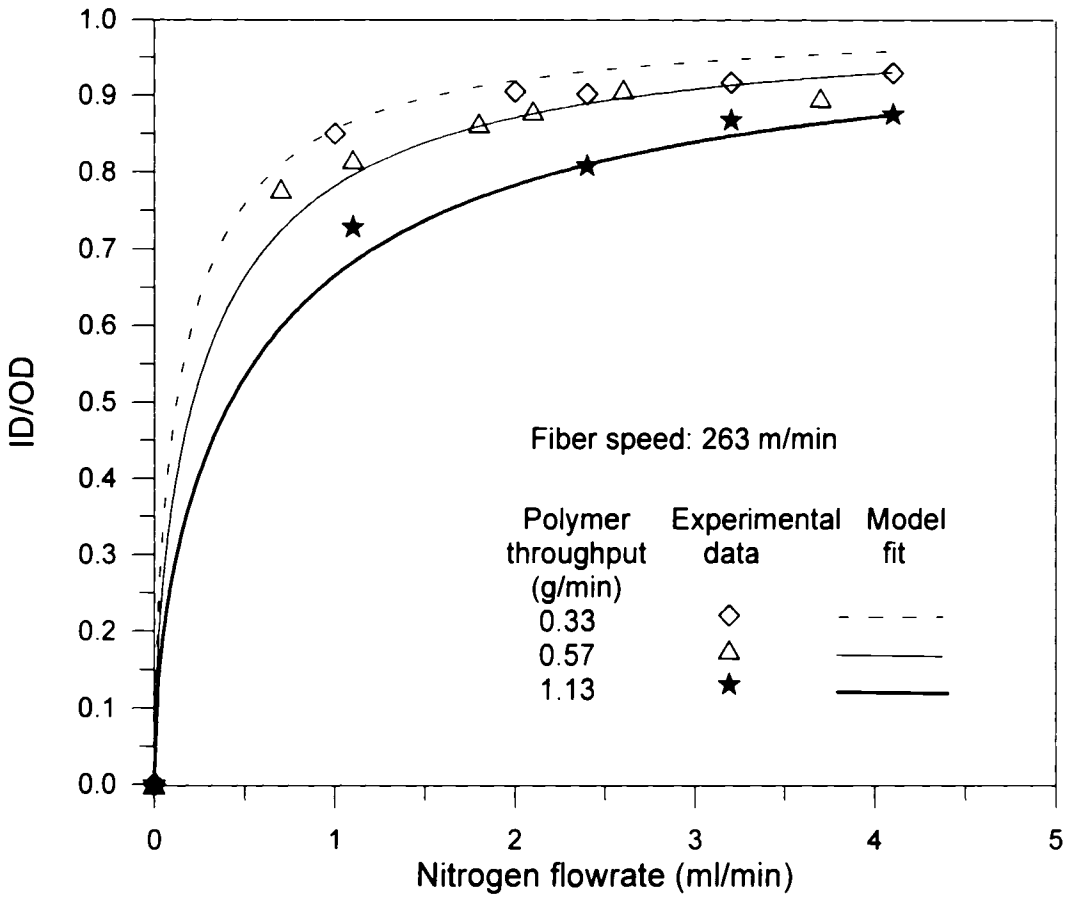

Figure 2.16: Effect of polymer throughput on ratio of inner to outer diameter.

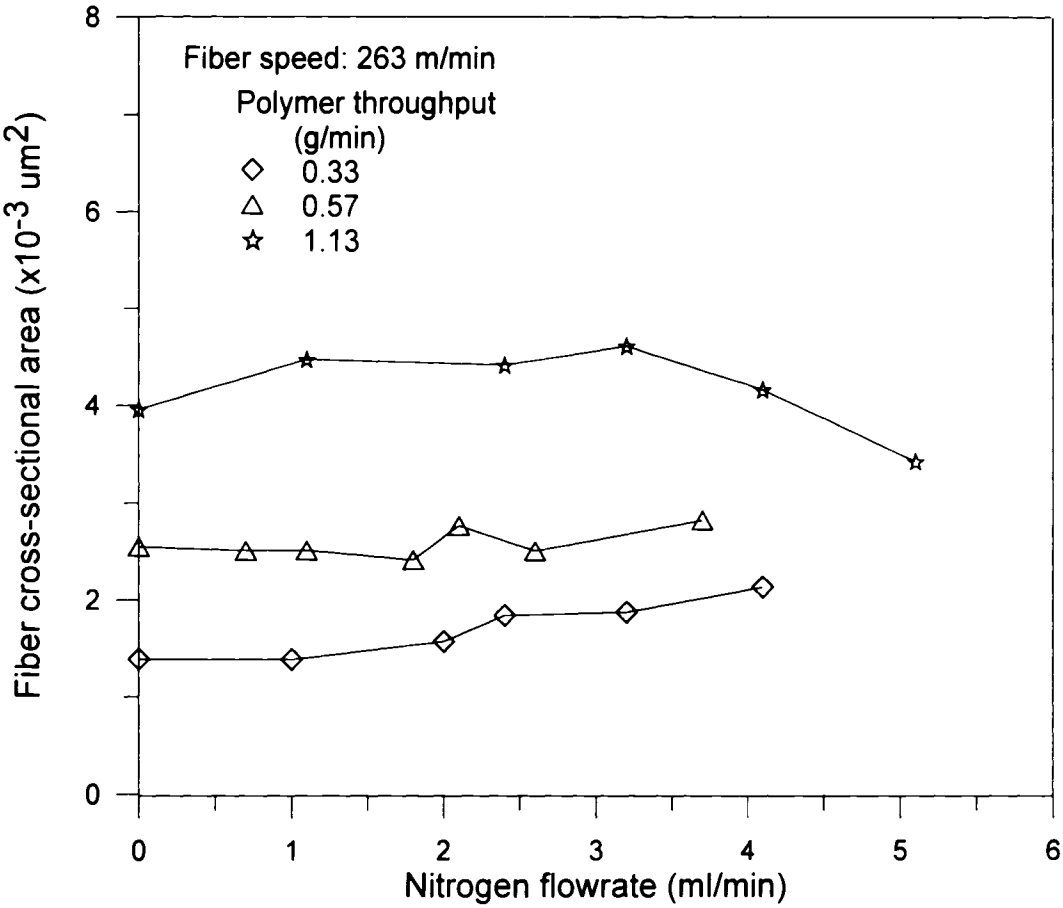

Figure 2.17: Effect of polymer flowrate on cross-sectional area.

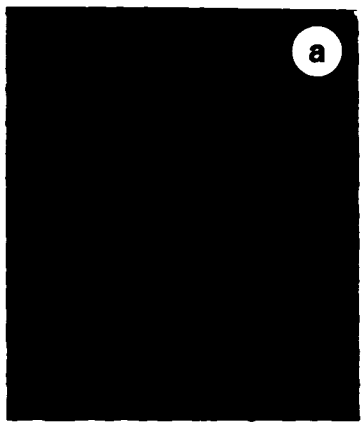

OD = 36.5 μm,
ID = 1.5 μm,
h = 0.21 %

OD = 55 μm,
ID = 33 μm,
h = 36 %

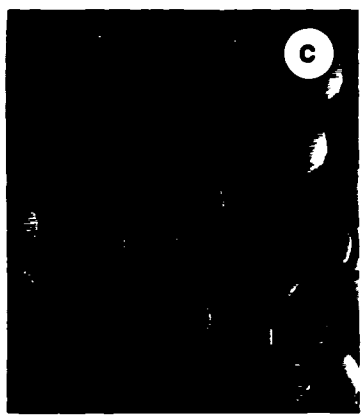

OD= 72 μm,
ID = 60 μm,
h = 69 %

Figure 2.18: Photographs of various hollow fiber cross-sections.

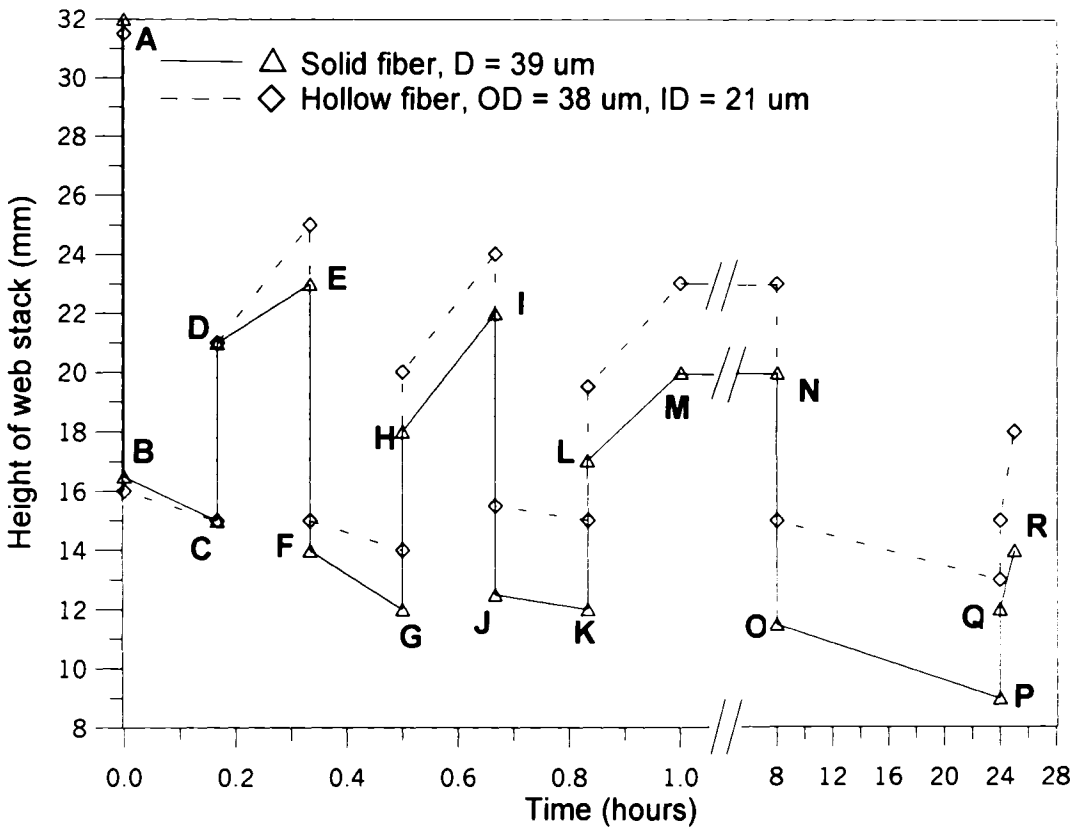

Figure 2.19: Compression-Recovery graph for solid filament D = 39 μm (sample weight = 9g) and hollow fiber OD =37.75 μm, ID = 20.75 μm (sample weight = 6.28 g). The letters from A to R correspond to the web's height as described in paragraph 2.2.2.

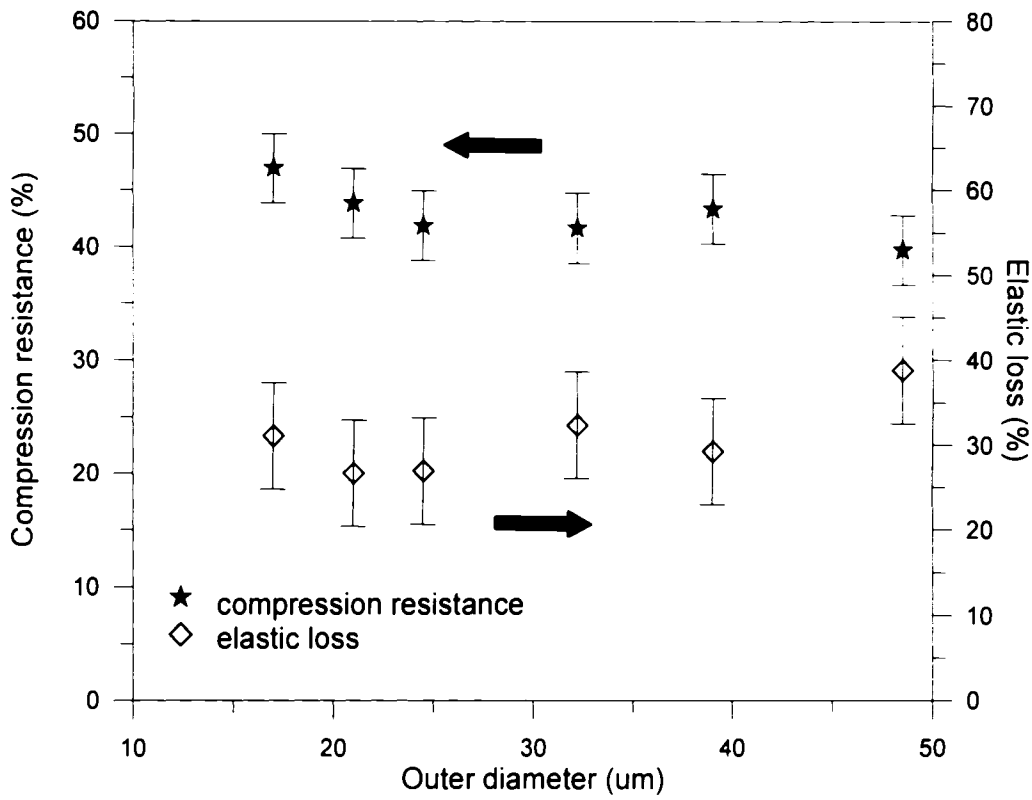

Figure 2.20: Compression resistance and elastic loss for solid fibers.

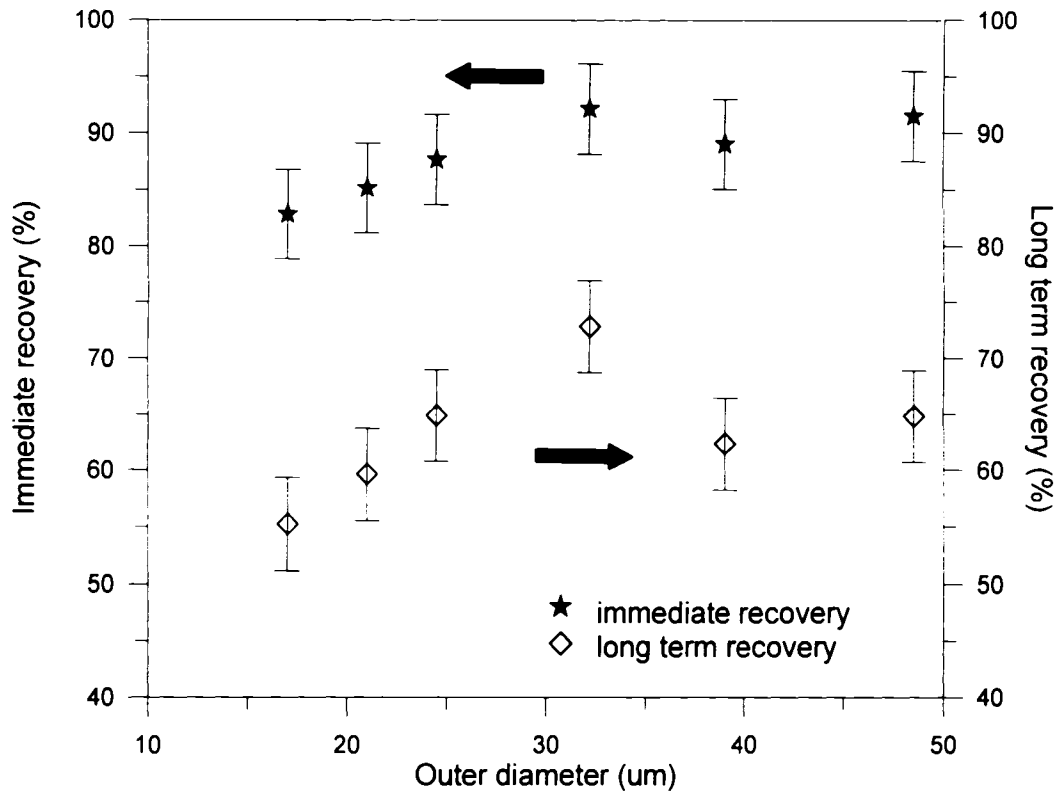

Figure 2.21: Immediate and long term recovery for solid fibers.

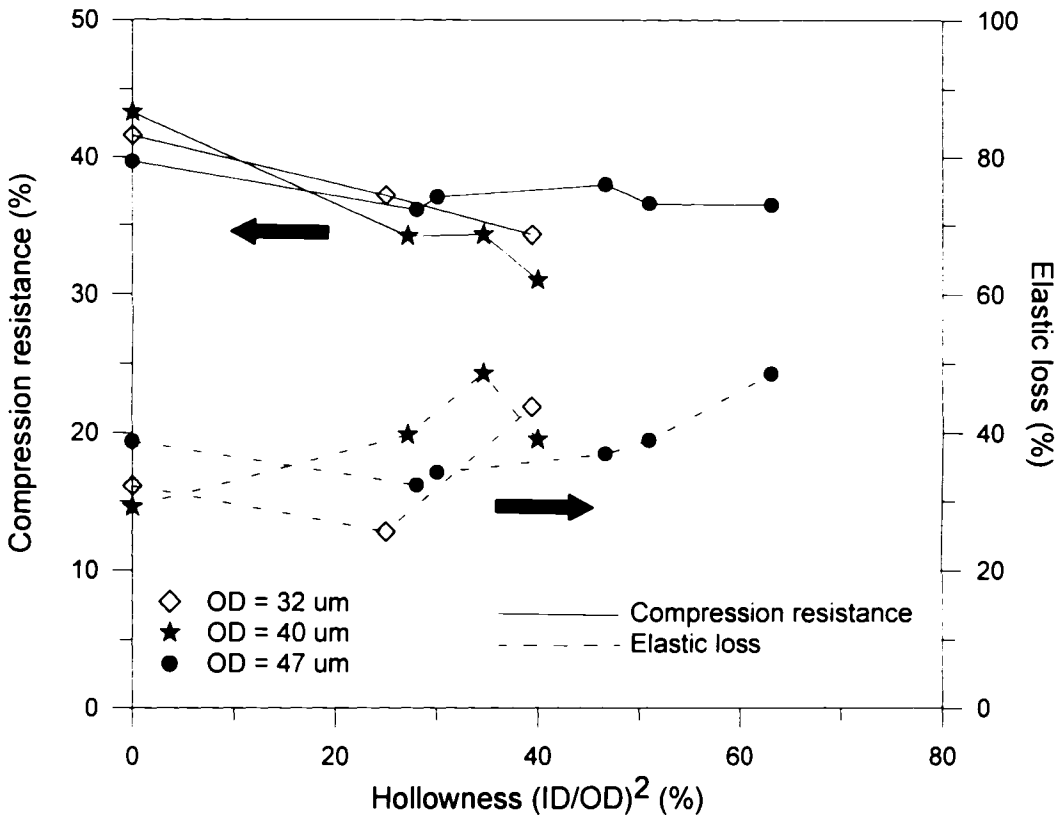

Figure 2.22: Effect of hollowness on compression resistance and elastic loss.

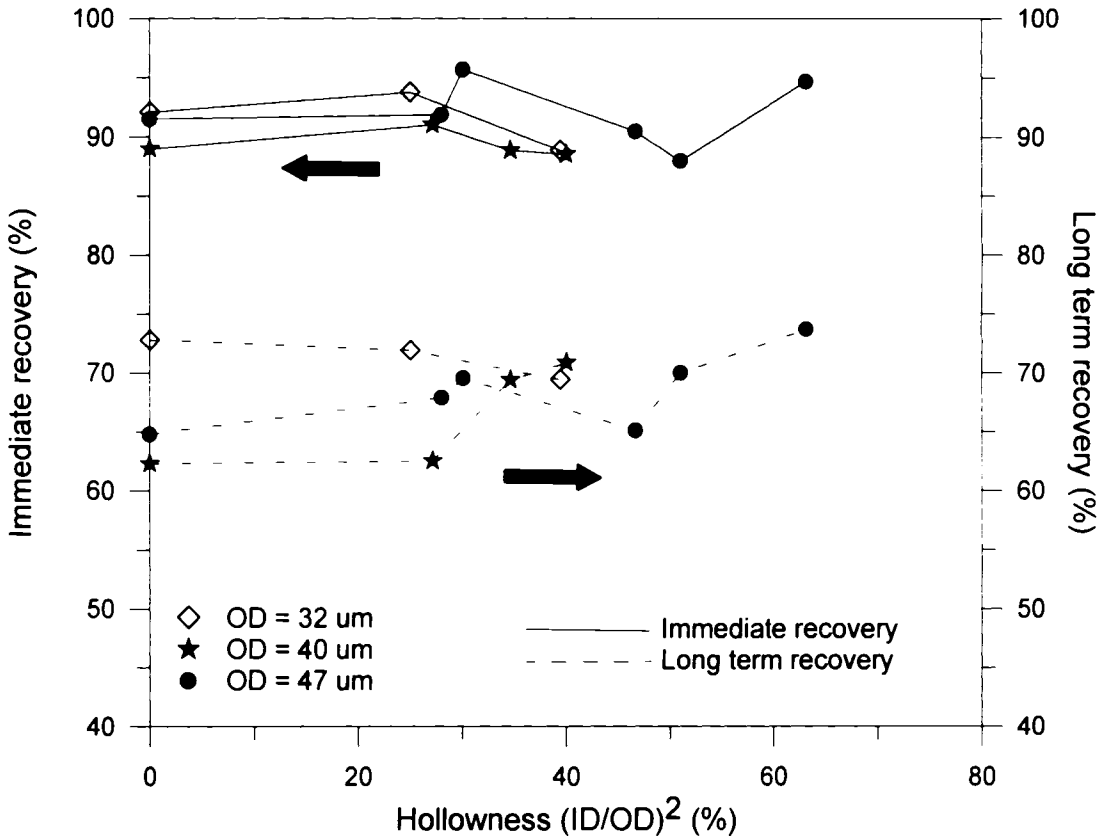

Figure 2.23: Effect of hollowness on immediate and long term recovery.

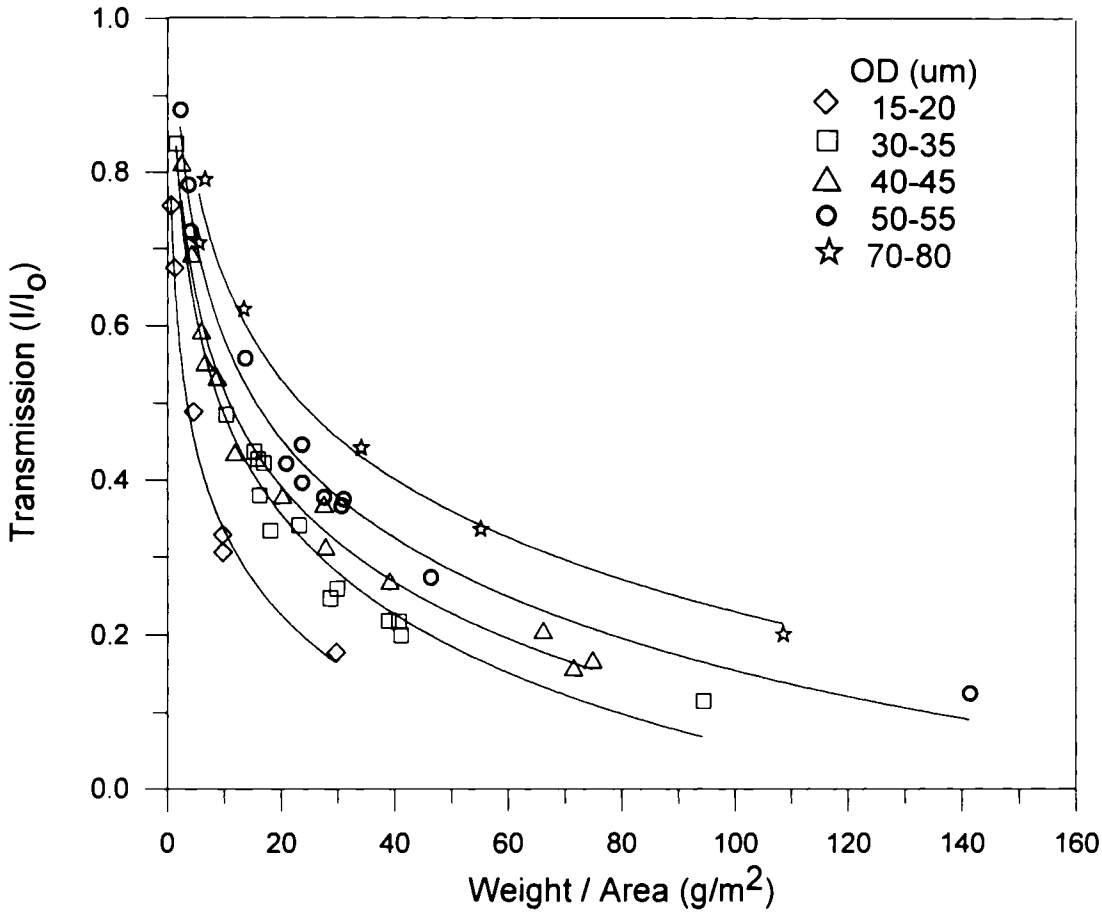

Figure 2.24: Effect of weight per area on transmission for solid fibers.

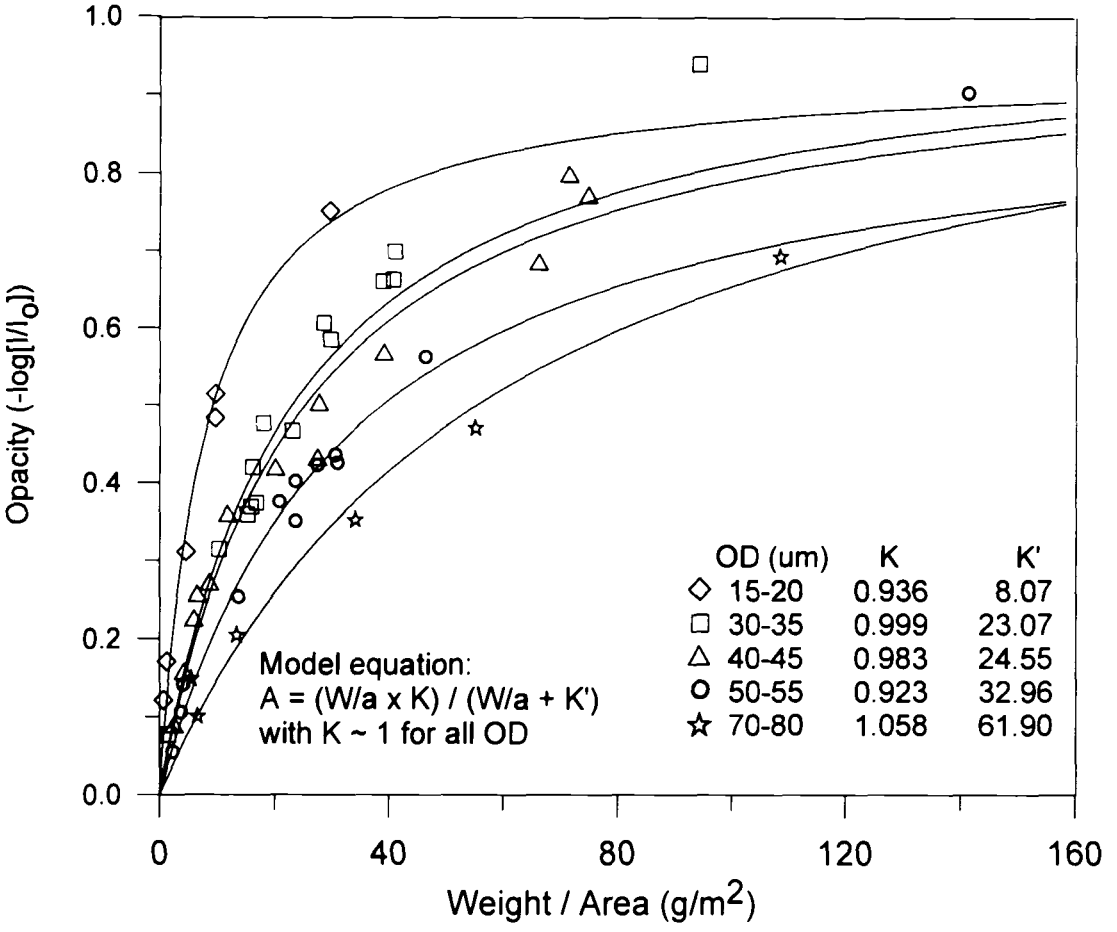

Figure 2.25: Effect of weight per area on opacity for solid fibers.

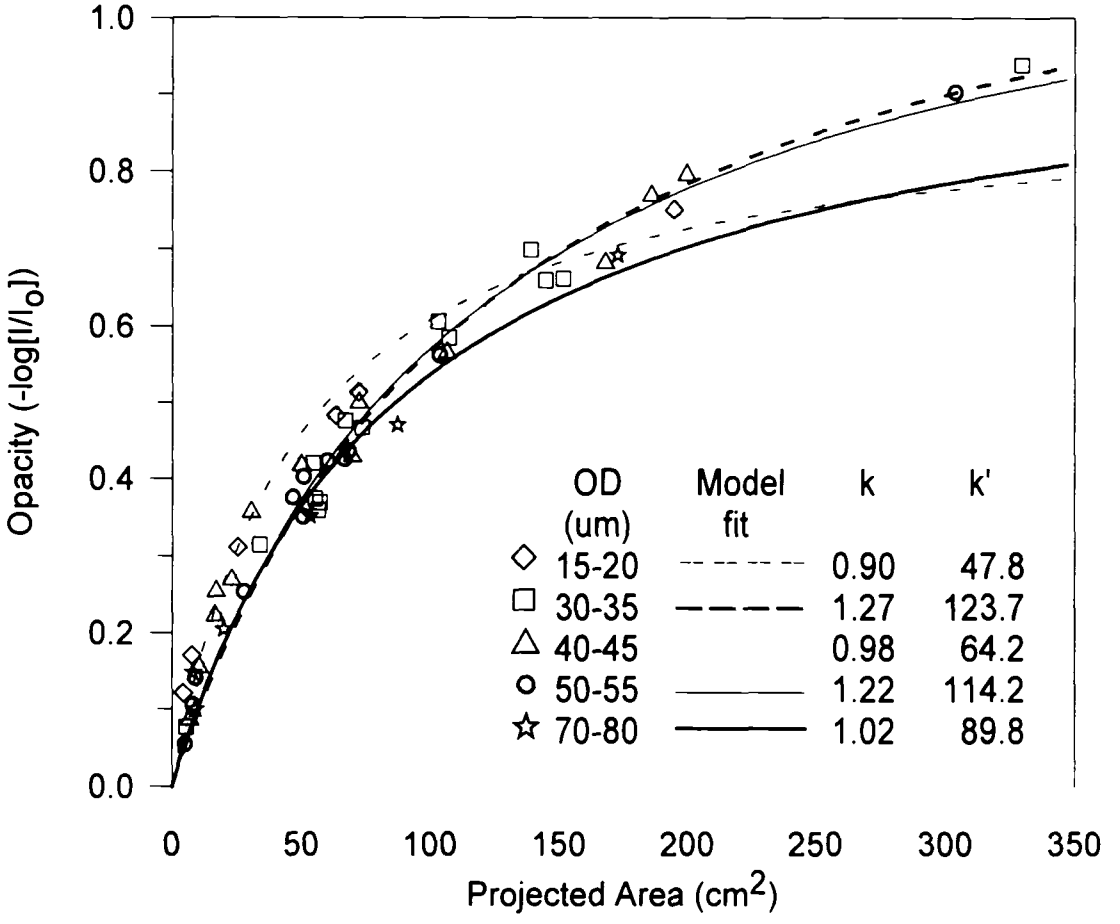

Figure 2.26: Effects of projected area on opacity for solid fibers.

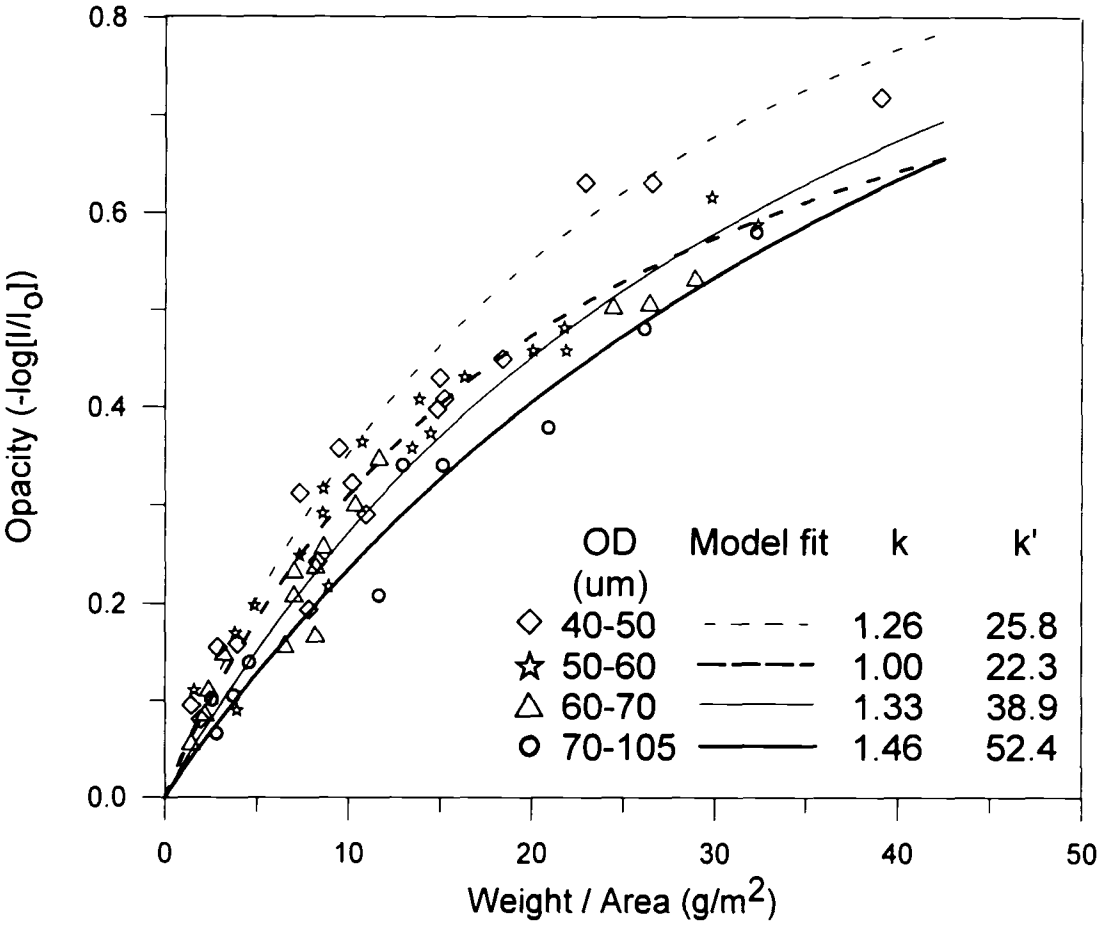

Figure 2.27: Effect of weight per area on opacity for hollow fibers (with various inner diameters).

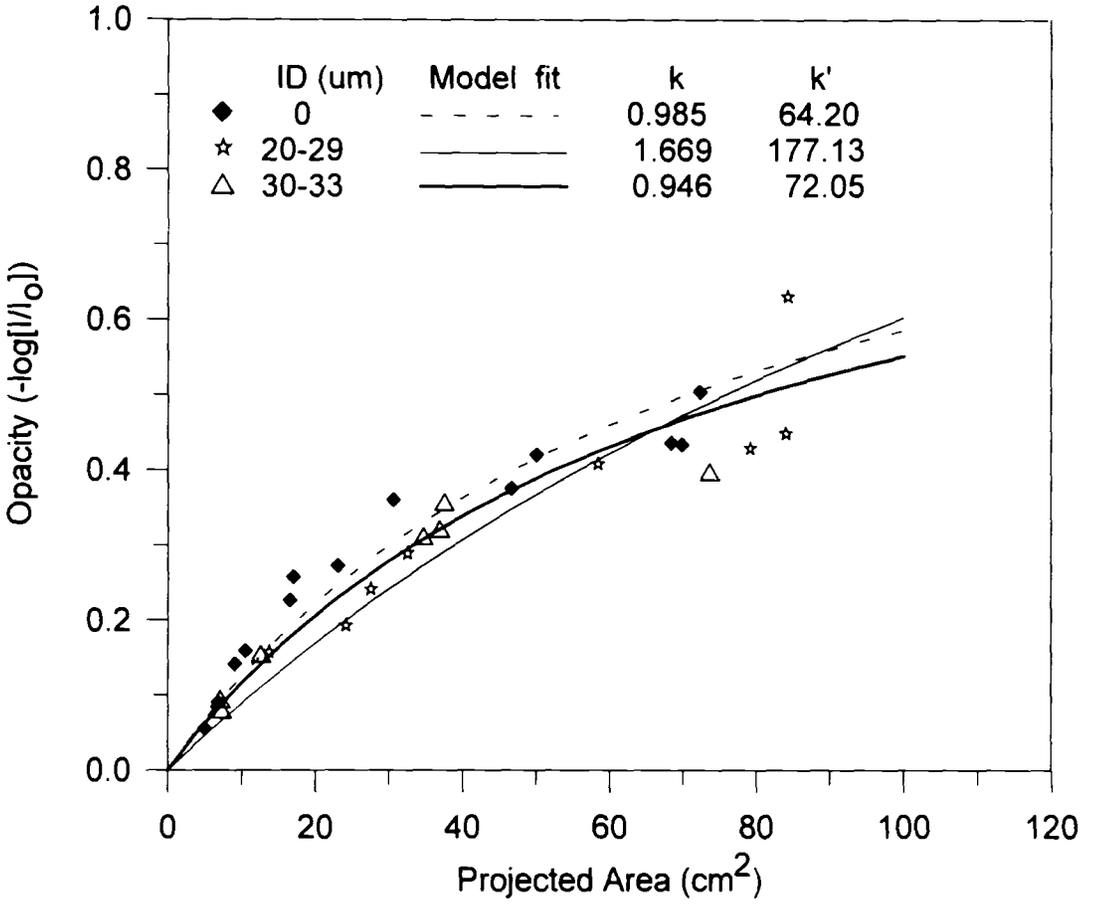

Figure 2.28: Effect of total projected area on opacity for OD = 40-50 μm.

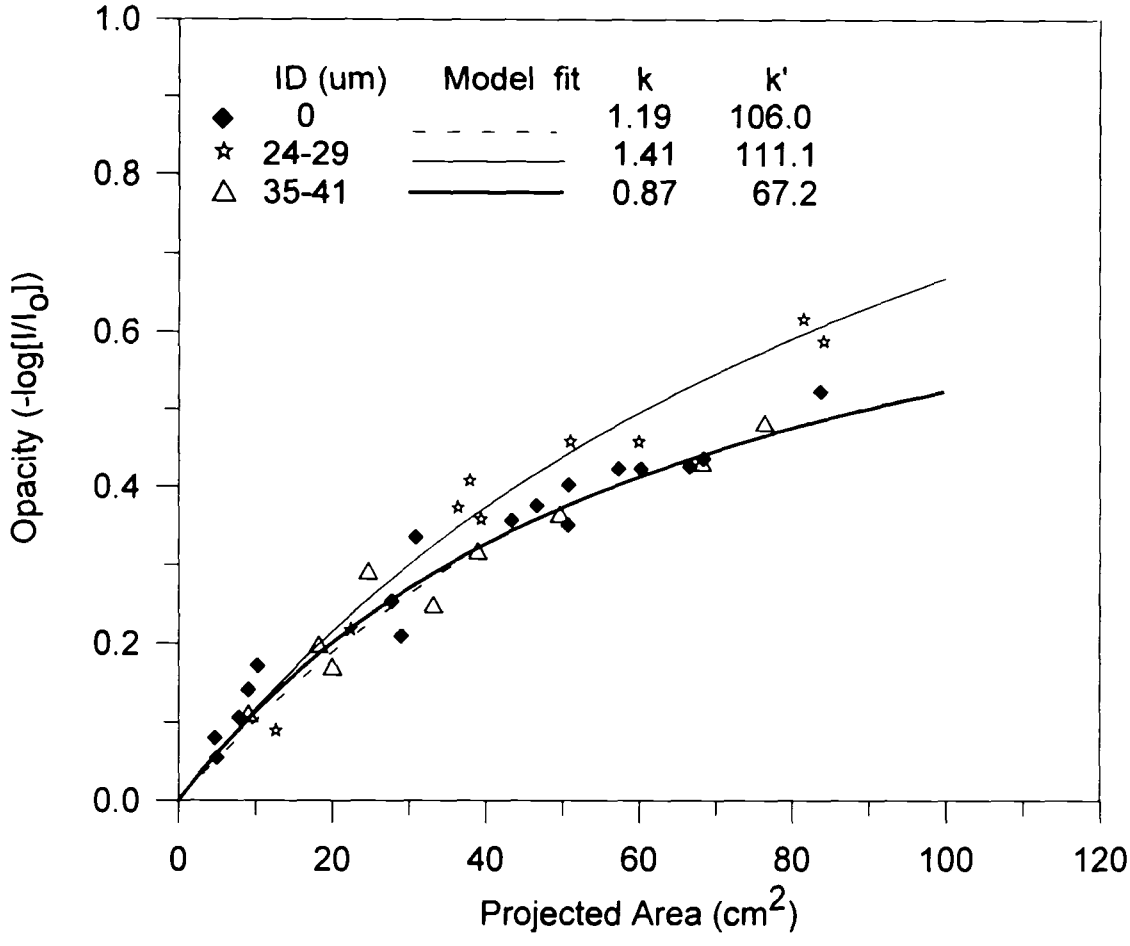

Figure 2.29: Effect of total projected area on opacity for OD = 50-60 μm.

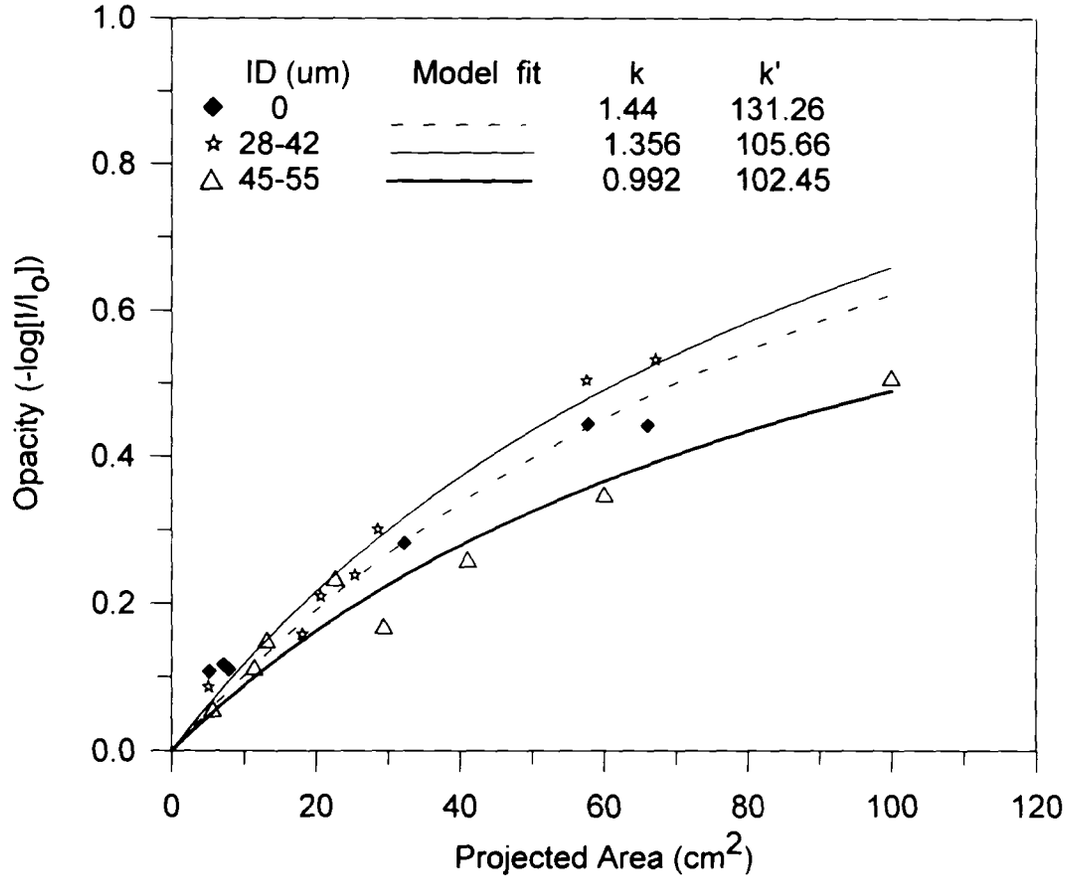

Figure 2.30: Effect of total projected area on opacity for OD = 60-70 μm.

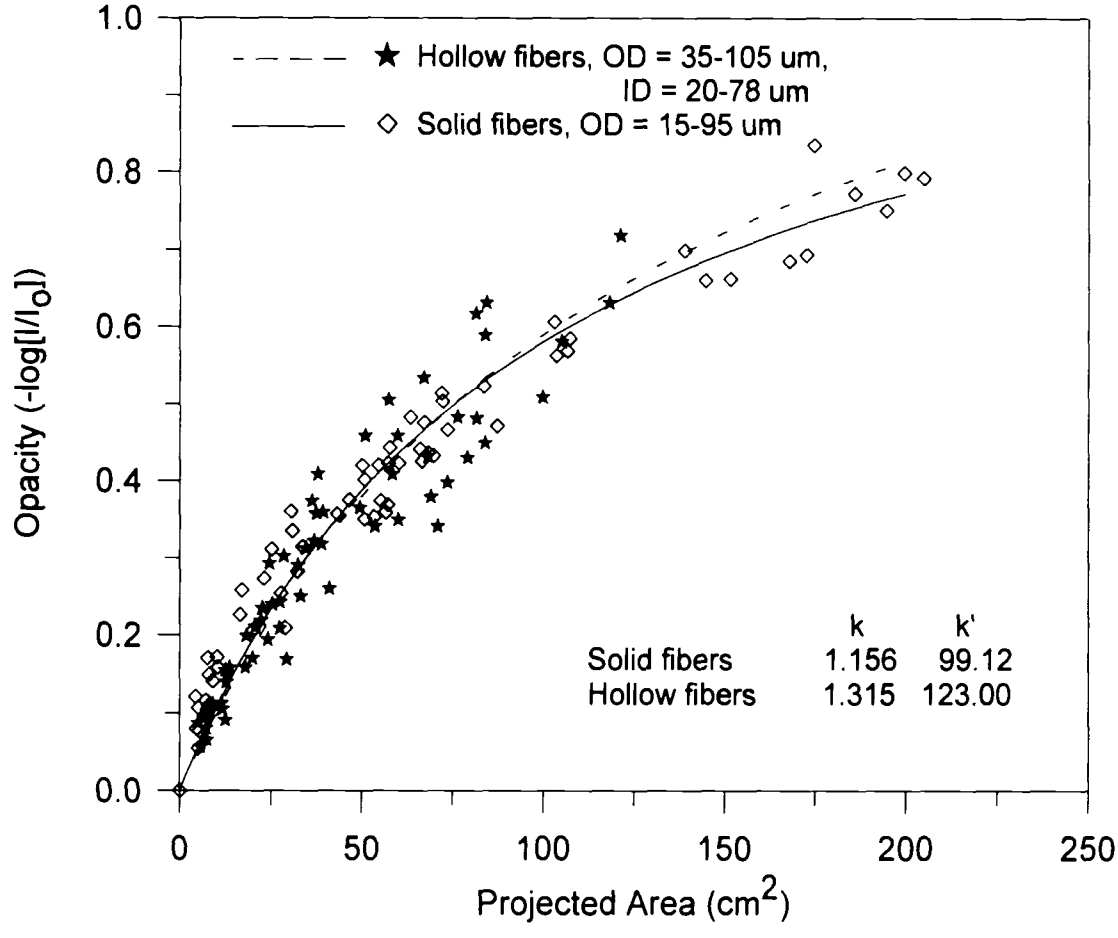

Figure 2.31: Effect of total projected area on opacity for solid and hollow fibers.

CHAPTER 3

ON-LINE BEHAVIOR OF SOLID AND HOLLOW FILAMENTS DURING MELT SPINNING

(The content of this chapter will be submitted to the journal *Polym. Eng. Sci.*)

ABSTRACT

Information about hollow fiber spinning was collected via on-line measurements along the spinline. The combination of four on-line variables (outer diameter, velocity, temperature, and birefringence) with the two continuity equations for polymer and lumen fluid provided a complete characterization of the on-line behavior of the fiber. On-line crystallization was identified under certain conditions of windup speed and nitrogen flowrate.

3.1 INTRODUCTION

The production of polyolefin fibers from both polypropylene and polyethylene is one of the fastest growing segments of the synthetic fiber industry. Melt spinning is

the most common way of converting thermoplastic polymers into fibers. Melt spinning of polypropylene has been and is still extensively studied, especially for one goal: designing the ideal process that will produce fibers with a high degree of orientation and crystallinity. High levels of orientation and crystallinity are usually achieved via high-speed spinning. Recent advances in the technology of fiber spinning lead to windup speeds as high as 6000 m/min. In the more restricted field of hollow fibers, fiber wall properties are of great importance in most of hollow membrane applications, and high-spinning speed has not been the principal issue so far. However, if no particular filtration properties are expected, hollow fibers can be produced at relatively high spinning speeds. To get a better understanding of the hollow fiber spinning process, both off-line and on-line studies are important. Off-line properties depend greatly on experimental conditions since they are closely related to the transformations happening to the fiber during the spinning process. Thus, on-line measurements can provide crucial information about the fiber final properties, and can help with the optimization of the process: obtaining strong, highly crystalline and highly oriented fibers.

Several on-line studies have been performed in the past for different types of polymer. Matsui [1985] measured temperature, crystallization, stress and orientation on a fast moving PET filament. Bansal and Shambaugh [1996, 1998] developed a technique for measuring on-line density on a moving filament. They applied that technique to melt spinning of polypropylene [Bansal and Shambaugh, 1996] and of polyethylene terephthalate [Bansal and Shambaugh, 1998]. Hollow fiber dimensions

(outside and inside diameters) were measured on-line by Oh et al. [1998]. They captured the spinning filament at various positions along the spinline, and measured the outer and inner diameters using a microscope.

This paper describes the experimental measurements of on-line outside diameter, temperature, birefringence, and velocity profiles of hollow fibers for various operating conditions. On-line techniques for diameter, temperature and velocity measurements described by Bansal and Shambaugh [1996] were applied to our hollow fiber spinning line. Since these techniques are non-destructive, measurements could be done all along the threadline, while keeping the spinning process continuously running. From these on-line measurements, additional information about the fiber behavior along the spinline was obtained: inside diameter and fiber density were calculated using polymer and nitrogen continuity equations.

3.2 MATERIAL AND EQUIPMENT

Polypropylene pellets were melted and pressurized in a Brabender screw extruder. The barrel had a 19.0 mm diameter, a 381 mm length, a 20:1 L/D ratio, and a 3:1 compression ratio. The extruder temperature was set at 225°C for all experiments. After exiting the extruder, the polymer was fed to a spin pack containing a modified Zenith pump which in turn fed the tube-in-orifice spinneret assembly [Moch, 1991]. The polymer exited from an annular ring in the spinneret, and a center hole allowed nitrogen to be injected into the core of the polymer stream. Two different spinnerets (A and B) were used; the dimensions and spinning conditions of

these spinnerets are given in Table 3.1. For both spinnerets, spinneret and spin pack temperatures were set at 200°C. For speeds up to 2000 m/min, the fibers were spun using a mechanical take-up roll placed 140 cm below the spinneret. For higher speeds (2500 m/min), the roll was replaced by an air-powered venturi, and the fibers were collected on an open screen placed underneath the venturi (see Figure 1.1).

3.2.1 Measurement of on-line diameter

Fiber diameters were measured via high-speed flash photography. The camera used was a Nikon 90S camera mounted with a 105 mm Nikon lens. The flash system used to provide the illumination was a Nikon ring flash (Macro Speedlight SB-21). Kodak Tri-X black and white film with ISO 400 was used. The camera was mounted on a tripod that permitted measurements at any position along the threadline. Figure 3.1a is a schematic of the experimental set-up for taking pictures. The diameter of the fiber along the threadline was measured by viewing the negatives under a Nikon microscope (Labphot2-pol) equipped with a micrometer eyepiece. The microscope was calibrated once a week using a calibration slide. Pictures of a nylon fiber of known diameter were taken at the beginning of each roll of film, and used as calibration reference to calculate the on-line polypropylene fiber diameters. Outer diameters were measured with a typical standard deviation that ranged from ±5% at the spinneret to ±2% at the windup.

3.2.2 Measurement of polymer flowrate

The polymer mass throughput was determined (with a standard deviation of ±3.3%) by collecting and weighing the polymer extrudate over a period of one minute.

3.2.3 Measurement of on-line temperature

On-line fiber temperature profiles were measured using an Inframetrics® model 600 infrared camera. The infrared camera measures the radiation emitted by the object and correlates this energy to the object's temperature via the Stephan-Boltzmann law. See Bansal and Shambaugh [1996] for more details. The camera was set to a working distance of 13 cm from the fiber (see Figure 3.1a). The emittance of the polypropylene fiber was found to be 0.8 in our experimental set up. Temperatures were measured with ±10% accuracy. Figure 3.1b shows a typical infrared image of a hollow fiber.

3.2.4 Measurement of on-line velocity

On-line velocity measurements were performed using a Laser Doppler Velocimeter (TSI, St.Paul, MN). The Laser Doppler method is based on the principles of light scattering interferometry. Measurements are made at a small probe volume defined by the intersection of two laser beams. The intersection of the two beams creates a fringe pattern within the probe volume. As a particle passes through the probe volume, it scatters light from the beams. The LDV measures velocity by detecting the Doppler shift of light scattered from a moving object. In our experimental set-up, the laser probe was placed at a working distance of about 6 cm

from the moving fiber. The laser source used was a 35 mW He-Ne laser (Uniphase, CA). Further details about the laser equipment and techniques are given in Wu and Shambaugh [1992]. Due to the transparency of the molten filaments, velocities could only be measured with ±20% accuracy near the spinneret.

3.2.5 Measurement of on-line orientation

The on-line orientation was estimated via birefringence. Birefringence provides a convenient measure of the extent of molecular alignment along the fiber axis. Two polarizing filters were mounted crossed-polars on each side of the spinning fiber (in the 45 position). Figure 3.2 shows the experimental set-up that was used. A source of white light was installed behind one of the filters, while the birefringence was observed through the other filter. The retardation was estimated by comparing the fiber's color to the Michel-Levy color chart (Deer et al., 1992). The birefringence was calculated according to the following formula:

$$\text{birefringence} = \text{retardation (nm)} / 1000 \times \text{sample thickness } (\mu\text{m}) \qquad (3.1)$$

For solid filaments, the sample thickness was defined as the filament diameter. For hollow fibers, the thickness was defined as the difference between the outer diameter and the inner diameter, which is twice the wall thickness (since the refracted light went through the fiber walls twice).

3.3 RESULTS AND DISCUSSION

Fiber outside diameter, temperature, velocity and birefringence were measured along the spinline of solid and hollow fibers. In conventional melt spinning, polymer throughput (m_p) and take-up speed are the most common parameters which effects are studied [Bansal and Shambaugh, 1996; Bansal and Shambaugh, 1998]. In hollow fiber spinning, the lumen gas (nitrogen) flowrate Q_n is also a very important parameter of the process since it determines the final dimensions and hollowness of the product. Hollowness is defined as the ratio of inner to outer diameter, squared. In order to study the effect of polymer mass throughput, two spinnerets were designed (Table 3.1). Spinneret A was run at high polymer throughput (m_p = 2.33 g/min) with spinning speeds up to 2500 m/min, and spinneret B was run at low polymer throughput (m_p = 0.66 g/min), with a maximum winding speed of 940 m/min (breakage in the spinline occurred for higher spinning speeds).

3.3.1 High polymer throughput

Because of its geometry, spinneret A could be used to produce fibers with a polymer throughput as high as 2.33 g/min. Fiber final dimensions (outside and inside diameters) were measured off-line and are presented in Table 3.2. Fibers were collected on the take-up roll for speeds up to 2000 m/min, or on a screen placed below the venturi for higher speeds. Then, they were sectioned and observed under an optical microscope equipped with a micrometer. Off-line outer (OD) and inner (ID) diameters were determined from the sample cross-sections. The theoretical dimensions shown in Table 3.2 were calculated using both polymer and nitrogen

continuity equations. The polymer mass throughput stays constant all along the spinline, so:

$$m_p = \rho_p v\left(\frac{\pi}{4}\right)\left(d_2^{\,2} - d_1^{\,2}\right) \tag{3.2}$$

where

m_p = polymer mass throughput

ρ_p = polymer density

v = fiber velocity

d_2 = outside diameter

d_1 = inside diameter

Nitrogen gas was used as lumen fluid, and also keeps a constant mass rate along the spinline:

$$m_n = \rho_n v\left(\frac{\pi}{4}\right)d_1^{\,2} \tag{3.3}$$

where

m_n = nitrogen mass throughput

ρ_n = nitrogen density

Assuming a polymer density of 0.895 g/cm^3 and a nitrogen density of 0.00113 g/cm^3 for the final products, equations 3.2 and 3.3 were combined to predict the final outside and inside diameters. In Table 3.2, experimental dimensions compare well with the calculated OD and ID (final product dimensions).

Figure 3.3a shows the effect of nitrogen flowrate on the outside diameter, for a final take-up speed of 1000 m/min. The initial data point at the beginning of the

threadline (z = 0) corresponds to the spinneret annulus outside diameter. The next data point down the spinline corresponds to the maximum die swell, that occurred at about z = 0.38 mm for all windup speeds and nitrogen flowrates used. The die swell ratio (ratio of maximum die swell diameter to initial diameter) was estimated at about 1.25 for all runs. In Figure 3.3a, solid fibers exhibit a lower diameter profile than hollow fibers all along the spinline. The difference is less significant between the two hollow fiber profiles. Figures 3.3b and 3.3c represent the effect of nitrogen on outer diameter for windup speeds of 2000 and 2500 m/min, respectively. At these speeds, increasing nitrogen flowrate also increases the outer diameter. This effect is particularly distinct between solid and hollow fibers. Same observations can be made on the final experimental and theoretical dimensions reported in Table 3.2. Solid and hollow fibers spun at 1000 m/min (Figure 3.3a) have not yet reached a constant diameter for the lowest position analyzed down the spinline, whereas fibers spun at 2500 m/min do not show much variation after z = 90 cm. In the rest of this discussion, we will only show the graphs for the lowest (1000 m/min) and the highest (2500 m/min) windup speed studied, since the behavior at 2000 m/min is intermediate between the behaviors observed at 1000 and 2500 m/min.

Figures 3.4a and 3.4b show the temperature profiles for solid and hollow fibers spun at 1000 and 2500 m/min. In Figure 3.4a, hollow fibers present a lower temperature profile than solid fibers: fibers cool down faster as nitrogen flowrate increases. Large nitrogen rates produce larger external filament areas, that in turn

result in increased heat loss. Since hollow fibers are quenched faster at high nitrogen flowrates, these fibers should have higher degree of orientation than solid fibers.

Figures 3.5a and 3.5b show the change in birefringence with nitrogen flowrate at different take-up speeds. As expected, birefringence increases as nitrogen flow increases. At 1000 m/min, the birefringence of solid and hollow fibers varies almost linearly with z. At 2500 m/min, solid fiber birefringence still varies linearly as z increases, while hollow fiber birefringence increases sharply at about 90 cm below the spinneret. This dramatic increase of birefringence reflects a sudden increase in fiber molecular orientation, which is most certainly due to the fast quenching that characterizes hollow fiber spinning. Comparison of Figures 3.5a and 3.5b shows that birefringence increases with increasing spinning speed. But even at the highest speed (2500 m/min), the birefringence of solid fibers never rises above 0.0045, while hollow fiber birefringence reaches 0.012, with Q_n = 1.7 ml/min. Ziabicki and Jarecki (1985) described how rapid deformation and quenching are closely related to the high tensile stress acting on the polymer melt during the spinning process. They were referring to speeds as high as 4000 m/min. In our work, the maximum speed used was 2500 m/min, but the fast quenching observed for hollow fibers most certainly contributes to increase the stress on-line, inducing high orientation.

The quenching of hollow fibers may also be observed on velocity profiles. Figures 3.6a and 3.6b represent the effect of nitrogen flowrate on velocity profiles at 1000 and 2500 m/min. Hollow fibers present higher velocity profiles as the nitrogen rate increases. Because hollow fibers cool down faster, they reach their final velocity

sooner (at smaller z). At 1000 m/min (Figure 3.6a), none of the profiles seem to have reached their final velocity. Even for the lowest position analyzed below the spinneret, velocities still present a fast increasing profile. But at the highest spinning speed tested (Figure 3.6b), the increase of velocity starts to attenuate around z = 90 cm below the spinneret. These results corroborate what was found for the outer diameter and birefringence profiles: their rate of change starts to slow down around 90 cm below the spinneret.

Further information can be obtained from on-line measurements. Inside diameter cannot be measured directly without disrupting the stability of the threadline [Oh et al., 1998]. However, inner diameter profiles can be calculated based on the nitrogen continuity equation (Eq. 3.3) as follows:

$$d_1 = \sqrt{\frac{m_n}{\rho_n v\left(\frac{\pi}{4}\right)}} \tag{3.4}$$

The ratio of inner to outer diameter is actually a more convenient way to characterize the hollow structure of these fibers. After combining polymer and nitrogen continuity equations, the ratio of inner to outer diameter was found to be independent of fiber velocity:

$$\frac{d_1}{d_2} = \sqrt{\frac{m_n}{\rho_n}\Big/\left(\frac{m_n}{\rho_n} + \frac{m_p}{\rho_p}\right)} \tag{3.5}$$

Nitrogen density along the spinline was calculated using the following correlation between nitrogen density and temperature (K):

$$\rho_n = \frac{0.3389}{T^{1.001}} \tag{3.6}$$

This expression fits Vargaftik data [1975] for nitrogen density within 0.03% for the temperature range of our experiments.

Polymer density could be calculated using the polymer continuity equation (Eq. 3.2). Then, three on-line measurements would be needed: outer diameter, velocity, and temperature (needed to obtain the inside diameter). It was found that, due to the propagation of errors, the combination of the three on-line measurements could not give accurate results for polymer density. The uncertainty in the velocity measurements was the factor that contributed the most to increase the standard deviation of polymer density (up to 50% error).

Instead, polymer densities were estimated via temperature measurements alone. Bansal and Shambaugh [1996] found polypropylene fiber density to be independent of polymer throughput and windup speed, for non-crystalline material. When crystallization occurred on-line, fiber density jumped to higher levels and followed the crystalline behavior described by Newman [1960]. Newman used dilatometers to evaluate changes in polypropylene specific volume with temperature (in the range 20-200°C). His experiments took several days, since a very slow heating rate was used, so the densities he found applied to crystallized material. We developed two correlations to characterize fiber density versus temperature for crystallized and non-crystallized fibers. We used Newman data [1960] for the former and Bansal data [1996] for the later. Figure 3.7 shows both correlations (polypropylene density versus temperature). Newman densities reach higher levels

than Bansal densities, since they describe crystallized material. For temperatures higher than 170°C, crystalline and non-crystalline material correlations become almost identical, since they have reached the melting temperature of polypropylene (165°C), where no crystallized material can exist. On-line crystallization was estimated through birefringence measurements, using Bansal and Shambaugh results [1996]: a crystallization point was assumed when birefringence reached 0.03 (maximum birefringence that can be obtained with polypropylene fibers).

Figures 3.8a and 3.8b show the effect of nitrogen flowrate on polymer density. From Figures 3.5a and 3.5b, since the highest birefringence reached was 0.012, the fibers were assumed to be non-crystalline all along the threadline, and Bansal correlation was applied to all runs. For a take-up speed of 1000 m/min, hollow fibers show higher polymer density than solid fibers. The difference is even more striking at 2500 m/min: hollow fiber density profiles are distinctly higher than solid fibers most of the time. These results agree well with the increase of orientation observed at high nitrogen flowrates.

Based on the polymer densities shown in Figures 3.8, the ratio of inside to outside diameter (Eq. 3.5) was calculated and is given in Figure 3.9 for a final speed of 2500 m/min. Identical graphs were obtained at 1000 and 2000 m/min since the ratio d_1/d_2 was found independent of take-up speed. The ratio shows a decreasing profile for both nitrogen flowrates, even though the difference between initial (top of spinline) and final (end of spinline) ratios is very small (9% for 1.0 ml/min and 7% for 1.7 ml/min). Oh et al. [1998] also found a decreasing profile for the ratio d_1/d_2.

The slope of the profile is mostly due to the large change of nitrogen density occurring along the spinline as the temperature drops down.

3.3.2 Low polymer throughput

Experiments were run for a low polymer throughput m_p = 0.66 g/min using spinneret B. Due to the unusual large size of the polymer annulus, no significant die swell was observed. Table 3.3 summarizes experimental and theoretical dimensions of solid and hollow fibers produced using this spinneret. Figures 3.10a to 3.10c show the effect of nitrogen flowrate on fiber outer diameter. For slow spinning speed (330 m/min), fibers spun with high rates of nitrogen flow present larger diameters all along the threadline, while hollow fibers attenuate much faster than solid fibers at high speeds. At high spinning speed and high nitrogen rate, fiber diameters appear to plateau: not much change appears at 940 m/min after z = 65 cm for fibers spun with Q_n =1.7 ml/min, and z = 50 cm for fibers spun with Q_n = 3.2 ml/min.

At m_p = 0.66 g/min, solid and hollow fibers cool down the same way as was previously discussed for large polymer throughput: in Figures 3.11a to 3.11c, hollow fibers are quenched faster for large nitrogen flowrates. This observation is particularly obvious at 940 m/min. The fast quenching at large nitrogen rate and relatively high speed agrees well with the rapid attenuation of hollow fibers diameters revealed in Figures 3.10.

Fibers spun at low polymer throughput exhibit a much larger degree of orientation than ones produced with large polymer throughput. Figure 3.12a shows the effect of nitrogen flow rate on birefringence, for a windup speed of 330 m/min. At

that speed, birefringence reaches 0.015 for the largest gas rate used. At larger windup speeds (Figures 3.12b and 3.12 c), birefringence of fibers spun with 3.2 ml/min nitrogen present a sharp increase at the beginning of the threadline (z ~20 cm), followed by a slowly increasing plateau that finally reaches a birefringence of 0.03, indicative of on-line crystallization. Crystallization is observed from z = 65 cm for a windup speed of 690 m/min, and from z = 50 cm for 940 m/min, which agrees with diameter plateaus observed in Figure 3.10c.

The largest windup speed used was 940 m/min. That speed is comparable to the lowest speed (1000 m/min) used with spinneret A (m_p = 2.33 g/min). Figure 3.13 compares the birefringence of solid fibers and hollow fibers (Q_n = 1.7 ml/min) spun at 940 and 1000 m/min using two different polymer throughput (m_p). With 1.7 ml/min nitrogen, fibers spun with the low polymer throughput show a maximum birefringence of 0.022, while birefringence of fibers spun at high m_p reaches 0.0065 only. In fact, the ratio of polymer throughput (3.53) is almost identical to the ratio of birefringence (3.38). The increase in birefringence might be directly proportional to the decreases of polymer throughput.

Velocity profiles are shown in Figures 3.14a to 3.14c. Previously, for m_p = 2.33 g/min, we observed that hollow fibers reached the windup velocity sooner with large nitrogen rates. The same is observed at low m_p for speeds of 690 and 940 m/min (Figure 3.14b and 3.14c). Surprisingly, the largest hollow fibers spun at 330 m/min exhibit lower velocities during the first 80 cm below the spinneret. Due to the large

diameter of the fiber and the low windup speed, the fiber might be slowed down by air drag effects.

Figures 3.15a to 3.15c show the effect of nitrogen flowrate on polymer density. Based on the birefringence results shown in Figures 3.12a to 3.12c, fibers spun at Q_n = 0 and 1.7 ml/min were assumed non-crystalline all along the spinline and for all windup speeds. Their densities were determined using Bansal [1996] correlation. Fibers spun with Q_n = 3.2 ml/min were assumed to have reached on–line crystallinity at z = 65 cm for a windup speed of 690 m/min, and z = 50 cm for 940m/min. Bansal correlation was used to determine the densities below the crystallization point, while Newman correlation was used to determine the densities of the crystallized material. As was observed at large m_p, increase of nitrogen increases the on-line density. The difference between solid and hollow fibers increases for larger windup speeds. As expected, the hollow fibers that we assumed to be crystalline exhibit a sharp rise in density at the supposed position of crystallization. Figure 3.16 shows the profile of d_1/d_2 as a function of nitrogen rate for a windup speed of 330 m/min. The ratio decreases of about 3.1% and 2.1% respectively for 1.7 and 3.2 ml/min nitrogen. Windup speed was found to have very little effect on the ratio of inner to outer diameter.

3.4 CONCLUSION

Combination of on-line measurement techniques with polymer and nitrogen continuity equations allowed us to follow the on-line density of hollow fibers. High degrees of orientation were obtained for large windup speeds, large nitrogen flow rates (large inner diameters), and low polymer throughput. In conventional melt spinning (solid filaments), windup speed is known as an important factor influencing stress-induced crystallization. In hollow fiber spinning, we showed that nitrogen flowrate (inner diameter size) also plays an important role in on-line stress. At low polymer throughput, where spinning speeds higher than 940 m/min could not be obtained to get to high orientation levels, birefringence was increased by using larger rates of lumen gas flow.

3.5 NOMENCLATURE

D = diameter, μm
d_1 = inside diameter of fiber, μm
d_2 = outside diameter of fiber, μm
ID = final product inside diameter, μm
m_n = nitrogen mass rate, g/min
m_p= polymer mass rate, g/min
OD = final product outer diameter, μm
Q_p = volumetric polymer flow rate, cm^3/min
v = fiber velocity, m/min
z = axial position in model, cm
ρ_n = nitrogen density, g/cm^3
ρ_p = polymer density, g/cm^3

3.6 REFERENCES

V. Bansal and R. L. Shambaugh, "On-line determination of density and crystallinity during melt spinning", *Polymer Engineering and Science*, **36** (22), 2786-2798 (1996).

V. Bansal and R. L. Shambaugh, "On-line density and crystallinity of polyethylene terephthalate during melt spinning", *Polymer Engineering and Science*, **38** (12), 1960-1968 (1998).

W.A. Deer, R.A., Howie, and J. Zussman, *An introduction to the rock-forming minerals*, Longman Scientific & Technical, 2nd Ed. (1992).

M. Matsui, "Fiber formation process in high-speed spinning of polyethylene terephthalate", in *High-speed fiber spinning*, pp. 137-150, A. Ziabicki and H. Kawai, John Wiley & Sons, NewYork (1985).

I. Moch, "Hollow Fiber Membranes", *Encyclopedia of Chemical Technology*, **13**, 4th edition, Wiley, NewYork, p. 334 (1991).

S. Newman, "On the characterization of stereoregular polymers. II. Polypropylene", *Journal of Polymer Science*, **47**, 111-137 (1960).

T. H. Oh; M. S. Lee; S. Y. Kim; and H. J. Shim, "Studies on Melt-Spinning Process of Hollow Fibers", *J. Appl. Polym. Sci*, **68**, 1209-1217 (1998).

N. B. Vargaftik, *Handbook of Physical Properties of Liquids and Gases – Pure Substances and Mixtures*, 2nd edition, Hemisphere Publishing, New York, (1975).

T. T. Wu and R. L. Shambaugh, "Characterization of the melt blowing process with laser Doppler velocimetry", *Ind. Eng. Chem. Res.*, **31** (1), 379-89 (1992).

A. Ziabicki and L. Jarecki, "The Theory of Molecular Orientation and Oriented Crystallization in High-Speed Spinning", in *High Speed Fiber Spinning*, Ziabicki and Kawai, John Wiley and Sons, New York (1985).

	SPINNERET A	SPINNERET B
OD of polymer annulus (mm)	1.98	7.01
ID of polymer annulus (mm)	1.22	3.78
D of nitrogen capillary (mm)	0.76	1.00
Polymer flowrate (g/min)	2.33	0.66
Fiber speed (m/min)	1000, 2000, and 2500	330, 690, and 940
Nitrogen flowrate (ml/min)	0, 1, and 1.7	0, 1.7, and 3.2

Table 3.1: Spinneret dimensions and experimental conditions used to produce fibers.

		Final Experimental Dimensions*		Final Theoretical Dimensions**	
Take-up Speed (m/min)	**Nitrogen Flowrate (ml/min)**	**OD** (μm)	**ID** (μm)	**OD** (μm)	**ID** (μm)
	0	55	0.0	57.5	0
1000	**1**	68.0	35.0	67.7	35.6
	1.7	75.0	46.0	74.0	46.5
	0	40.0	0.0	40.7	0.0
2000	**1**	48.0	25.0	47.9	25.2
	1.7	52.0	33.0	52.3	32.8
	0	35.0	0.0	36.4	0.0
2500	**1**	42.0	23.0	42.8	22.5
	1.7	47.0	30.0	46.8	30.0

Table 3.2: Final experimental and theoretical fiber dimensions for fibers produced at a polymer throughput of 2.33 g/min with spinneret A.
* Measured at room temperature (25°C);
** Calculated using continuity equations assuming room temperature at the end the spinline.

		Final Experimental Dimensions*		Final Theoretical Dimensions**	
Take-up Speed (m/min)	**Nitrogen Flowrate (ml/min)**	**OD** (μm)	**ID** (μm)	**OD** (μm)	**ID** (μm)
	0	50.0	0.0	53.3	0.0
330	**1.7**	96.0	80.0	96.6	80.9
	3.2	120.0	110.0	123.2	111.1
	0	35.0	0.0	36.8	0.0
690	**1.7**	64.0	54.0	67.0	56.0
	3.2	84.0	77.0	85.2	76.8
	0	33.5	0.0	31.6	0.0
940	**1.7**	58.0	48.0	57.4	47.9
	3.2	72.0	66.0	73.0	65.8

Table 3.3: Final experimental and theoretical fiber dimensions for fibers produced at a polymer throughput of 0.66 g/min with spinneret B.
* Measured at room temperature (25°C);
** Calculated using continuity equations assuming room temperature at the end the spinline.

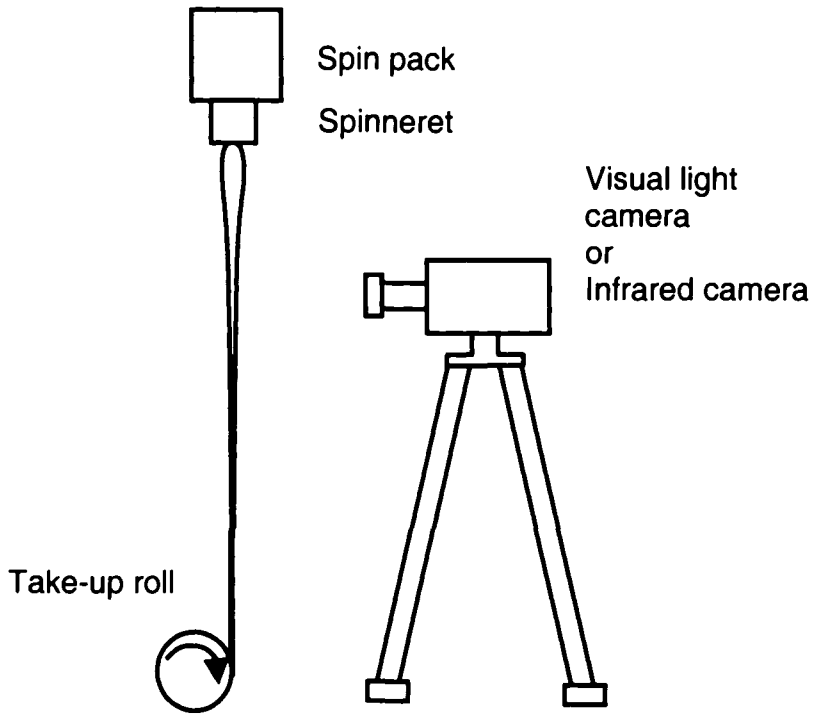

Figure 3.1a: On-line diameter and temperature experimental equipment.

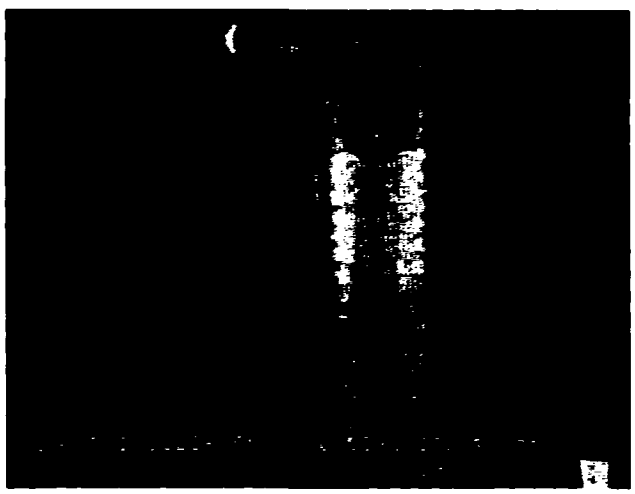

Figure 3.1b: Infrared image of hollow fiber.

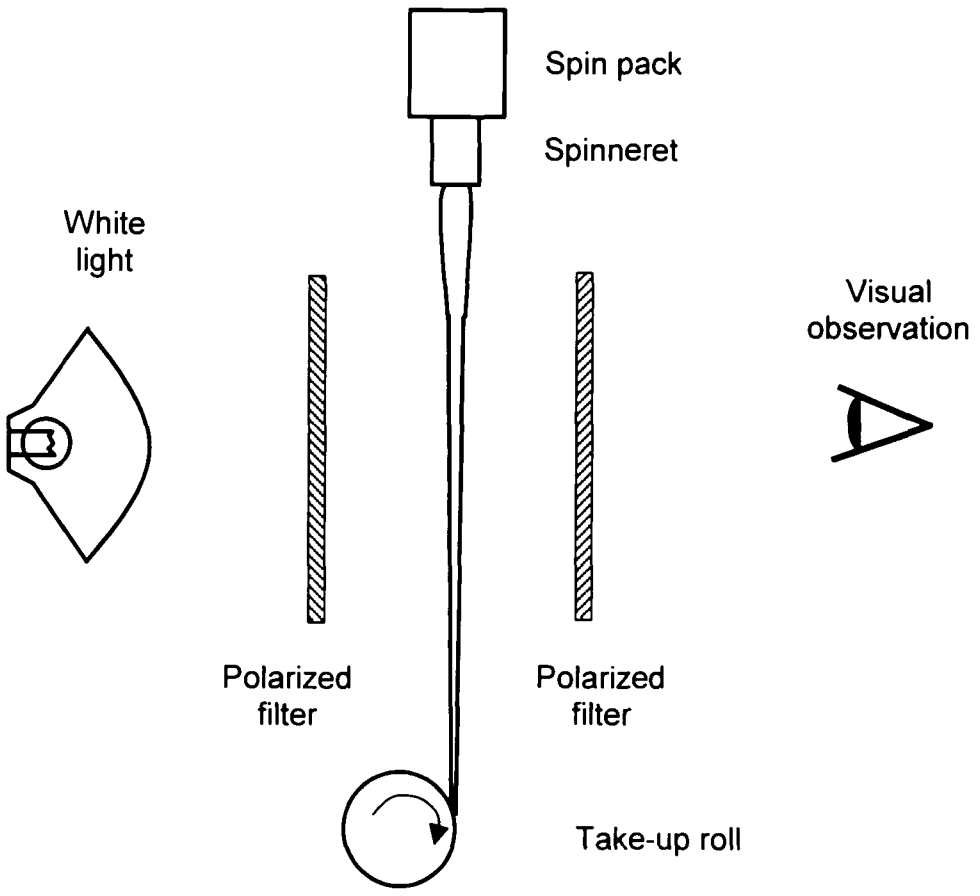

Figure 3.2: Birefringence Experimental Set-up.

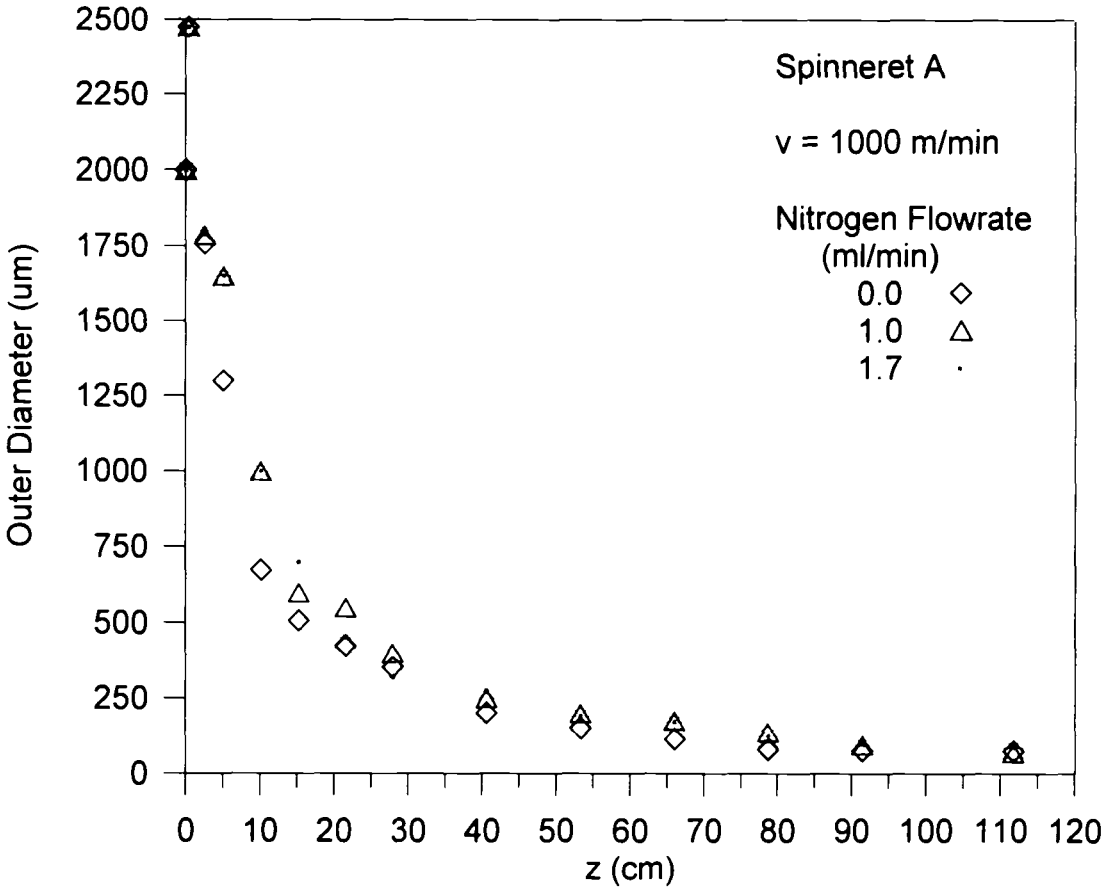

Figure 3.3a: Effect of nitrogen flowrate on outer diameter for a windup speed of 1000 m/min.

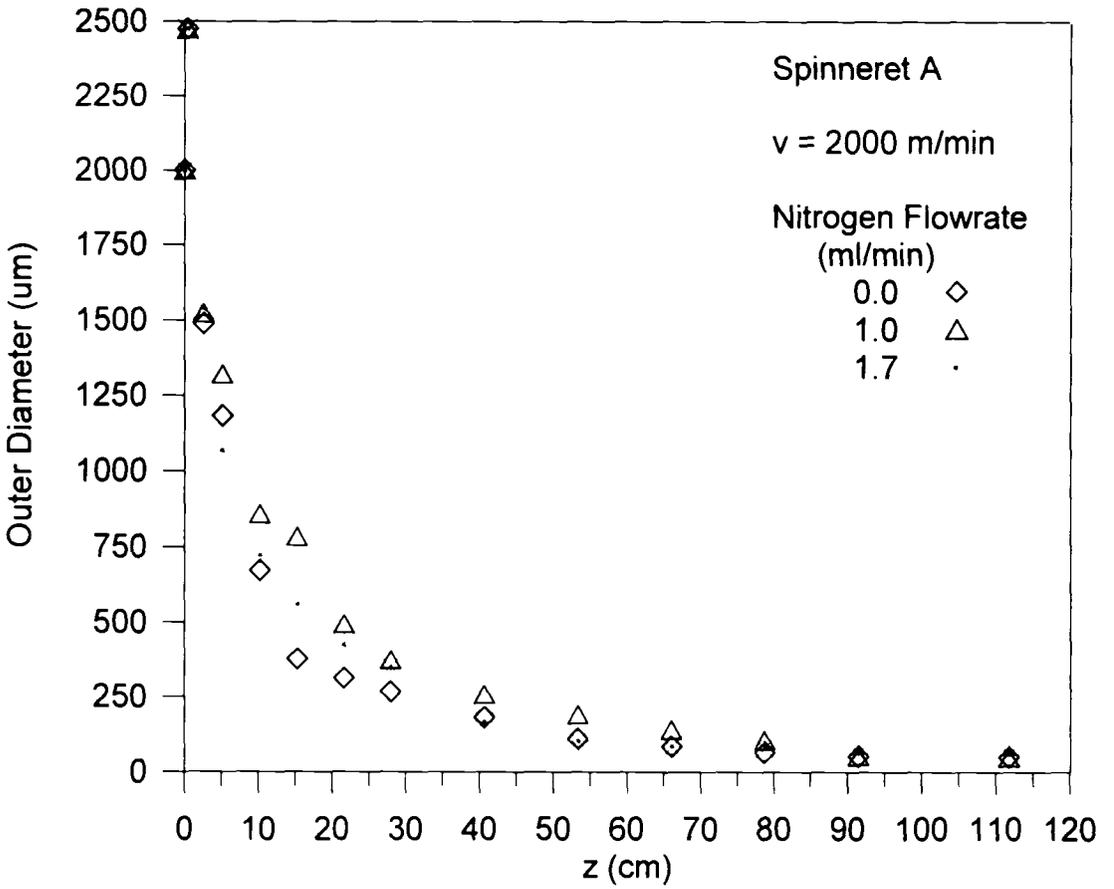

Figure 3.3b: Effect of nitrogen flowrate on outer diameter for a windup speed of 2000 m/min.

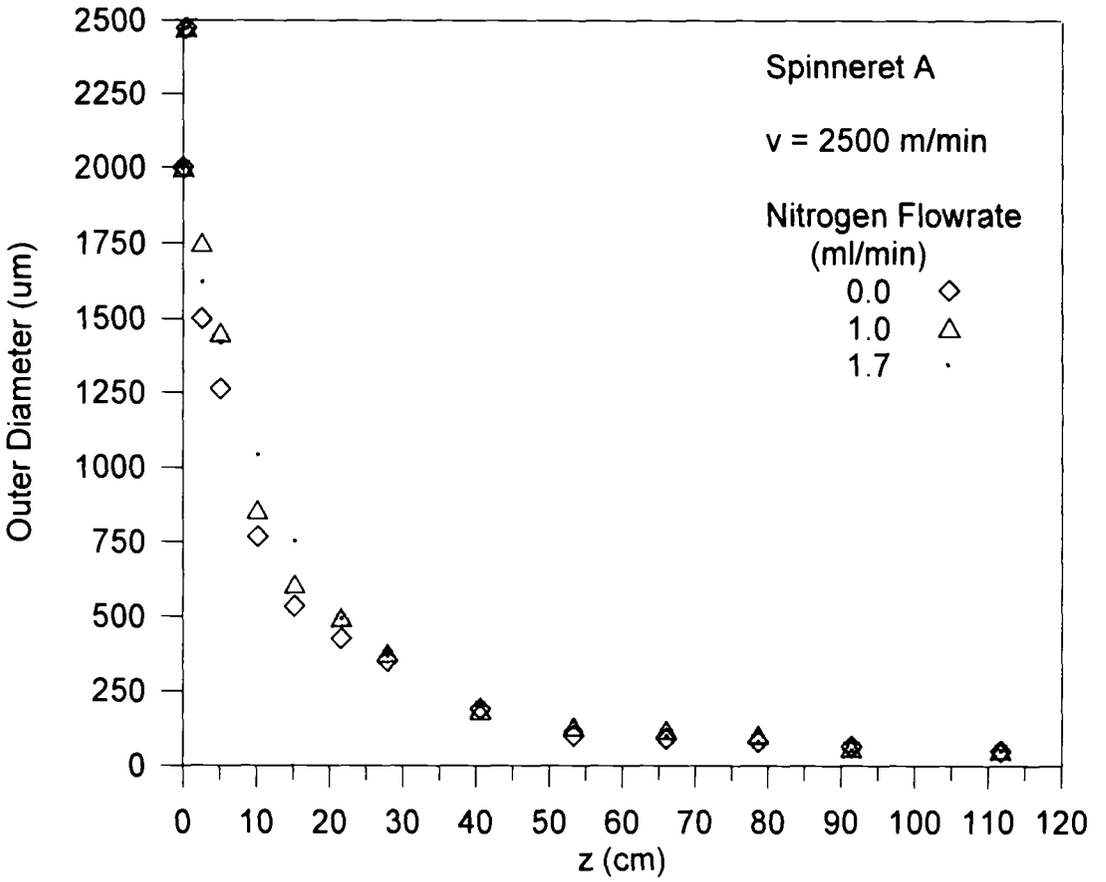

Figure 3.3c: Effect of nitrogen flowrate on outer diameter for a windup speed of 2500 m/min.

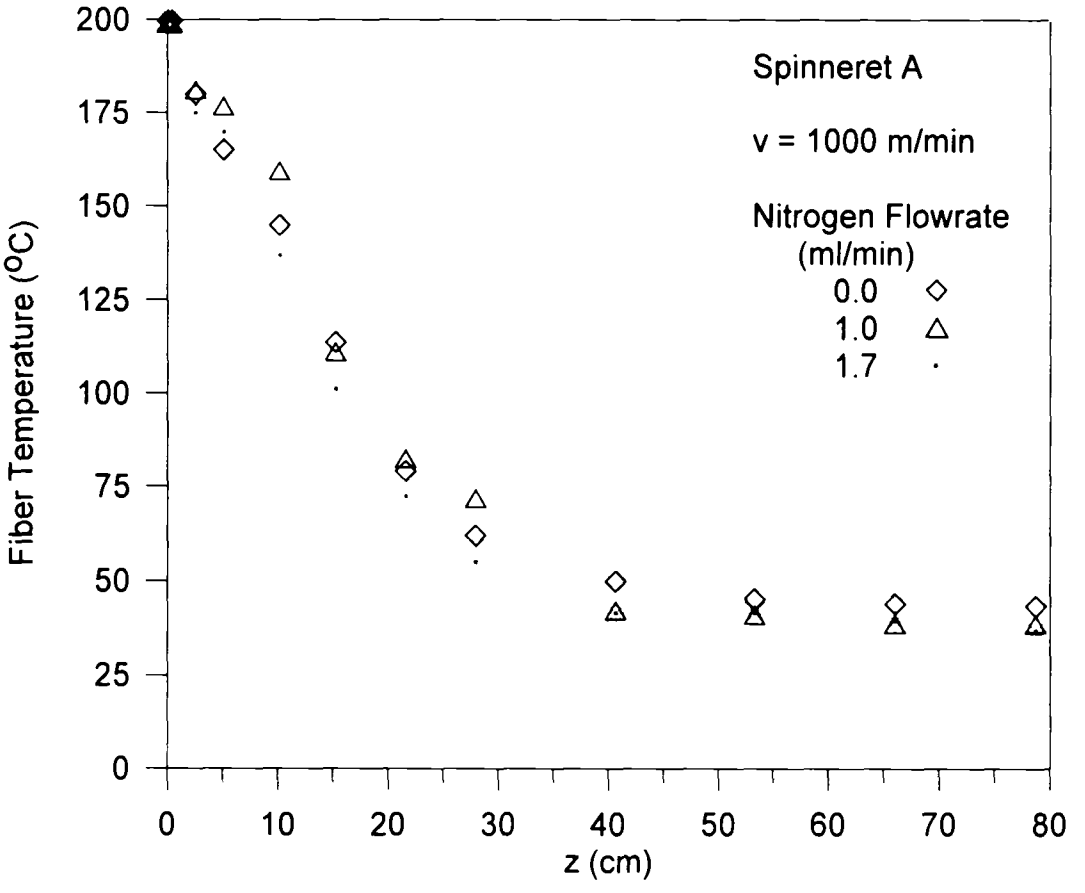

Figure 3.4a: Effect of nitrogen flowrate on fiber temperature for a windup speed of 1000 m/min.

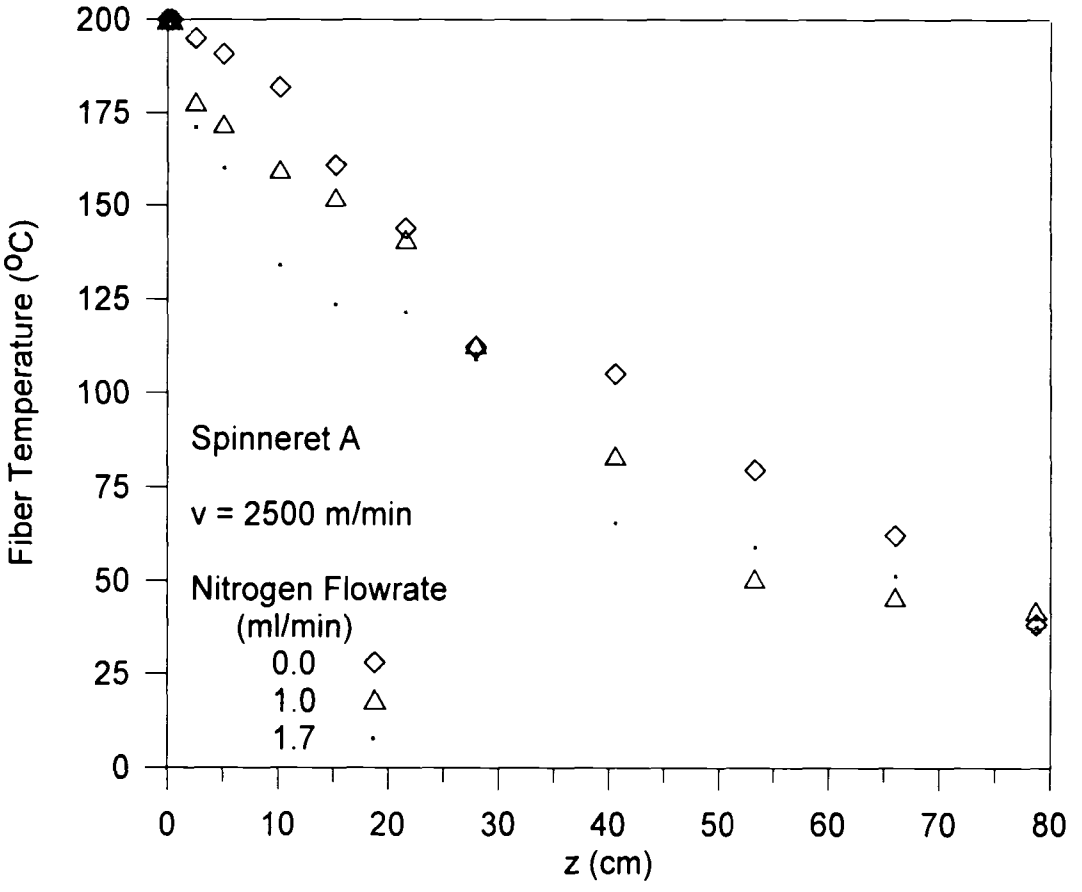

Figure 3.4b: Effect of nitrogen flowrate on fiber temperature for a windup speed of 2500 m/min.

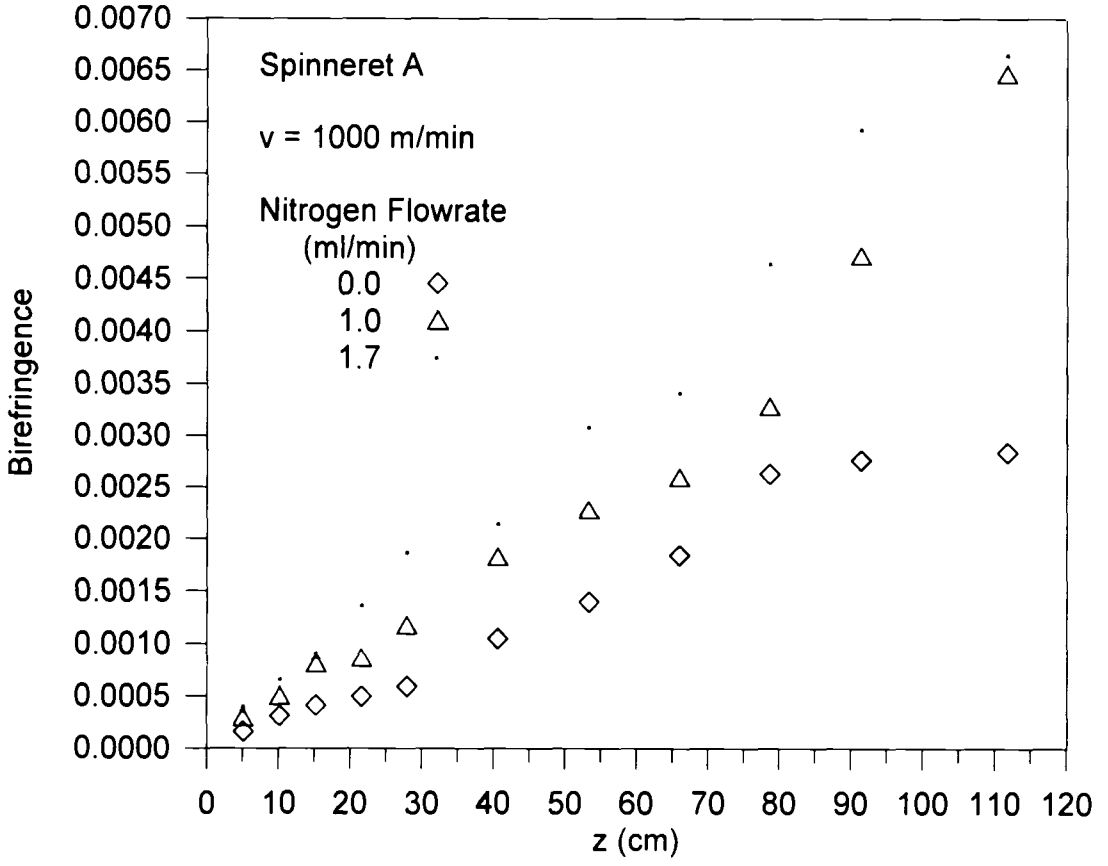

Figure 3.5a: Effect of nitrogen flowrate on birefringence for a windup speed of 1000 m/min.

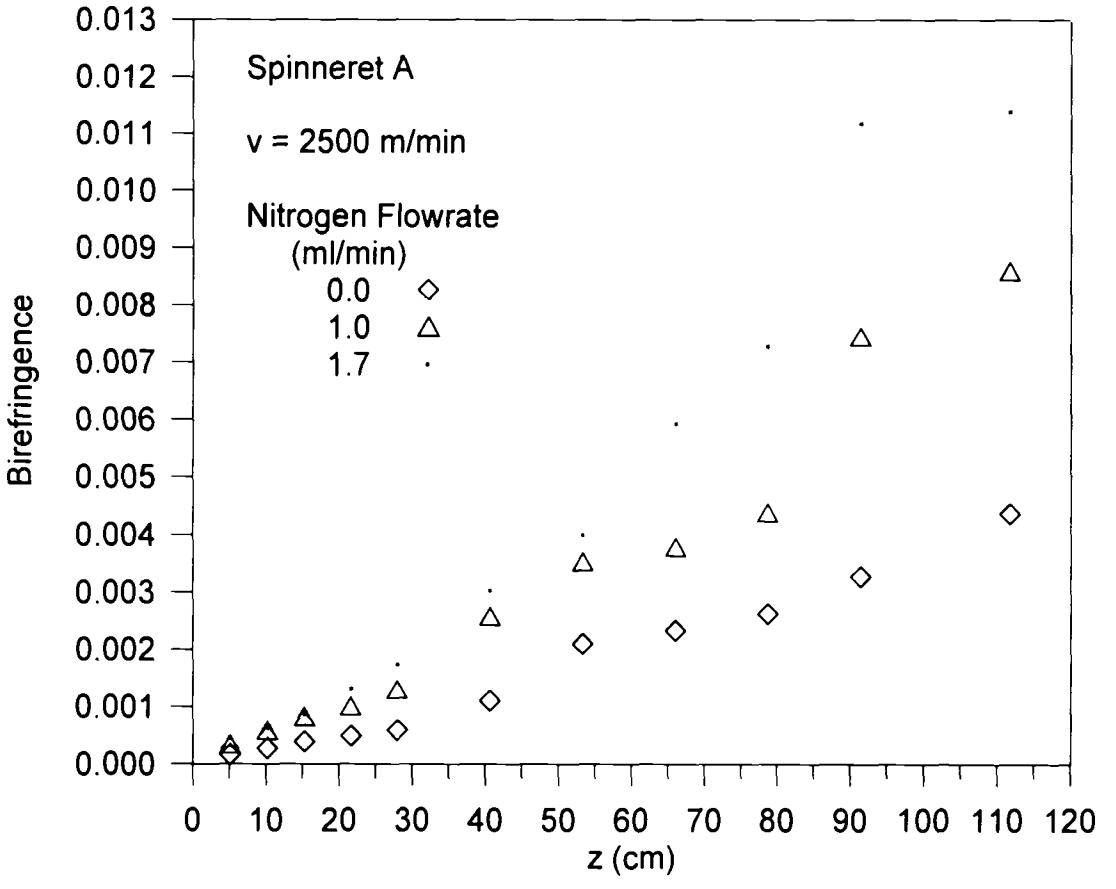

Figure 3.5b: Effect of nitrogen flowrate on birefringence for a windup speed of 2500 m/min.

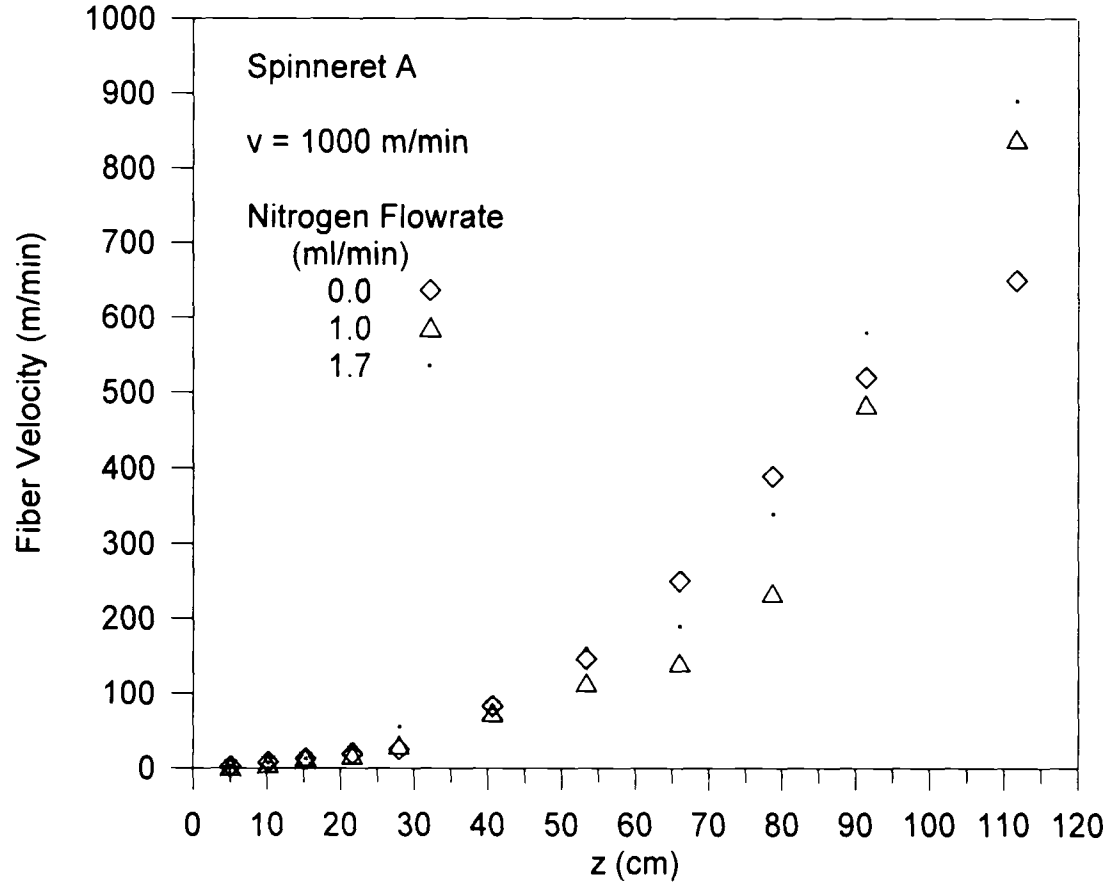

Figure 3.6a: Effect of nitrogen flowrate on velocity for a windup speed of 1000 m/min.

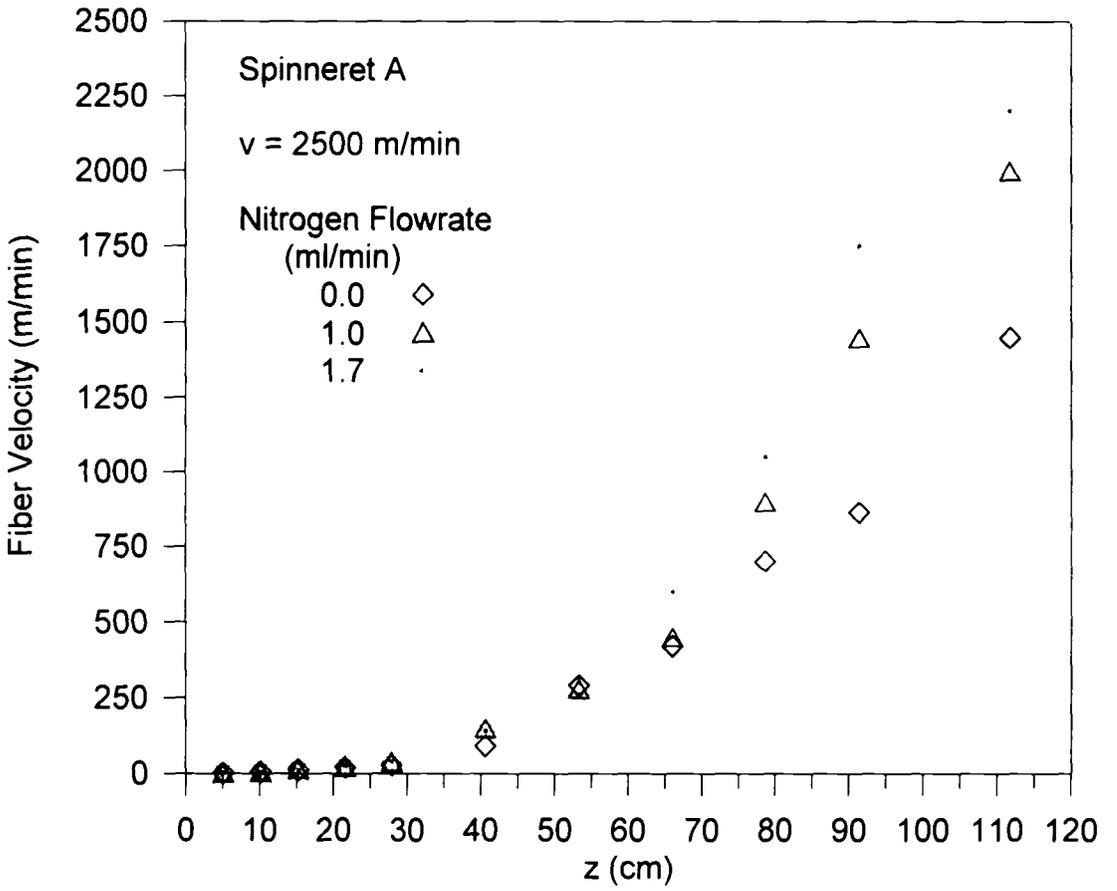

Figure 3.6b: Effect of nitrogen flowrate on velocity for a windup speed of 2500 m/min.

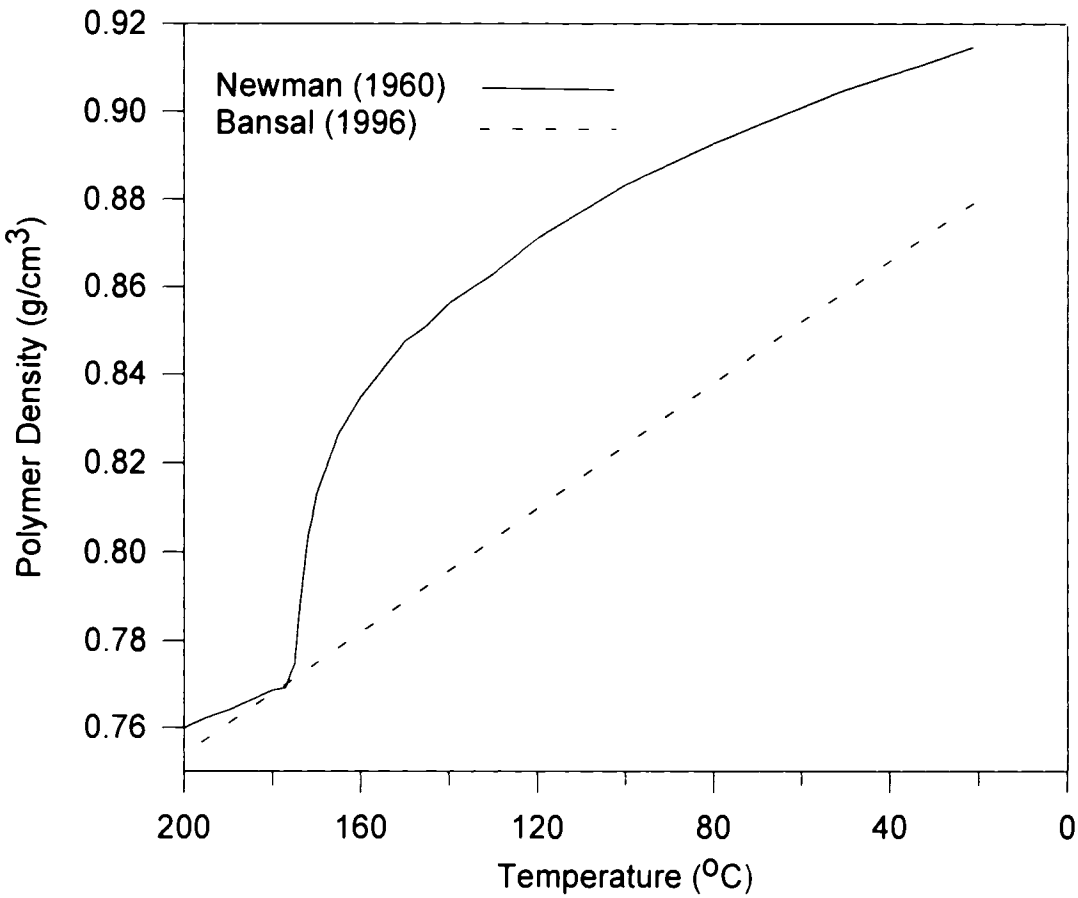

Figure 3.7: Bansal and Newman correlations for polymer density versus temperature. Bansal correlation applies to non-crystalline material and Newman correlation applies to crystalline material.

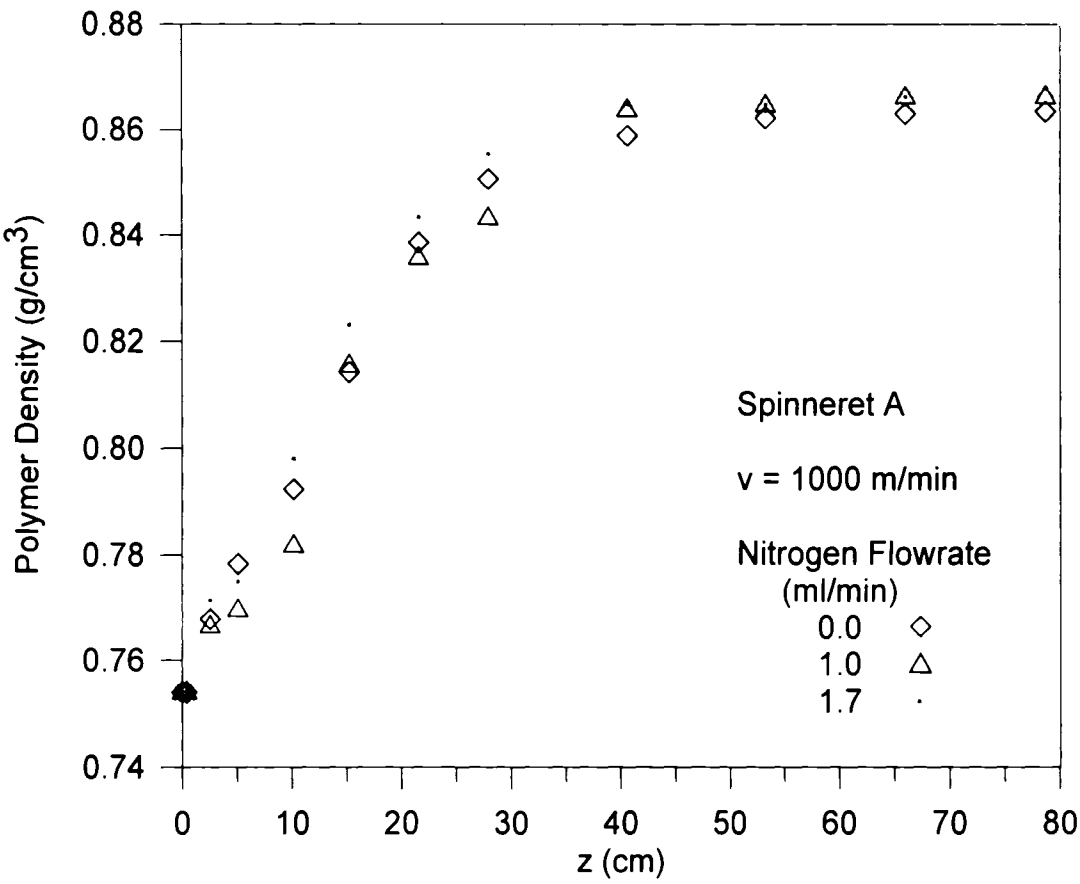

Figure 3.8a: Effect nitrogen flowrate on polymer density for a windup speed of 1000 m/min.

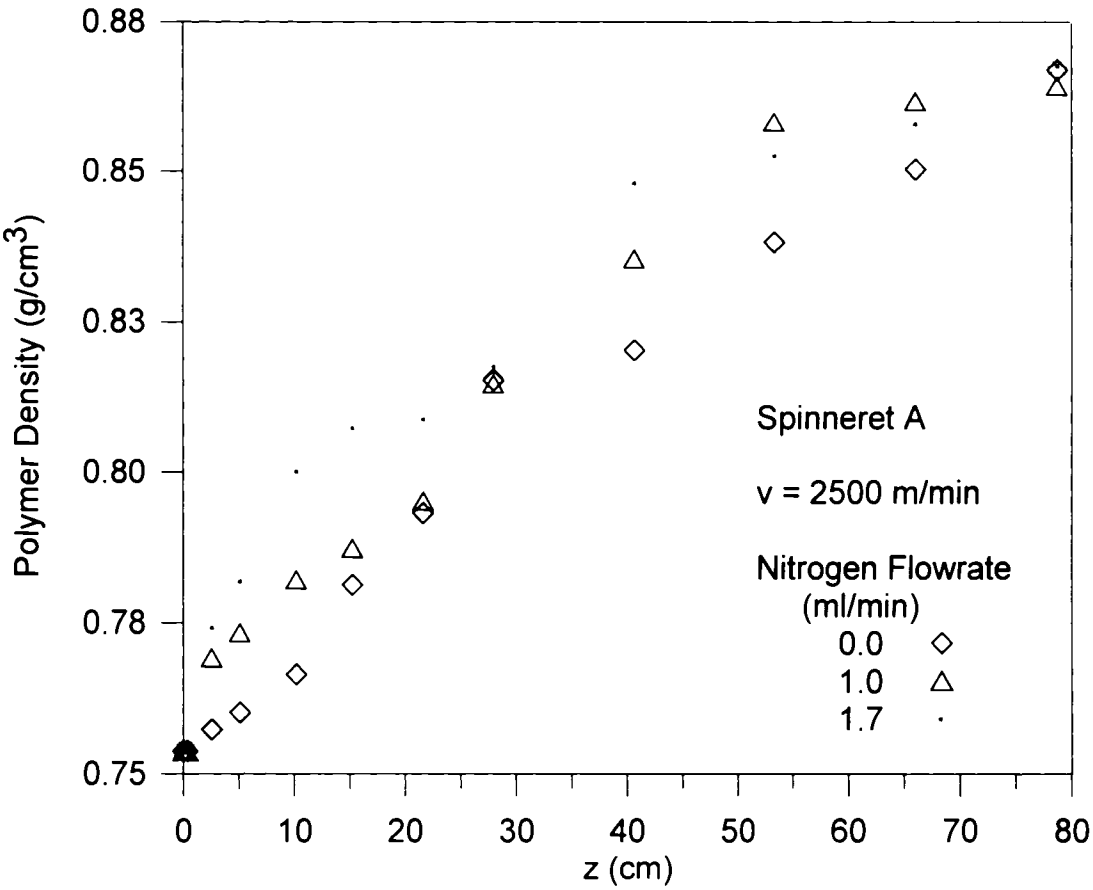

Figure 3.8b: Effect of nitrogen flowrate on polymer density for a windup speed of 2500 m/min.

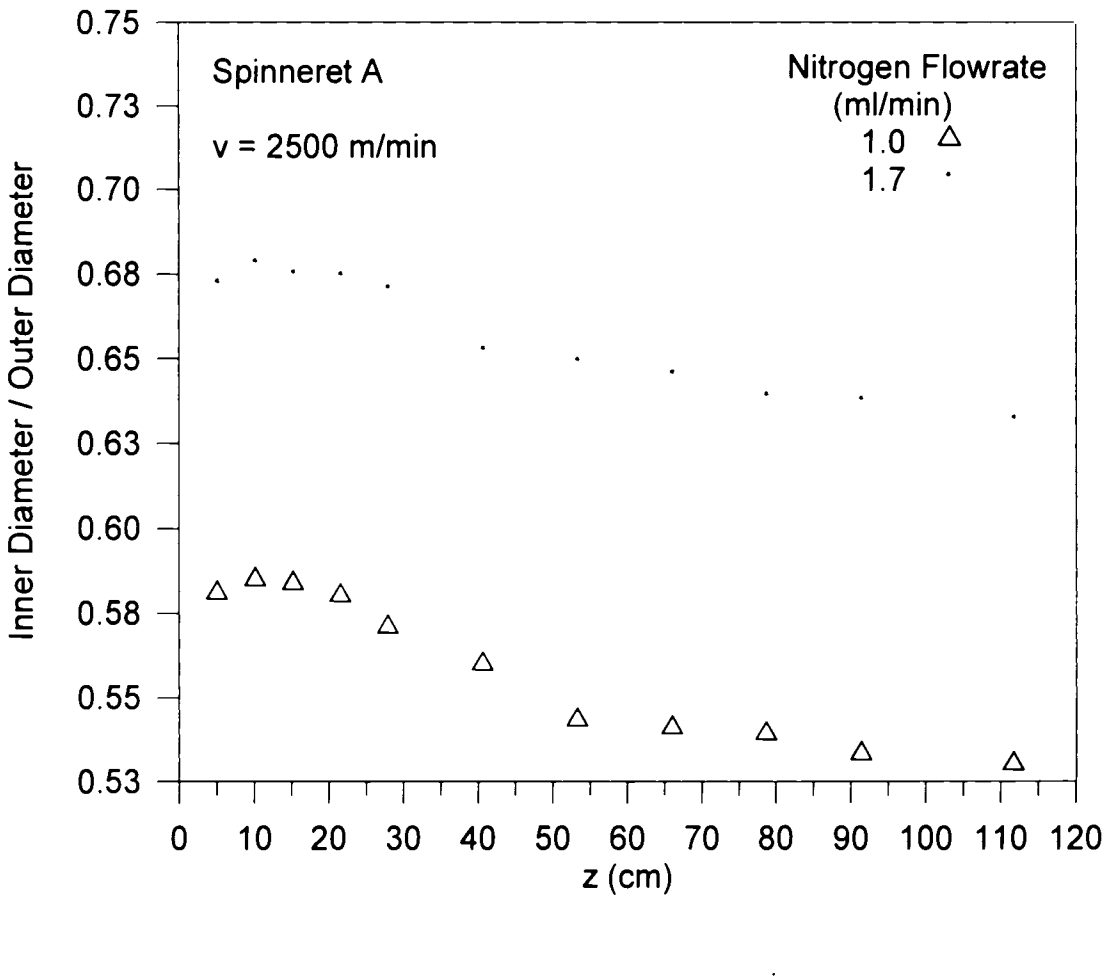

Figure 3.9: Effect of nitrogen flowrate on ratio d_1/d_2 for a windup speed of 2500 m/min.

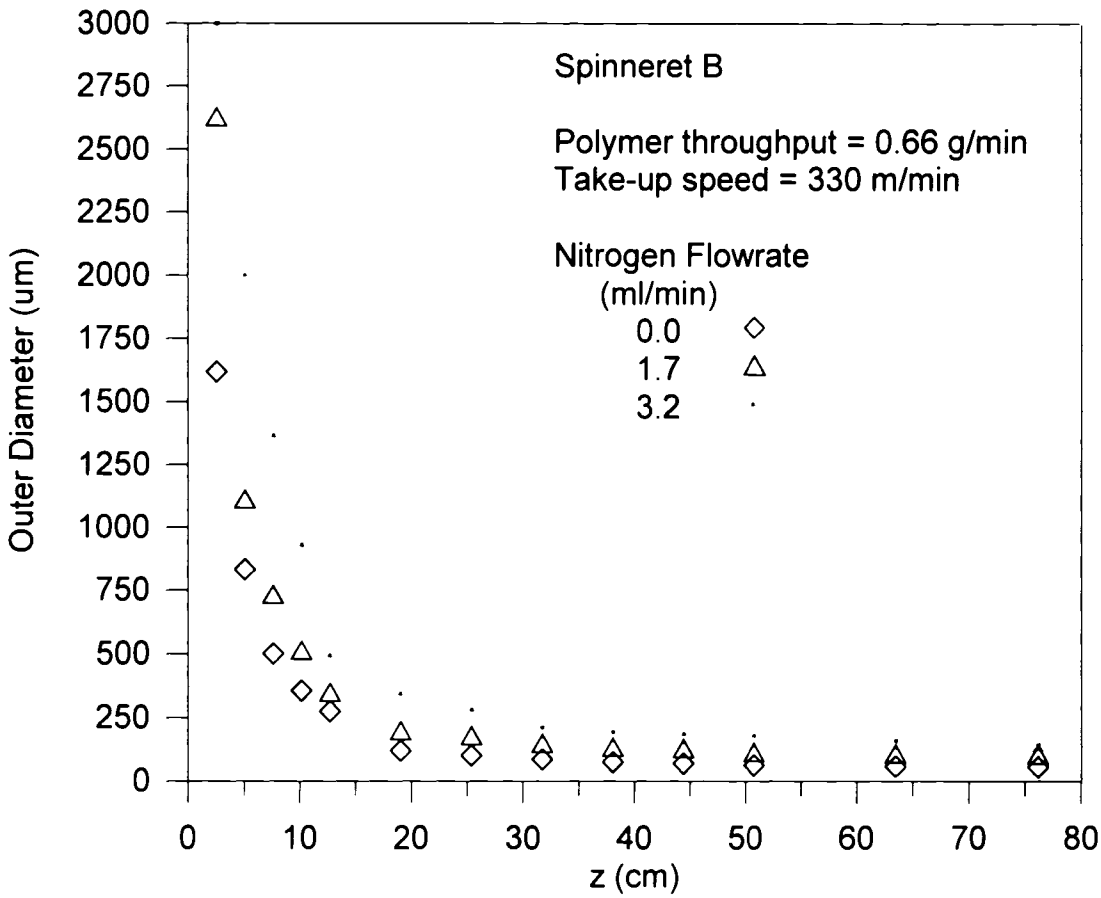

Figure 3.10a: Effect of nitrogen flowrate on outer diameter for a windup speed of 330 m/min.

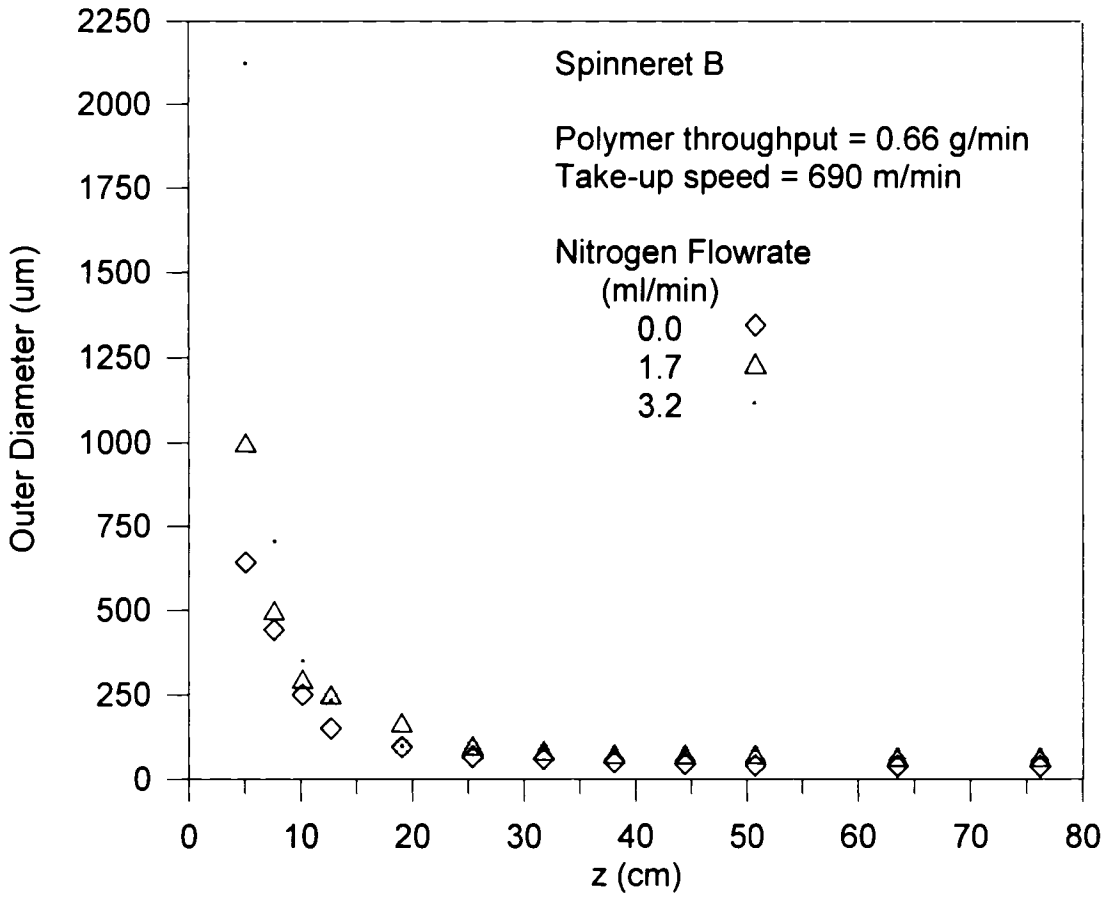

Figure 3.10b: Effect of nitrogen flowrate on outer diameter for a windup speed of 690 m/min.

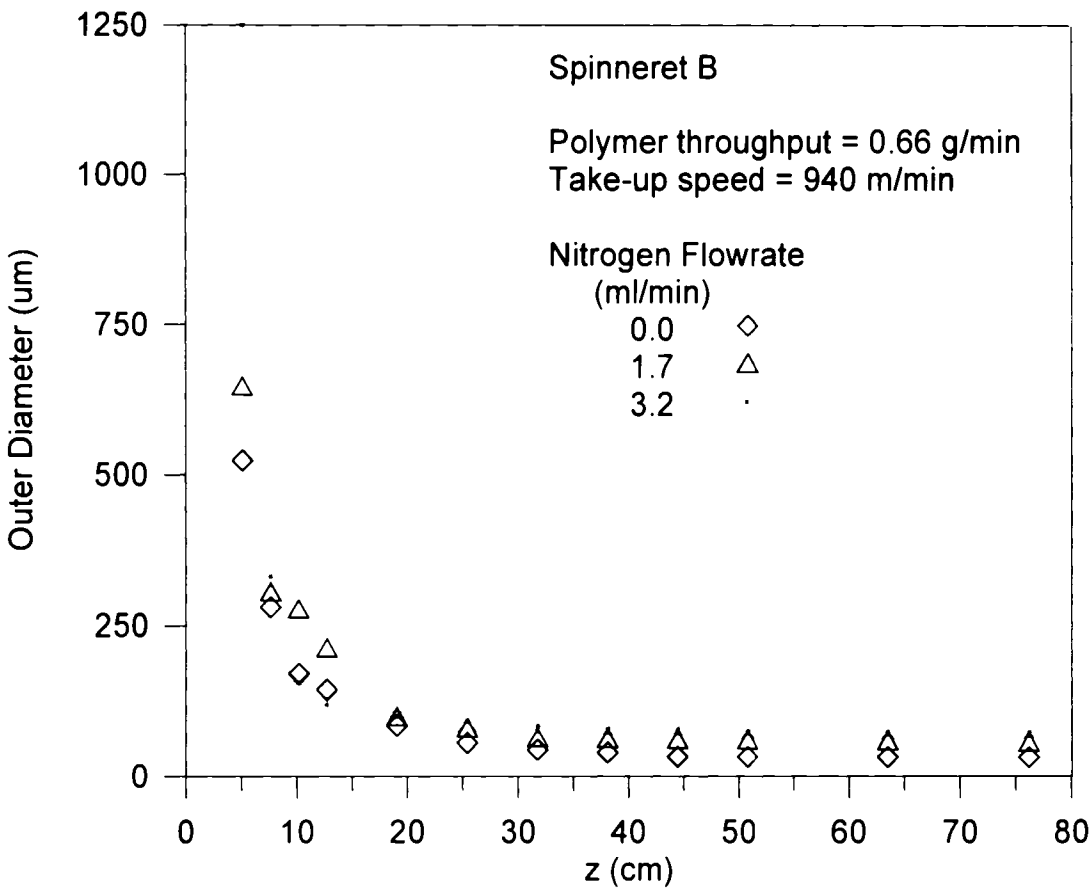

Figure 3.10c: Effect of nitrogen flowrate on outer diameter for a windup speed of 940 m/min.

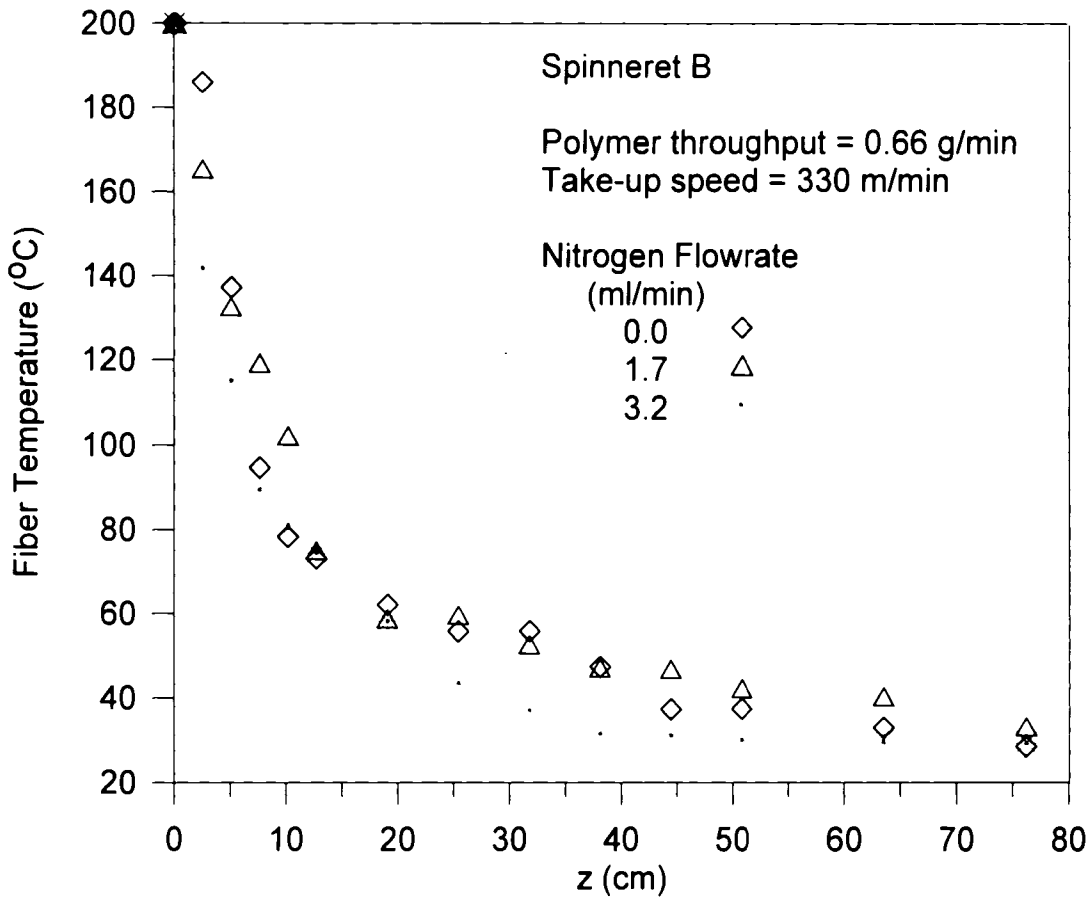

Figure 3.11a: Effect of nitrogen flowrate on fiber temperature for a windup speed of 330 m/min.

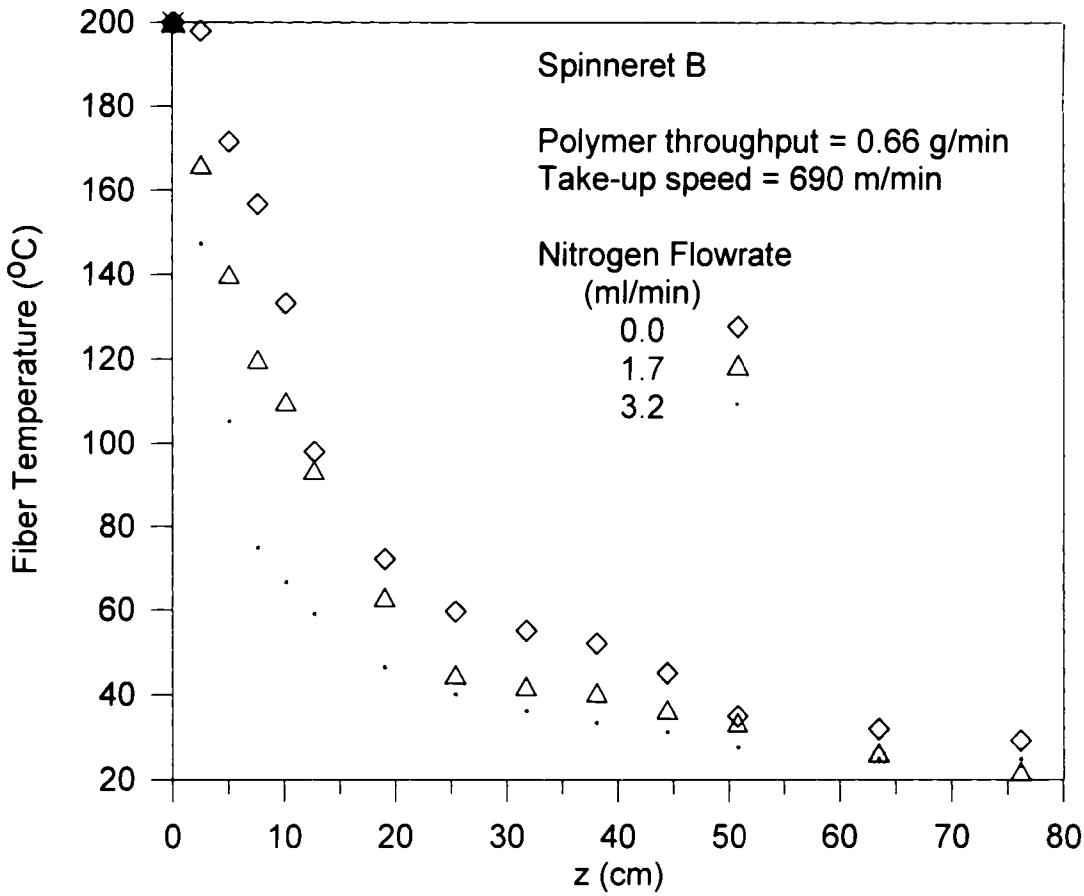

Figure 3.11b: Effect of nitrogen flowrate on fiber temperature for a windup speed of 690 m/min.

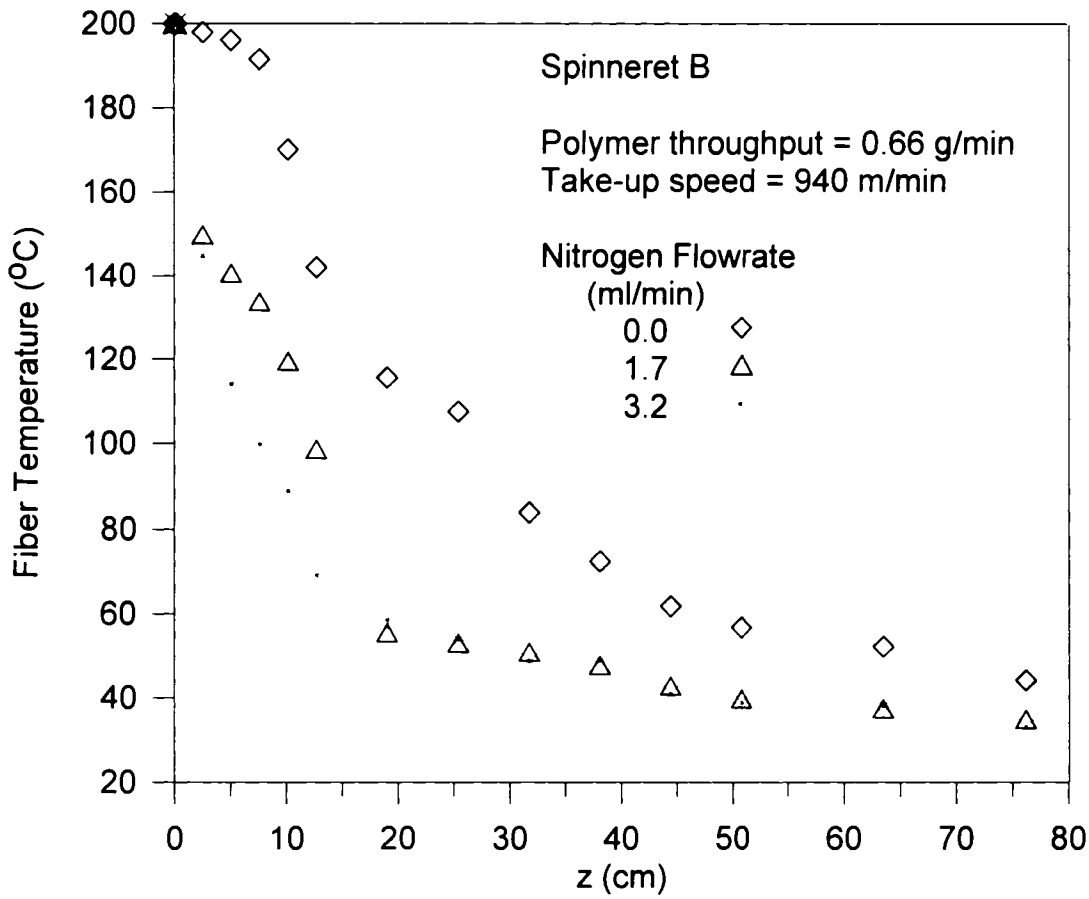

Figure 3.11c: Effect of nitrogen flowrate on fiber temperature for a windup speed of 940 m/min.

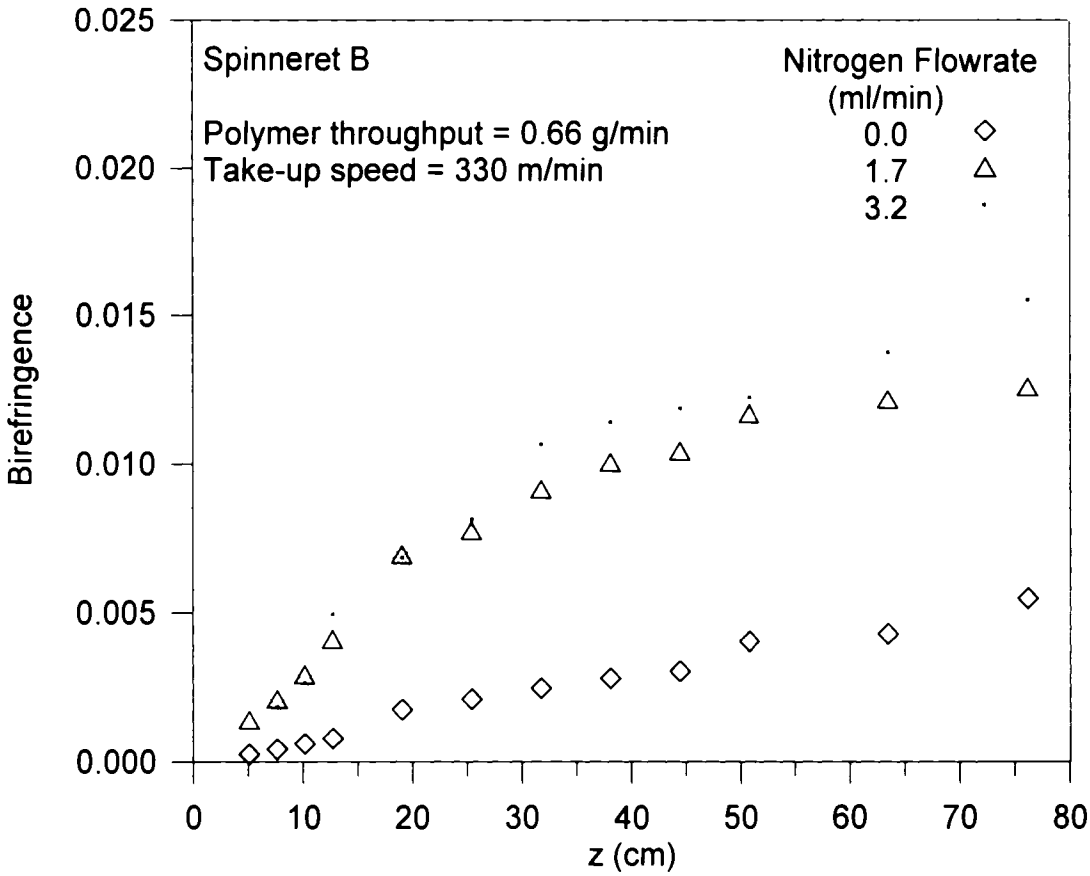

Figure 3.12a: Effect of nitrogen flowrate on birefringence for a windup speed of 330 m/min.

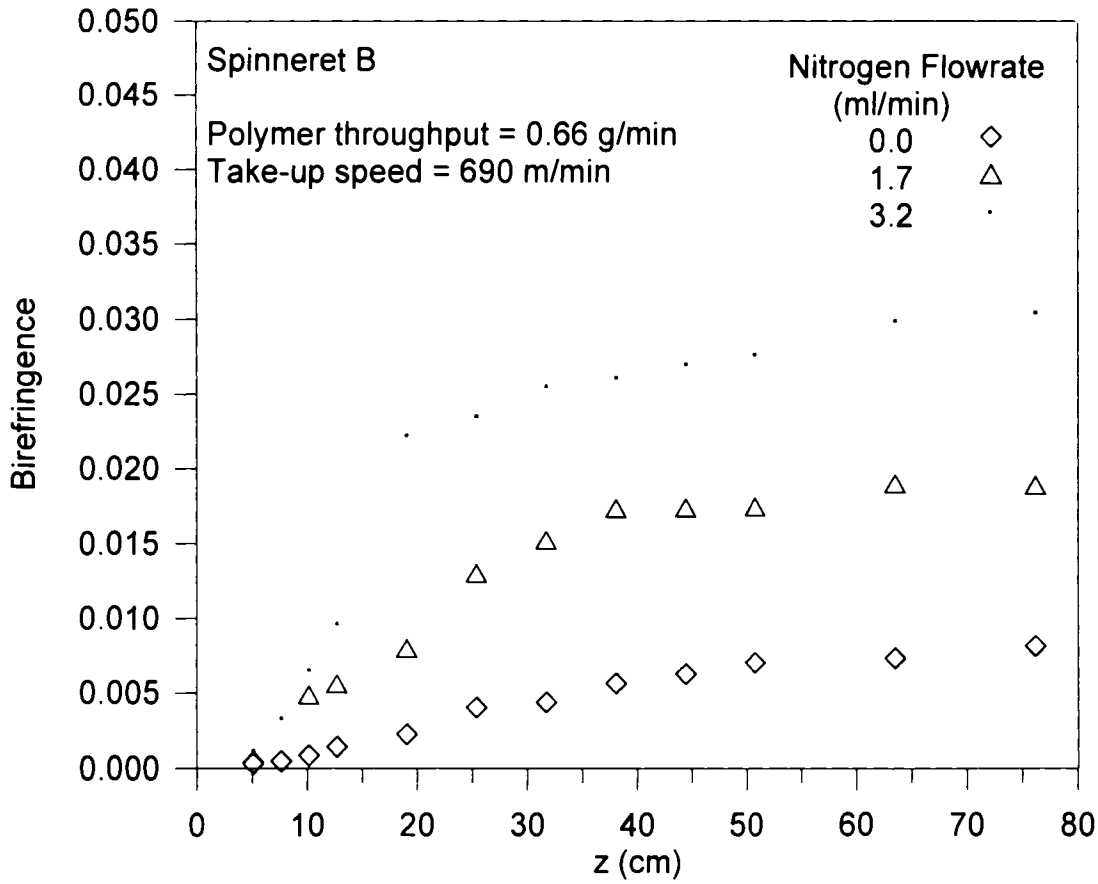

Figure 3.12b: Effect of nitrogen flowrate on birefringence for a windup speed of 690 m/min.

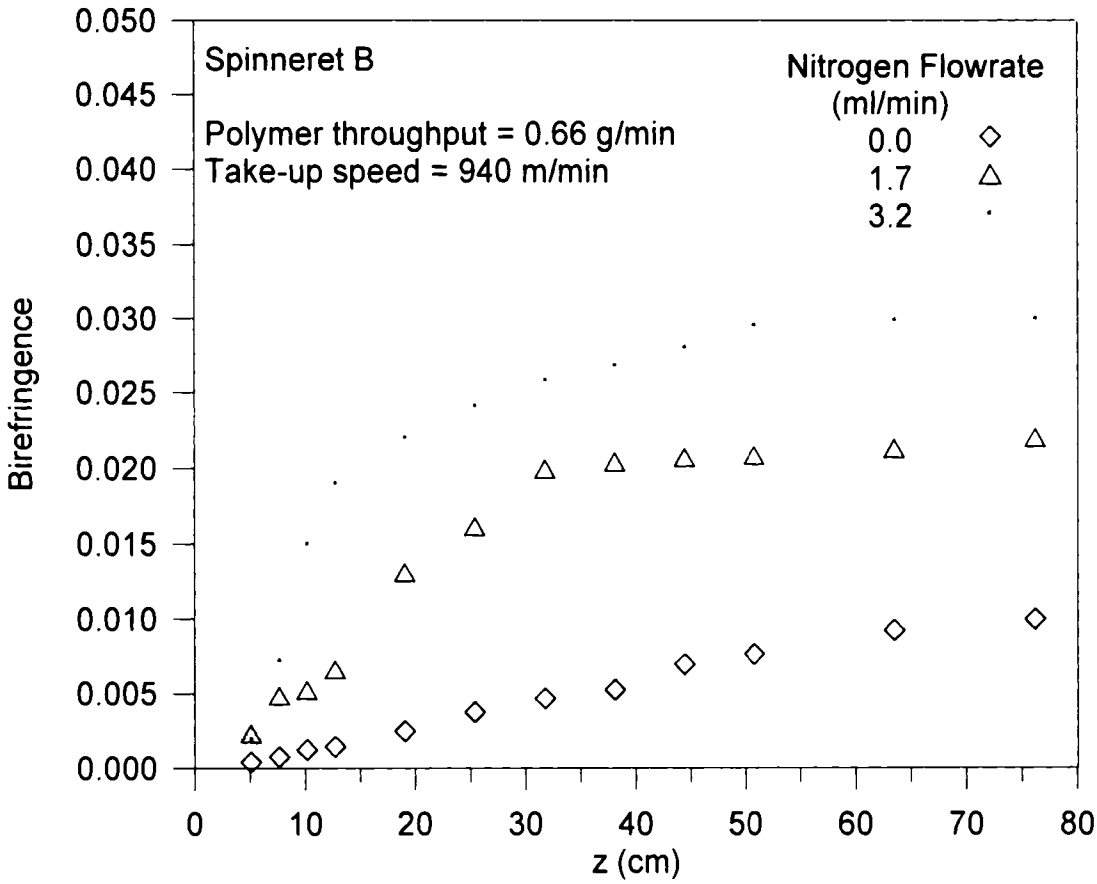

Figure 3.12c: Effect of nitrogen flowrate on birefringence for a windup speed of 940 m/min.

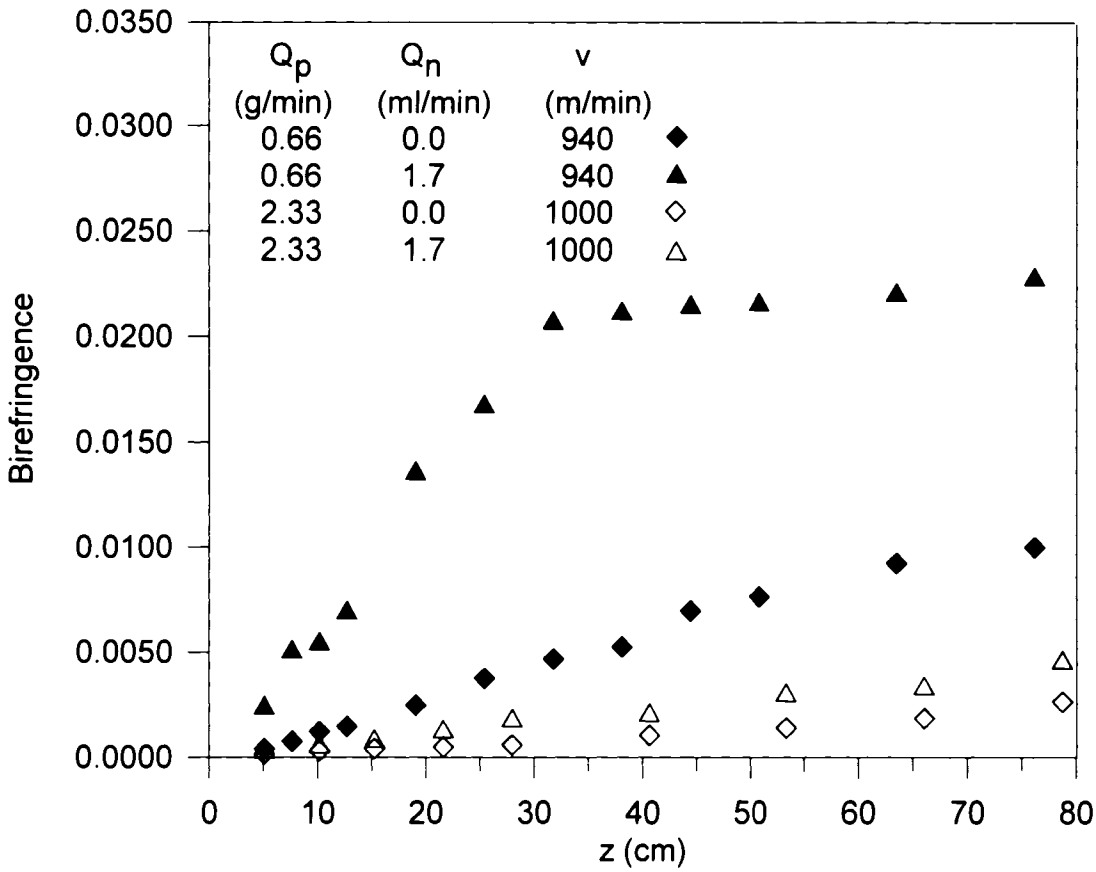

Figure 3.13: Effect of polymer throughput on birefringence for a windup speed of about 1000 m/min.

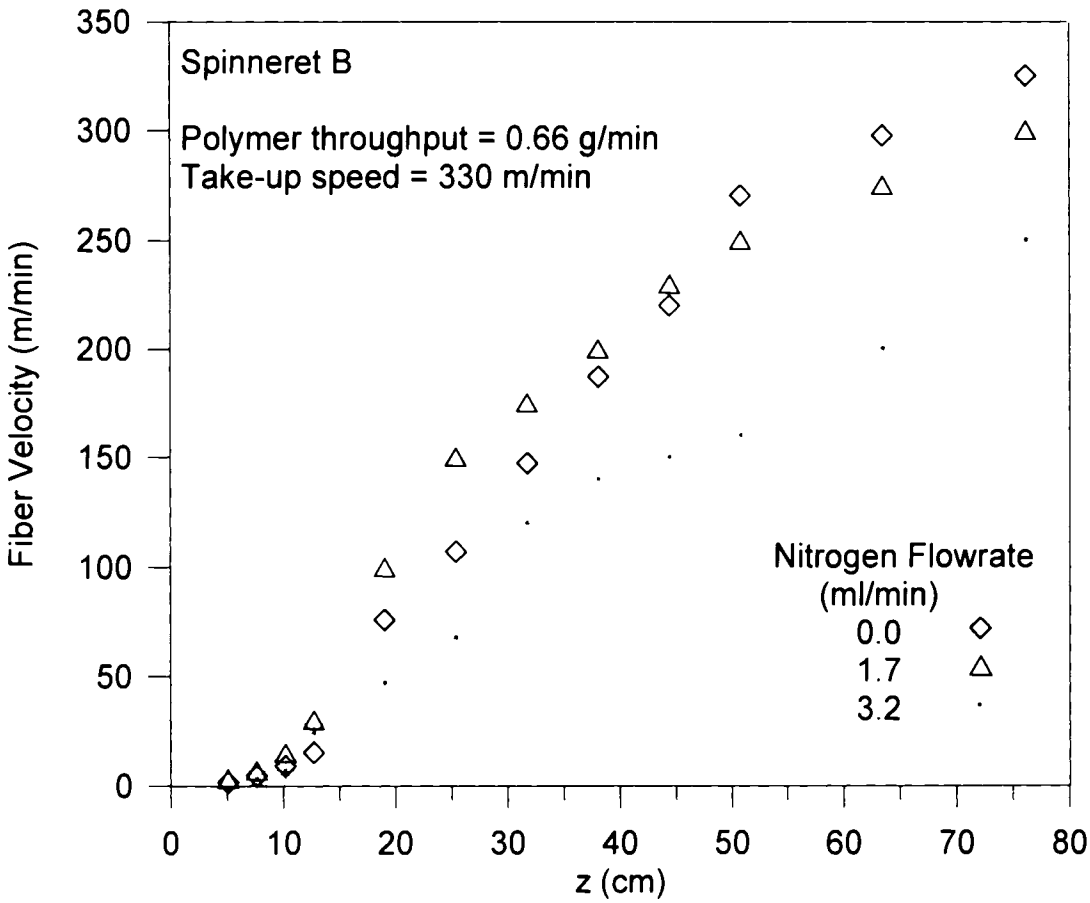

Figure 3.14a: Effect of nitrogen flowrate on velocity for a windup speed of 330 m/min.

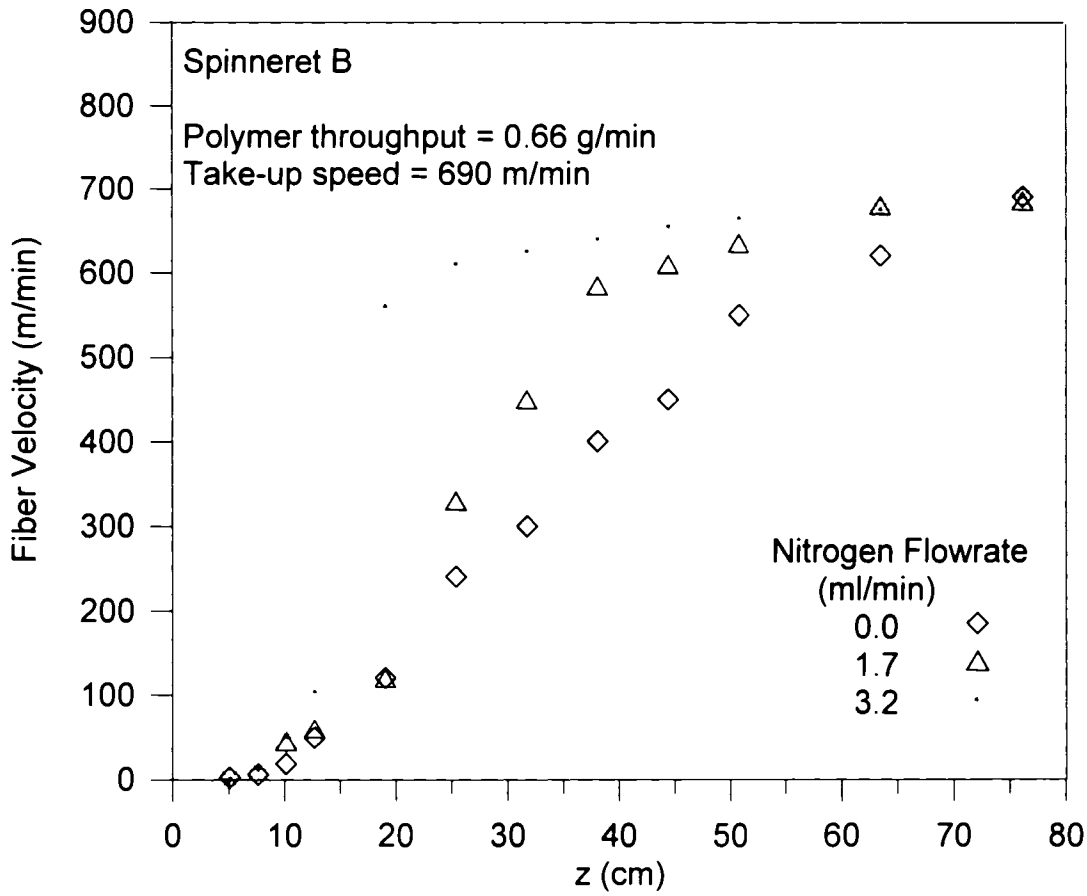

Figure 3.14b: Effect of nitrogen flowrate on velocity for a windup speed of 690 m/min.

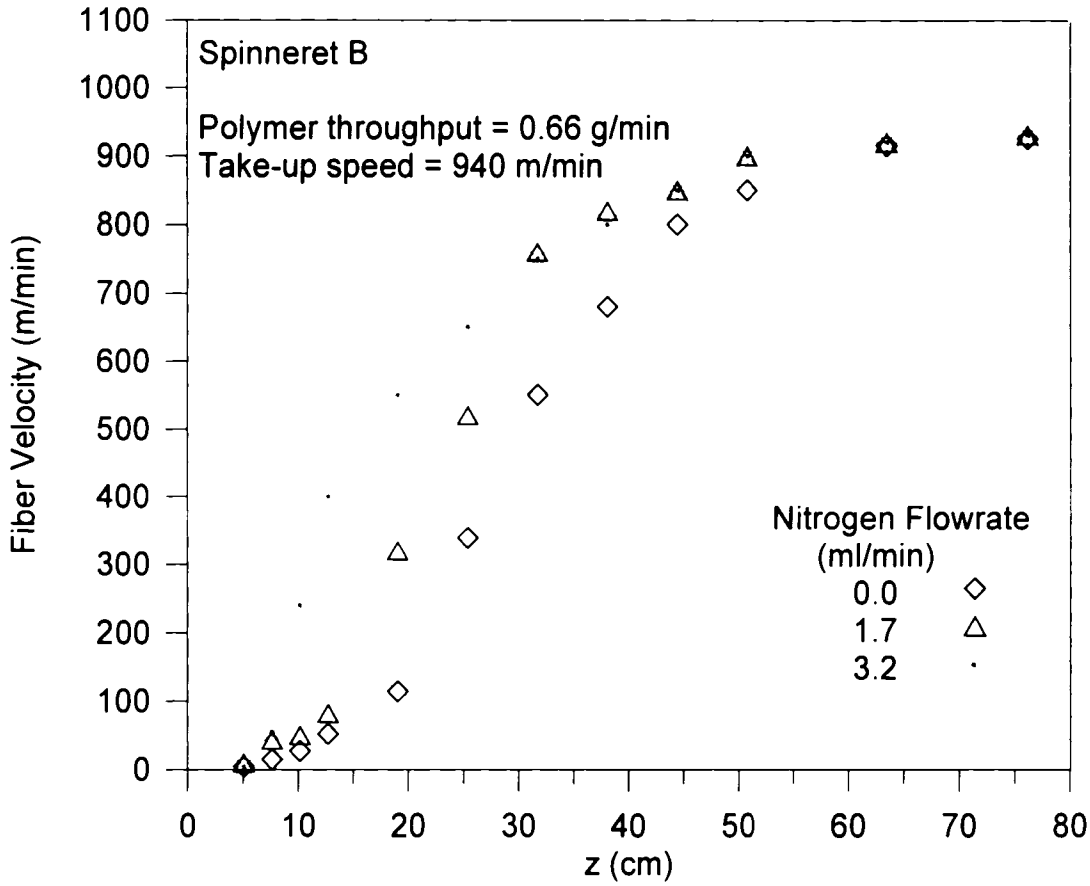

Figure 3.14c: Effect of nitrogen flowrate on velocity for a windup speed of 940 m/min.

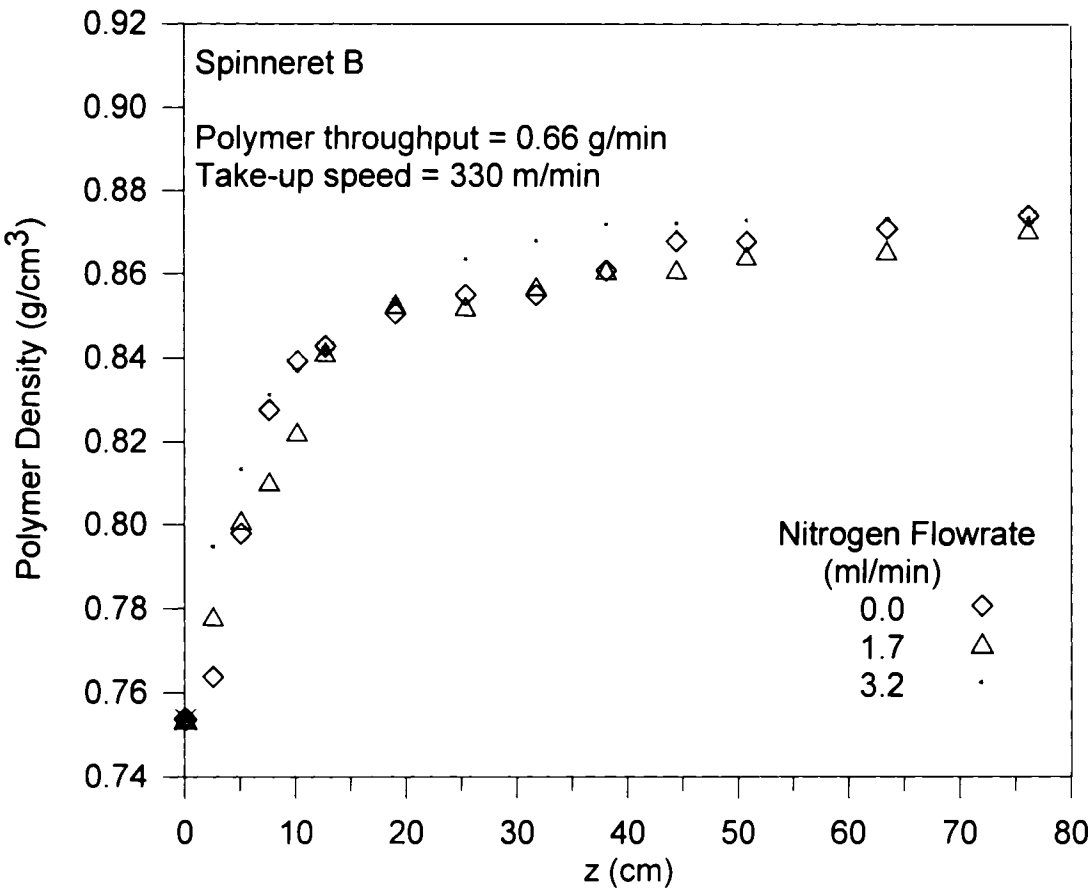

Figure 3.15a: Effect of nitrogen flowrate on polymer density for a windup speed of 330 m/min.

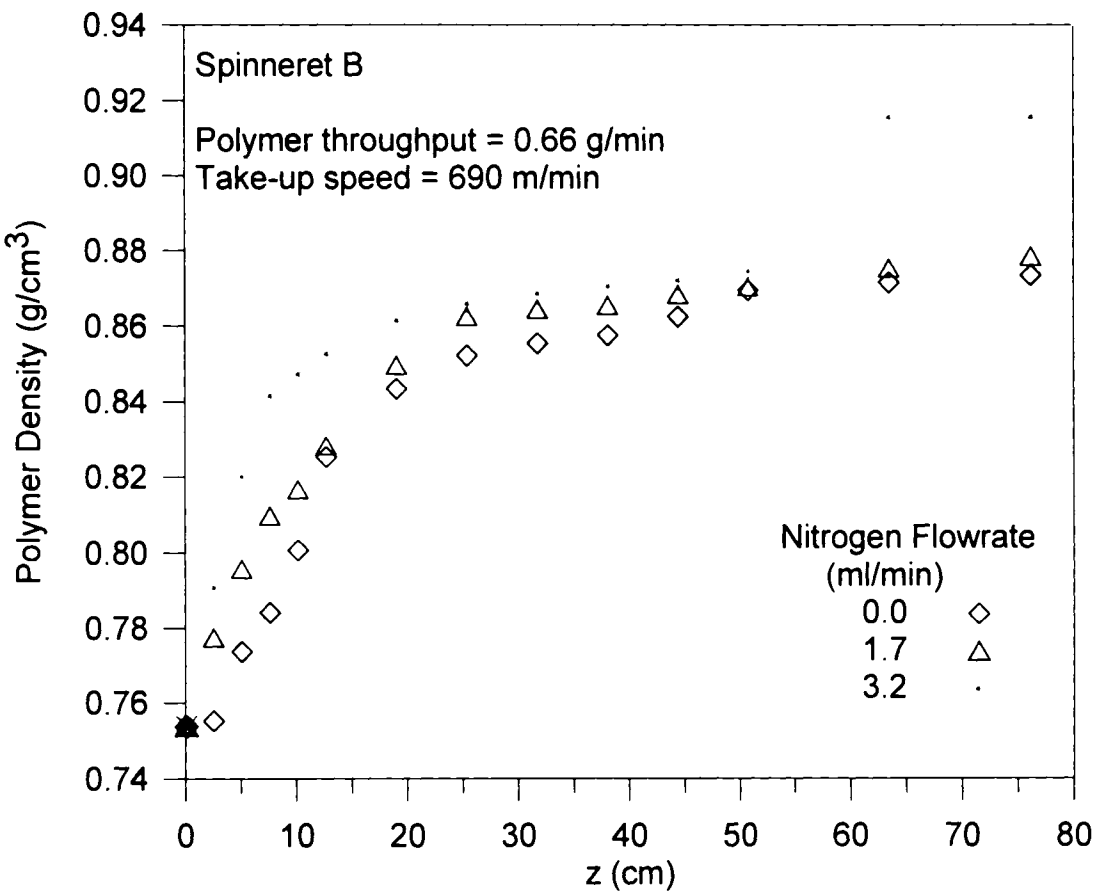

Figure 3.15b: Effect of nitrogen flowrate on polymer density for a windup speed of 690 m/min.

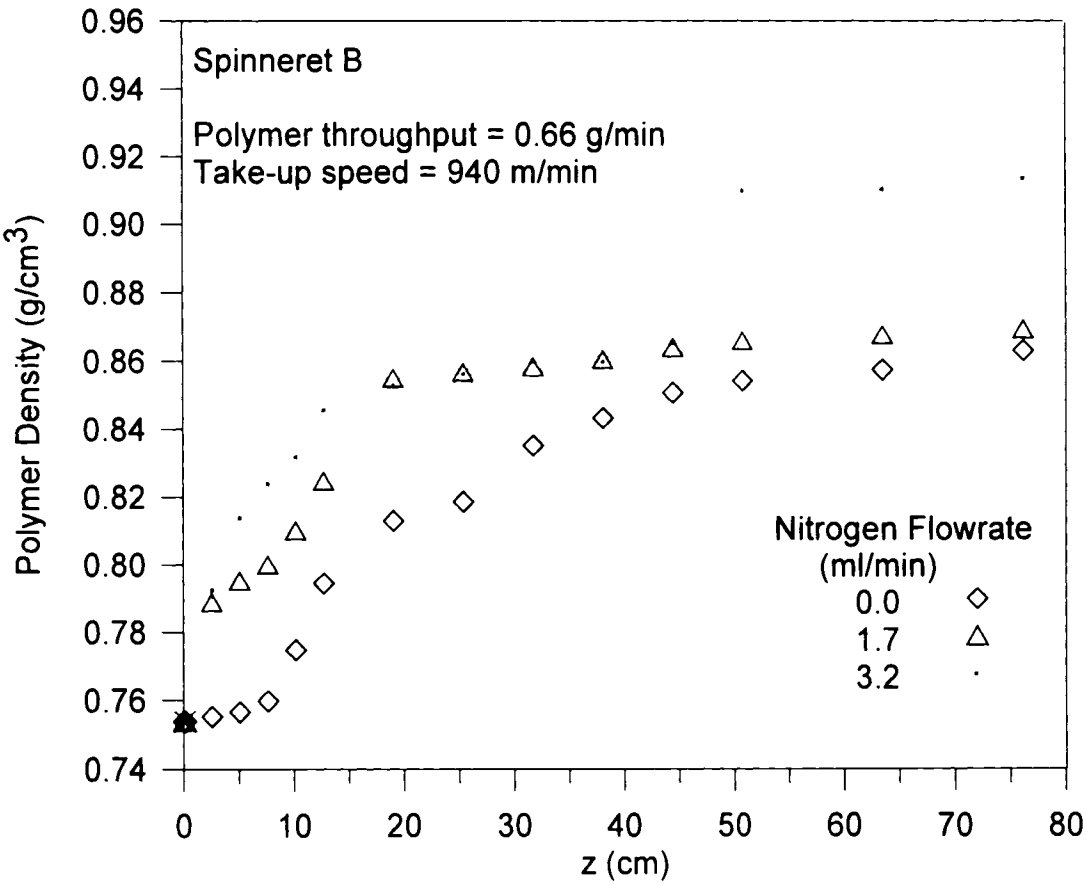

Figure 3.15c: Effect of nitrogen flowrate on polymer density for a windup speed of 940 m/min.

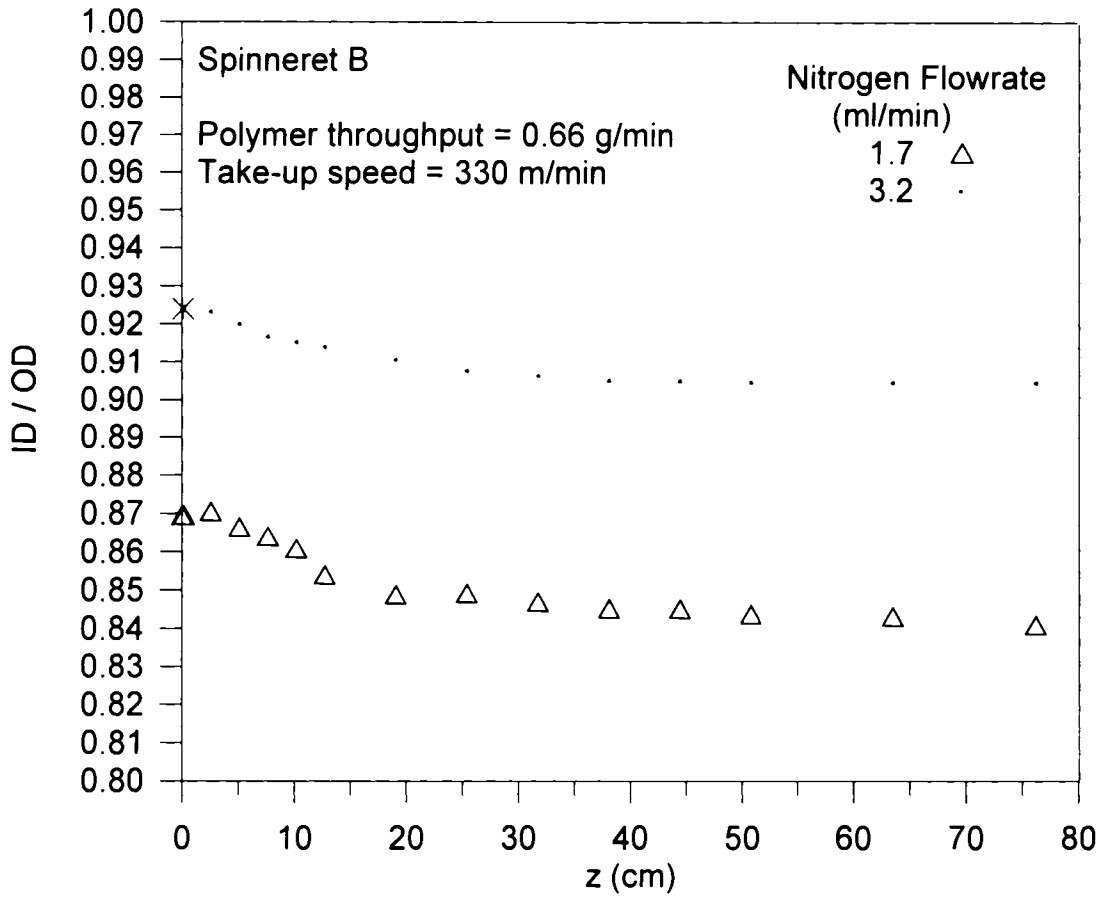

Figure 3.16: Effect of nitrogen flowrate on ratio d_1/d_2 for a windup speed of 330 m/min.

CHAPTER 4

MELT-SPUN HOLLOW FIBERS:

MODELING AND EXPERIMENTS

(The first part of this chapter has been submitted to a journal as: A. de Rovere and R. L. Shambaugh, Melt-spun hollow fibers: Modeling and Experiments, *Polymer Engineering and Science*.)

ABSTRACT

Polypropylene hollow fibers were prepared via melt spinning at speeds of 330-2500 m/min. The outside diameters of the fibers were measured on-line with high-speed photography. The fiber formation process was modeled with momentum, energy, and two continuity equations (one for the polymer, and one for the lumen fluid). The equations were solved numerically, and the results were compared to the on-line diameter data. Both Newtonian and viscoelastic constitutive equations were considered.

4.1 INTRODUCTION

Hollow fibers are used commercially for reverse osmosis, hemodialysis, gas separation, microfiltration, and pervaporation. As described by Baum et al. [1976], hollow fibers can be prepared by wet spinning, dry spinning or melt spinning. Melt spinning is the fastest (in terms of spinning speed) and most economical of these three processes. This paper concerns a study of the melt spinning of hollow fibers.

Melt spinning of hollow fibers has much in common with the melt spinning of conventional (solid) fibers. Figure 4.1 shows the conventional melt spinning process. Polymer is extruded at high pressure through a spinneret (a fine capillary). Generally, the polymer is extruded into ambient air that both cools the fiber and exerts a drag force on the fiber. At some distance below the spinneret (a meter or more), a mechanical roll provides the force that drives the process. Substantial attenuation of the filament diameter occurs along the fiber.

Figure 4.2 shows the melt spinning of a hollow fiber. In this case, the polymer exits from an annular hole. Inside the annulus is a hole through which a lumen fluid (nitrogen is typical) is injected. This is referred to as a tube-in-orifice spinneret. Besides the outside diameter (d_2) that is present in ordinary melt spinning, the hollow fiber also has an inside diameter (d_1) that varies along the fiber threadline. It is also possible to melt spin hollow fibers with a segmented arc spinneret. In this situation, no lumen fluid needs to be injected. Instead, ambient air is entrained and trapped within the fiber core.

Models for melt spinning have been developed over a number of years. Ziabicki and Kedzierska [1960, 1961], Ziabicki [1961], Kase and Matsuo [1965], and Matovich and Pearson [1969] developed the basic momentum, continuity and energy balances that apply to a spinning threadline. Extension of this early work to viscoelastic fluids was done by Gagon and Denn [1981]. All of these researchers approximated the threadline as extensional flow (i.e., as thin filament equations). Ziabicki [1976] provides an excellent overview of melt spinning, while Ziabicki and Kawai [1985] give an overview of high speed melt spinning.

Freeman et al. [1986] developed spinning equations for hollow fibers. They added a new variable, the inside diameter. They also used a finite element technique to analyze the flow near the spinneret. Their calculations showed that, after a short region of shear flow and profile rearrangement, extensional flow equations can be used to predict the filament profile. The work of Freeman et al. was strictly theoretical – no experimental data were included in their study. Oh et al. [1998] used a two-dimensional finite element method to analyze the melt spinning of hollow fibers. They used a segmented arc die in their studies, and they collected experimental data that were fitted well by their model.

4.2 MODEL FORMULATION

As has been done in the past for melt spinning, we will assume that the momentum and mass conservation equations can be averaged over the fiber cross-section. A hollow fiber, like a conventional solid fiber, exhibits a die swell at the

spinneret. The equations will be assumed accurate for locations beyond the die swell (this assumption will be experimentally tested). Uyttendaele and Shambaugh [1990] developed the continuity, momentum, and energy equations for melt blowing, which is a special case of melt spinning (mathematically, only the boundary conditions change). We will use the equation format of Uyttendaele and Shambaugh as a starting point for our development of spinning equations for hollow fibers.

4.2.1 Continuity equations

The continuity equation for the polymer in the threadline is:

$$Q_p = \frac{m_p}{\rho_p} = \left(\frac{\pi}{4}\right)\left(d_2^{\,2} - d_1^{\,2}\right)v \tag{4.1}$$

where

Q_p = volumetric polymer flow rate

d_1, d_2 = the variable inside and outside diameters of the fiber (see Figure 4.2)

m_p = polymer mass rate

ρ_p = polymer density

v = fiber velocity

The common practice in modeling melt spinning is to assume that polymer density is constant along the threadline [Uyttendaele and Shambaugh, 1990].

For the core fluid (nitrogen), the mass balance equation is:

$$m_n = \rho_n\left(\frac{\pi}{4}\right)d_1^{\,2}v \tag{4.2}$$

where

m_n = nitrogen mass rate

ρ_n = nitrogen density

In order to use equation 4.2, information about the nitrogen density (ρ_n) along the spinline is needed. The ρ_n is a function of pressure and temperature. The pressure in the spinline is greater than the ambient atmospheric pressure. This difference can be calculated from the fundamental equation of capillarity which is [Adamson, 1967]:

$$\Delta P = \gamma\left(\frac{1}{R_1} + \frac{1}{R_2}\right) \tag{4.3}$$

where

ΔP = the pressure difference between two phases

R_1, R_2 = radii of curvature of the interface between the two phases

γ = surface energy

For a cylindrical fiber, one of the radii is infinite. Thus, the capillarity equation becomes:

$$\Delta P = \gamma\left(\frac{1}{R}\right) \tag{4.4}$$

Bicerano [1996] gives data for the surface energies of polypropylene and polyethylene at temperatures of 20-180°C. His data show that temperature has relatively little effect on γ. Based on Bicerano's data, it can be assumed that $\gamma \approx 25$ dyne/cm for the air-polypropylene interface and the nitrogen-polypropylene interface. Because the hollow fiber has both an inner and outer surface, equation 4.4 must be applied twice. At the die swell, the fiber has its largest diameter. Assuming that d_2

and d_1 are 2.47 mm and 1.64 mm, respectively, at the die swell (these are typical values: see experimental results), then the difference between the inside and outside pressure of the fiber is only 50.7 Pa, or about 0.05%. The pressure difference becomes greater as the fiber diameters decrease. However, even at the final (product) diameters, the pressure difference is small. For example, if the final outer diameter (d_2) is 70 microns and the inner diameter (d_1) is 40 microns, the pressure in the core nitrogen is only 1964 Pa higher than the outside pressure (i.e, 1.9% higher than the ambient pressure). It is therefore safe to approximate the inner core pressure as atmospheric.

Equation 4.2 can be used to eliminate d_1 in equation 4.1 to give:

$$Q_p = \left(\frac{\pi}{4}\right)\left[d_2^{\,2}v - \frac{4m_n}{\rho_n \pi}\right] \tag{4.5}$$

Since the nitrogen is a gas, its density change along the threadline is significant. The nitrogen gas ranges in temperature from 200°C at the spinneret to ambient temperature at the windup. For this temperature range, the data of Vargaftik [1975] were fitted with the expression:

$$\rho_n = \frac{0.3389}{T^{1.001}} \tag{4.6}$$

where T is absolute temperature in °K. This equation fits the Vargaftik data to within 0.03% for the temperature range of our experiments. Equation 4.6 was used in our modeling work.

4.2.2 Momentum Equation

The momentum equation accounts for rheological force, gravitational force, air drag force, and inertial force. For solid filaments, the appropriate equation is [Uyttendaele and Shambaugh, 1990]:

$$\frac{d}{dz}\left[\pi\frac{d^2}{4}\left(\tau^{zz}-\tau^{xx}\right)\right]=\pi dC_f\rho_a\frac{v^2}{2}+\rho_pQ_p\frac{dv}{dz}-\frac{\pi d^2}{4}\rho_pg \tag{4.7}$$

where

v = fiber velocity

z = axial position

d = diameter of solid fiber

τ^{zz}, τ^{xx} = components of the extra stress in the spinning and transverse directions, respectively

C_f = air drag coefficient

ρ_a= air density

g = gravitational acceleration

The drag coefficient C_f was correlated by the following relation that was developed for fine polymer fibers [see Majumdar and Shambaugh, 1990]:

$$C_f = 0.78(\mathrm{Re})^{-0.61} \tag{4.8}$$

The Reynolds number in the above equation is

$$\mathrm{Re}=\frac{d_2v}{\upsilon_a} \tag{4.9}$$

where υ_a is the kinematic viscosity of air.

Equation 4.7 can be easily modified to accommodate the modeling of hollow fiber spinning. In hollow fiber spinning, the rheological term only acts on the annular part of the fiber. Hence, the area factor must be changed in the term on the left side of the equation. In the first term on the right side of the equation, d becomes d_2, since the drag acts on the outer diameter and is independent of the value of d_1. The second term on the right side remains unchanged, although the definition of Q_p is different for hollow fiber spinning (see equation 4.5). Finally, the third term on the right side must be modified to show that gravity is acting on an annular solid. With these modifications, the momentum equation becomes:

$$\frac{d}{dz}\left[\pi\frac{(d_2^{\,2}-d_1^{\,2})}{4}\left(\tau^{zz}-\tau^{xx}\right)\right]=\pi d_2 C_f \rho_a \frac{v^2}{2}+\rho_p Q_p \frac{dv}{dz}-\frac{\pi(d_2^{\,2}-d_1^{\,2})}{4}\rho_p g \qquad (4.10)$$

4.2.3 Energy Equation

We assume steady state conditions, no conductive resistance in the radial direction, no conduction in the axial direction, and no viscous dissipation. Then the equation of energy for an annular fiber is:

$$\rho_p C_p v\frac{dT}{dz}=-\frac{4hd_2}{\left(d_2^{\,2}-d_1^{\,2}\right)}\left(T-T_a\right) \qquad (4.11)$$

where

C_p = polymer heat capacity

T = polymer temperature

T_a = ambient air temperature

h = convective heat transfer coefficient

To estimate h we used the correlation [Kase and Matsuo, 1965]:

$$Nu = \gamma (Re)^m \tag{4.12}$$

where Nu is the Nusselt number and γ and m are empirical constants. For γ and m we used values of 0.42 and 0.334, respectively [see Uyttendaele and Shambaugh, 1990]. Unlike the melt blowing process where ambient air temperature and velocity vary along the threadline, in melt spinning the air temperature is constant and was assumed equal to 25°C, while the air velocity is equal to zero at all position below the spinneret.

4.2.4 Constitutive Equations

Both Newtonian and viscoelastic constitutive equations were used in our studies. For the Newtonian case, the τ^{zz} and τ^{xx} components of the extra stress tensor are:

$$\tau^{zz} = 2\eta \frac{\partial v}{\partial z} \tag{4.13}$$

$$\tau^{xx} = -\eta \frac{\partial v}{\partial z} \tag{4.14}$$

Equations 4.10, 4.11, 4.13, and 4.14 are the four equations that describe Newtonian, nonisothermal melt spinning of hollow fibers. By using the previous expressions of τ^{xx} and τ^{zz} into equation 4.10, Trouton elongational viscosity $\bar{\eta}$ (that describes the normal stress difference) is recovered: $\bar{\eta} = 3\eta$.

We selected the Phan-Thien constitutive equations [Phan-Thien, 1978] to model viscoelastic spinning. The equations are:

$$\tau^{zz} = \sum_i \tau_i^{zz} \tag{4.15}$$

$$\tau^{xx} = \sum_i \tau_i^{xx} \tag{4.16}$$

$$K_i \tau_i^{zz} + \lambda_i \left[v \frac{d\tau_i^{zz}}{dz} - 2(1-X)\tau_i^{zz} \frac{dv}{dz} \right] = 2G_i \lambda_i \frac{dv}{dz} \tag{4.17}$$

$$K_i \tau_i^{xx} + \lambda_i \left[v \frac{d\tau_i^{xx}}{dz} - 2(1-X)\tau_i^{xx} \frac{dv}{dz} \right] = -G_i \lambda_i \frac{dv}{dz} \tag{4.18}$$

and

$$K_i = \exp\left[\frac{E}{G_i} \left(\tau_i^{zz} + 2\tau_i^{xx} \right) \right] \tag{4.19}$$

A discrete spectrum of relaxation times can be used with the Phan-Thien model. The factor X is a viscous shear thinning parameter, and E is a parameter related to stress saturation at high extension rates. The counter i defines the number of relaxation times. When both parameters (X and E) are set equal to zero, the Maxwell fluid model is recovered. Equations 4.10, 4.11, 4.17 and 4.18 describe the viscoelastic spinning of hollow fibers. All equations were solved numerically (fourth order Runge-Kutta-Gill method) using Fortran 77 on an HP 4550 Z computer. The model code is given in Appendix A.

4.3 EXPERIMENTAL DETAILS

The experiments were carried out in a single hole melt spinning device. Polymer pellets were melted and pressurized in a Brabender screw extruder. The extruder barrel had a 19.0 mm diameter, a 381 mm length, a 20 to 1 L/D ratio, and a 3:1 compression ratio. The extruder temperature was set to 225°C for all experiments. After exiting the extruder, the polymer was fed to a modified Zenith pump which in turn fed the spinneret assembly. Two different tube-in-orifice spinnerets (A and B) were used to produce hollow fibers using two different polymer throughputs. Spinneret A was run with a polymer throughput of 2.33 g/min and spinneret B with a polymer throughput of 0.66 g/min. The spinnerets had an annulus through which polymer was ejected and a center hole through which the lumen fluid (nitrogen) was passed. The spinnerets were kept at 200°C for all experiments. Hence, both the polymer and the nitrogen were at a temperature of 200°C as they exited the spinneret. Table 4.1 gives the dimensions and the spinning conditions used for spinnerets A and B. Table 4.2 gives the properties of ambient air. For spinning speeds of 1000 and 2000 m/min, the melt spun hollow filaments were collected on a mechanical takeup roll placed 140 cm below the spinneret. For the highest spinning speed (2500 m/min), the roll was replaced with an air venturi, and the filaments were collected on a screen placed below the venturi. Fina Dypro® isotactic polypropylene pellets were used for all experiments. The polymer had an MFR (Melt Flow Rate) of 88, an M_w of 165,000 g/mol, and a polydispersity of 4. The zero shear rate viscosity of this polymer can be described by the relation [Cooper, 1987]:

$$\eta_o = 0.00376 \exp\left(\frac{5754.71}{T}\right) \tag{4.20}$$

For the Phan-Thien model, we let i = 1 (only 1 relaxation time was considered), G = 28 kPa, X = 0.1, and E = 0.015. These were the same values chosen by Uyttendaele and Shambaugh [1990] to describe melt spinning of polypropylene.

On-line fiber diameters (d_2 only) were determined by taking high-speed flash pictures with a Nikon 90S camera and a 105 mm Nikon macro lens. Kodak Tri-X film with ISO 400 was used. Fiber diameters were measured by examining photographic negatives under a microscope with micrometer eyepiece. Off-line fiber diameters (d_2 and d_1) were determined by cross-sectioning fibers and then examining the sections under a microscope. On-line velocities were determined using a TSI Laser Doppler Velocimeter, and on-line temperatures were determined using an Inframetrics Infrared Camera (see Chapter 3 for further details).

4.4 COMPARISON OF EXPERIMENTAL RESULTS WITH THE MODEL AT HIGH POLYMER FLOWRATE

4.4.1 Boundary Conditions

In conventional melt spinning calculations (i.e., the spinning of solid filaments), the speed of the take-up roll fixes the final velocity of the filament and thus provides a boundary condition which allows the solution of the model equations. With minor modifications, the numerical solution of hollow filament spinning can proceed in the same way. A value of F_o (the force at the spinneret) is guessed, and iteration proceeds down the threadline until the final fiber velocity is calculated.

Then, the value of F_o is adjusted until the correct (experimental) fiber velocity is achieved.

A transition zone from die flow to extensional flow occurs just after the polymer exits the spinneret. An increase in fiber diameter (die swell) is a common characteristic of this zone. Strictly speaking, the thin filament equations (like those developed in this paper) do not apply to this transition zone. However, the zone is small enough that many researchers have ignored it and have started their model calculations by using the diameter dimension of the spinneret hole [e.g., see Gagon and Denn, 1981]. For the spinning of hollow filaments, Freeman et al. [1986] found that the transition zone was about one annular thickness ($[d_2 - d_1]/2$) in length. For our spinneret, the annular thickness is 0.38 mm.

Figure 4.3 shows diameter profile measurements taken with zero nitrogen flowrate and a 1000 m/min windup speed. The standard deviation of the diameter measurements (determined by taking replicate photographs) ranges from ± 5% at the spinneret to ± 2% at the windup. Figure 4.3 also shows Newtonian model fits based on three starting positions: (a) at the spinneret, (b) one annular thickness below the spinneret, and (c) 25.4 mm below the spinneret (Note: z refers to the variable in the model solution, while $\dot{z}$ refers to the experimental distance from the spinneret). As can be seen, starting at one annular thickness is as good as starting well below this point. Model fits similar to those on Figure 4.3 were also found for different windup speeds and for nitrogen flowrates of 1 and 1.7 ml/min. Therefore, all model fits were done by starting at one annular thickness below the spinneret. The maximum die

swell also occurred at about this same distance (one annular thickness) below the spinneret.

4.4.2 Model Fits

Figure 4.4a compares the Newtonian model with the Phan-Thien model for a 1000 m/min windup and zero nitrogen flowrate. As can be seen, the Newtonian model actually does a better job of predicting the diameter profile than does the viscoelastic model (The effects of changing the parameters in the Phan-Thien model will be discussed later). The viscoelastic model predicts a much more rapid attenuation than the Newtonian model because of the shear-thinning aspects of the viscoelastic model.

Figure 4.4b shows diameter profiles for the same conditions as Figure 4.4a, except that the nitrogen flowrate is 1 ml/min. The measured fiber diameters are, as expected, larger at every z˙ because of the presence of the lumen fluid. As before, the Newtonian model does the best job of fitting the data. Figure 4.4c shows the results for an even higher flowrate of nitrogen (1.7 ml/min). Again, the Newtonian model does the best job of fitting the data.

Figures 4.5a, 4.5b, and 4.5c show the diameter profiles for a 2000 m/min windup speed and nitrogen rates of 0, 1 and 1.7 ml/min. Again, the Newtonian model fits the data well at all nitrogen rates.

A 2500 m/min windup speed was the highest speed tested in our experiments. Figures 4.6a, 4.6b, and 4.6c show the diameter profiles at this speed. Also shown are the fits of the Newtonian and the Phan-Thien models. For a particular set of operating

conditions (temperature, windup speed, polymer throughput, etc.), a viscoelastic fluid will draw down more rapidly than a Newtonian fluid. Thus, the general difference between the Newtonian and Phan-Thien fits of Figures 4.4 - 4.6 is to be expected.

To best illustrate the effect of nitrogen flowrate on fiber diameter, the Newtonian model predictions were plotted on the same graph for nitrogen flowrates on 0 to 1.7 ml/min; see Figure 4.7a (Placing all the data on the same graph produces a tremendous clutter). As Figure 4.7a shows, larger diameters do occur when nitrogen flowrate increases. However, the percent increase is relatively small. Figure 4.7a shows results at a 1000 m/min spinning speed. Figures 4.7b and 4.7c show diameter versus position for higher speeds of 2000 and 2500 m/min. Results are similar to that shown for the 1000 m/min windup speed.

4.4.3 Model Predictions of Rheological Stress, Fiber Temperature, Velocity, and Internal Diameter

Figures 4.8a to 4.8c show some calculated spinline stresses as a function of threadline position. Higher stresses occur for higher nitrogen flowrates. Oh et al. [1998] also calculated that hollow fibers should have higher stresses than comparable solid filaments. Maximum stresses of about 1 x 10^6 Pa, 3 x 10^6 Pa, and 4.5 x 10^6 Pa occur just prior to the windup, respectively for the 1000, 2000, and 2500 m/min cases. Also shown on Figures 4.8 are the stresses for the Phan-Thien model. The Phan-Thien stresses are higher than the Newtonian stresses. This is to be expected since, under the same operating conditions, a viscoelastic fluid requires higher take-up tension than does a Newtonian fluid. Our calculated stresses are similar in magnitude

to on-line stress measurements taken by Matsui [1985] for melt spinning. He used a birefringence technique to determine that for polyester spinning in the range of 4000-6000 m/min, the stress is in the range of 10^6 to 10^7 Pa. Oh et al. [1998] calculated a maximum stress level of about $2x10^7$ Pa for polypropylene hollow fiber spinning from a segmented arc spinneret at speeds up to 350 m/min.

Figures 4.9a to 4.9c show some predicted and experimental (for Figure 4.9a only) fiber temperature profiles for both the Newtonian and the Phan-Thien models. Both Newtonian and Phan-Thien profiles are higher than experimental temperatures. The profiles for the Newtonian model are about 10°C higher than the corresponding profiles for the Phan-Thien model. As can be seen, the higher nitrogen flowrates result in more rapid fiber cooling. Keep in mind that ambient air, not the nitrogen, causes fiber cooling. The higher nitrogen rates produce larger external filament areas that in turn result in increased heat loss. The axial gradients in temperature are about 100°C/m for all windup speeds. In comparison, Gagon and Denn [1981] calculated a temperature gradient of about 380°C/m for high speed melt spinning of polyester. Since both our spinning temperature and spinning speeds are lower than theirs, our lower gradient is as expected.

Figures 4.10a to 4.10c show the fiber velocity as a function of spinning position for several different nitrogen flowrates. For a final speed of 1000 m/min, the Phan-Thien model predicts higher velocity than the Newtonian model all along the threadline. Newtonian predictions follow the same trend as the experimental data. For higher windup speeds, at positions nearer to the spinneret, the Phan-Thien model

predicts a higher velocity than the Newtonian model; the situation reverses at about the midpoint of the threadline. Of course, for each Figure, the final velocity is the same because of the conditions of the experiment (i.e, the windup speed). Unlike melt spinning of solid fibers, a simple application of the continuity equation cannot be used to determine velocity from measured (or calculated) fiber diameters (This calculation would involve equation 4.1 with $d_1 = 0$). Rather, the calculation of velocity involves the full use of the model's two continuity equations, the momentum equation, and the energy equation.

The ratio of the inner diameter to the outer diameter (d_1/d_2) is plotted in Figure 4.11. For the 1.0 ml/min nitrogen rate, the model ratio decreases from about 0.62 to 0.54 along the threadline. For the 1.7 ml/min rate, the ratio decreases from 0.71 to 0.65. For comparison, the figure also shows what would happen if the nitrogen density was assumed to be a constant 0.00113 g/cm^3 (the value at 25°C). Including the effect of nitrogen density change can affect the prediction of d_1/d_2 by nearly 20% for positions near the spinneret. Figure 4.11 applies to a spinning speed of 2500 m/min. Results are similar for speeds of 1000 and 2000 m/min, since the ratio d_1 to d_2 is independent of spinning speed.

4.4.4 Sensitivity to Parameters

As shown previously, the Newtonian model does a good job of predicting the outer diameter of the filament. To test how sensitive the model is to the viscosity, the Newtonian model was run with the viscosity reduced by 20% and 50%. Figure 4.12 shows the results of this test. Though the model is relatively insensitive to small

changes in viscosity, a lower viscosity gives the expected result -- a more rapid attenuation of the threadline.

Figure 4.13 shows the effect on the model of changing the drag. Our value for the leading coefficient in the drag relation was 0.78 (see equation 4.8). This value was compared to a coefficient of 0.37, a value originally determined by Matsui [1976]. The leading coefficient was also doubled to provide another comparison. As can be seen, changing the coefficient does not greatly affect the goodness of fit of the model to the data. The small effect is expected since, for our spinning speed range, drag is not the dominant force in the momentum equation (At 6000m/min, drag would be dominant; see Ziabicki and Kawai [1985]). Figure 4.13 applies to our highest spinning speed of 2500 m/min. At lower speeds, the affect of drag is even lower.

For the 1000 m/min case, Figure 4.14 shows what happens when the heat transfer coefficient h is reduced by 25%. This reduction has a more significant effect on the model than a reduction in either viscosity or drag coefficient. This is to be expected, since the quenching of the filament is a dominant occurrence in the melt spinning of fibers. Fiber diameter changes more slowly when heat transfer is reduced, since the viscosity at any z position is higher. Figure 4.15 shows the predicted fiber temperature resulting from the reduction in h. As expected, temperature changes more slowly when heat transfer is reduced.

The effects of changing E and X are shown in Figure 4.16. When E = X = 0, the Maxwell model is recovered, and the resulting fit is not as good as with the base case values for E and X. Increasing E and/or increasing X results in a better fit of the

Phan-Thien model to the data. Figure 4.17 shows that fit improves as G is increased with the Maxwell model (with E = X = 0). This improvement is as expected, since increasing G causes Maxwell model to approach the Newtonian model (which fits our data quite well).

4.5 COMPARISON OF EXPERIMENTAL RESULTS WITH THE MODEL AT LOW POLYMER THROUGHPUT

The accuracy of the model was tested with a low polymer throughput of 0.66 g/min. The experimental data were obtained using spinneret B. The spinneret dimensions and experimental conditions that were used are shown in Table 4.1. The effect of starting position was also studied on the accuracy of the fits at low polymer throughput. Figures 4.18 and 4.19 show the effect of starting position on Newtonian fits for solid fibers and hollow fibers (Q_n = 1.7 ml/min) spun at 690 m/min. Only two positions were considered, $z^* = 0$ and $z^* = 25.4$ mm (the die swell was negligible for this spinneret). Because of the large size of the polymer annulus (7.01 mm), the transition from die flow to extensional flow took longer to stabilize, and better fits were obtained when models were started 25.4 mm below the spinneret. In the rest of the chapter, simulations with spinneret B were started at z_0 = 25.4 mm. The initial conditions (outer diameter and temperature) were determined using high-speed photography and infrared camera at 25.4 mm below the spinneret.

Figures 4.20 compare actual experimental data with the prediction of the Newtonian and Phan-Thien models for a take-up speed of 330 m/min. As was

observed for large polymer throughput, the Newtonian model does a very good job at fitting the data for solid and hollow fibers, while the Phan-Thien model predicts a faster attenuation. Figures 4.21a to 4.21c show the experimental and predicted diameter profiles for a take-up speed of 690 m/min. For nitrogen rates up to 1.7 ml/min, the Newtonian model fits the data very well. But for the highest nitrogen flowrate (3.2 ml/min), the experimental outer diameter attenuates much faster than the diameter predicted by the Newtonian model (Figure 4.21c). Large nitrogen rates increase the fiber outside surface area. Thus, with high nitrogen flowrates, the fiber cools down faster. At this point, for the highest nitrogen flowrate tested, it is reasonable to assume that the polymer stream freezes somewhere along the threadline. The position where the solidifying filament stops attenuating is the freezing point. It is mainly due to stress-induced crystallization [Ahmed, 1982; Ziabicki and Kawai, 1985]. In melt spinning, crystallization occurs non-isothermally under molecular orientation. Crystallization is usually a very strong function of temperature, but under stress, crystallization depends also on molecular orientation. The molecular orientation in a spinning fiber is mostly a function of tensile stress at the freezing point. Since both the rate of cooling and the tensile stress at crystallization point change in a very complex manner, it is very difficult to predict the position of the freezing point. In order to account for the on-line crystallization, model calculations were stopped at the assumed freezing position by using shorter threadlines. Figure 4.21c shows the effect of the position of the freezing point on diameter profiles for a take-up speed of 690 m/min and nitrogen flowrate of 3.2

ml/min. The freezing position was varied from 140 cm to 80 cm below the spinneret. The freezing point assumed at 80 cm below the die gave the best fit. It is interesting to note that in Chapter 3, for the same set of experimental data points, on-line crystallization was found to occur around 65 cm below the spinneret, which is very close to the predicted value of 80cm.

Figures 4.22a to 4.22c represent model (Newtonian and Phan-Thien) and experimental diameter profiles for solid and hollow fibers spun at a final speed of 940 m/min. The Newtonian model still provides the best fit for the solid filament, but does not fit very well the experimental data of hollow fibers. Since the final take-up speed is larger than the one presented in Figures 4.21, the stress acting on the fibers is larger. As we observed earlier, high stress combined with rapid quenching is responsible for stress-induced crystallization, and the model calculations must be stopped at the freezing position. In Figure 4.22b, the experimental data (1.7 ml/min nitrogen) were fitted assuming a freezing point 90 cm below the spinneret. For larger gas flowrates, hollow fibers cool down faster and thus reach their freezing point earlier. Fibers produced at the largest gas rate (3.2 ml/min) freeze at z' = 50 cm (Figure 4.22c). An identical freezing point was found in Chapter 3 for this set of data.

The effects of nitrogen on fiber temperature predicted by the Newtonian model are shown in Figures 4.23a and 4.23b, respectively for windup speeds of 330 and 940 m/min. Figure 4.23a also shows experimental data. Even though experimental data exhibit cooler temperatures than predicted by the model, experimental data and the Newtonian model predict the same effect of nitrogen on

temperature. As was observed for larger polymer throughput, hollow fibers cool down much faster than solid fibers at both speeds. Hollow fibers spun with a windup speed of 940 m/min reach their final temperature at the assumed freezing position (90 cm and 50 cm respectively for 1.7 and 3.2 ml/min nitrogen rate).

Figures 4.24a and 4.24b show the effect of nitrogen flowrate on velocity profiles predicted by the Newtonian model at 330 and 940 m/min windup speed. Figure 4.24a also shows experimental data. Experimental data and model exhibit the same effect of nitrogen on fiber velocity. At 330 m/min, no major difference can be observed between the three profiles. At higher take-up speed, we obtain the same results that were obtained for large polymer flowrate with spinneret A: for large nitrogen flowrates, fibers reach their final velocity sooner. Fibers actually reach their final velocity at the freezing positions that were assumed earlier to fit the diameter data points.

Figure 4.25 shows the effect of the threadline length on the ration d_1 / d_2. As expected, the ratio reaches its final value sooner at high speed (where on-line freezing points were assumed).

4.6 CONCLUSIONS

In the melt spinning of hollow fibers, the effects of heat transfer (cooling) on the threadline are more important than the choice of constitutive equation. Hence, a Newtonian model fits the data quite well. However, more complex constitutive equations are useful for stress predictions along the threadline. On-line measurements

of outer diameter illustrate how increased nitrogen (lumen fluid) rate increases the outer diameter. Both nitrogen and polymer continuity equations are needed to predict the inner diameter. The effect of temperature on nitrogen density must be considered. Hollow fibers presented on-line freezing behavior when spun with low polymer rate, high nitrogen rate, and high windup speed.

4.7 NOMENCLATURE

C_f = air drag coefficient
C_p = polymer heat capacity, J/kg.K
d = diameter of solid fiber, μm
d_1 = inside diameter of fiber, μm
d_2 = outside diameter of fiber, μm
E = Phan-Thien and Tanner model parameter related to stress saturation at high extension rates
F_o = initial force at the spinneret
g = gravitational acceleration, m/s^2
G_i = shear modulus, Pa
h = convective heat transfer coefficient, $W/m^2.K$
i = number of relaxation time
K_i = Phan-Thien and Tanner model variable
m = empirical exponent in equation 4.12
m_n = nitrogen mass rate, g/min
m_p= polymer mass rate, g/min
M_w = weight average molecular weight, g/mol
ΔP = the pressure difference between two phases, Pa
Q_p = volumetric polymer flow rate, cm^3/min
Q_n = volumetric nitrogen flow rate, cm^3/min
R_1, R_2 = radii of curvature of the interface between the two phases, m
Re = Reynolds number (see equation 4.9)
T = polymer temperature, °C
T_a = ambient air temperature, °C
v = fiber velocity, m/min
X = Phan-Thien and Tanner model parameter related to viscous shear thinning
z = axial position in model, cm
z = measured axial position below spinneret, cm

Greek letters

γ = empirical constant in equation 4.12, or surface energy in equation 4.3, N/m
$\bar{\eta}$ = Trouton elongational viscosity
η = dynamic shear viscosity, Pa.s
λ_i = stress relaxation time, s
ν_a = kinematic viscosity of air, m^2/s
ρ_a= air density, g/cm^3

ρ_n = nitrogen density, g/cm^3
ρ_p = polymer density, g/cm^3
τ^{zz}, τ^{xx} = components of the extra stress in the spinning and transverse directions, respectively, Pa

4.8 REFERENCES

A. W. Adamson, *Physical Chemistry of Surfaces*, 2nd edition, Interscience, New York, pp. 3-6 (1967).

M. Ahmed, *Polypropylene Fibers – Science and Technology*, Elsevier Scientific Publishing Company, New York (1982).

B. Baum; W. Holley; R. A. White, "Hollow Fibres in Reverse Osmosis, Dialysis, and Ultrafiltration", in *Membrane Separation Processes* by P. Meares, Elsevier, New York, pp. 187-227 (1976).

J. Bicerano, *Prediction of Polymer Properties*, 2nd edition, Marcel Dekker, New York, p. 195 (1996).

S. D. Cooper, American Petrofina, Deer Park, TX, private communication (1987).

B. D. Freeman; M. M. Denn; R. Keunings; G. E. Molau; J. Ramos, "Profile Development in Drawn Hollow Tubes", *J. Polym. Eng.*, ***6***, 172-186 (1986).

D. K. Gagon; M. M. Denn, "Computer Simulation of Steady Polymer Melt Spinning", *Polym. Eng. Sci.*, ***21***, 844 (1981).

S. Kase; T. Matsuo, "Studies on Melt Spinning. I. Fundamental Equations on the Dynamics of Melt Spinning,", *J. Polym. Sci.*, ***A-3***, 2541 (1965).

B. Majumdar; R. L. Shambaugh, "Air Drag on Filaments in the Melt Blowing Process", *J. Rheol.*, ***34***, 591-601 (1990).

M. A. Matovich; J. R. A. Pearson, "Spinning a Molten Threadline: Steady State Isothermal Viscous Flows", *Ind. Eng. Chem. Fund.*, ***8*** (3), 512 (1969).

M. Matsui, "Air Drag on a Continuous Filament in Melt Spinning", *Trans. Soc. Rheol.*, ***20*** (3), 465 (1976).

M. Matsui, "Fiber Formation Process in High-Speed Spinning of Polyethylene Terephthalate", in *High-Speed Fiber Spinning* by A. Ziabicki and H. Kawai, Wiley-Interscience, New York, pp.141-143 (1985).

T. H. Oh; M. S. Lee; S. Y. Kim; H. J. Shim, "Studies on Melt-Spinning Process of Hollow Fibers", *J. Appl. Polym. Sci.*, ***68***, 1209-1217 (1998).

N. Phan-Thien, "A Nonlinear Network Viscoelastic Model", *J. Rheol.*, ***22***(3), 259 (1978).

N. B. Vargaftik, *Handbook of Physical Properties of Liquids and Gases – Pure Substances and Mixtures*, 2nd edition, Hemisphere Publishing, New York (1975).

M. A. J. Uyttendaele; R. L. Shambaugh, "Melt Blowing: General Equation Development and Experimental Verification", *AIChE J.*, ***36*** (2), 175-186 (1990).

A. Ziabicki, Mechanical Aspects of Fibre Spinning Process in Molten Polymers: 3. Tensile Force and Stress, *Kolloid-Z*, ***175***, 14 (1961).

A. Ziabicki, *Fundamentals of Fibre Formation*, Wiley, New York (1976).

A. Ziabicki; H. Kawai, *High-Speed Fiber Spinning: Science and Engineering Aspects,* Wiley, New York (1985).

A. Ziabicki; K. Kedzierska, "Mechanical Aspects of Fibre Spinning Process in Molten Polymers: 1. Stream Diameter and Velocity Distribution Along the Spinning Way", *Kolloid-Z*, ***171***, 51 (1960).

----------, "Mechanical Aspects of Fibre Spinning Process in Molten Polymers: 2. Stream Broadening after the Exit from the Channel of Spinneret", *Kolloid-Z*, ***171***, 111 (1961).

	SPINNERET A	SPINNERET B
OD of polymer annulus (mm)	1.98	7.01
ID of polymer annulus (mm)	1.22	3.78
D of nitrogen capillary (mm)	0.76	1.00
Polymer flowrate (g/min)	2.33	0.66
Fiber speed (m/min)	1000, 2000, and 2500	330, 690, and 940
Nitrogen flowrate (ml/min)	0, 1, and 1.7	0, 1.7, and 3.2

Table 4.1: Experimental conditions used to produce fibers with spinnerets A and B.

Velocity (m/min)	0
Temperature (K)	298
Density *	$\rho = \frac{363.06}{T^{1.005}}$
Viscosity *	$\mu = 10^{-5}(0.147 + 0.0069T - 4.449.10^{-6}T^{2} + 1.614.10^{-9}T^{3})$
Thermal conductivity *	$k_a = 0.000337T^{0.761}$

Table 4.2: Surrounding air properties
(*) : Correlations developed by Uyttendale (1990) that fit the best Kreith (1965) and Schlichting (1979) density, viscosity and thermal conductivity data at 1 atm.

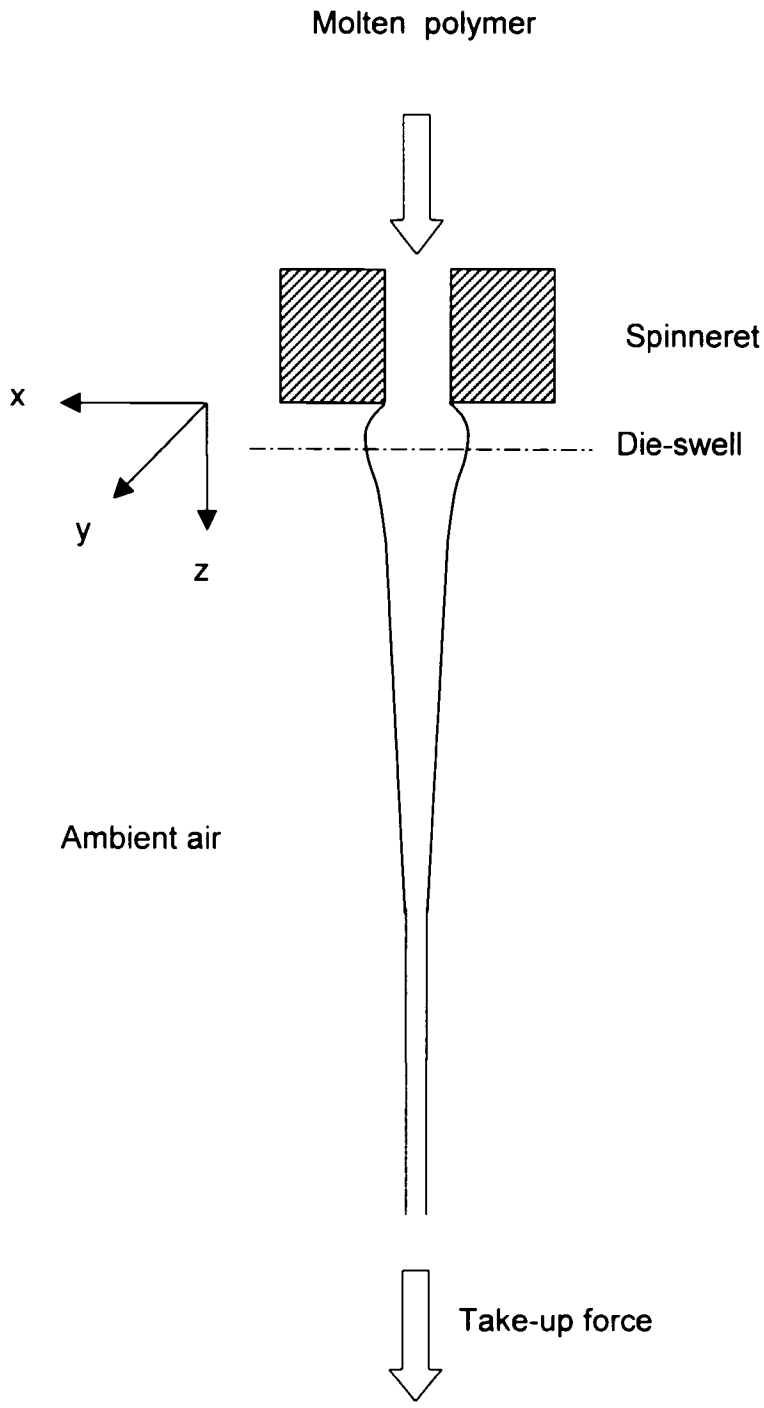

Figure 4.1: Schematic of conventional melt spinning.

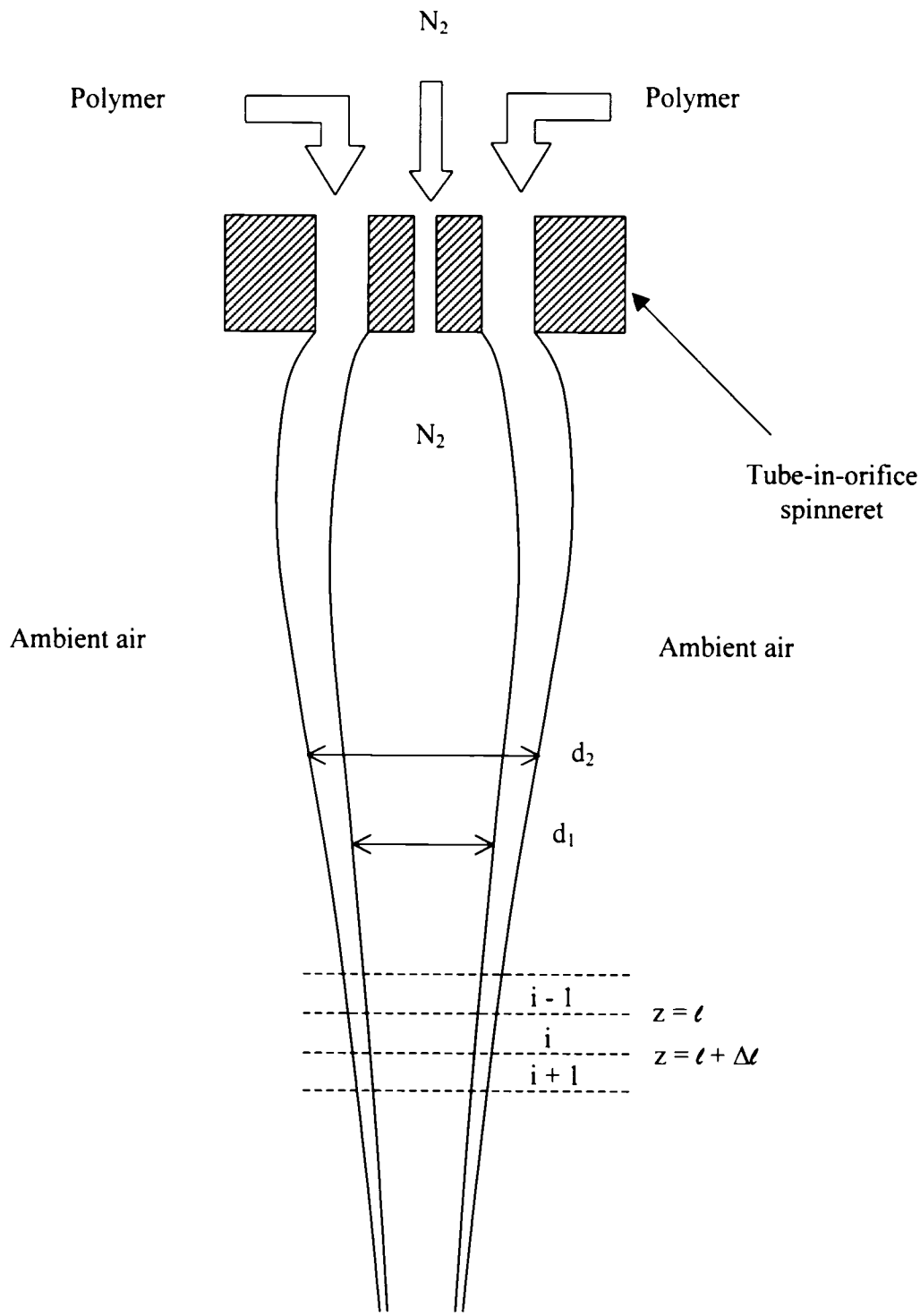

Figure 4.2: Hollow Fiber Spinline.

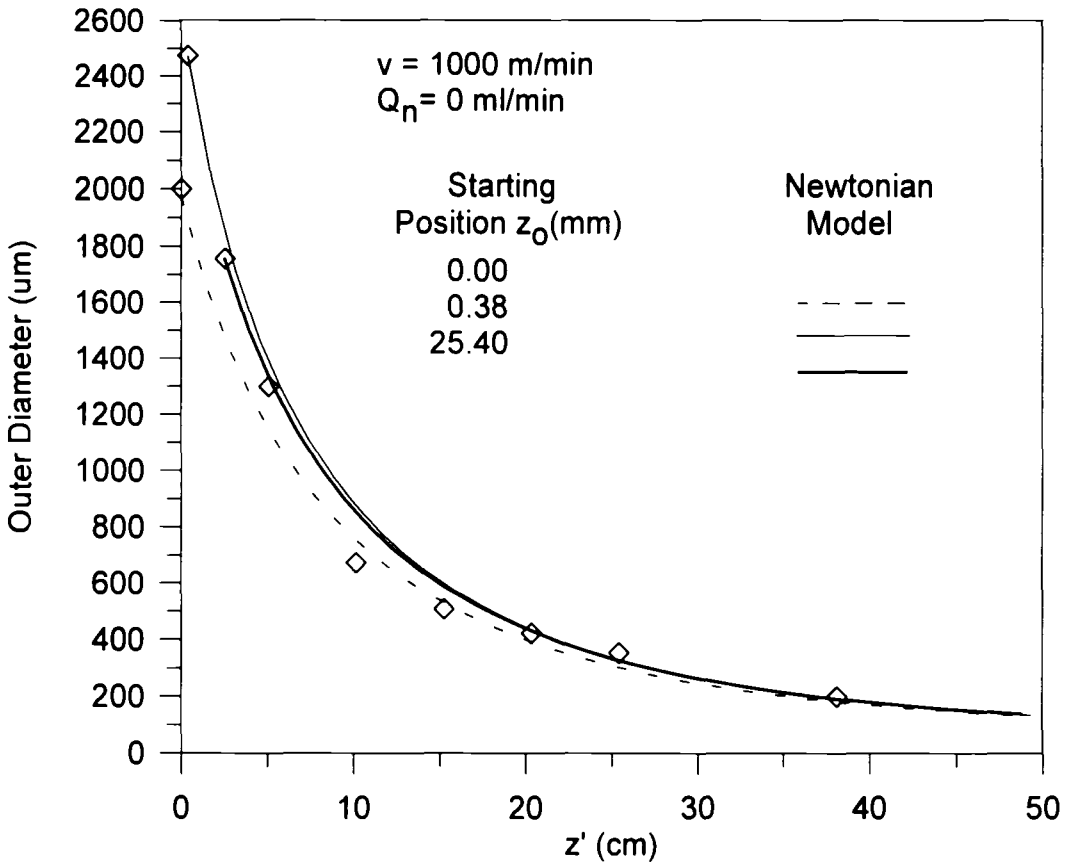

Figure 4.3. Effect of starting position on the results of the model for spinneret A.

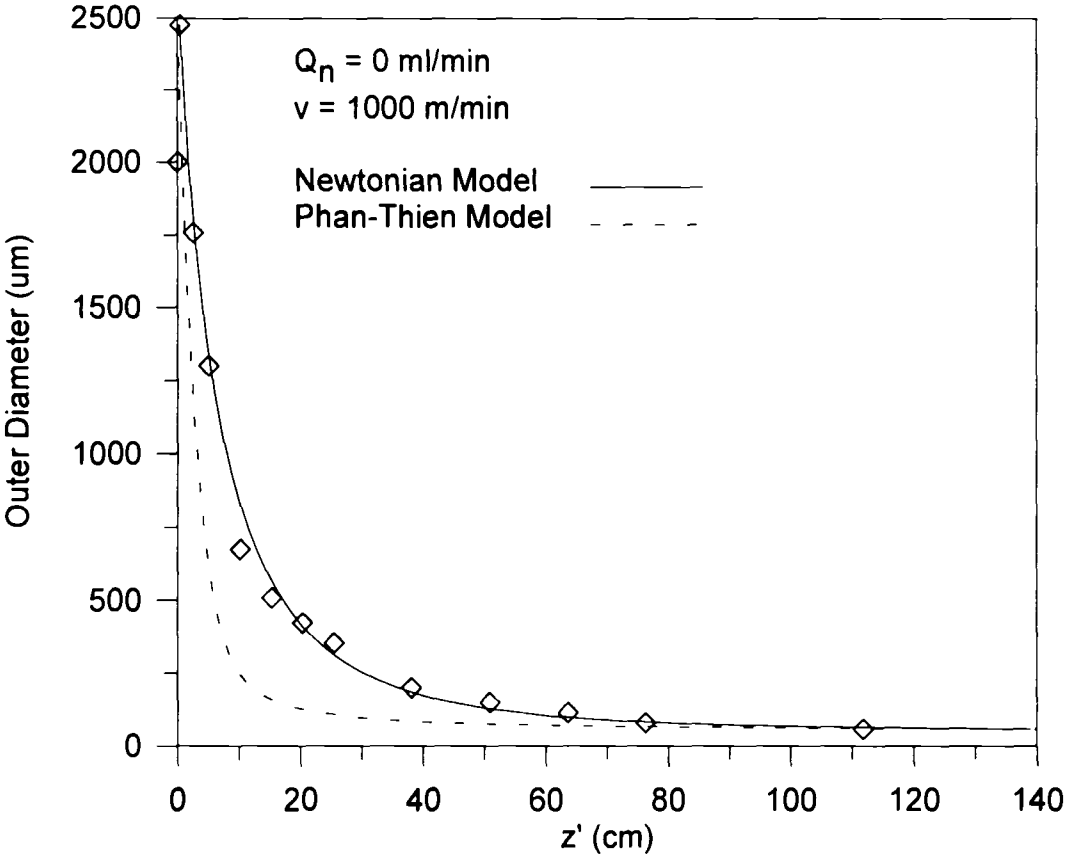

Figure 4.4a: Experimental data compared to the predictions of the Newtonian and Phan-Thien models. The nitrogen rate was 0 ml/min, and the windup speed was 1000 m/min.

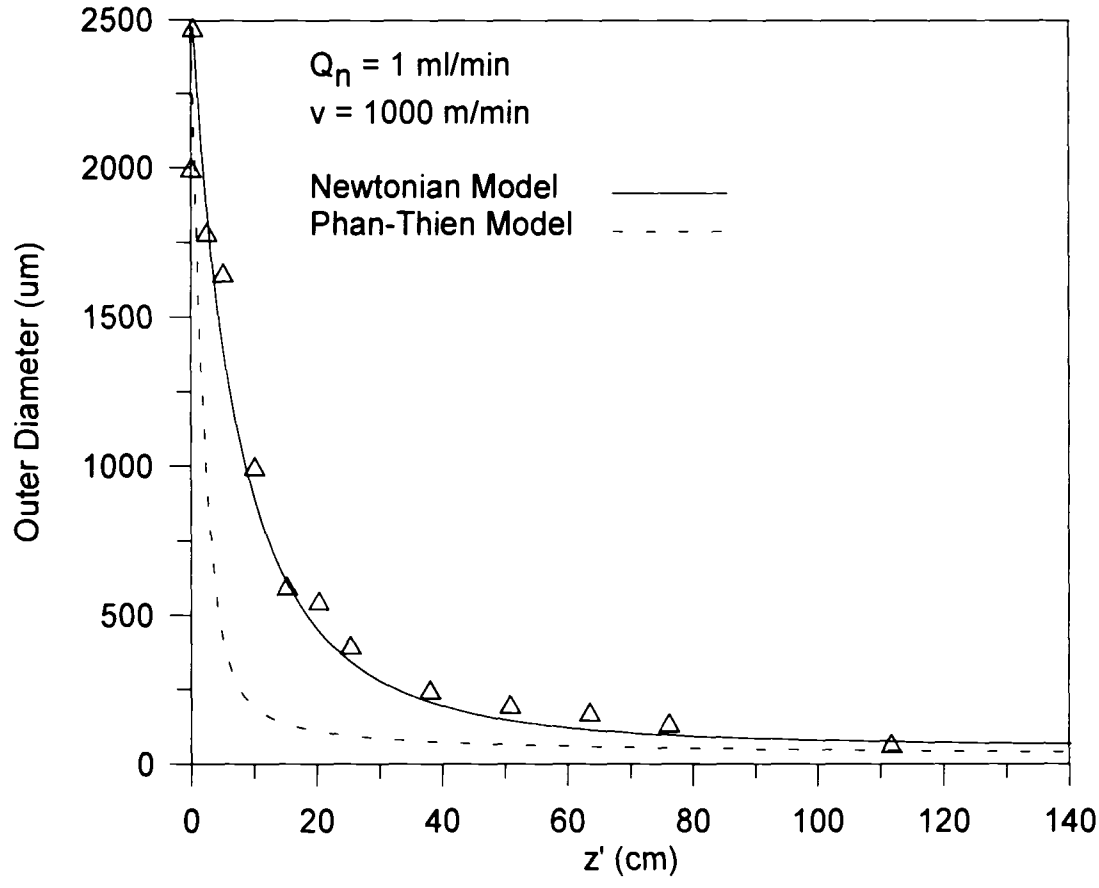

Figure 4.4b: The same comparison as in Fig. 4.4a, except the nitrogen rate was 1 ml/min.

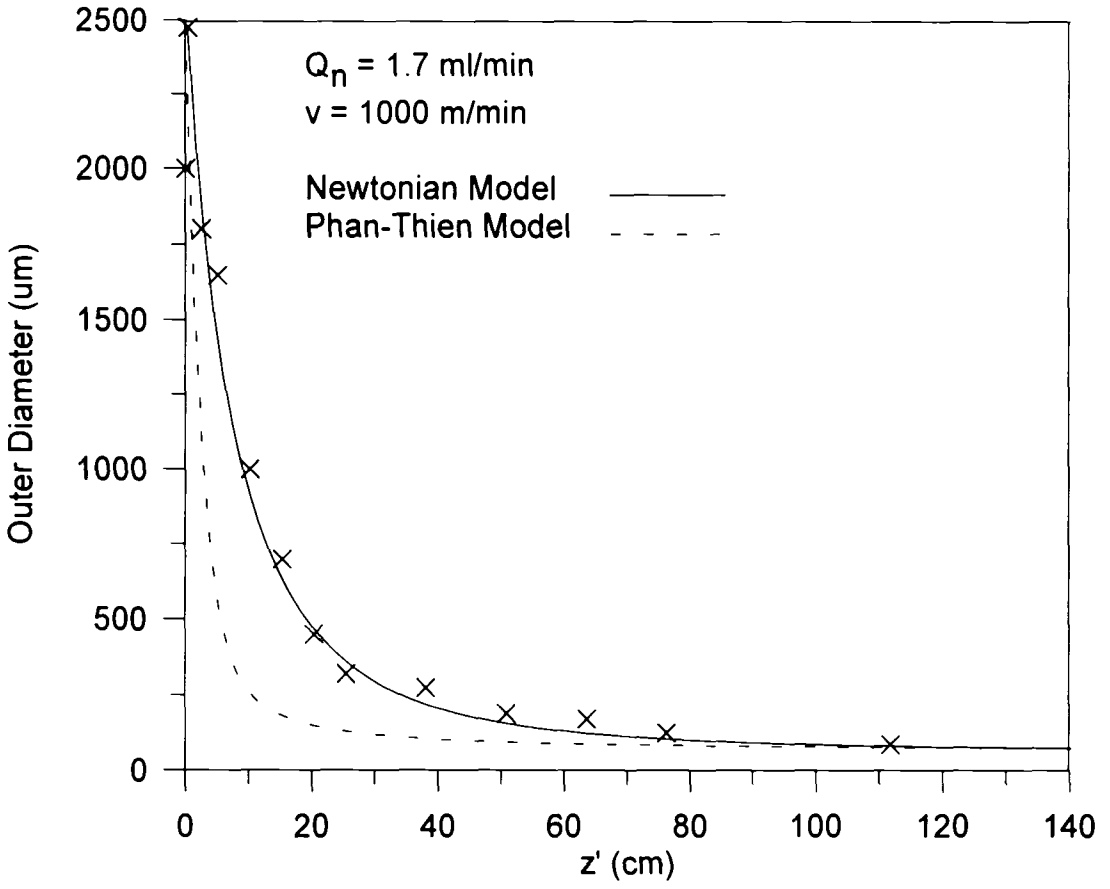

Figure 4.4c: The same comparison as in Fig. 4.4a, except the nitrogen rate was 1.7 ml/min.

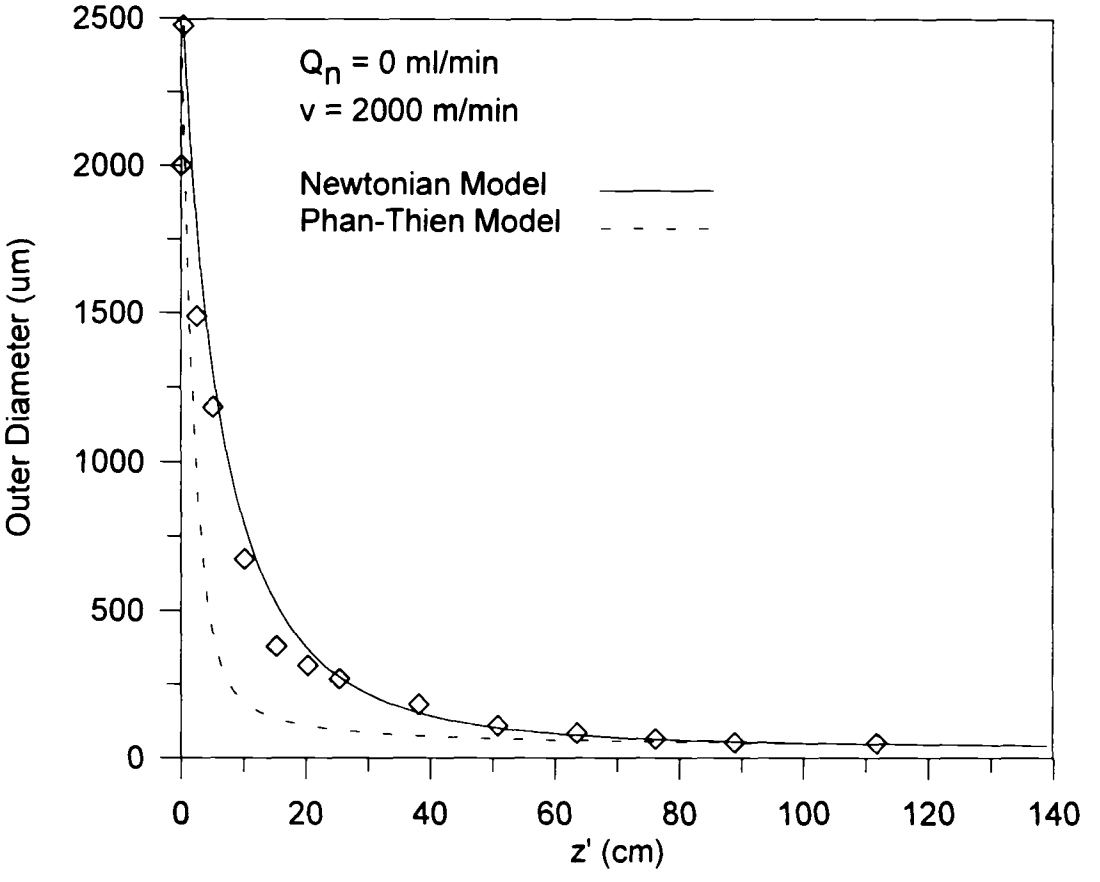

Figure 4.5a: Experimental data compared to the predictions of the Newtonian and Phan-Thien models. Results are shown for a mid-range windup speed of 2000 m/min and a nitrogen rate of 0 ml/min.

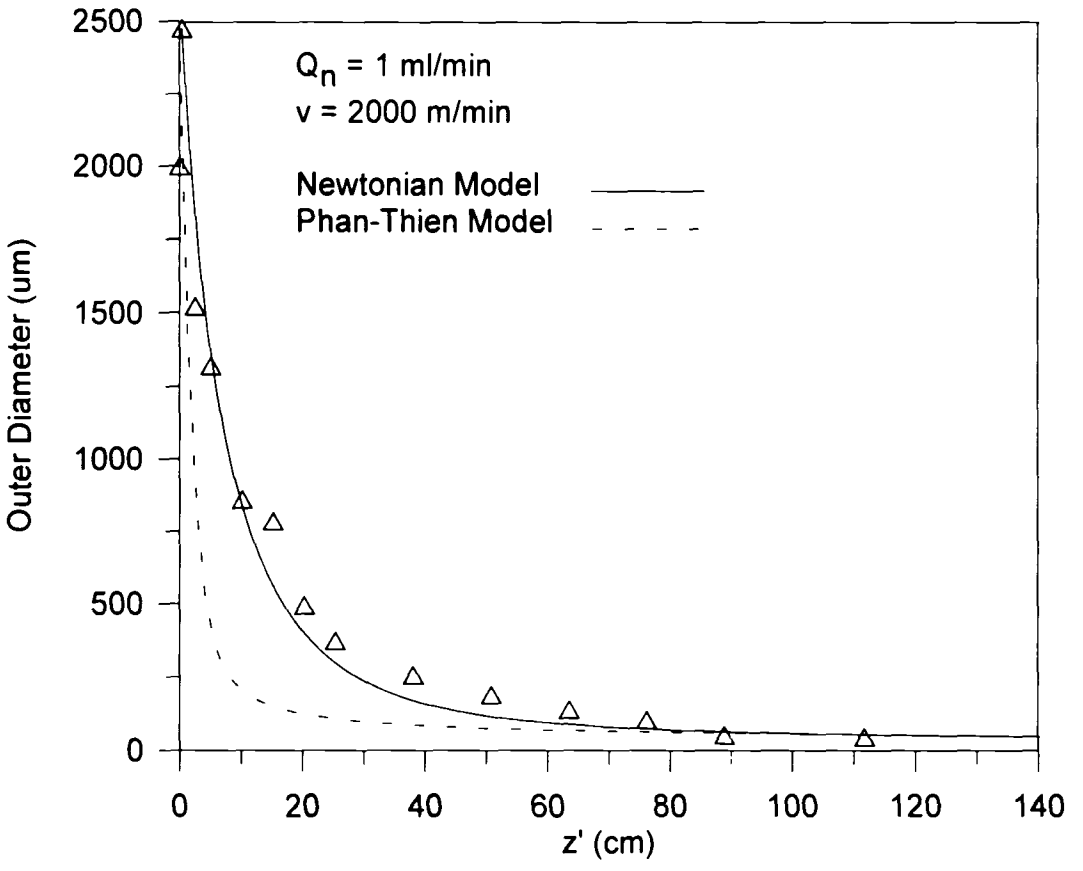

Figure 4.5b: The same comparison as in Fig. 4.5a, except the nitrogen rate is 1 ml/min.

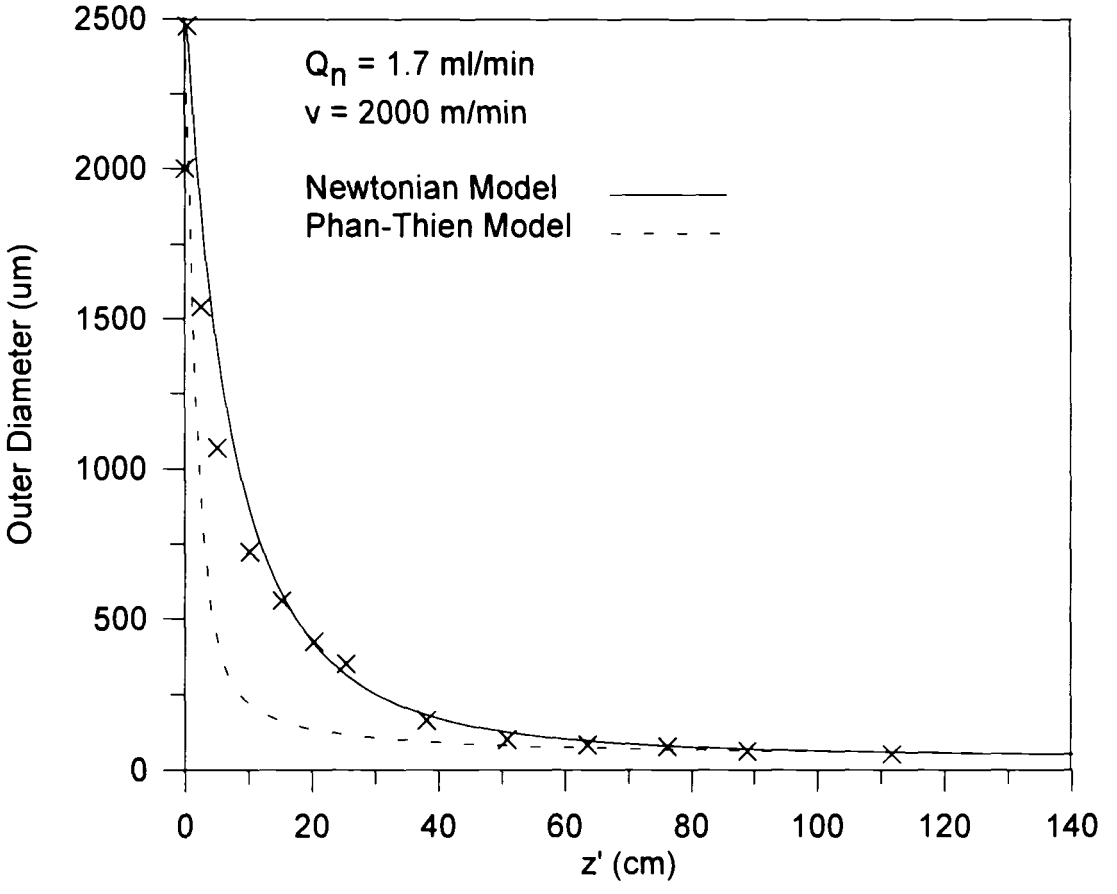

Figure 4.5c: The same comparison as in Fig. 4.5a, except the nitrogen rate is 1.7 ml/min.

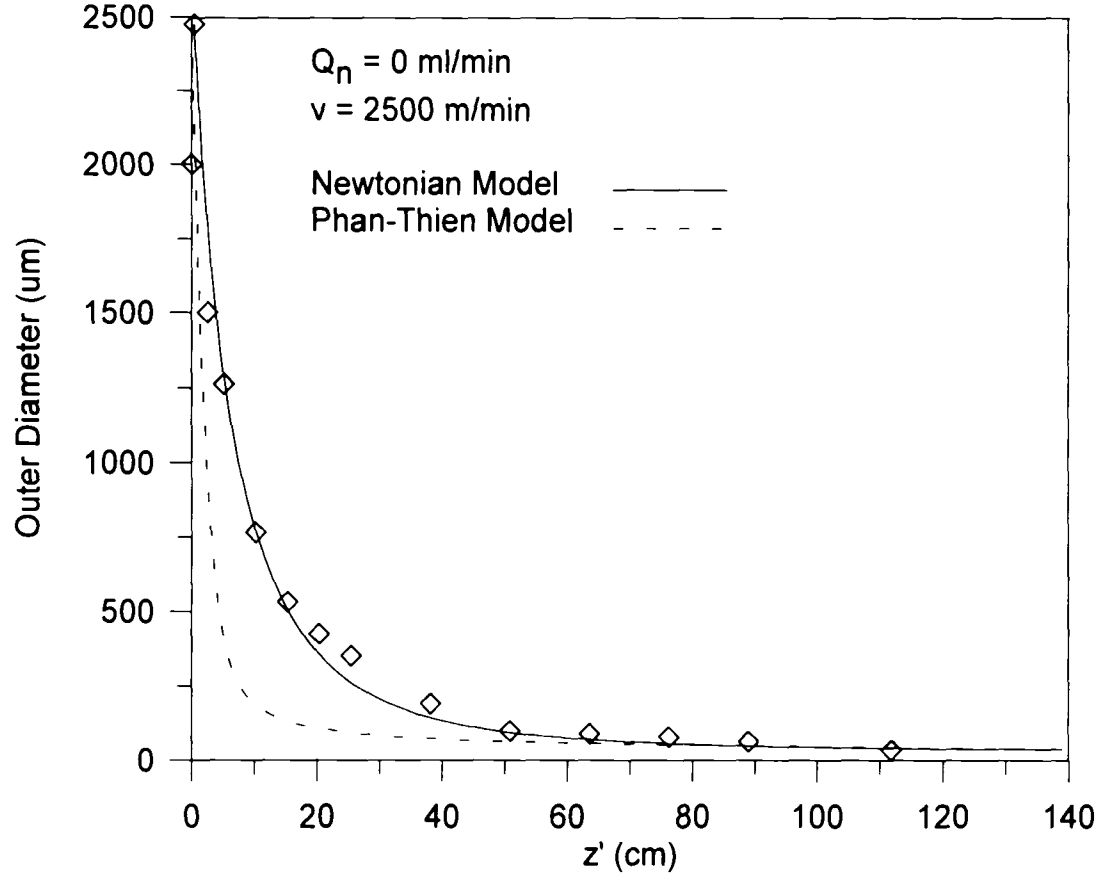

Figure 4.6a: Experimental data compared to the predictions of the Newtonian and Phan-Thien models. Results are shown for a high windup speed of 2500 m/min and a nitrogen rate of 0 ml/min.

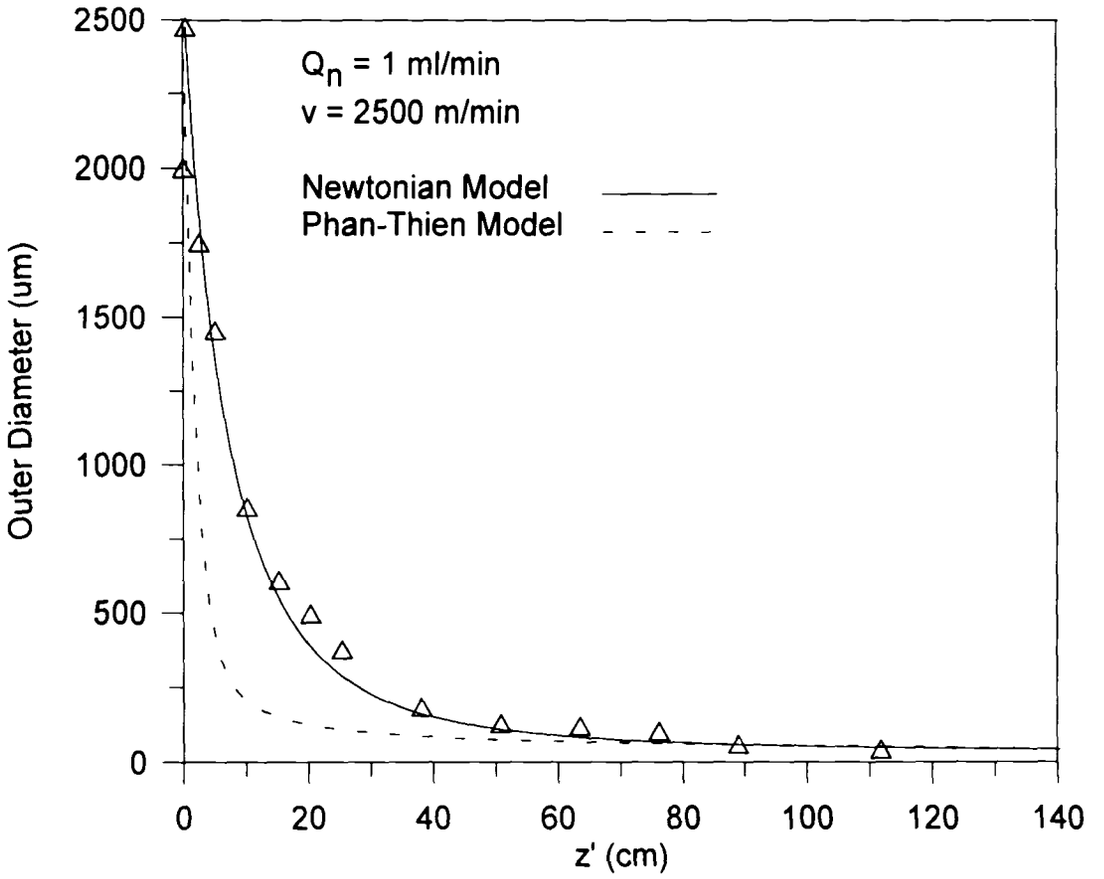

Figure 4.6b: The same comparison as in Fig. 4.6a, except the nitrogen rate is 1 ml/min.

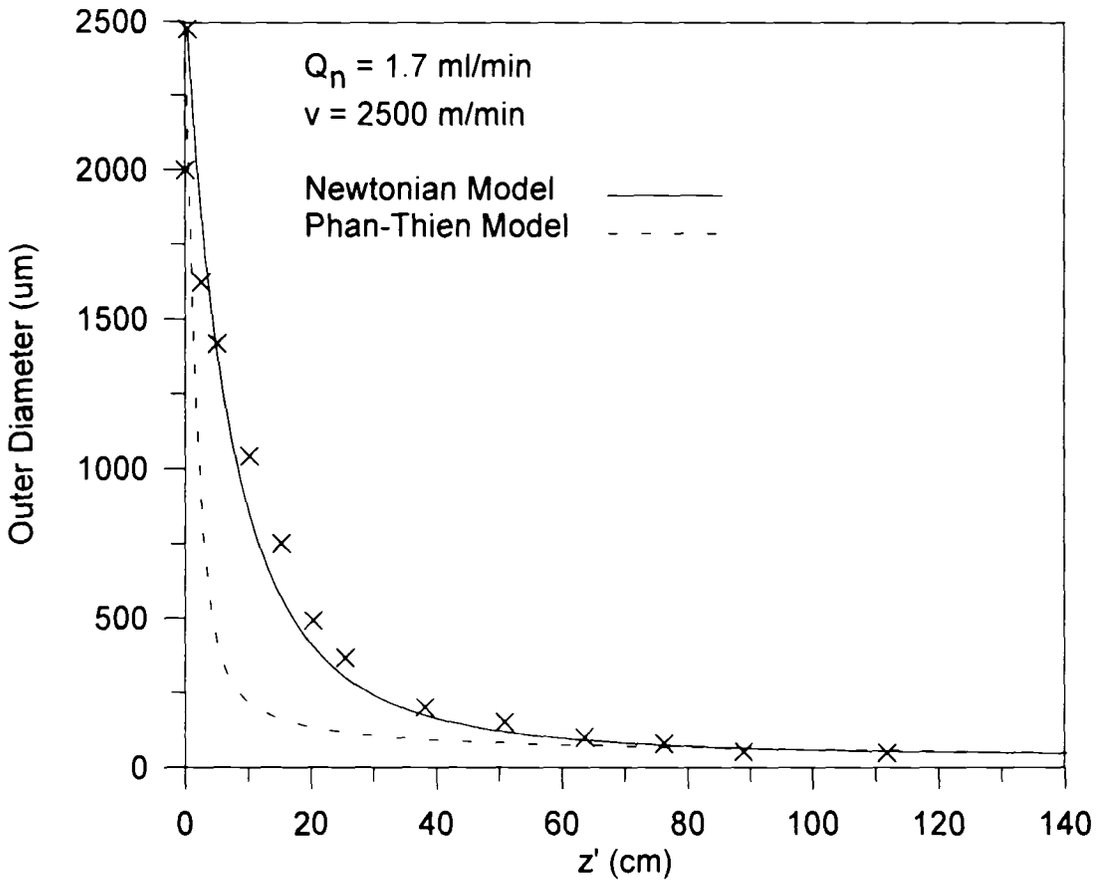

Figure 4.6c: The same comparison as in Fig. 4.6a, except the nitrogen rate is 1.7 ml/min.

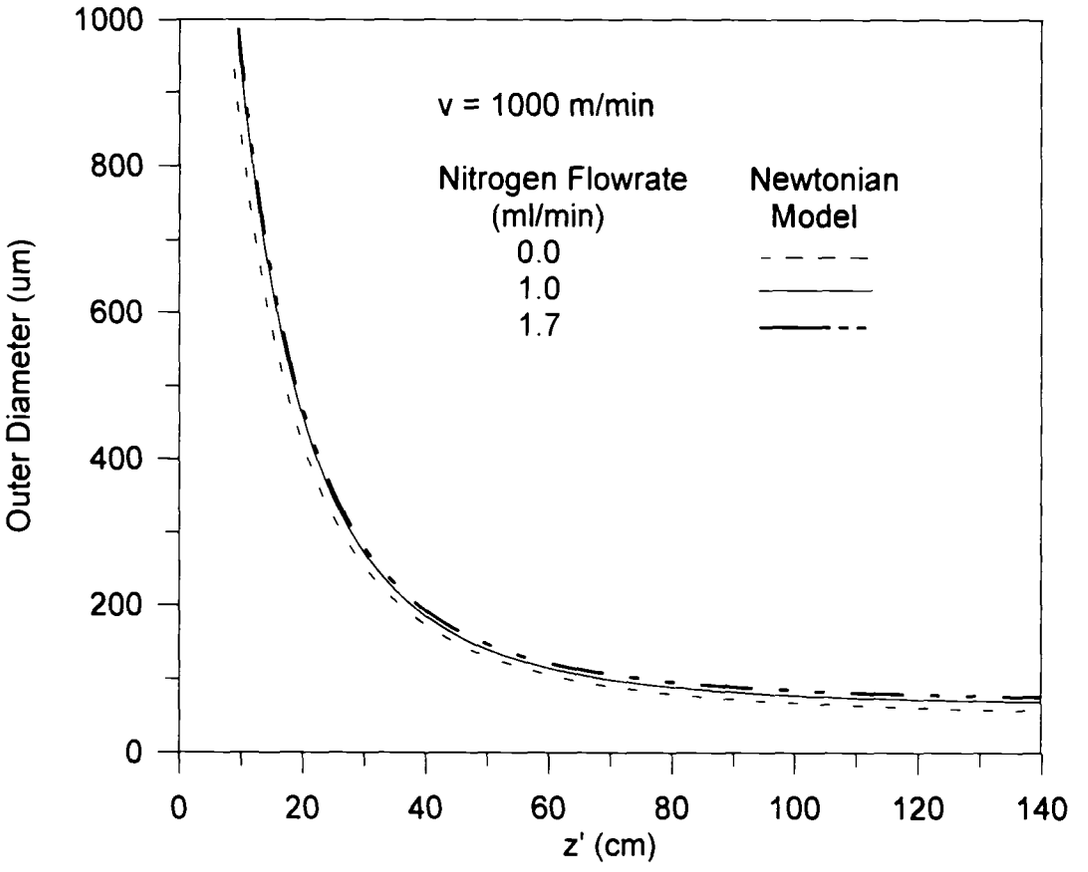

Figure 4.7a: Model predictions of the effect of nitrogen flowrate on fiber diameter at a windup speed of 1000 m/min.

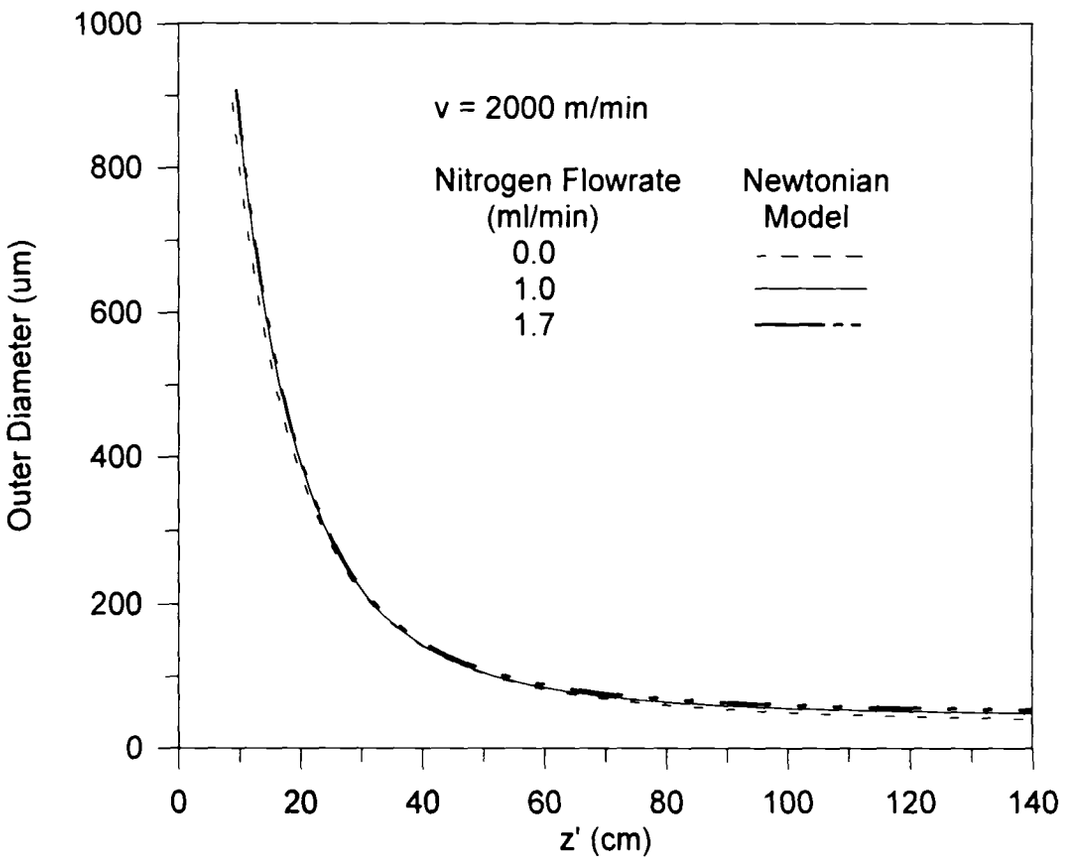

Figure 4.7b: The same comparison as in Figure 4.7a, except the windup speed is 2000m/min.

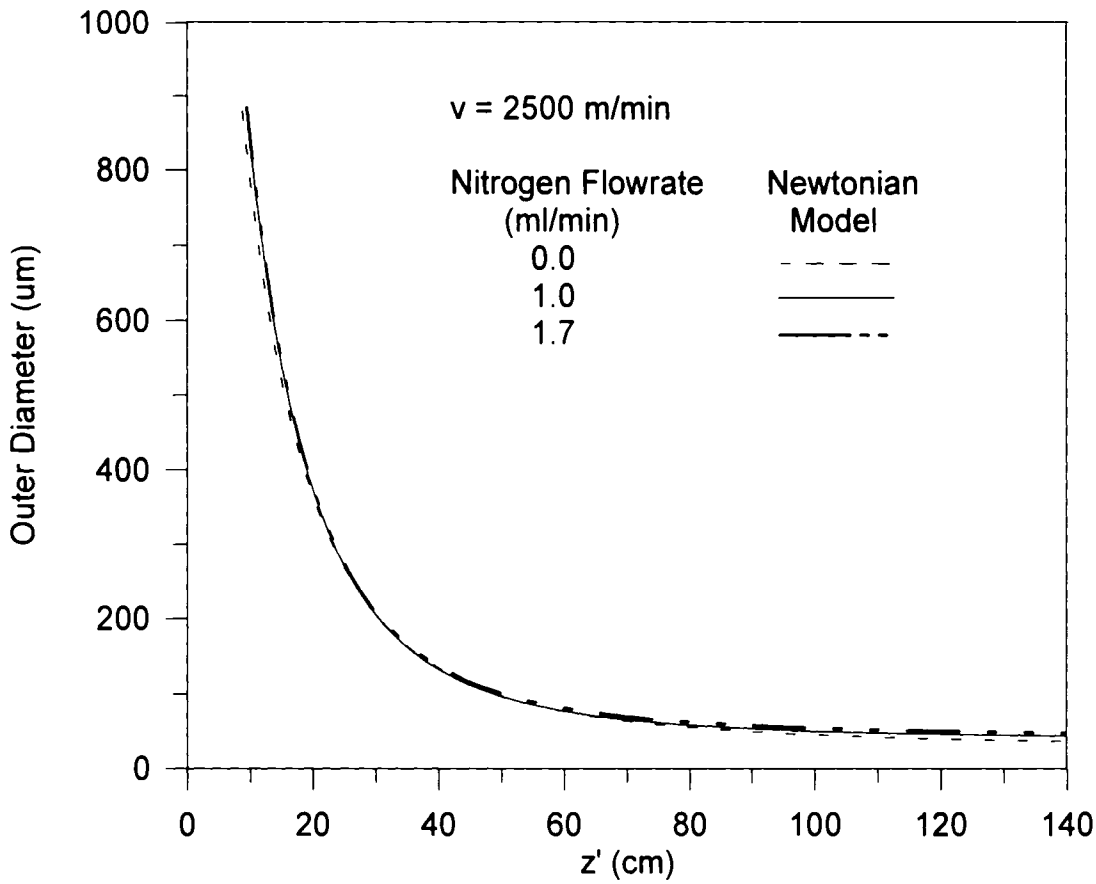

Figure 4.7c: The same comparison as in Figure 4.7a, except the windup speed is 2500m/min.

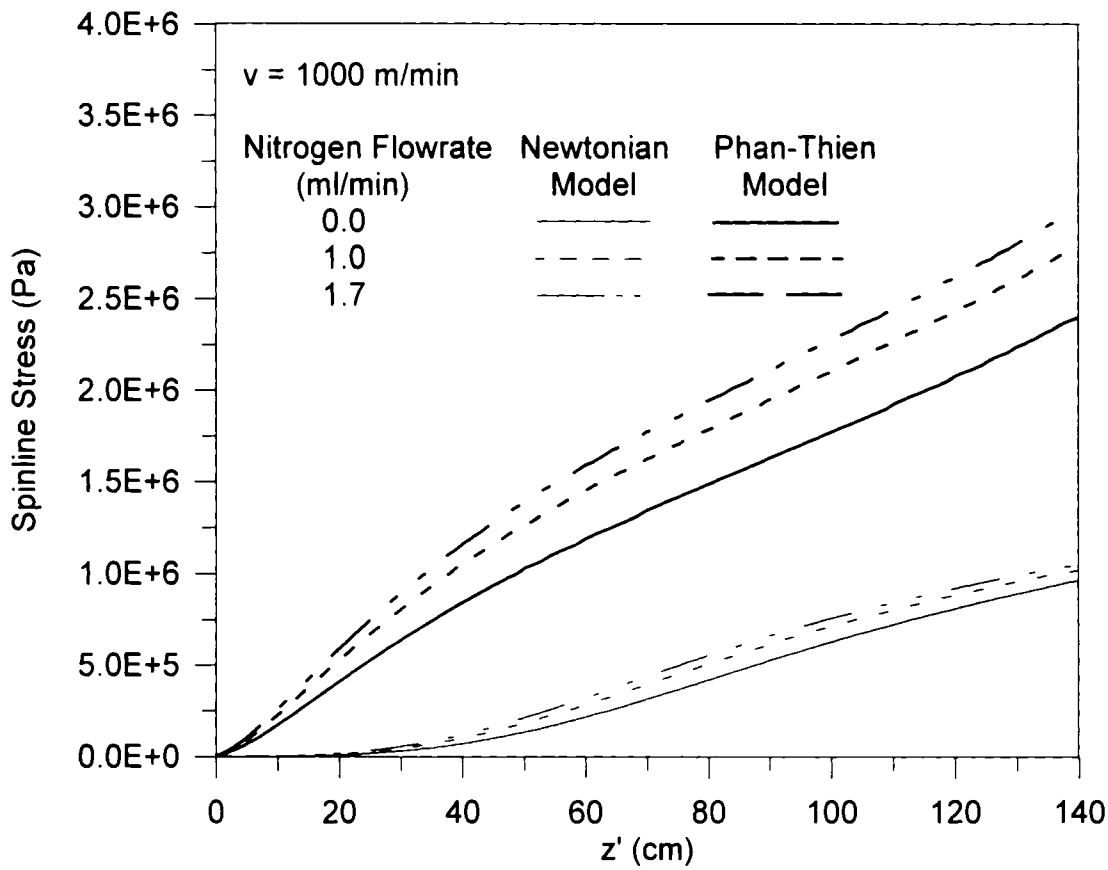

Figure 4.8a: The effect of nitrogen flowrate on rheological stress for both the Newtonian and Phan-Thien models at a windup speed of 1000 m/min.

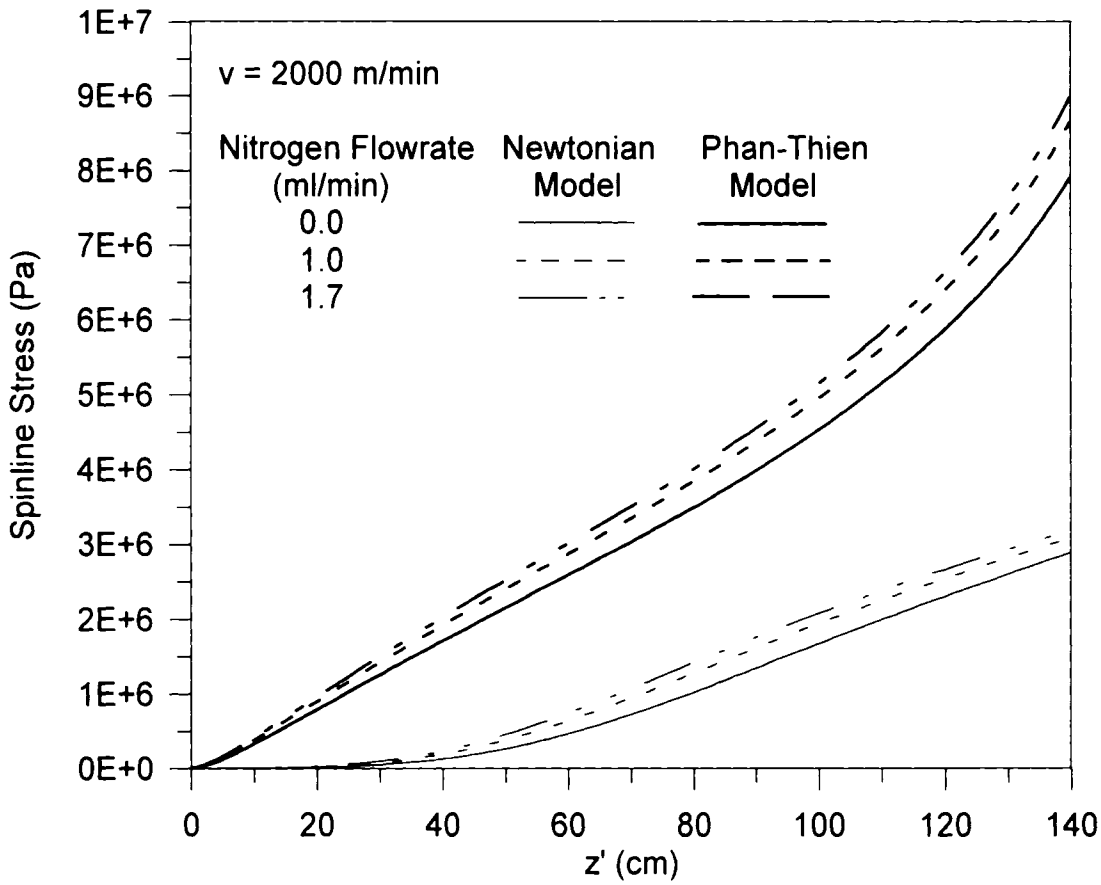

Figure 4.8b: The effect of nitrogen flowrate on rheological stress for both the Newtonian and Phan-Thien models at a windup speed of 2000 m/min.

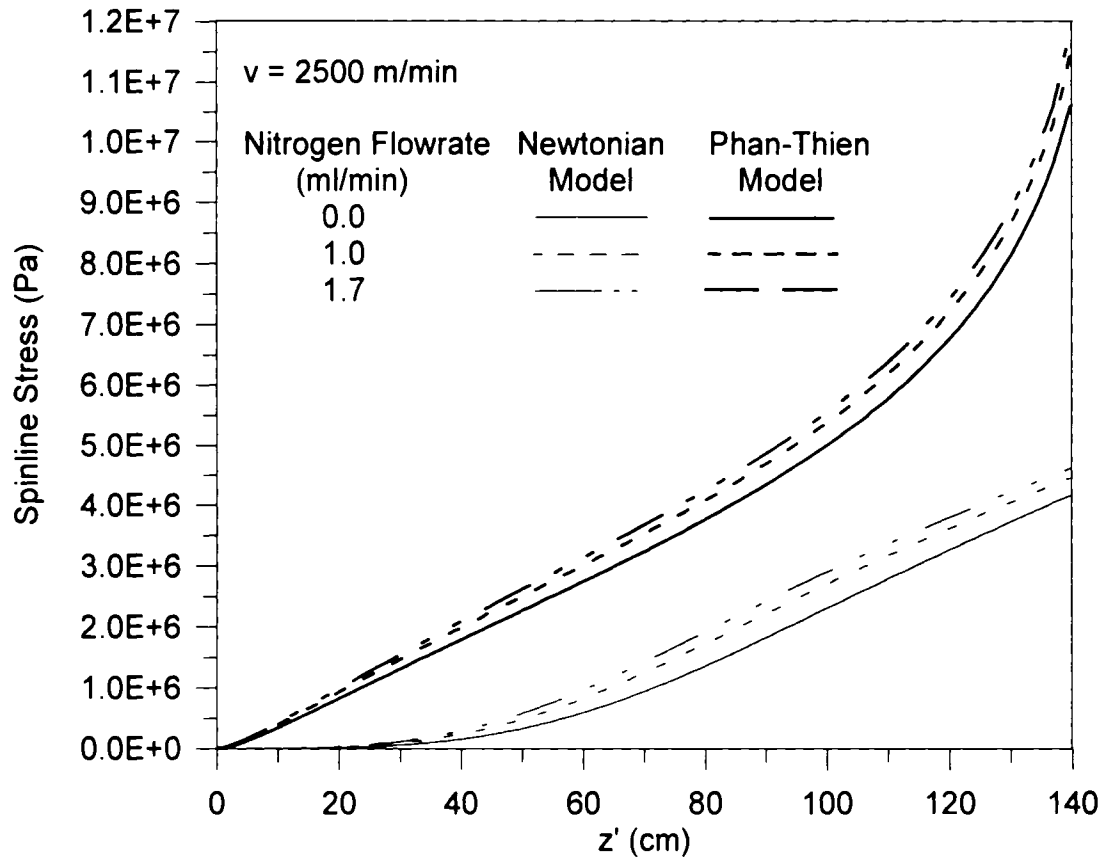

Figure 4.8c: The effect of nitrogen flowrate on rheological stress for both the Newtonian and Phan-Thien models.

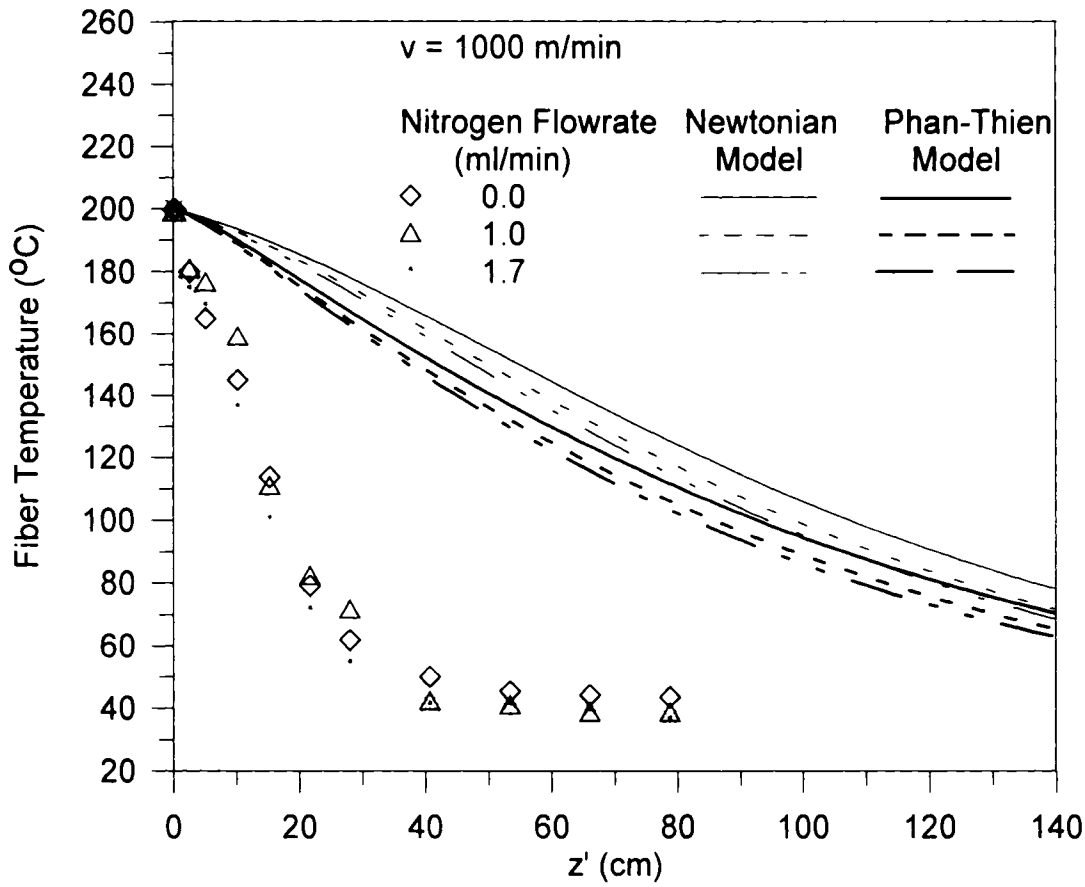

Figure 4.9a: Effect of nitrogen flowrate on fiber temperature for a final take-up speed of 1000 m/min. Symbols represent experimental data points.

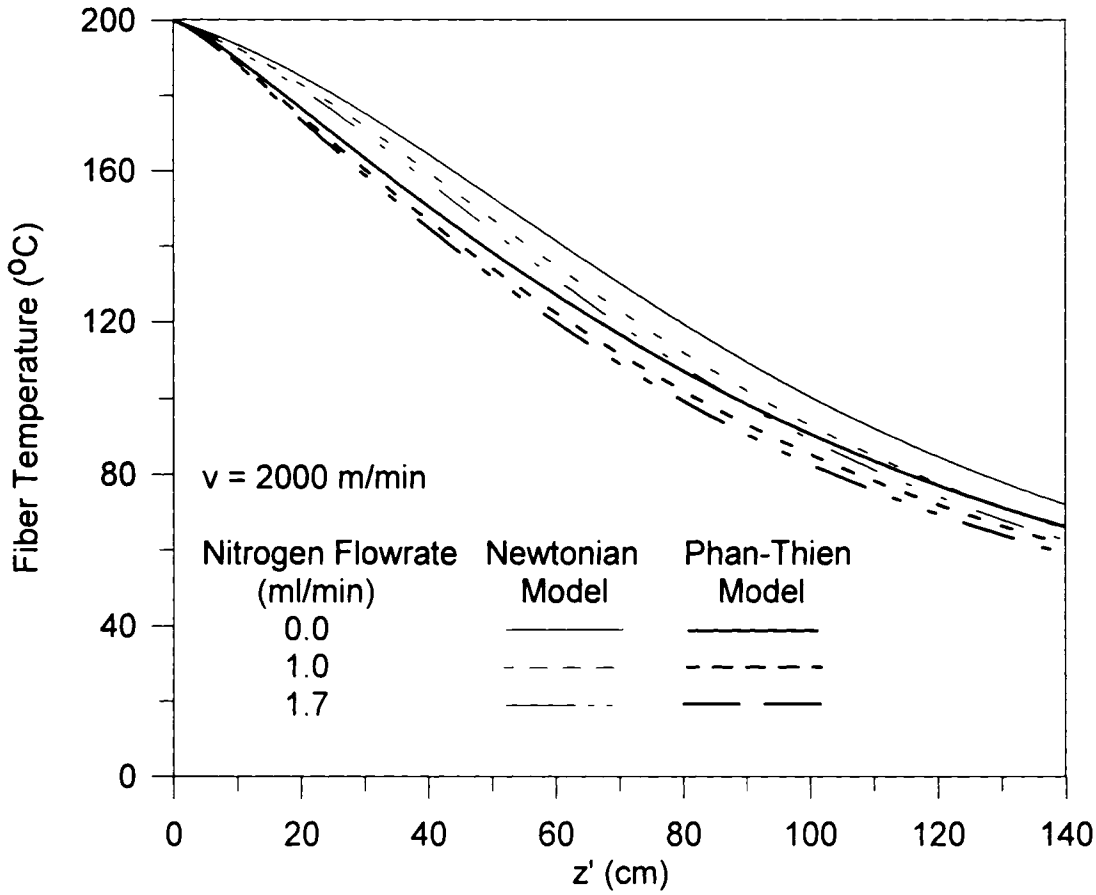

Figure 4.9b: Effect of nitrogen flowrate on fiber temperature for a final take-up speed of 2000 m/min.

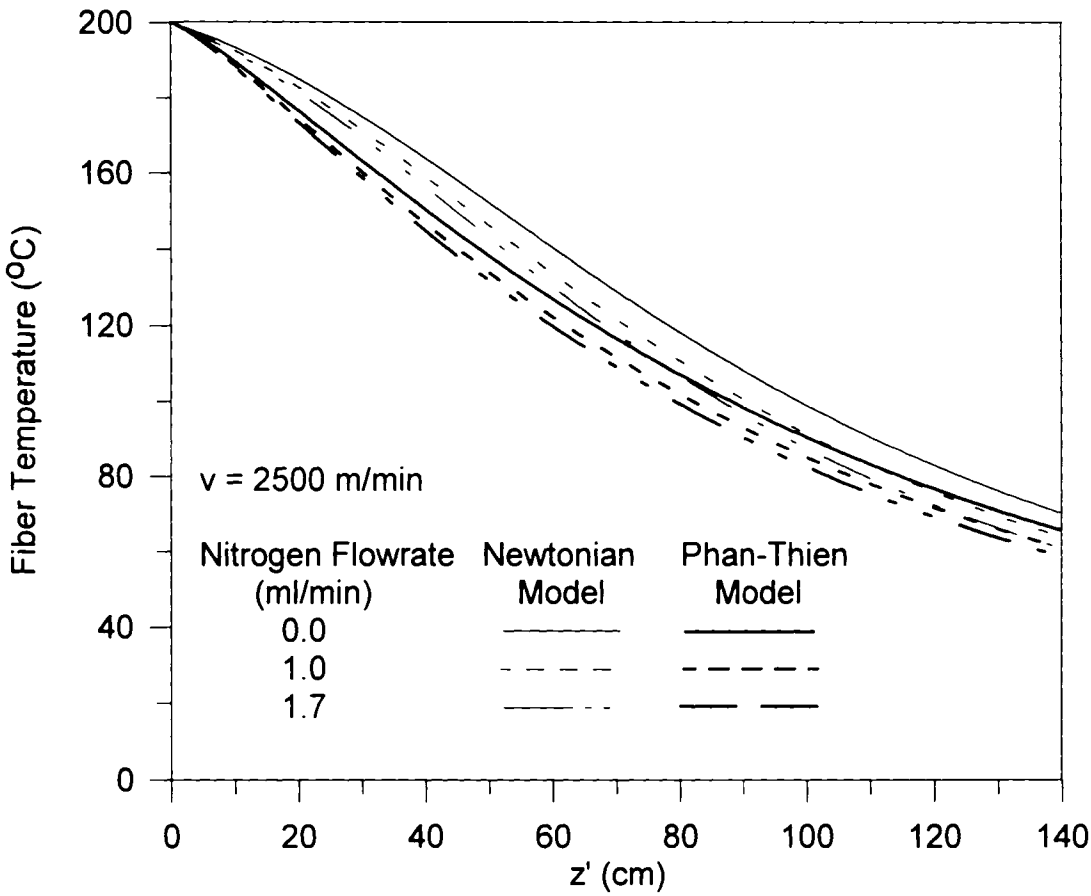

Figure 4.9c: Effect of nitrogen flowrate on fiber temperature for a final take-up speed of 2500 m/min.

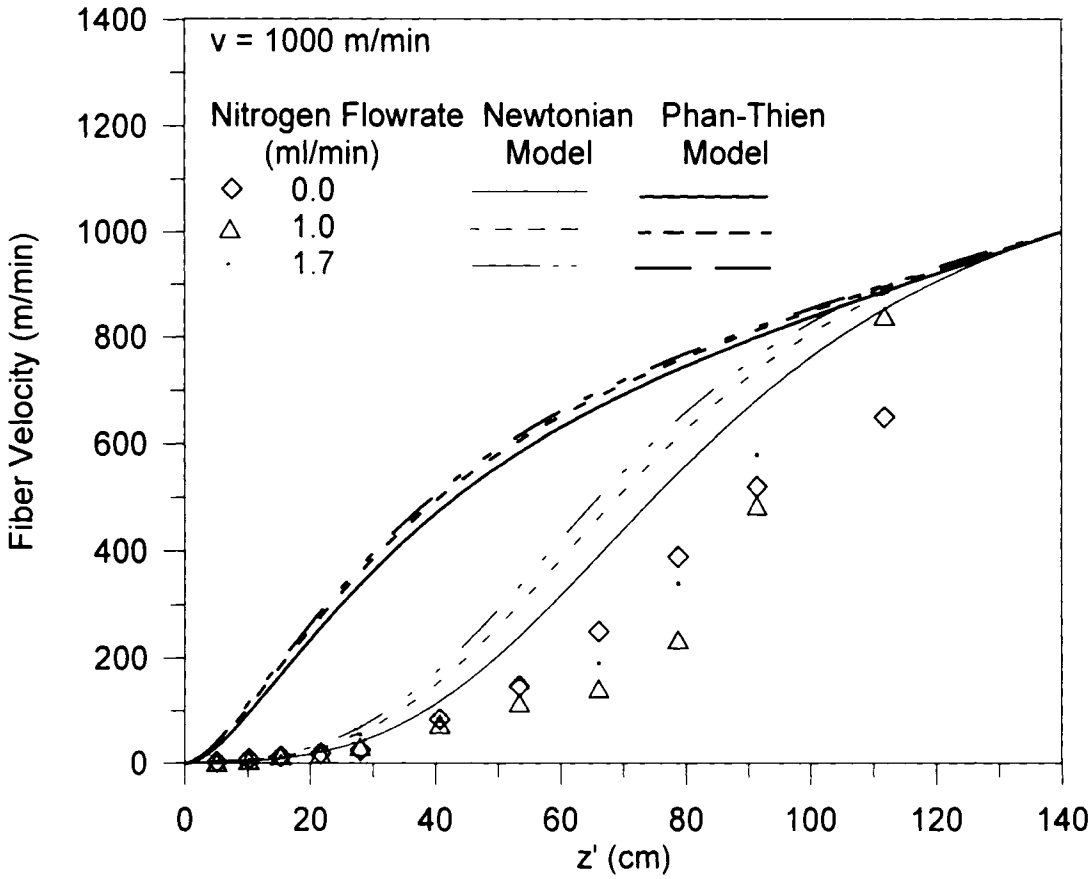

Figure 4.10a: Effect of nitrogen flowrate on fiber velocity for a takeup speed of 1000 m/min. Symbols represent experimental data points.

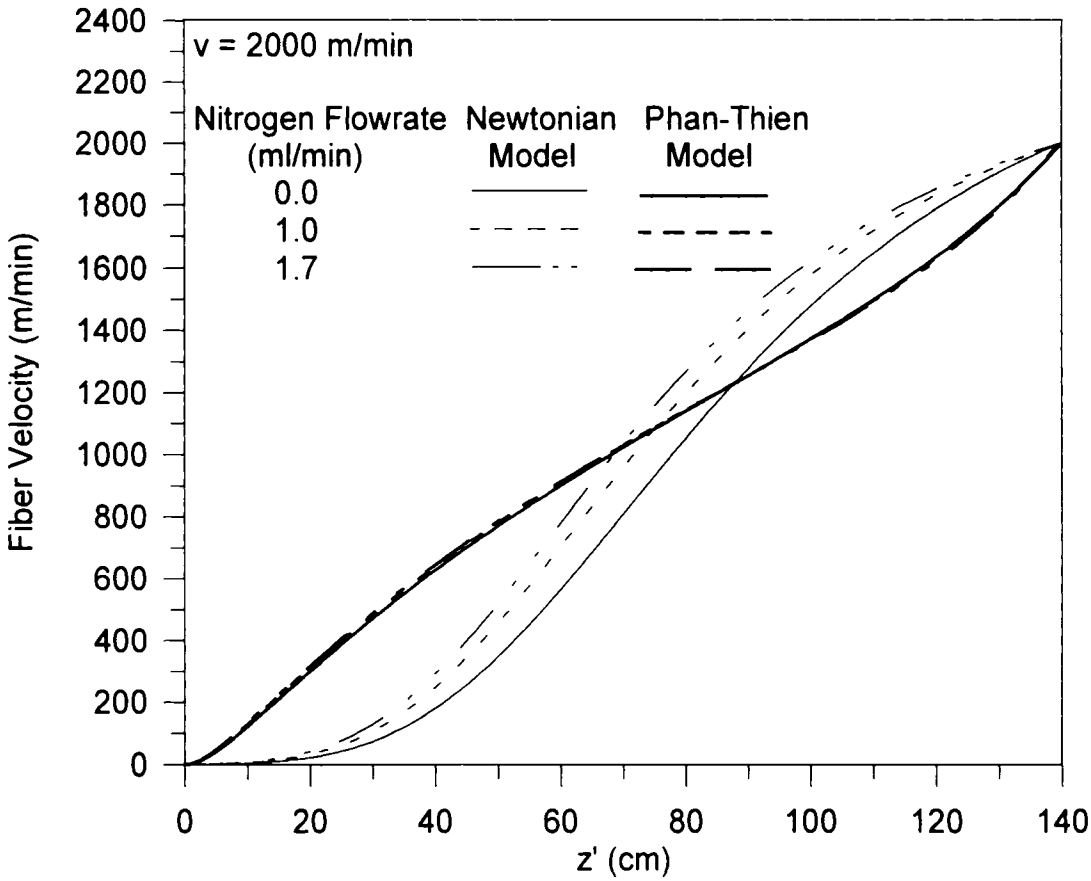

Figure 4.10b: Effect of nitrogen flowrate on fiber velocity for a takeup speed of 2000 m/min.

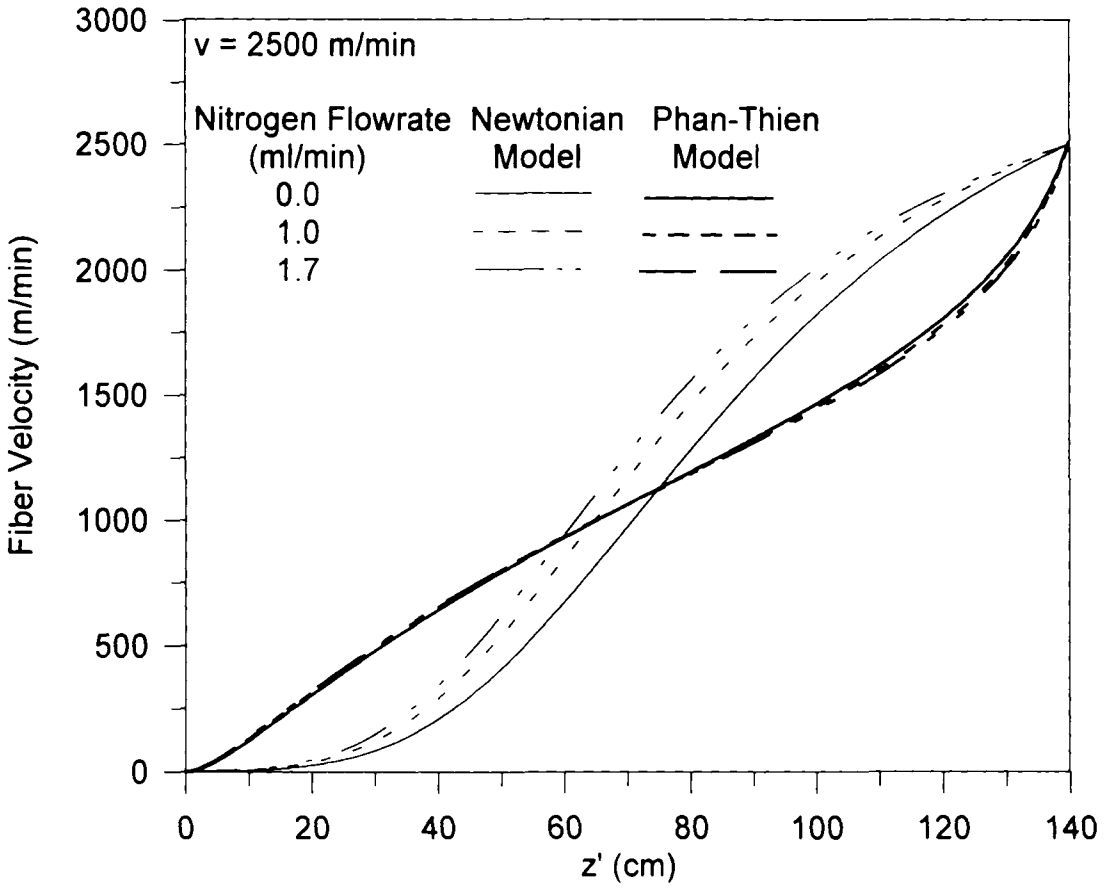

Figure 4.10c: Effect of nitrogen flowrate on fiber velocity for a takeup speed of 2500 m/min.

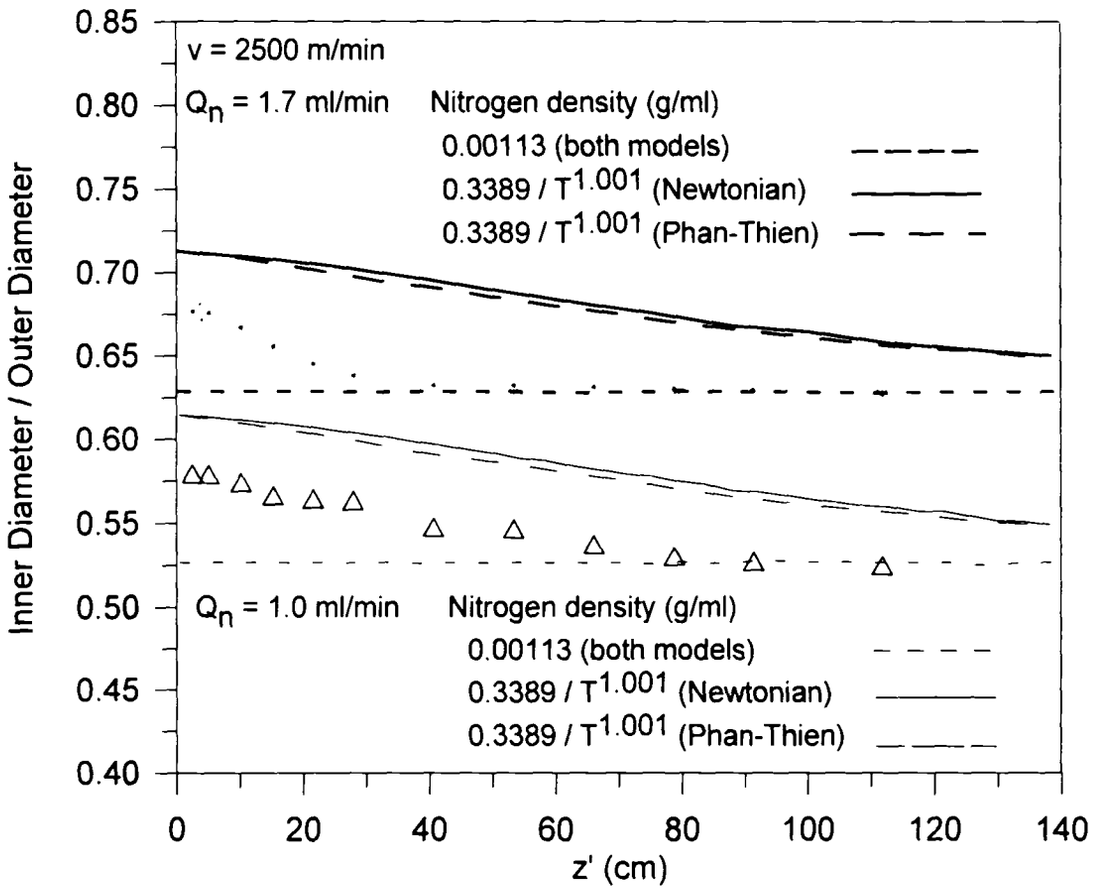

Figure 4.11: The ratio of inner to outer diameter for a final takeup speed of 2500 m/min. The stars are the experimental data points for Q_n = 1.7 ml/min, and the triangles are the experimental data points for Q_n = 1.0 ml/min.

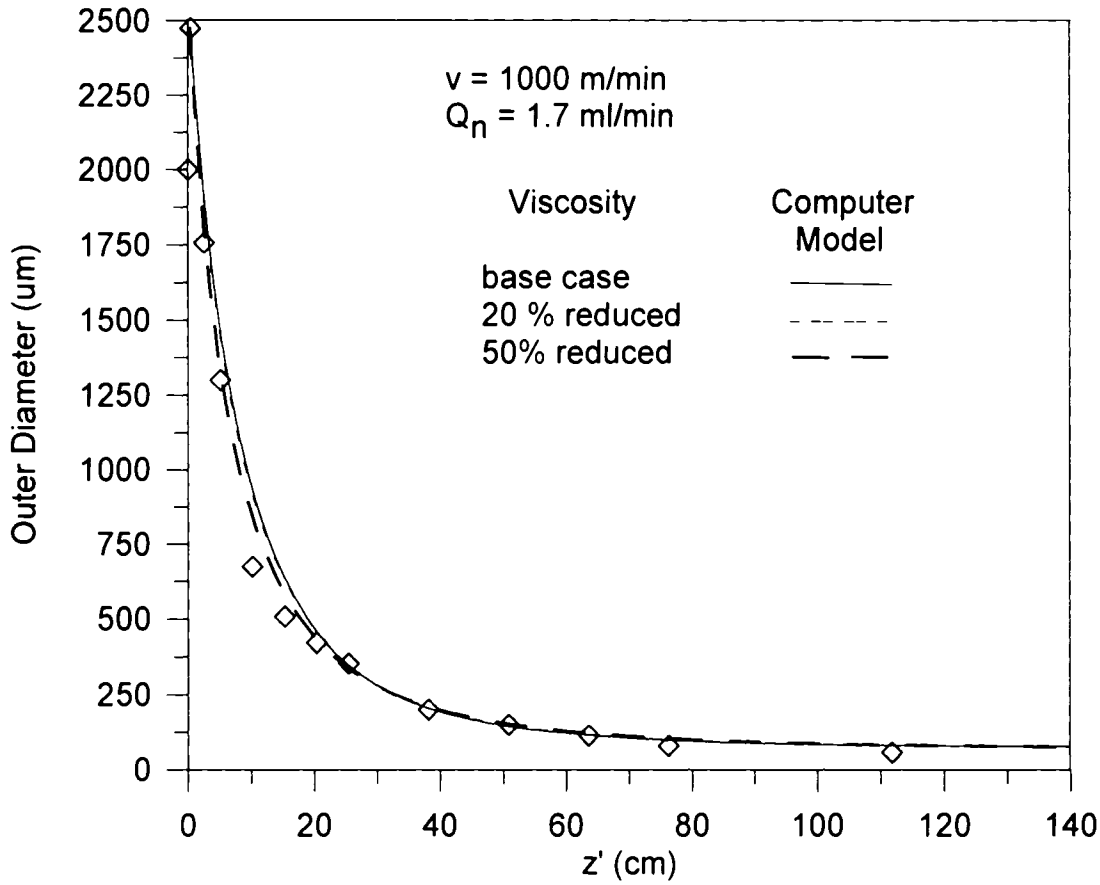

Figure 4.12: The effect of a reduction in viscosity on the model predictions.

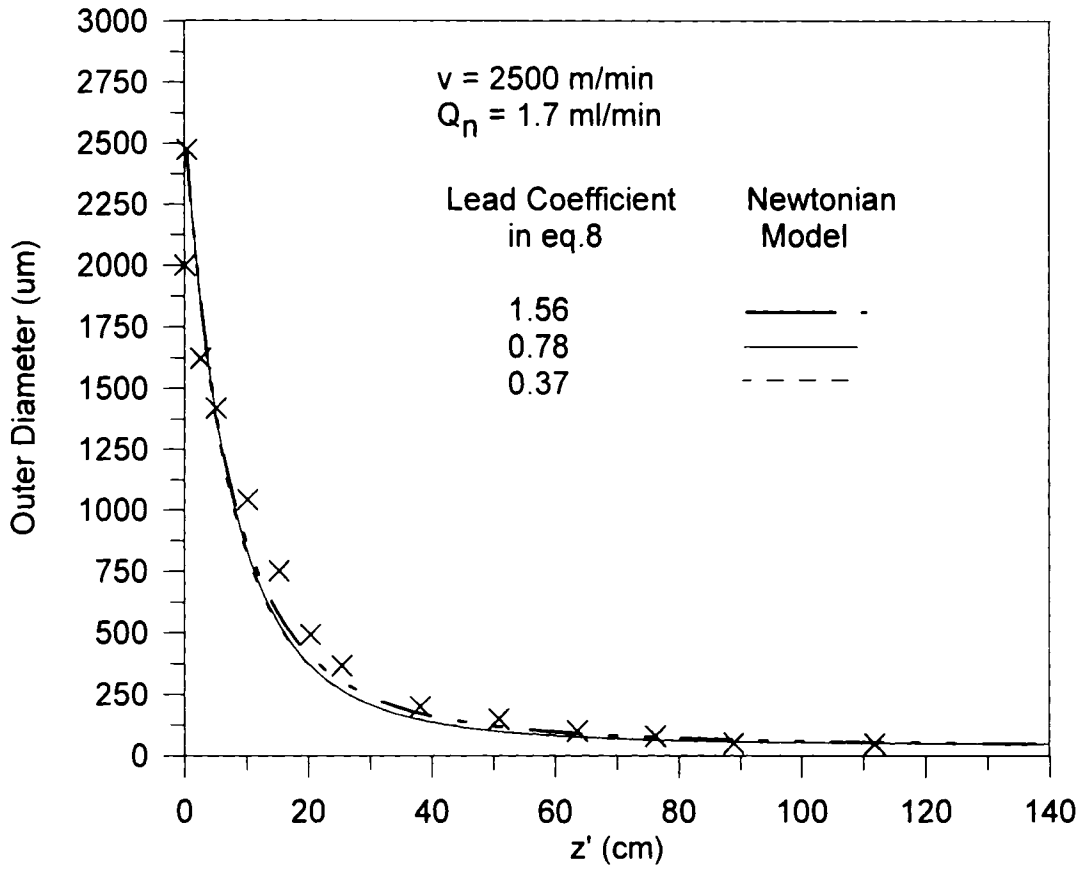

Figure 4.13: How the drag coefficient affects the prediction of outer diameter.

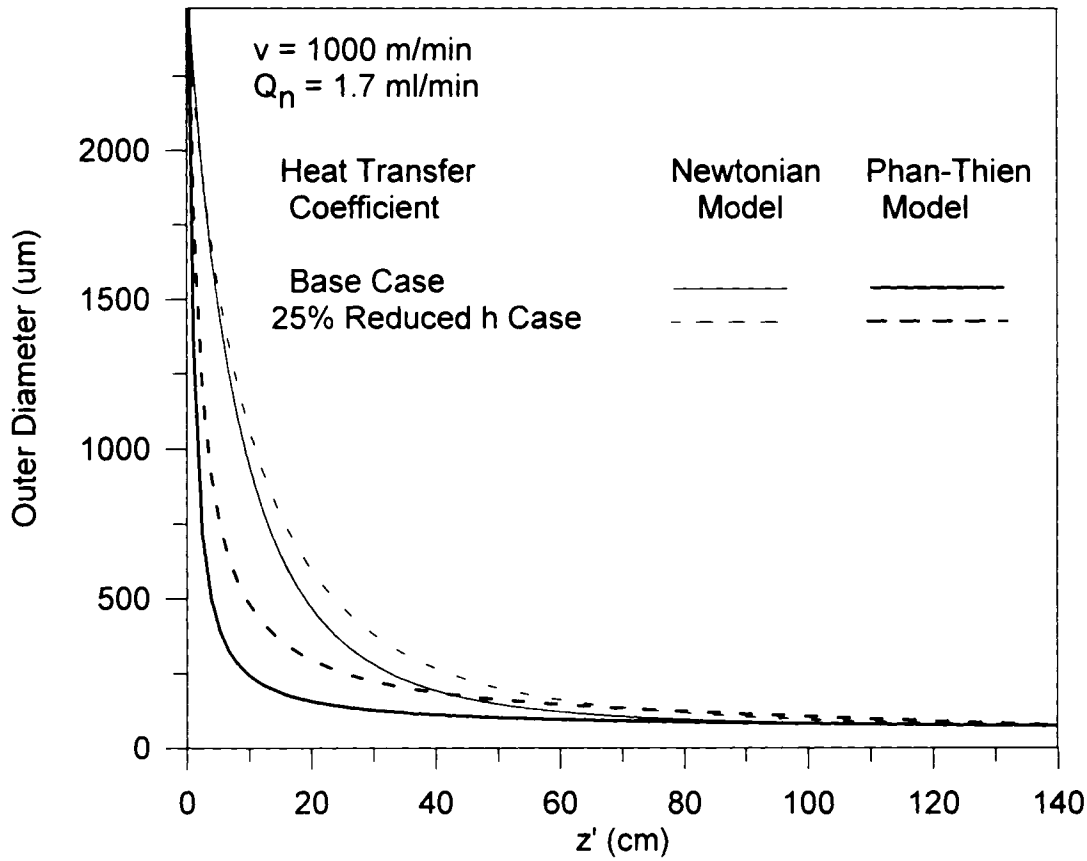

Figure 4.14: How the fiber diameter changes when the heat transfer coefficient is reduced.

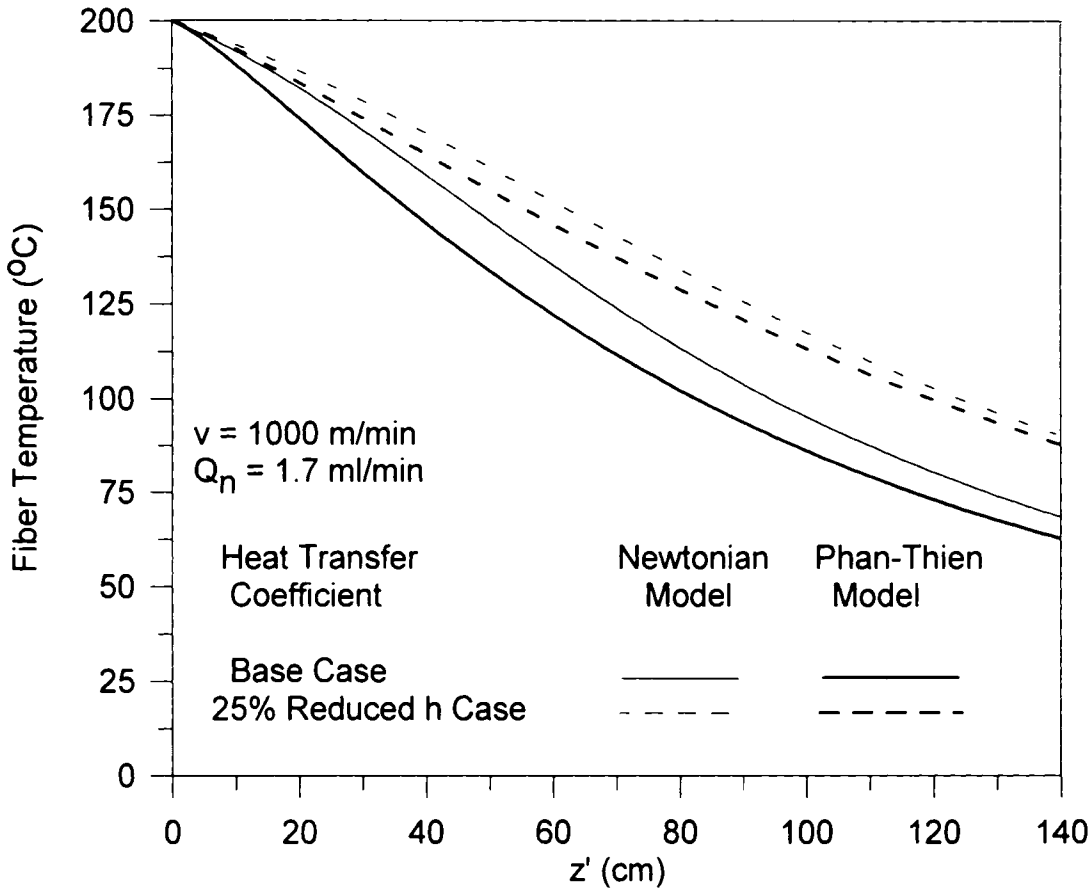

Figure 4.15: The change in fiber temperature which corresponds with Figure 4.14.

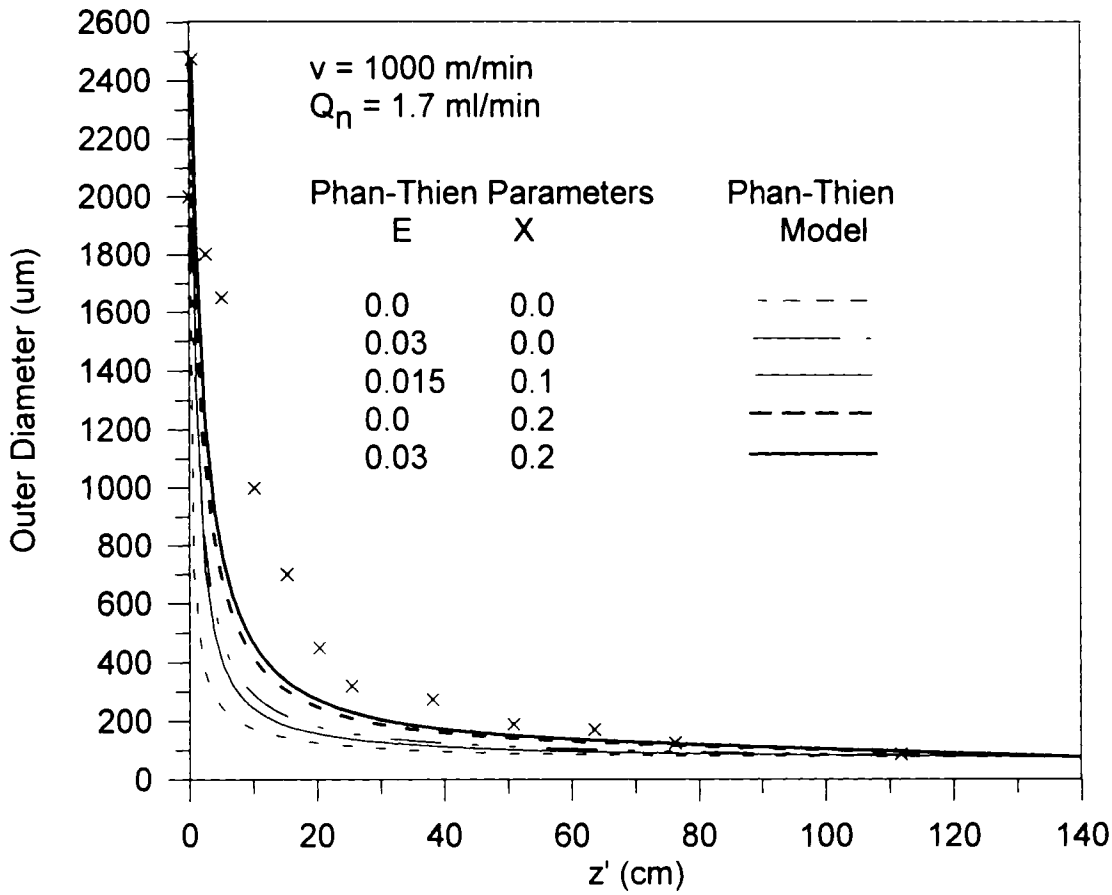

Figure 4.16: The effects of changing the E and X parameters in the Phan-Thien model.

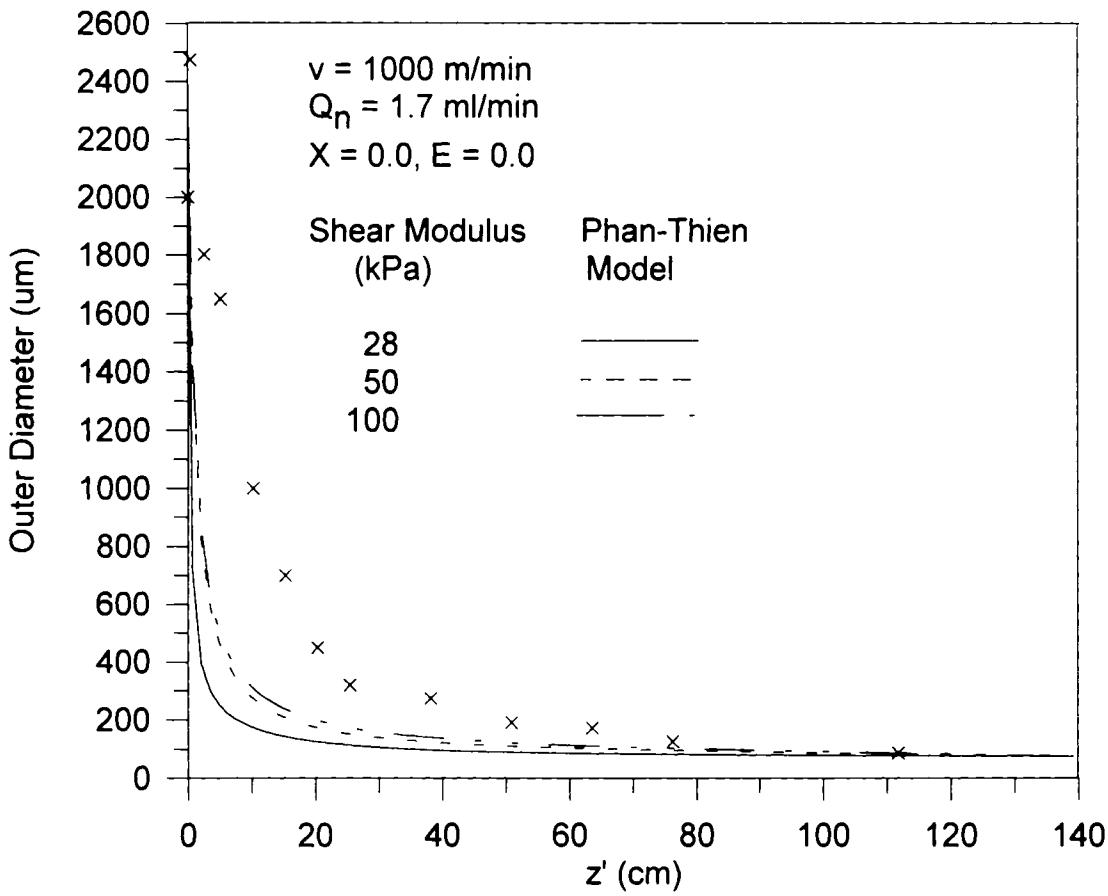

Figure 4.17: The effect of changing G.

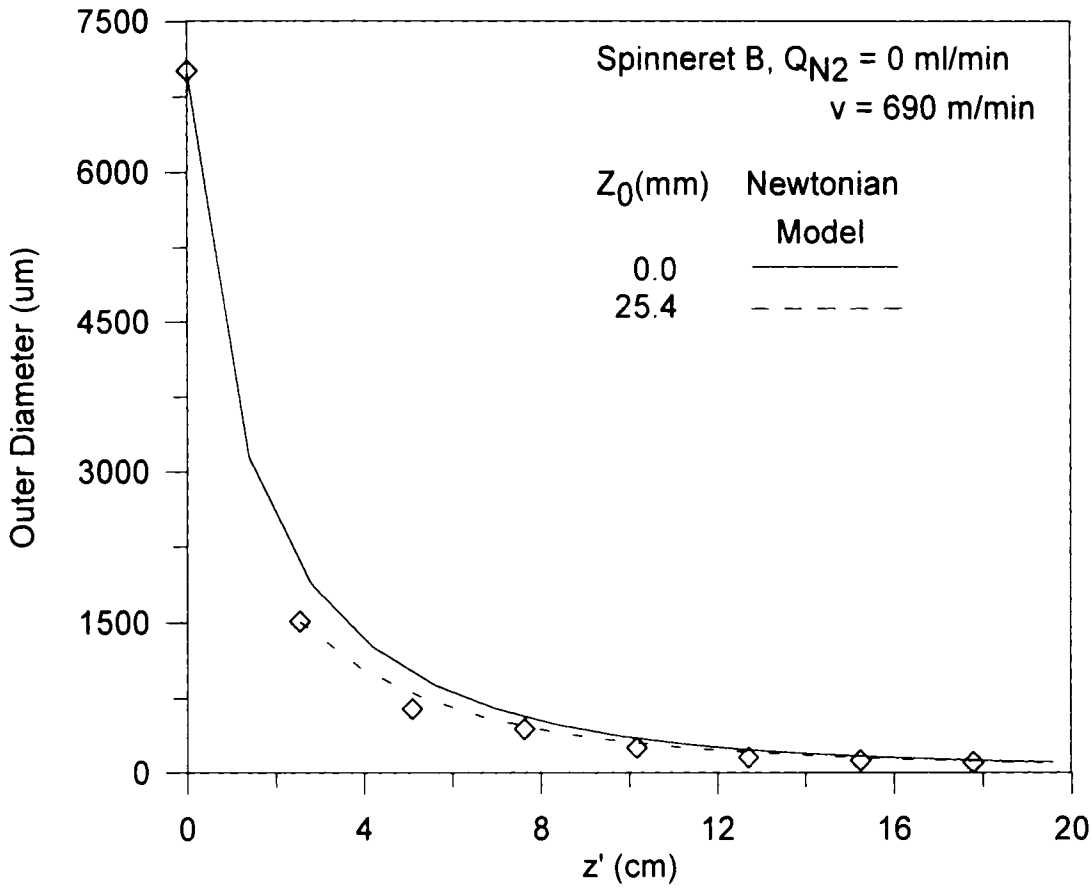

Figure 4.18: Effect of starting position on the Newtonian model for a windup speed of 690 m/min and Q_n = 0 for spinneret B.

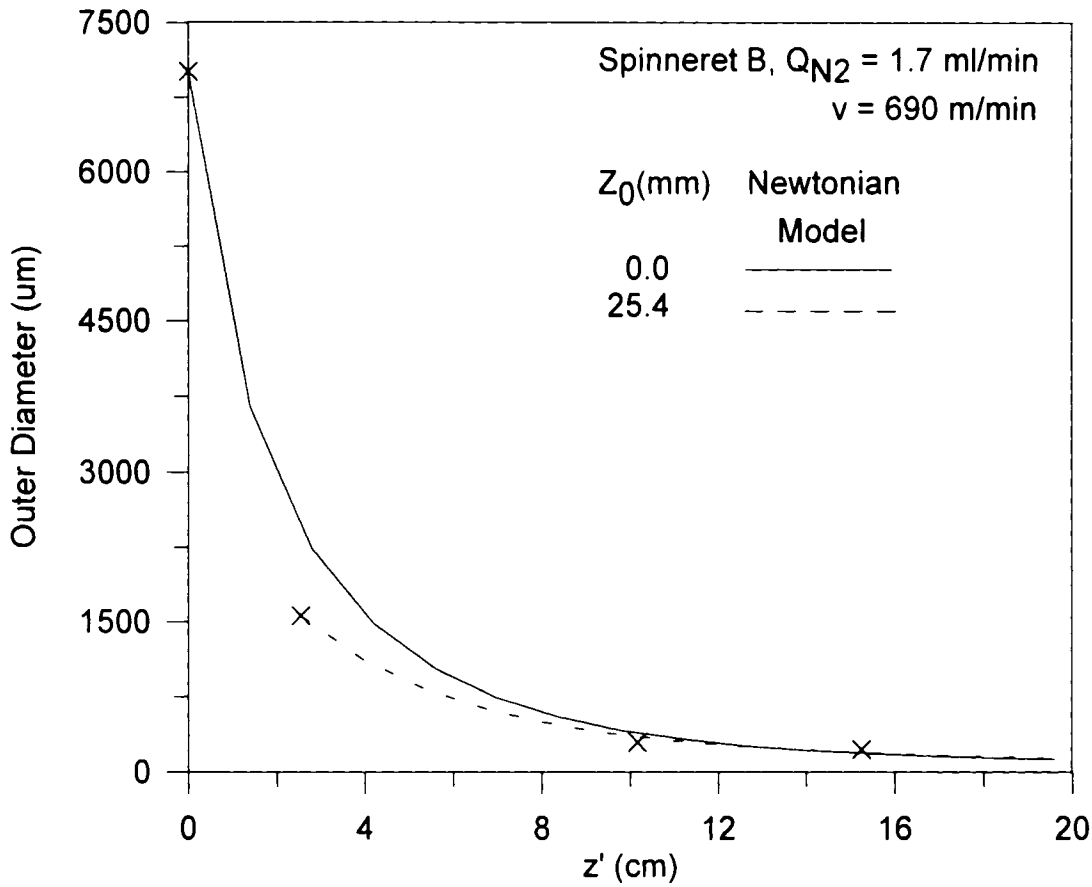

Figure 4.19: Effect of starting position on the Newtonian model for a windup speed of 690 m/min and Q_n = 1.7 ml/min for spinneret B.

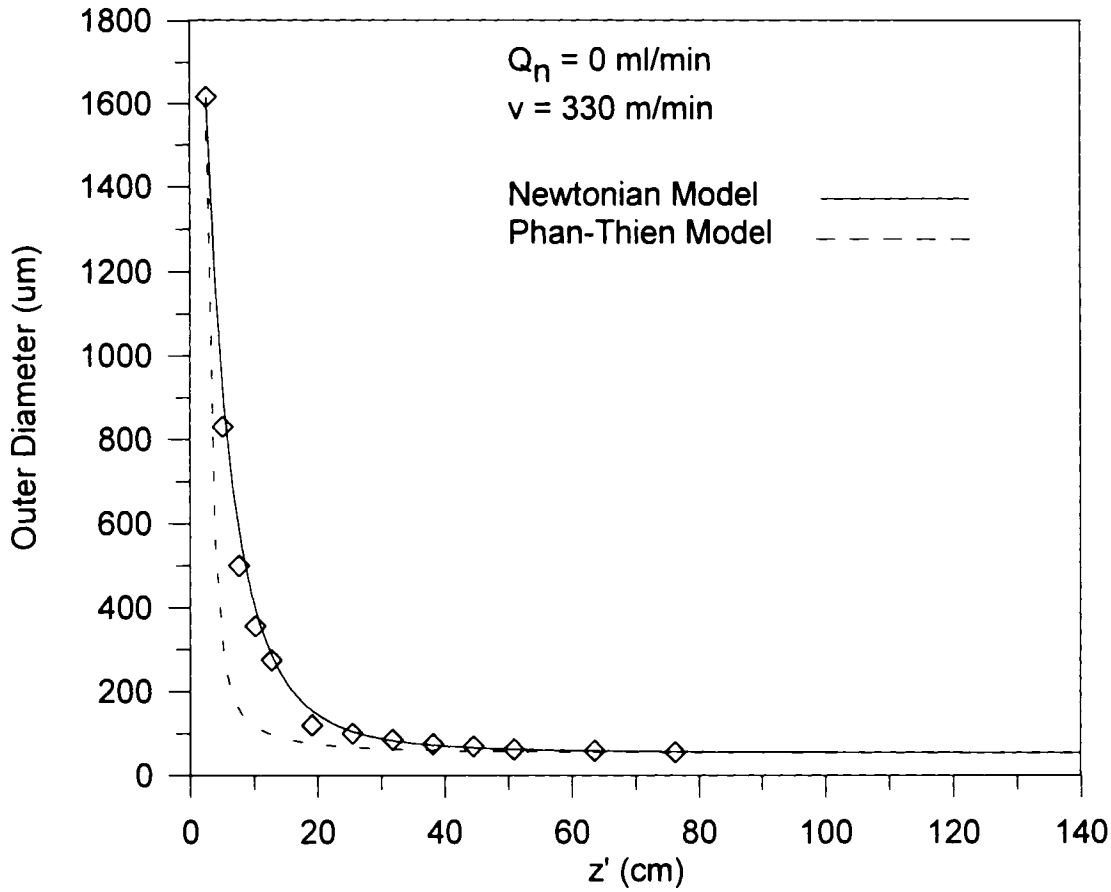

Figure 4.20a: Experimental data compared to the predictions of the Newtonian and Phan-Thien models. Results are shown for a high windup speed of 330 m/min and a nitrogen rate of 0 ml/min.

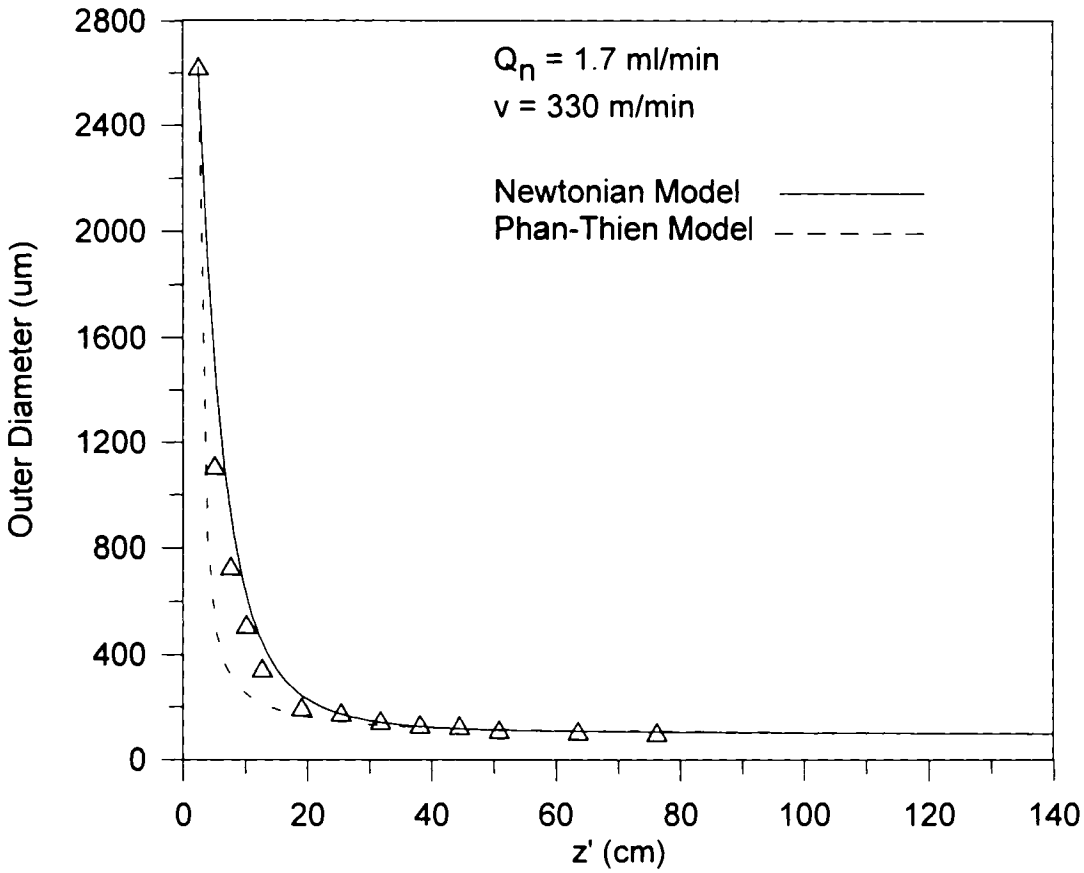

Figure 4.20b: The same comparison as in Fig. 4.20a, except the nitrogen rate is 1.7 ml/min.

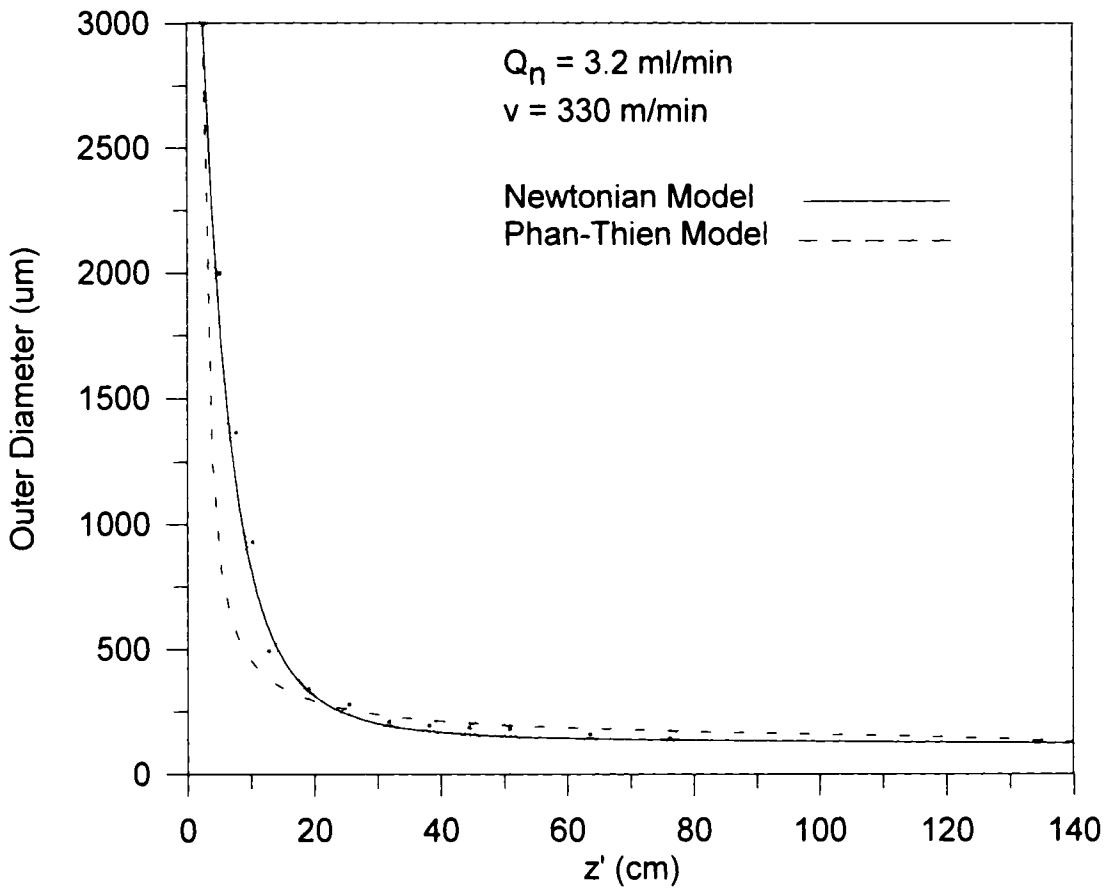

Figure 4.20c: The same comparison as in Fig. 4.20a, except the nitrogen rate is 3.2 ml/min.

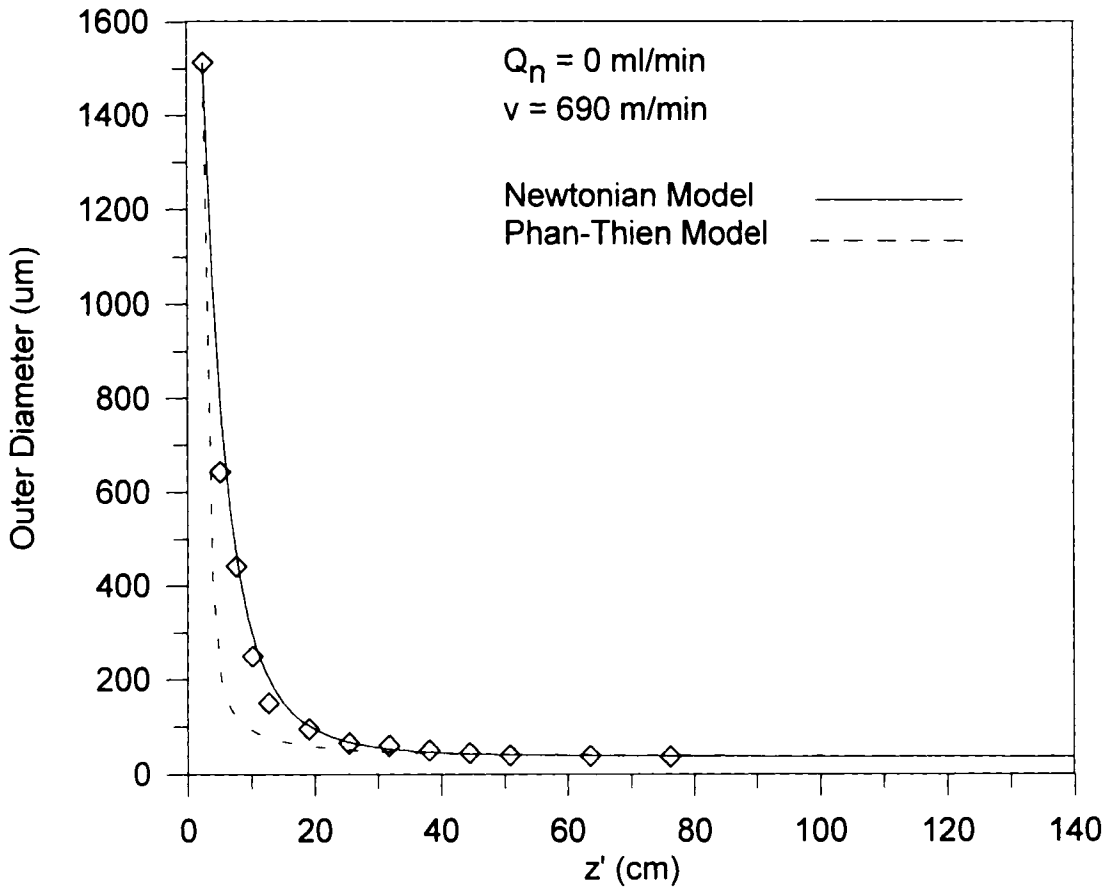

Figure 4.21a: Experimental data compared to the predictions of the Newtonian and Phan-Thien models. Results are shown for a high windup speed of 690 m/min and a nitrogen rate of 0 ml/min.

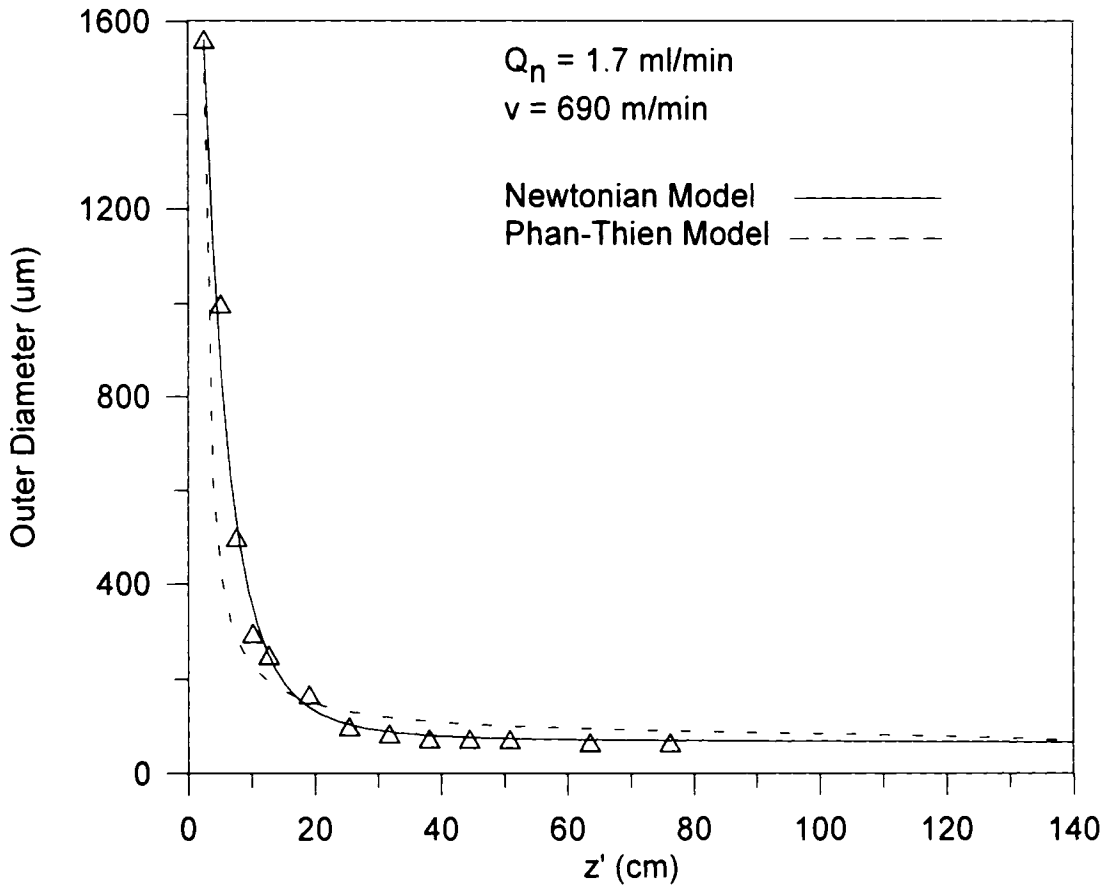

Figure 4.21b: The same comparison as in Fig. 4.21a, except the nitrogen rate is 1.7 ml/min.

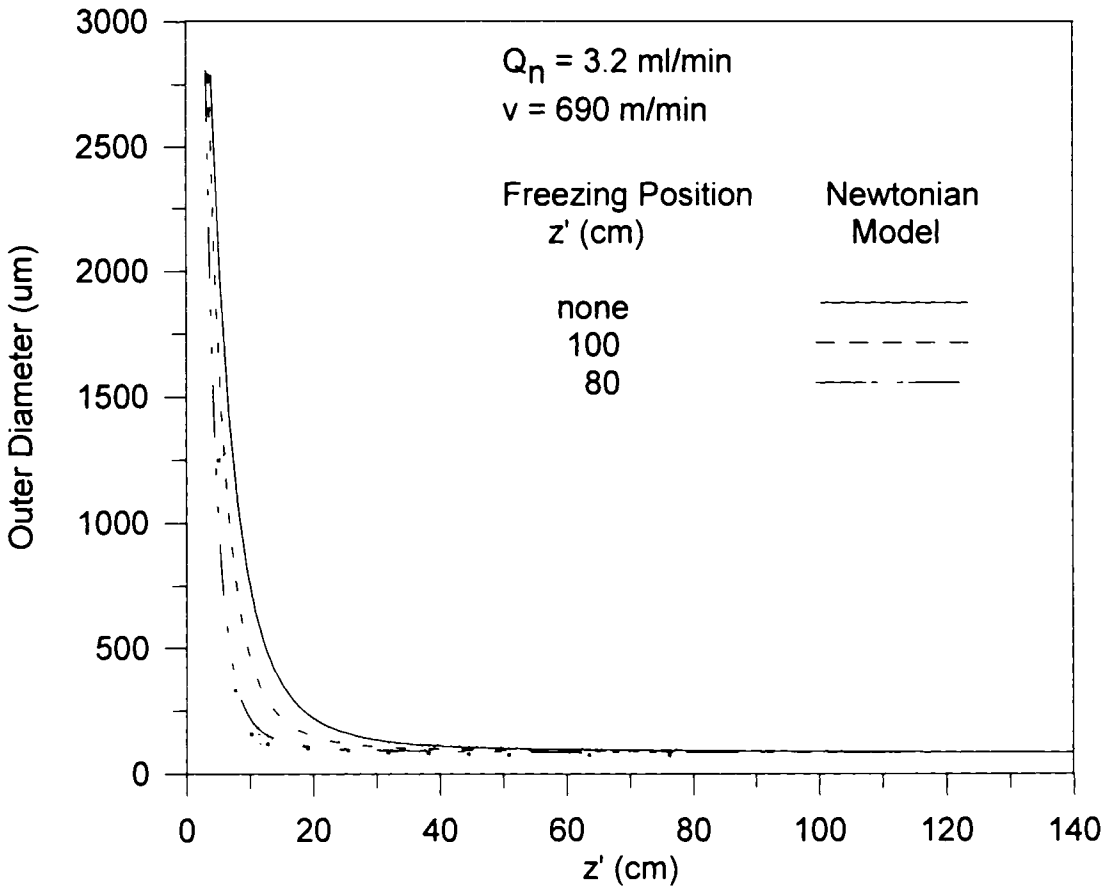

Figure 4.21c: Effect of freezing position on hollow fibers spun with 1.7 ml/min nitrogen with a windup speed of 690 m/min.

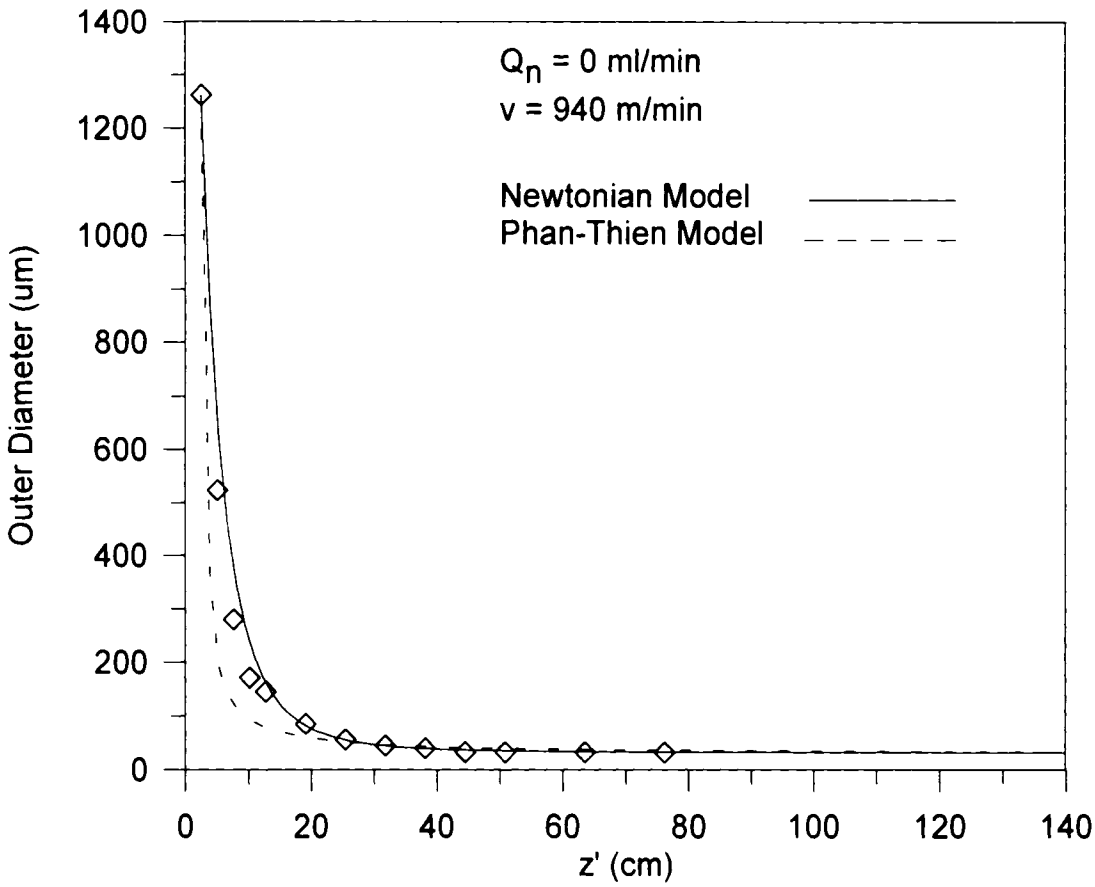

Figure 4.22a: Experimental data compared to the predictions of the Newtonian and Phan-Thien models. Results are shown for a high windup speed of 940 m/min and a nitrogen rate of 0 ml/min.

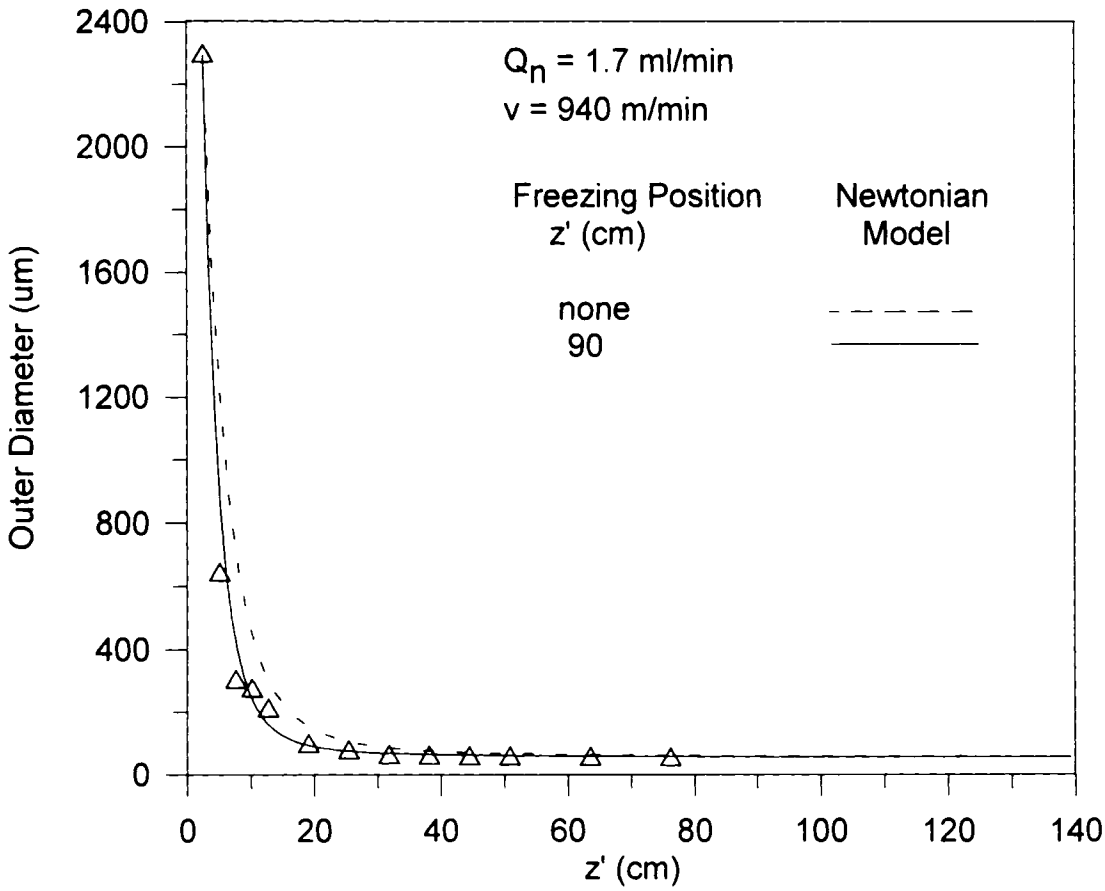

Figure 4.22b: Effect of freezing position for 1.7 ml/min nitrogen with a windup speed of 940 m/min.

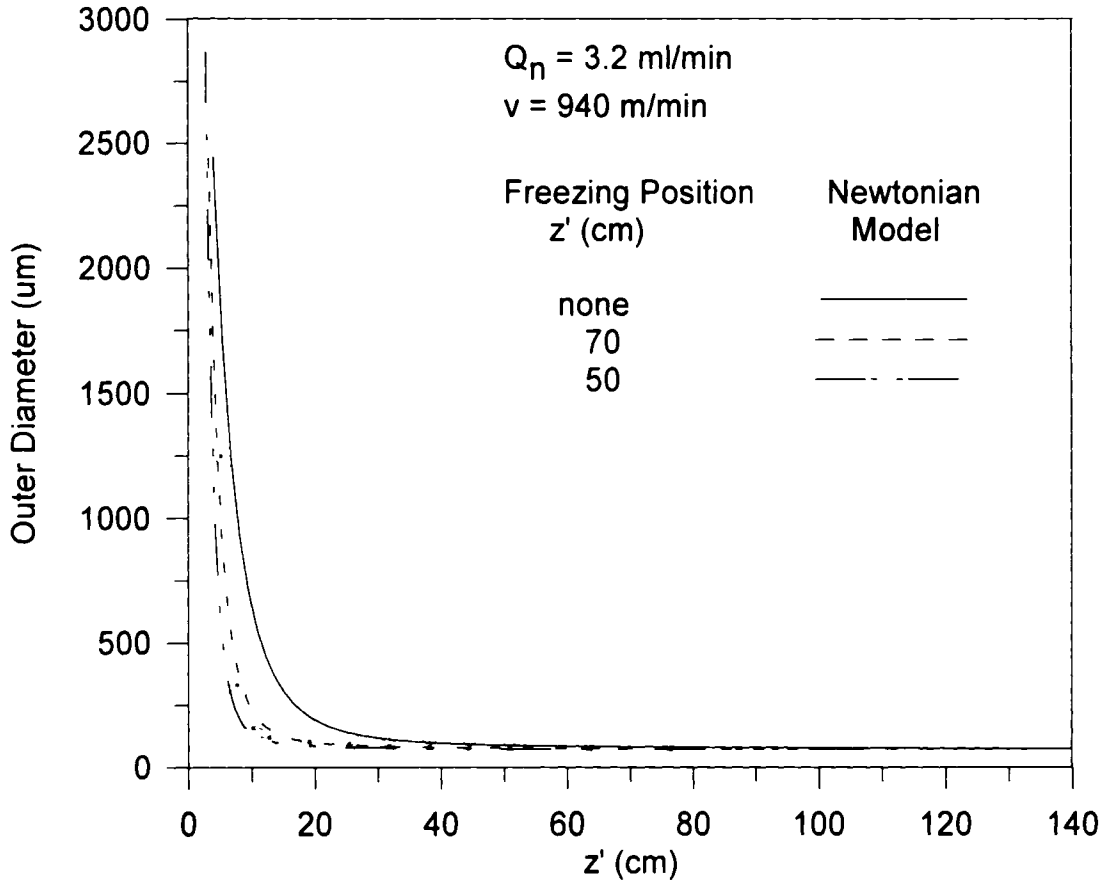

Figure 4.22c: Effect of freezing position for 3.2 ml/min nitrogen with a windup speed of 940 m/min.

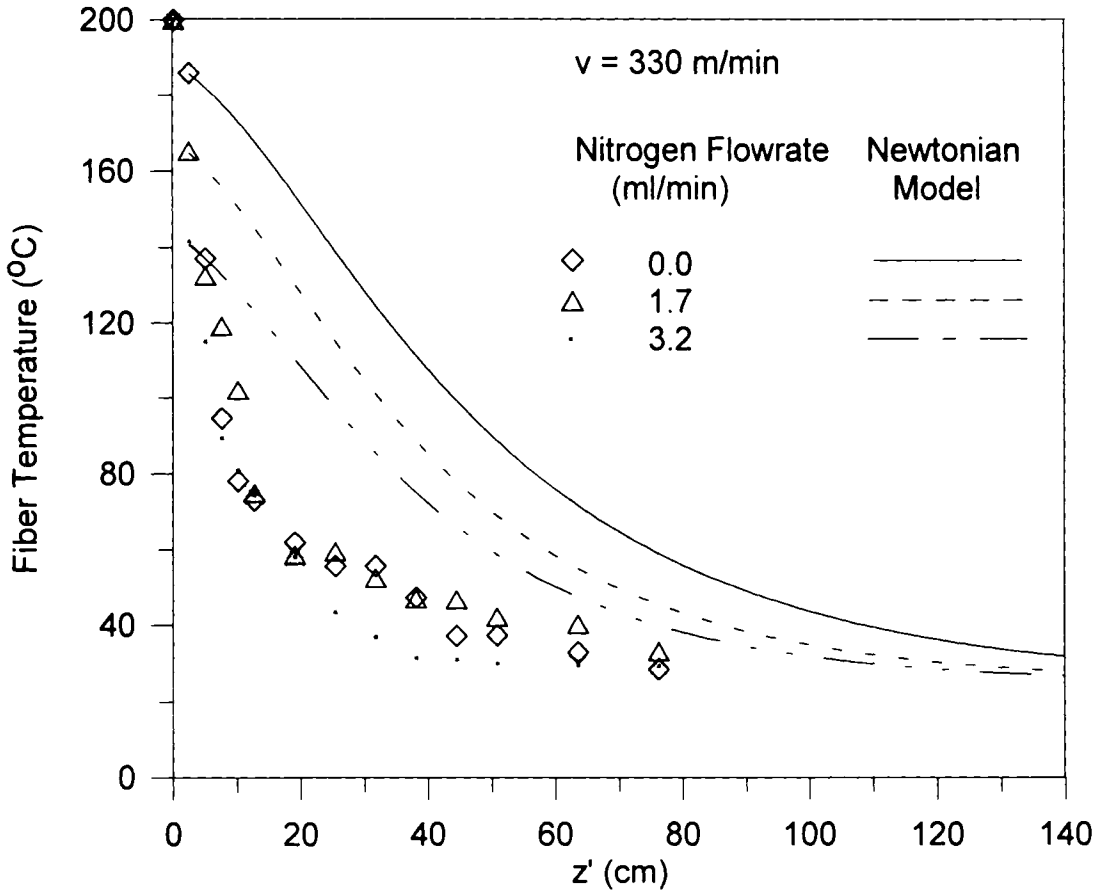

Figure 4.23a: Effect of nitrogen on fiber temperature for a windup speed of 330 m/min. Symbols represent experimental data points.

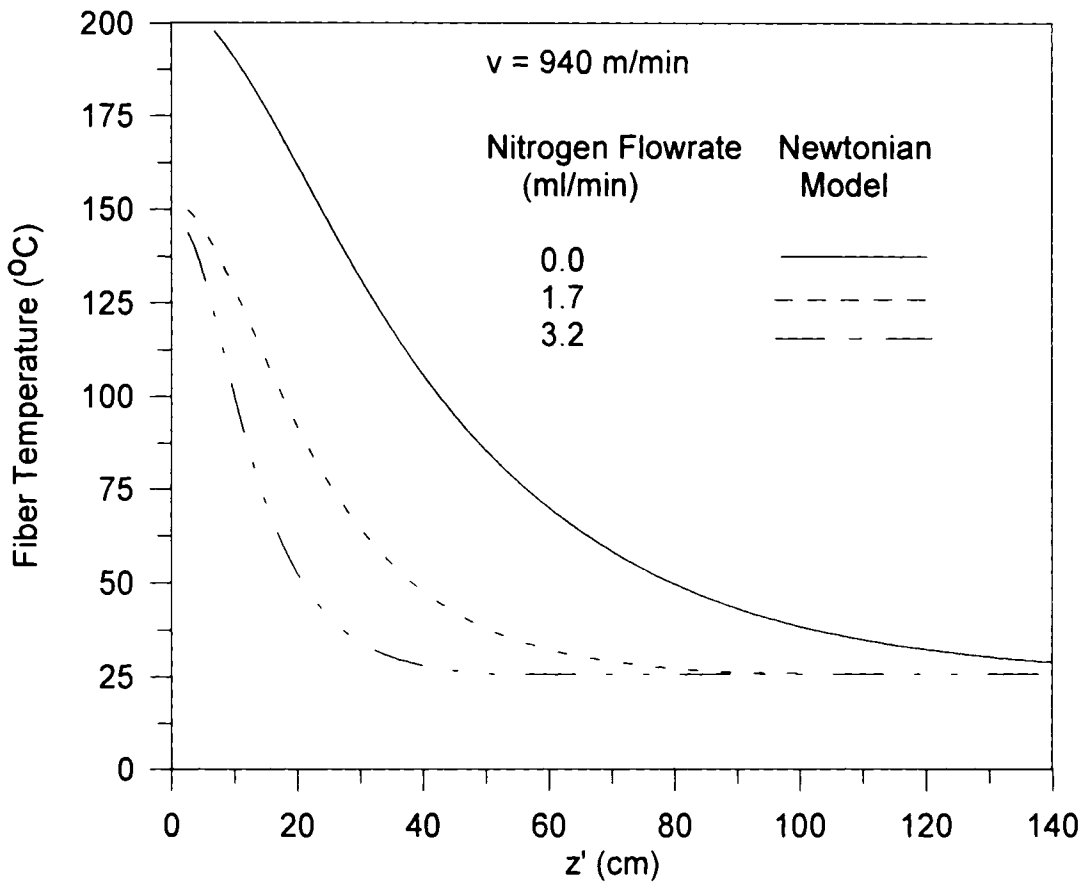

Figure 4.23b: Effect of nitrogen on fiber temperature for a windup speed of 940 m/min.

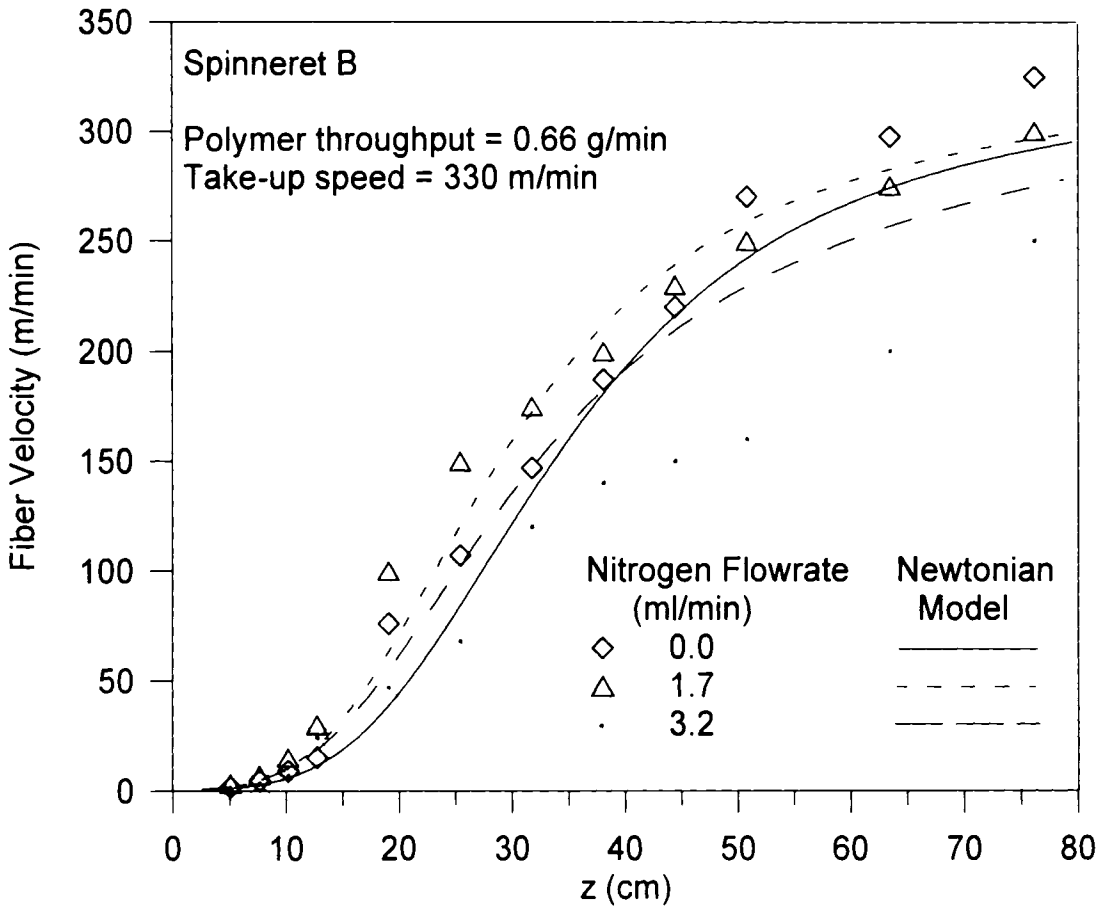

Figure 4.24a: Effect of nitrogen on fiber velocity for a windup speed of 330 m/min. Symbols represent experimental data points.

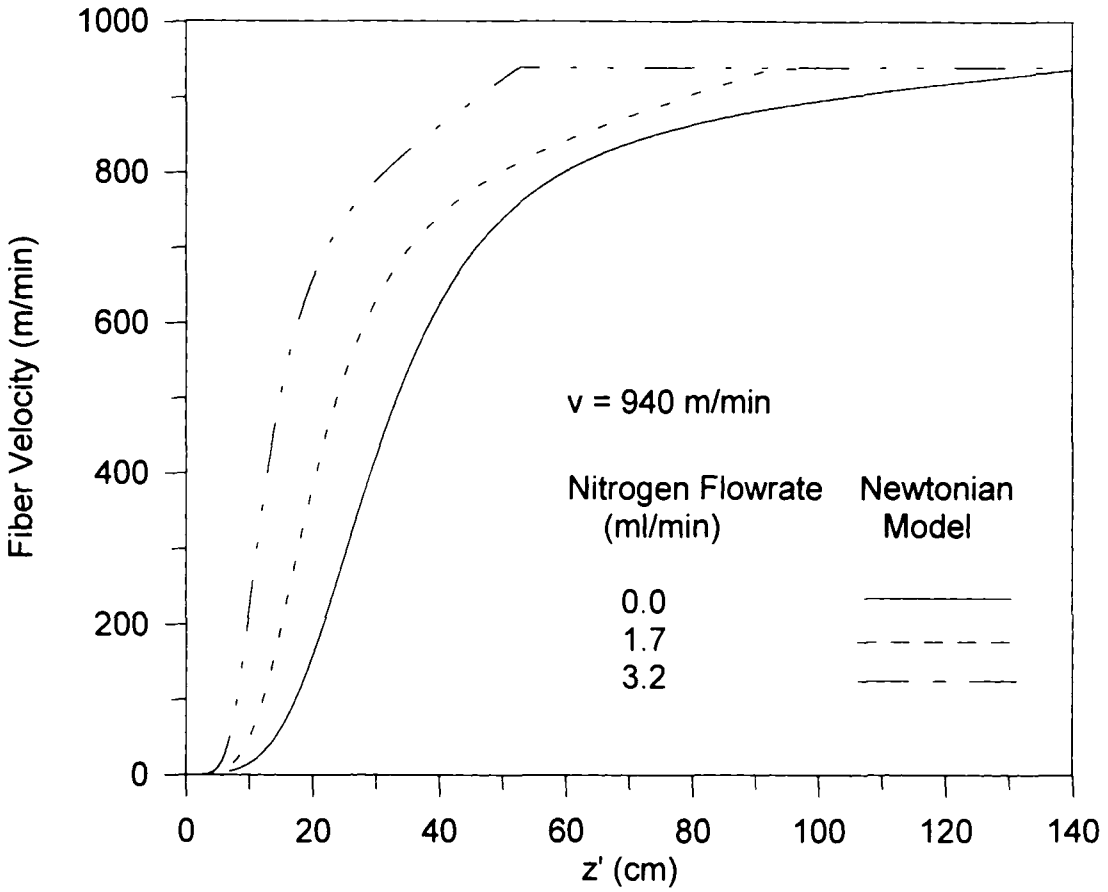

Figure 4.24b: Effect of nitrogen on fiber velocity for a windup speed of 940 m/min.

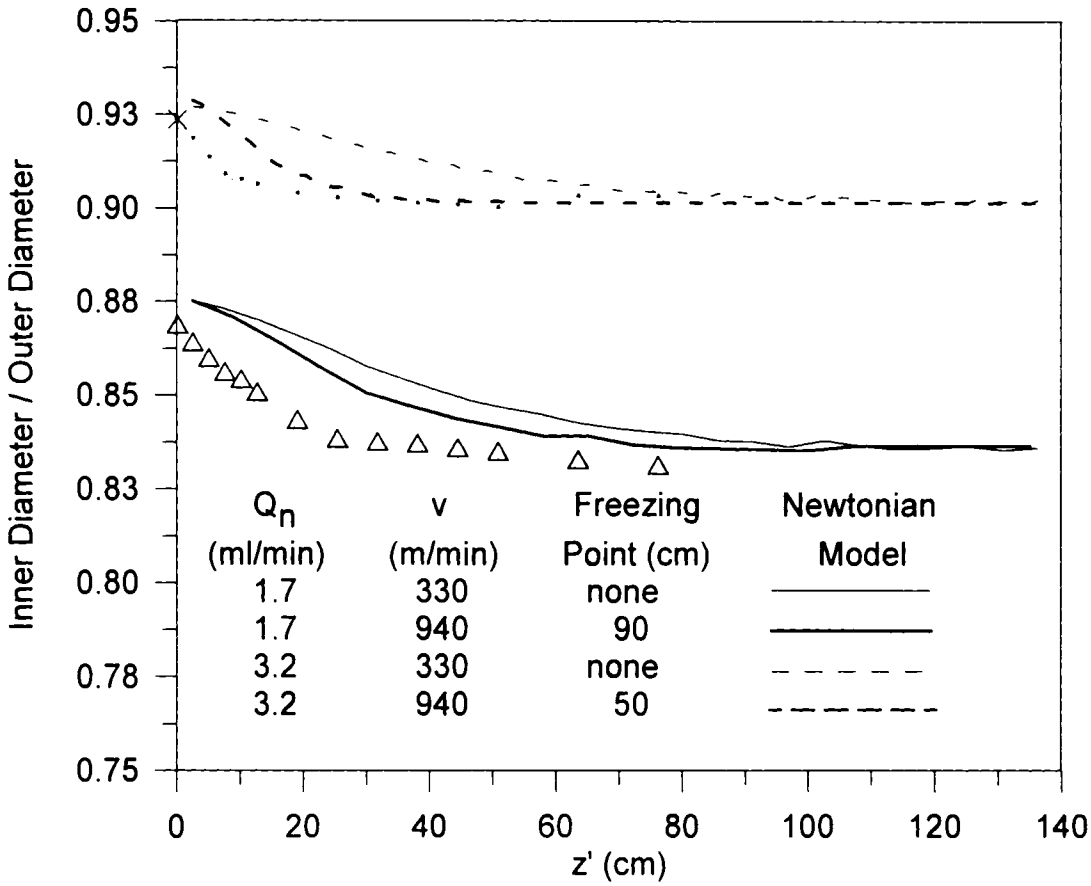

Figure 4.25: Effect of freezing point on ratio inner diameter to outer diameter. The stars represent the experimental data points at Q_n = 3.2 ml/min, and the triangles represent the experimental data points at Q_n = 1.7 ml/min.

CHAPTER 5

THE INFLUENCE OF PROCESSING PARAMETERS ON THE PROPERTIES OF MELT-SPUN POLYPROPYLENE HOLLOW FIBERS

(The content of this chapter will be submitted to the journal *Polym. Eng. Sci.*)

ABSTRACT

Isotactic polypropylene hollow fibers with different hole sizes were produced by melt spinning with windup speeds up to 1880 m/min. The samples were characterized using dynamic mechanical analysis, birefringence, tensile testing, and differential scanning calorimetry. Hollow fibers exhibit higher crystallinity, orientation and strength than solid fibers. In fact, the orientation produced in a hollow fiber was much larger than that which could be produced in a solid fiber, even when the spinning speed of the latter was much larger. Larger inner diameters improved fiber properties up to a certain point, after this point fiber properties declined slightly. At a given ratio inner to outer diameter (constant polymer and nitrogen rates), increased windup speed increased modulus and tenacity.

5.1 INTRODUCTION

Hollow fibers have been primarily used in separation processes; for example artificial kidneys [Baum et al., 1976]. Such fibers are difficult to produce because the required filtration properties necessitate strict control of wall properties. These properties (microporous walls, asymmetric walls, etc.) mean that hollow fiber membranes are spun at relatively slow spinning speeds. For example, Kim et al. [1994] produced polypropylene hollow fibers with take-up speeds as slow as 76.6 cm/min while a maximum spinning speed of 350 m/min was reported by Oh et al. [1998].

The rate of fiber spinning as well as any subsequent cold drawing changes the properties of a fiber dramatically. The high modulus and tensile strength of semicrystalline commercial synthetic fibers, including polypropylene, are usually due to morphological transformations and chain orientation procedures [Capiati and Porter, 1975]. High performance fibers are usually obtained when both crystallinity and orientation are increased. For polyethylene, techniques such as ultra-drawing [Capiata and Porter, 1975], and extrusion at high pressure and high shear [Weeks and Porter, 1974] are used to increase orientation and crystallinity. These processes impart much higher strength and modulus to the fibers.

Melt draw ratio, spinneret temperature, and annealing temperature are also important factors influencing a fiber's structure and performance. Kim et al. [1994, 1995] studied the effects of cold drawing and spinning temperatures on polypropylene hollow fibers morphology. Annealing at 60 to 140°C was found to

increase fiber crystallinity without changing orientation. High melt-draw ratios (1000 to 1250 %) were found to increase hollow fiber orientation in the spinning direction [Kim et al., 1994].

Although filtration and separation are the main applications for hollow fibers, they are not their only market. Hollow fibers can also be produced for other applications where fiber walls properties are not critical. The advantage of hollow fibers over solid fibers is their lower cost and lighter weight on a per outside diameter basis.

In this paper, we show how lumen gas rate, spinning speed, and ratio inner (ID) to outer (OD) diameter affect hollow fibers morphology and strength. Fiber morphology was described in terms of percent crystallinity, molecular orientation (of crystallite and amorphous regions). Dynamic mechanical analysis (DMA) was used to find the glass transition temperature (T_g) and estimate the elastic modulus as a function of temperature. Fractional crystallinity and melting temperature were obtained using Differential Scanning Calorimetry. Molecular orientation was obtained using birefringence, while ultimate properties were determined from tensile tests.

5.2 EXPERIMENTAL

5.2.1 Materials

Fina Dypro® isotactic polypropylene pellets with an average molecular weight of 165,000 g/mol (88 MFR) and a polydispersity of 4 were melted and spun at 200°C

to produce the fibers. Hollow and solid fibers were obtained by melt extrusion using a tube-in-orifice spinneret [Moch, 1991]. Nitrogen gas was injected in the center of the molten filament to produce the hollow structure. Solid fibers were spun with the same spinneret, operated without nitrogen gas. All fibers were obtained by a single step drawing process, using a mechanical take-up roll to collect the fibers.

Fiber diameters were measured under an optical microscope equipped with a micrometer. Solid fiber diameters were measured from side views of the fibers. For hollow fibers, outer and inner diameters were determined from cross-sectional views obtained by first microtoming the samples. A distinction needs to be made between polymer and fiber cross-sectional area. The polymer cross-sectional area (S_p) represents the area of the polymer annulus only, while fiber cross-sectional area (S_f) represents the total cross-sectional area of the fiber. Hence, S_f is larger than S_p, except in the case of solid fiber, where the two are equal. Throughout this chapter, we will be careful to designate which convention was used when calculating mechanical properties etc.

5.2.2 Tensile test equipment

A model TT-B-L Instron Tensile Tester was used to measure tensile properties. A B-load cell, with a sensitivity in the range of 100 to 2,000 grams, was used in all experiments. Special pneumatic grips with a working pressure of 0.138 MPa (20 psi) were used to hold the samples in place. A crosshead speed (stretching rate) of 2.54 cm/min was set for all experiments. The initial length of the sample was set at 2.2 cm. Careful attention was taken not to stretch the fiber before testing and

while placing the sample in the grips. The procedure followed is described in ASTM D 2101-93.

The Young's modulus was calculated from the initial slope of each tensile curve. The elongation and stress at break were determined at the position of rupture. Toughness was obtained by integrating the area under the stress-strain curve, from 0% elongation to elongation at break. The unit was converted into g/den using the following equation [Ahmed, 1982]:

$$\text{Tensile strength (lb/in}^2\text{)} = 12{,}800 \times \text{Specific gravity} \times \text{Tenacity (g/den)} \qquad (5.1)$$

where the specific gravity was assumed to be 0.895, i.e. changes in the density with crystallinity were ignored. Denier is a unit based on the weight of a fiber per its unit length; in the U.S., denier is measured in grams of 9,000 m of material (the lower the number, the finer the fiber). Reported values were averages from three repeat experiments. The confidence intervals for a reliability of 0.95 were ± 20% for tenacity and rupture elongation, and ± 15% for Young's modulus. Polypropylene fibers are available in the range of 2-4 g/den for carpeting, 3-6 g/den for textiles, and 6-9 g/den for industrial purposes [Ahmed, 1982]. Polypropylene fibers also differ widely in their elastic moduli, ranging from 120 g/den for well-annealed monofilaments to 25 g/den for carpet staple. For textile fibers, a mean value of 50 to 60 g/den is common.

5.2.3 Dynamic mechanical analysis

A Solid Analyser RSA-II (Rheometric Scientific) was operated in a nitrogen gas atmosphere using tensile deformation mode and Static Force Tracking Dynamic Force. The test sequence is given in Table 5.1. The temperature increment was set at 2°C between −30 to +40°C to more accurately measure the glass transition temperature. Dynamic mechanical analyzers require a certain pretension since the sinusoidal deformations cannot be applied on slackened samples. All samples were mounted with approximately 0.5 g of pretension before starting the test; once the test started an initial static force of 5 g (applied at −100°C) was used. All experiments were performed with a 10 Hz frequency, and 0.1% strain. Khanna et al. [1989,1991] observed an increase of PET yarns moduli around their T_g with an increase of pretension. In our study, the pretension applied to the fiber at −100°C was varied around the base case of 5 g for a solid fiber. The change of pretension did not affect the value of the modulus, or the value of the T_g within the error shown in Figure 5.1. The strain was also varied around the base case of 0.1%, and no difference was found on either E' or E". Thus, the results reported in this chapter are characteristic to fiber properties, and are not an artifact of pretension or strain. Modulus calculations were based on the polymer cross-sectional area (S_p), except where noted.

In order to test reproducibility, two fibers were taken from the same sample and run with the conditions described in Table 5.1. The sample was a solid filament of 45.6 μm OD, spun with a final take-up speed of 840 m/min. As Figure 5.1 shows, E' and E" curves are almost perfectly overlapping from −100°C to 100°C, and only

differ slightly for temperatures higher than these. The reproducibility also attests to the fact that any stretching of the samples during loading was minimal. T_g was determined from the peak of the loss modulus curves E". The curves were fitted with a 6^{th} order polynomial function and the maximum (dE"/dT = 0) was used to determine T_g. Glass transition temperatures of 1.41°C and –0.28°C were obtained from the two duplicate samples. These values fit within the range of T_g (–30°C to 25°) typical of polypropylene [Ahmed, 1982; Brandrup and Immergut, 1989]. The difference of T_g between the two repeat tests is within a reasonable range; thus the reproducibility obtained with the RSA between two identical samples is quite good.

5.2.4 Birefringence

A Nikon polarized microscope (LabPhot2-pol) was used for measuring the birefringence of a sample. The Senarmont compensator technique was used to determine the retardation (phase difference between the light wave oriented parallel and perpendicular to the stretch direction). The retardation is proportional to the birefringence according to the following formula:

$$\text{birefringence} = \text{relative retardation (nm)} / \text{specimen thickness (nm)} \qquad (5.2)$$

For solid filaments, the specimen thickness was defined as the filament diameter. For hollow filaments, the thickness was defined as the difference between the outer diameter and the inner diameter, which is twice the wall thickness (since the refracted

light went through the fiber wall twice). This measurement gave the overall orientation of both the crystalline and amorphous regions.

5.2.5 Differential Scanning Calorimetry

Differential scanning calorimetry (DSC) was used to measure the experimental heat of fusion ΔH_f and the melting temperature T_m. The instrument used was a Perkin-Elmer DSC-2 with a heating rate of 1.25°C/min. This very slow heating rate was selected since Bershtein and Egorov [1994] studied the effect of heating rate on DSC melting peaks, and showed that the lower the heating rate, the more accurate the melting point. According to the literature, the melting point measured at this heating rate is less than a degree different from what would be measured at infinitely slow heating rate. Lower heating rates also give more resolved peak shapes according to the same reference. Sample weights of 1.0 to 4.0 mg were determined with an accuracy of 0.01 mg and placed in an aluminum pan. The temperature scale was calibrated with an indium standard (T_m = 156.6°C).

The preparation of fiber samples for reproducible results presents special problems for the DSC analysis of polymer fibers. To avoid any heat transfer limitations between fibers and aluminum pan, polypropylene fibers were cut in pieces of about 0.5 mm in length using a fresh razor blade for each sample. Special attention was taken to avoid stretching of the fibers. The pieces of fibers were placed in aluminum pans together with a drop of silicone oil to provide good thermal contact between sample and pan [Smook and Pennings, 1984]. To test for possible unwanted side-effects (i.e. plasticization), a solid fiber was immersed in silicone oil for 12 hours.

The diameter was measured before and after immersion, and no swelling was observed. Further, the silicone oil was carefully wiped off, and the fiber was tested with DMA. No change was observed for the elastic and the loss modulus curves before and after immersion in oil. Thus, silicone oil does not modify the fiber properties at ambient temperature, and we assumed it could be used safely at elevated temperatures as well.

The melting temperatures quoted in this paper are peak melting temperatures, i.e. the temperature corresponding to the maximum of the melting endotherm peaks. Crystallinity content of the fiber samples was determined using the commonly used relation [Dole, 1967]:

$$\% \text{ crystallinity} = \frac{\Delta H_f}{\Delta H_0} \cdot 100 \tag{5.3}$$

where ΔH_f is the heat of fusion of the sample and ΔH_0 is the heat of fusion of the same material with 100% crystallinity. A value of 146.5 J/g was assumed for ΔH_0 [Huda et al., 1985]. Heats of fusion ΔH_f were determined by comparing the areas under the sample melting endotherms to the areas for fusion of indium samples, with a known indium heat of fusion of 6.8 cal/g. The accuracy of the DSC measurements for melting temperature and crystallinity was estimated for both solid and hollow fibers. Three repeat experiments on solid fibers of 44 μm diameter, and three repeat experiments on hollow fibers of 55.6 μm OD and 28.8 μm ID were performed. The confidence interval, for a reliability of 0.95, was ± 1.5°C for the T_m, and ± 2% for the

fractional crystallinity, for both solid and hollow fiber samples. The low standard deviations obtained prove the good reproducibility of our sample preparation.

5.3 RESULTS AND DISCUSSION

5.3.1 Effect of inner diameter

In order to study the effect of the inner diameter, two different approaches were considered. In a first part, we considered the effect of inside diameter with a constant polymer cross-sectional area (S_p is constant), and in a second part we considered the effect of inside diameter with a constant outside diameter (S_f is constant).

Constant S_p

Fibers with constant polymer cross-sectional area were experimentally obtained by spinning fibers at constant polymer throughput and constant take-up velocity. Since mass neither enters nor leaves the spinline during fibers melt processing, the mass throughput at the exit of the spinneret is equal to the mass throughput on the collection roll. The mass conservation equation can be written as:

$$m_p = \rho_p \cdot v \cdot S_p \tag{5.4}$$

where

m_p = polymer throughput

ρ_p = polymer density

v = fiber velocity

S_p = polymer cross-sectional area

Assuming a constant polymer density of 0.895 g/cm^3 (the effect of crystallinity on polymer density was neglected), and since polymer throughput and take-up speed are constant (respectively 1.35 g/min and 840 m/min), then the polymer cross-sectional area also stays constant. The inner diameter was increased by increasing the flow of nitrogen injected in the core of the molten filament. A dimensionless variable termed the hollowness (H) was used to characterize hollow fiber dimensions:

$$H = \left(\frac{ID}{OD} \right)^2 \tag{5.5}$$

This variable represents the ratio of the area of the hole to the total area of the fiber. Figure 5.2 shows the variation of the elastic modulus E' versus temperature for solid and hollow fibers spun with a polymer throughput of 1.35 g/min and a take-up speed of 840 m/min. The ID was varied to obtain a range of hollowness from 0 to 53.3 %. Hollow fibers show a higher melting temperature versus the solid fiber but there is little difference between the two hollow fibers as shown in Table 5.2. The increase in T_m indicates a larger crystal thickness for the hollow fibers, while the increase in fractional crystallinity in the hollow fibers, as measured by DSC, is reflected in the increased modulus at all temperatures versus the solid fibers. A significant increase in modulus for the fiber with 53.3% hollowness was found versus the fiber with 30.2% hollowness. Since the fractional crystallinities of these two samples were approximately identical, the increase in modulus is a reflection of the increase in orientation determined via birefringence.

Finally however, there was no significant difference in glass transition temperature for any of the three samples (Figure 5.3). Generally, T_g increases as the fractional crystallinity increases. The equivalence of the solid fibers with the hollow fibers is probably due to predictable result that the orientation of the amorphous regions is higher in the solid fibers than in the hollow fibers, which offsets the increase in T_g caused by a higher crystalline fraction in the hollow fibers. Possible higher amorphous orientation in the solid fibers was not reflected in the birefringence measurements; however these birefringence measurements cannot distinguish between crystalline and amorphous domains. We are proposing that the crystallite orientation is greater in the hollow fibers, while the amorphous orientation is higher in the solid fibers. This tradeoff is a reflection of the competitiveness between polymer crystallization and molecular orientation in amorphous regions [Ziabicki, 1976]. The equivalence of glass transition between the two hollow fibers is more difficult to understand since the orientations are different, while the melting temperatures and crystalline fractions are identical. Because birefringence cannot distinguish between amorphous and crystalline domains, this equivalence could be the result of some complicated morphological behavior, or perhaps this slight increase in orientation, even if fully in the amorphous regions, is not enough to cause a significant enough increase in glass transition temperature.

Crystallization in melt-spun fibers has been studied both theoretically and experimentally. Results from various experiments of melt-spinning indicate that the structures formed during the process are due to non-isothermal crystallization under

molecular orientation [Jinan et al., 1989]. During melt spinning, the fiber cools down by convection only. The loss of heat is proportional to the outside area of the fiber. When spinning hollow fibers with constant polymer cross-sectional area, hollow fibers have a larger outer diameter than solid fibers. Thus hollow fibers are quenched faster than solid fibers, leading to higher chain orientation. The higher crystallinity with increased hollowness is more difficult to explain, since generally faster quenching means lower crystallinity. However, the stress is not uniform along the length of the threadline, and stress can also significantly affect the amount of crystalline material.

Constant S_f

The effect of inner diameter was also studied while maintaining the OD constant. Various ID's were obtained using different combinations of polymer throughput, take-up speed, and nitrogen flowrate. Keeping OD constant is particularly interesting considering the replacement of solid fibers by hollow fibers, since replacement would probably require the same outer diameter fiber.

Figure 5.4 shows the effect of temperature on elastic modulus E' for fibers with constant OD and various ID. Once again hollow fibers show a higher melting temperature than the solid fiber as shown in Table 5.3. No difference in T_m was observed between the two hollow fibers. The increase of T_m indicates a larger crystallite long spacing in hollow fibers. The increase of fractional crystallinity between the solid and the 37% hollowness fiber is reflected in the increase of

modulus between the two fibers, as reported in Figure 5.4. An unexpected decrease in fractional crystallinity was observed as the hollowness changed from 37% to 59%, while the modulus increased slightly. The increase of molecular orientation with increasing hollowness as shown in Figure 5.6 probably compensated for the drop of fractional crystallinity and explains the slight increase of modulus between the two hollow fibers. The increase of orientation with increasing hollowness was certainly due to faster quenching. Faster quenching was due to the total amount of polymer being less with increasing hollowness. This quenching certainly limits the complete organization of the polymer chains in crystallites, thus reducing the crystallinity. This phenomenon was observed before; Galanti and Montell [1965] found that crystallinity can be significantly affected by the cooling conditions: polypropylene fibers that were quenched immediately after extrusion formed a paracrystalline structure with low crystallinity (45%).

The variation of the glass transition temperature (Figure 5.5 and Table 5.3) with hollowness was very complex. The glass transition temperature actually decreased between the solid fiber and the 37% hollow fiber even though the fractional crystallinity increased. Once again, we assign this counterintuitive observation to higher amorphous chain orientation in the solid fiber. The increase of T_g between 37 and 59% hollowness could be explained by the decrease of fractional crystallinity. The reduced fractional crystallinity would allow higher amorphous orientation in the 59% hollow fiber.

Data obtained using DMA were complemented with data provided by tensile tests. Figure 5.6 represents rupture elongation and birefringence versus hollowness for fibers with constant OD (40 μm). Three fibers with various hollowness were added compared to the previous DMA and crystallinity analysis. As expected, birefringence increased with increasing hollowness while rupture elongation decreased. Rupture elongation and birefringence are actually closely connected, since the high orientation limits the maximum elongation that can be reached. Birefringence almost reached the maximum orientation that can be achieved in polypropylene fibers (0.03) with a hollowness of 69%. The introduction of a hole had little effect on toughness, but a more complex effect on modulus and tenacity was observed (see Figure 4.7). Both modulus and tenacity increased with increasing birefringence up to a hollowness of 50% (birefringence of about 0.015). After that point, modulus and tenacity decreased while birefringence continued to increase. This phenomenon agrees well with the dual effect of hollowness observed with constant polymer cross-sectional area.

For hollowness up to about 50%, the increase of inner diameter increases crystallinity, orientation, modulus and tenacity. Above 50% hollowness, the orientation reaches such levels (0.015) that it starts limiting crystallinity and strength.

5.3.2 Effect of take-up velocity

The vertical stress applied on the fibers during melt spinning orients the molecular axis of the polymer chains in the direction of the stretching. The orientation is a function of the polymer throughput, take-up speed, polymer temperature, and

many other parameters. Figures 5.8 and 5.9 show the effect of take-up speed on respectively elastic modulus and loss modulus, for hollow fibers produced with a polymer throughput of 2.33 g/min, and a nitrogen flowrate of 1.7 ml/min. These fibers had identical hollowness (about 40%), since the ratio of inner to outer diameter is not a function of final take-up speed based on the nitrogen and polymer mass balance equations:

$$\left(\frac{ID}{OD}\right)^2 = \frac{\frac{m_n}{\rho_n}}{\frac{m_n}{\rho_n} + \frac{m_p}{\rho_p}} \tag{5.6}$$

where

m_p = polymer mass throughput

m_n = nitrogen mass flowrate

ρ_p = polymer density

ρ_n = nitrogen density

In Figure 5.8, hollow fibers spun with increasing take-up speed show increasing modulus at ambient temperature. The increase of fractional crystallinity and molecular orientation (Table 5.4) between 460 and 1090 m/min explains the increase of modulus. Between 1400 and 1880, the increase of orientation alone is responsible for the high modulus, since the fractional crytallinity decreases (Drawing has been shown to decrease crystallinity [Galanti and Mantell, 1965]). At high speeds, the stress acting on the fiber increases and might start destroying the crystallites. Moreover, the decrease of the polymer cross-sectional area with the increase of

spinning speed results in a faster quenching, which could reduce fractional crystallinity.

As also reported in Table 5.4, spinning speed had very little effect of T_m, thus spinning speed did not affect crystal size, or their perfection. Glass transition temperatures decreased significantly with increasing take-up speed as shown in Figure 5.9. For final spinning speeds between 460 and 1090 m/min, the decrease in T_g was probably a tradeoff between higher crystalline orientation and lower amorphous orientation. For higher speeds, T_g decreases as fractional crystallinity decreases, as expected.

Figure 5.10 represents stress-strain curves of the same fibers as analyzed in Figures 5.8 and 5.9. The increase of the degree of orientation achieved by drawing influences the mechanical properties of polypropylene filaments. Figure 5.10 was analyzed to obtain fiber typical mechanical properties. Rupture elongation and birefringence are plotted versus take-up speed in Figure 5.11. As expected, for increasing windup speeds, orientation increases, and thus elongation at break decreases. Figure 5.12 represents the variation of modulus, toughness, and tenacity as a function of birefringence. Toughness shows little variation, whereas modulus and tenacity increase as birefringence (thus take-up speed) increases. This is typical of solid fiber behavior [Ahmed, 1982]. In the previous section (constant S_f), a maximum in fractional crystallinity of 55% and a maximum in tenacity of 1.5 g/den were found at a birefringence and hollowness of 0.015 and 50% respectively. Here, the increase of take-up speed starts limiting fractional crystallinity around 1090 m/min, but has no

limiting effects on modulus and tenacity, probably because birefringence and orientation never reached their critical values.

5.4 CONCLUSION

A study was carried out of the mechanical properties of hollow fibers compared to solid fibers. Based on the combined experimental results presented in this chapter, hollow fibers exhibit stronger properties in terms of crystallinity, orientation, modulus, and tenacity, whether the outer diameter or the polymer cross-sectional area are kept constant. Larger inner diameter and higher spinning speed seem to improve hollow fibers properties to a certain extent. It was observed that the presence of the inner hole changed dramatically the tensile properties between solid and hollow fibers. We observed that the increase of spinning speed or inner diameter first increased fractional crystallinity. However, for high degree of orientation (birefringence higher than 0.015) or large hollowness (higher than 50%), the fractional crystallinity went down.

By keeping orientation and hollowness below their critical values, replacing solid fibers by hollow fibers would not only produce a cheaper and lighter material, it could also produce a stronger material.

5.5 GLOSSARY-NOMENCLATURE

ΔH_f : heat of fusion (J/g)
ΔH_0 : heat of fusion of 100% crystalline material
DMA : Dynamic Mechanical Analysis
DSC : Differential Scanning Calorimetry
E' : elastic modulus (dyn/cm^2)
E" : loss modulus (dyn/cm^2)
H : hollowness (%)
ID : inner diameter (μm)
m_n : polymer throughput (g/min)
m_p : polymer throughput (g/min)
OD : outer diameter (μm)
ρ_n : polymer density (g/cm^3)
ρ_p : polymer density (g/cm^3)
S_f : fiber cross-sectional area (μm^2)
S_p : polymer cross-sectional area (μm^2)
T_g : glass transition temperature (^oC)
T_m : melting temperature (^oC)
v : fiber velocity (m/min)

5.6 REFERENCES

M. Ahmed, *Polypropylene Fibers-Science and Technology*, Elsevier Scientific Publishing Company, New York (1982).

ASTM D 2101-93, "Standard Test Method of single man-made textile fibers taken from yarns and tows" (1993).

B. Baum; W. Holley; Jr. and R.A. White, "Hollow fibers in reverse osmosis, dialysis, and ultrafiltration" in *Membrane Separation Processes*, P. Meares, Elsevier Scientific Publishing Company, New York (1976).

V.A. Bershtein and V.M. Egorov, "*Differential scanning calorimetry of polymers*", Ellis Horwood, New York (1994).

J. Brandrup and E.H. Immergut, *Polymer Handbook*, 3rd Ed., John Wiley & Sons, New York (1989).

N.M. Capiati and R. S. Porter, "Tensile properties of ultradrawn polyethylene", *Journal of Polymer Science: Polymer Physics*, **13**, 1177-1186 (1975).

M. Dole, "Crystallinity from thermal measurements", *Journal of Polymer Science, Part C*, **18**, 57-68 (1967).

A. V. Galanti and C. L. Mantell, *Polypropylene fibers and Films*, Plenum Press, New York (1965).

M. N. Huda; H. Dragaun; S. Bauer; H. Muschik; and P. Skalicky, "A study of the crystallinity index of polypropylene fibres", *Colloid & Polymer Science*, **263**, 730-737 (1985).

C. Jinan; T. Kikutani; A. Takaku; and J. Shimizu, " Nonisothermal Orientation-Induced Crystallization in Melt Spinning of Polypropylene", *Journal of Applied Polymer Science*, **37**, 2683-2697 (1989).

Y.P. Khanna; W.M. Wenner; R. Kumar; and S. Kavesh, "Dynamic mechanical analysis of fibers. I. Effect of experimental variables and material type", *Journal of Applied Polymer Science*, **38**, 571-578 (1989).

Y.P. Khanna; T.J. Taylor; and R. Kumar, "Dynamic mechanical analysis of Fibers. II. Estimation of fiber orientation and characterization of heat set PET yarns", *Journal of Applied Polymer Science*, **42**, 693-699 (1991).

J. J. Kim; T. S. Jang; Y. D. Kwong; U. Y. Kim; and S. S. Kim, "Structural study of microporous polypropylene hollow fiber membranes made by the melt-spinning and cold-stretching method," *Journal of Membrane Science*, **93**, 209 (1994).

J. J. Kim; J. R. Hwang; U. Y. Kim; and S. S. Kim, "Operation parameters of melt spinning of polypropylene hollow fiber membranes", *Journal of Membrane Science*, **108**, 25-36 (1995).

I. Moch, "Hollow Fiber Membranes," *Encyclopedia of Chemical Technology*, **13**, 4th Ed. (1991).

T. H. Oh; M. S. Lee; S. Y. Kim; and H.J. Shim, "Studies on Melt-Spinning Process of Hollow Fibers", *Journal of Applied Polymer Science*, **68**, 1209-1217 (1998).

J. Smook and J. Pennings, "Influence of draw ratio on morphological and structural changes in hot-drawing of UHMW polyethylene fibres as revealed by DSC", *Colloid & Polymer Science*, **262**, 712-722 (1984).

N. Weeks and R.S. Porter, "Mechanical properties of ultra-oriented polyethylene", *Journal of Polymer Science: Polymer Physics*, **12**, 635-643 (1974).

A. Ziabicki, " Fundamentals of fibre formation", Editor John Wiley & Sons, New York (1976).

	Sequence 1	Sequence 2	Sequence 3
Initial temperature (°C)	-100	-30	40
Final temperature (°C)	-30	40	200
Temperature increment (°C)	8	2	4
Soak time (sec)	6	6	6
Strain (%)	0.1	0.1	0.1

Table 5.1: DMA test sequence.

Hollowness (%)	Birefringence	T_g (°C)	T_m (°C)	Crystallinity (%)
0	0.00372	-0.249	161	39.6
30.2	0.00587	0.809	164	50.3
53.3	0.00738	1.101	164	50.2

Table 5.2: Birefringence, T_g, T_m, and fractional crystallinity of fibers at constant polymer cross-sectional area.
Polymer throughput = 1.35 g/min;
Take-up speed = 840 m/min.

Hollowness (%)	Birefringence	T_g (°C)	T_m (°C)	Crystallinity (%)
0	0.00368	-0.28	161	39.6
37	0.0096	-10	164	55.7
59	0.0185	-7.22	164	44.5

Table 5.3: Birefringence, T_g, T_m, and fractional crystallinity for fibers with constant OD.

Take-up speed (m/min)	Birefringence	T_g (°C)	T_m (°C)	Crystallinity (%)
460	0.00563	5.0	162.6	26.4
790	0.0077	5.0	162.6	36.2
1090	0.01	2.2	163.8	59.8
1400	0.0123	0.5	163.5	50.3
1880	0.0144	-10.0	163.1	37.1

Table 5.4: Birefringence, T_g, T_m, and fractional crystallinity at various take-up speeds.
Polymer throughput = 2.33 g/min;
Nitrogen flowrate = 1.7 ml/min.

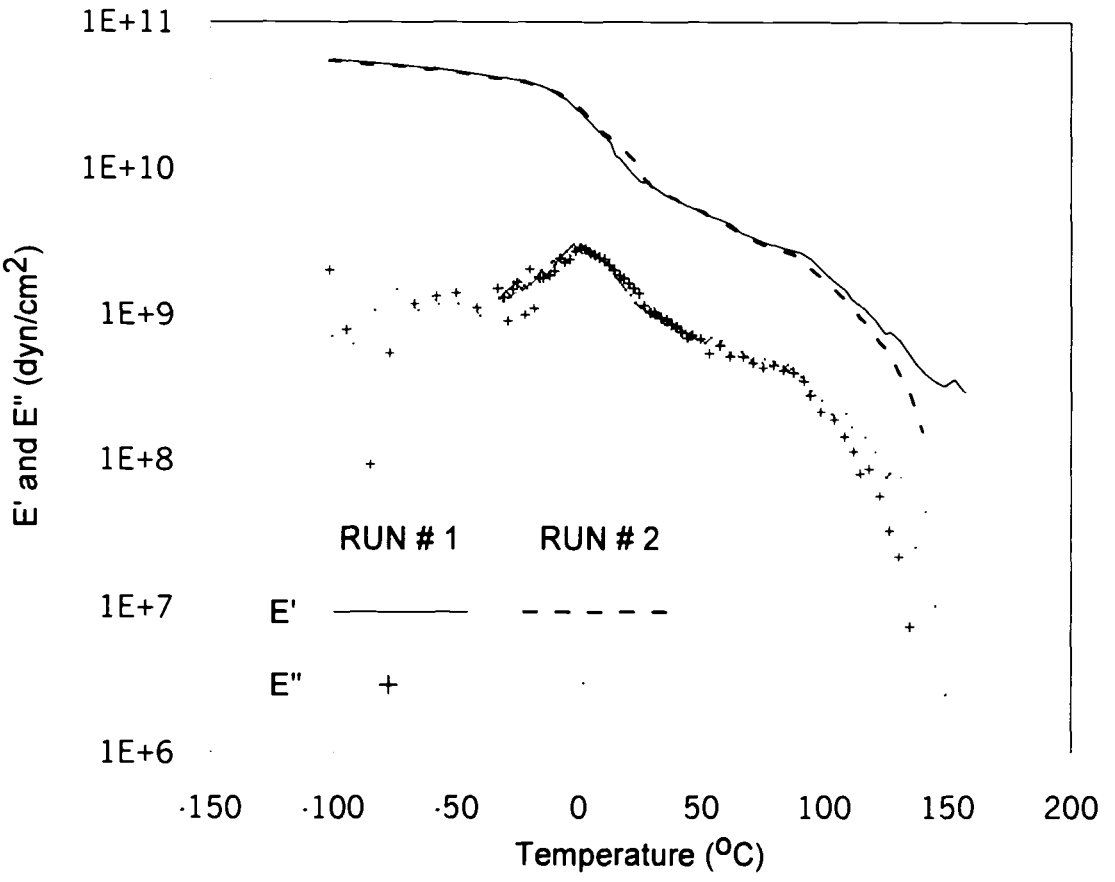

Figure 5.1: Elastic modulus E' and complex modulus E" as a function of temperature for two repeat runs of the same sample.
OD = 54.6 μm;
Take-up speed = 840 m/min.

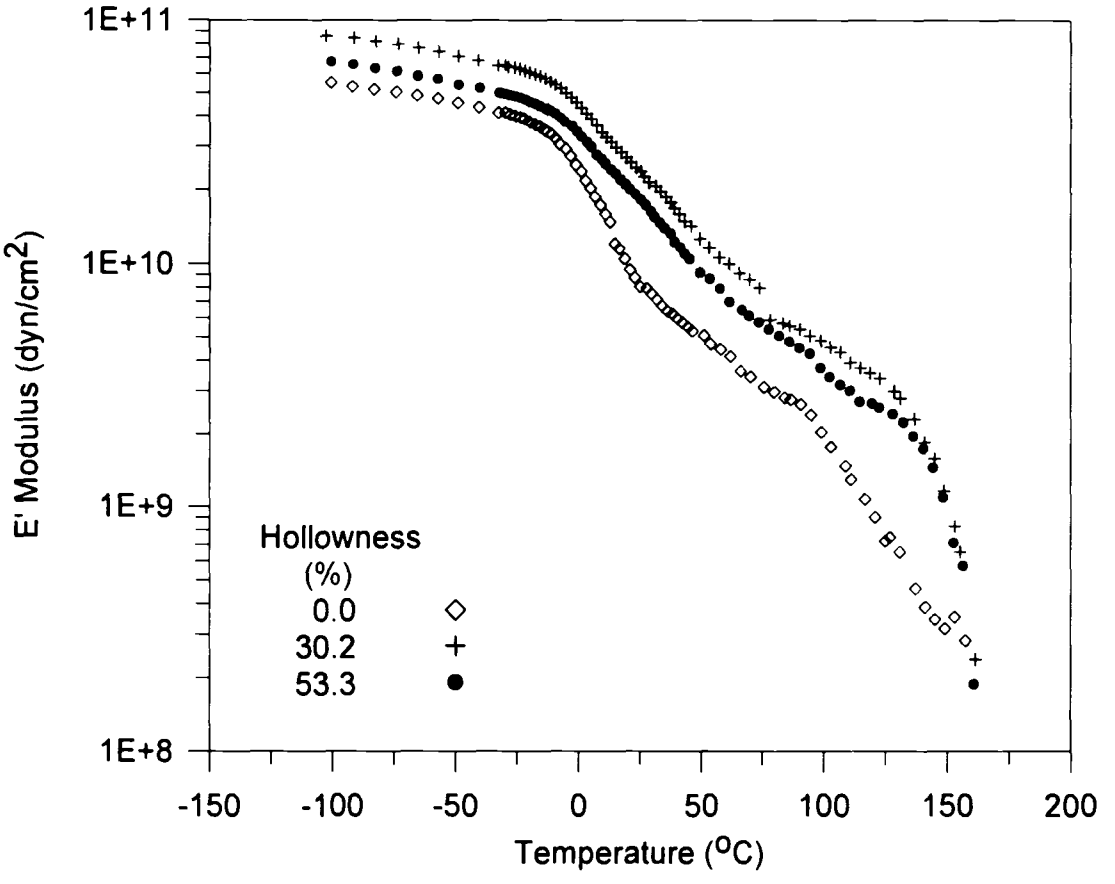

Figure 5.2: Elastic modulus E' as a function of temperature for fibers with constant cross-sectional area and various hollowness.
Polymer throughput = 1.35 g/min;
Take-up speed = 840 m/min.

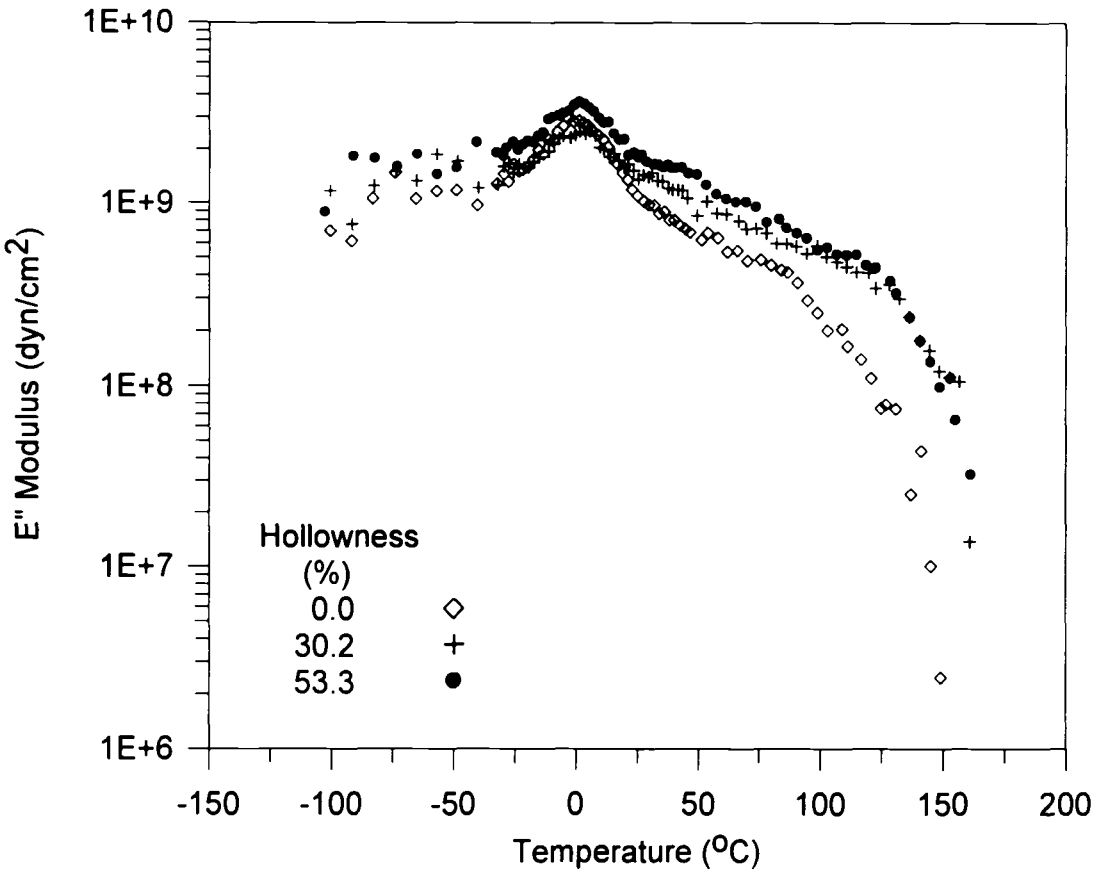

Figure 5.3: Loss modulus E" as a function of temperature for fibers with constant cross-sectional area and various hollowness.
Polymer throughput = 1.35 g/min;
Take-up speed = 840 m/min.

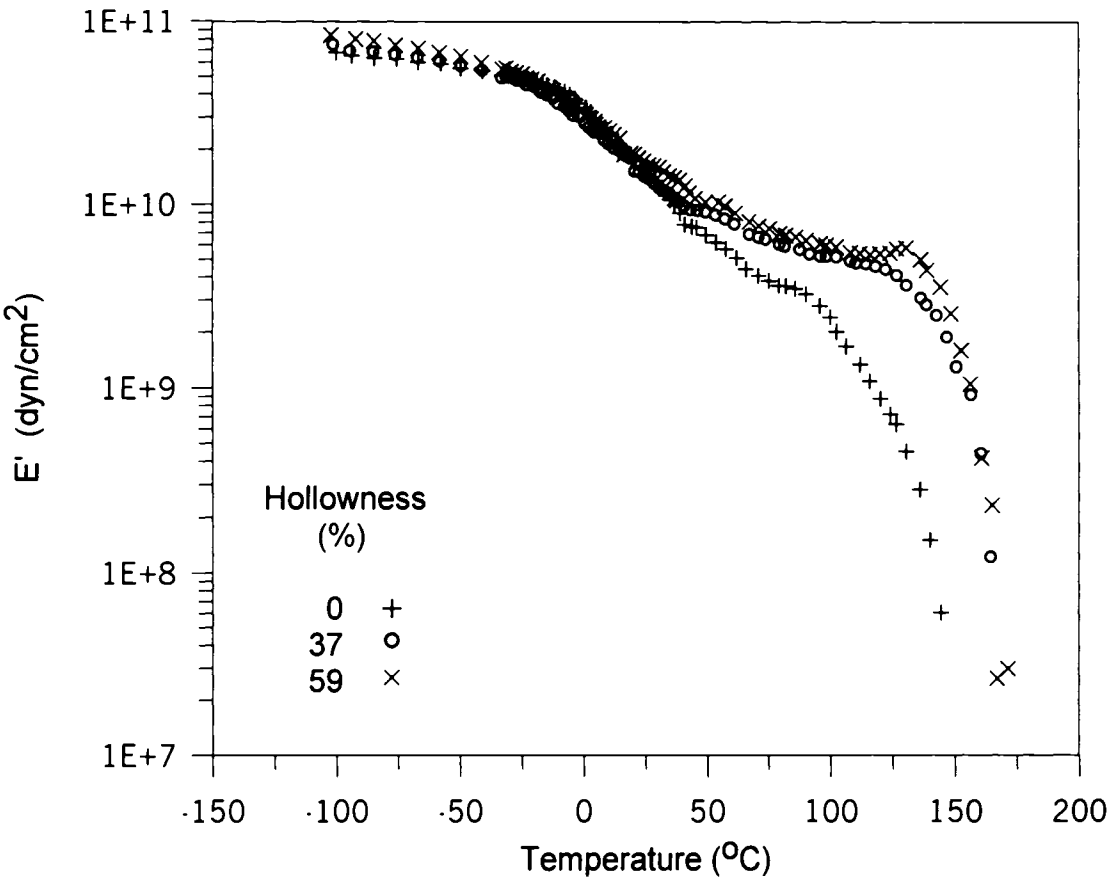

Figure 5.4: Elastic modulus E' versus temperature for fibers with constant outer diameter and various hollowness (OD = 40 μm).

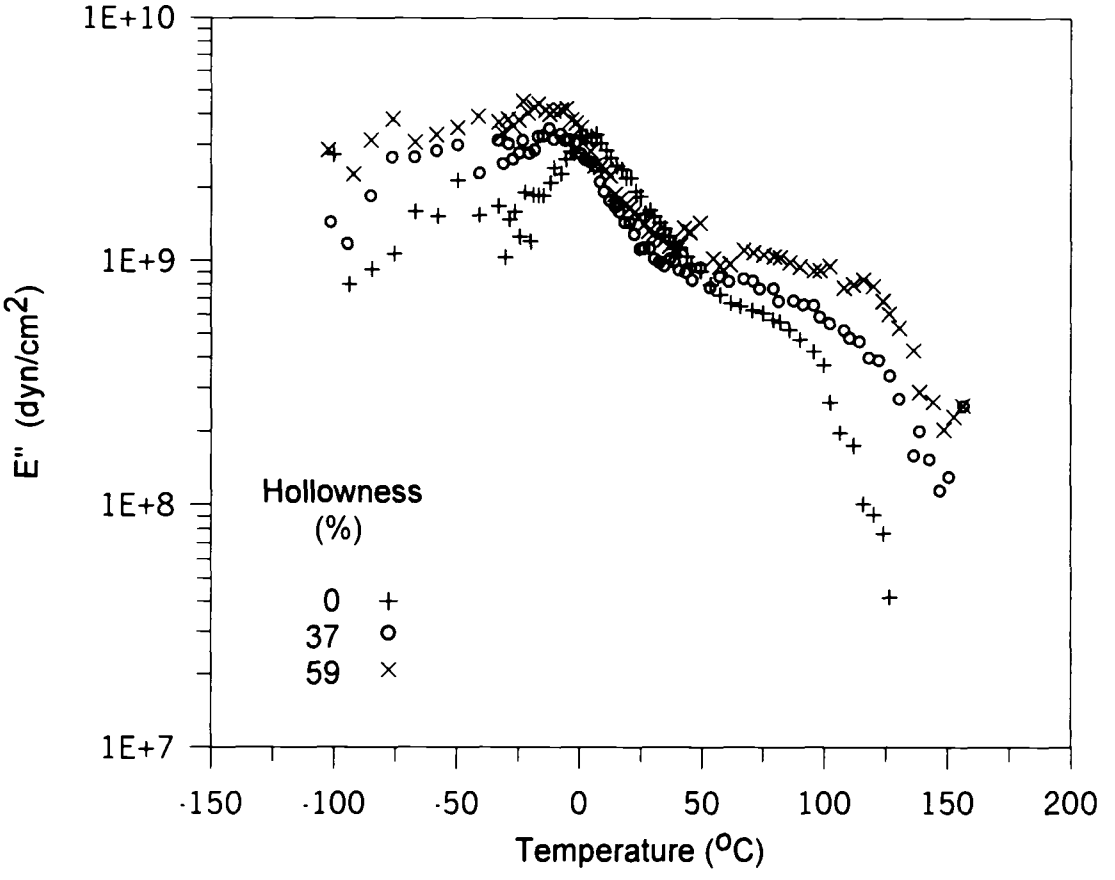

Figure 5.5: Loss modulus E" versus temperature for fibers with constant outer diameter (40 μm) and various hollowness.

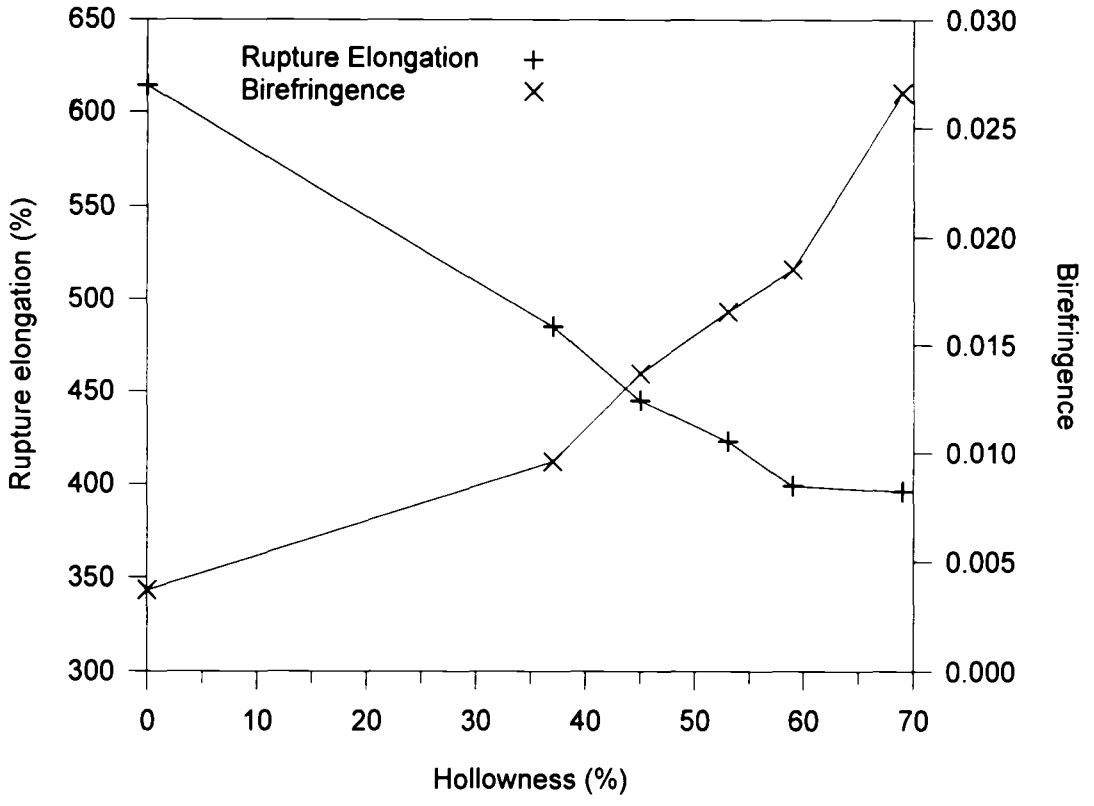

Figure 5.6: Rupture elongation and birefringence versus hollowness for fibers with a constant outer diameter of 40 microns.

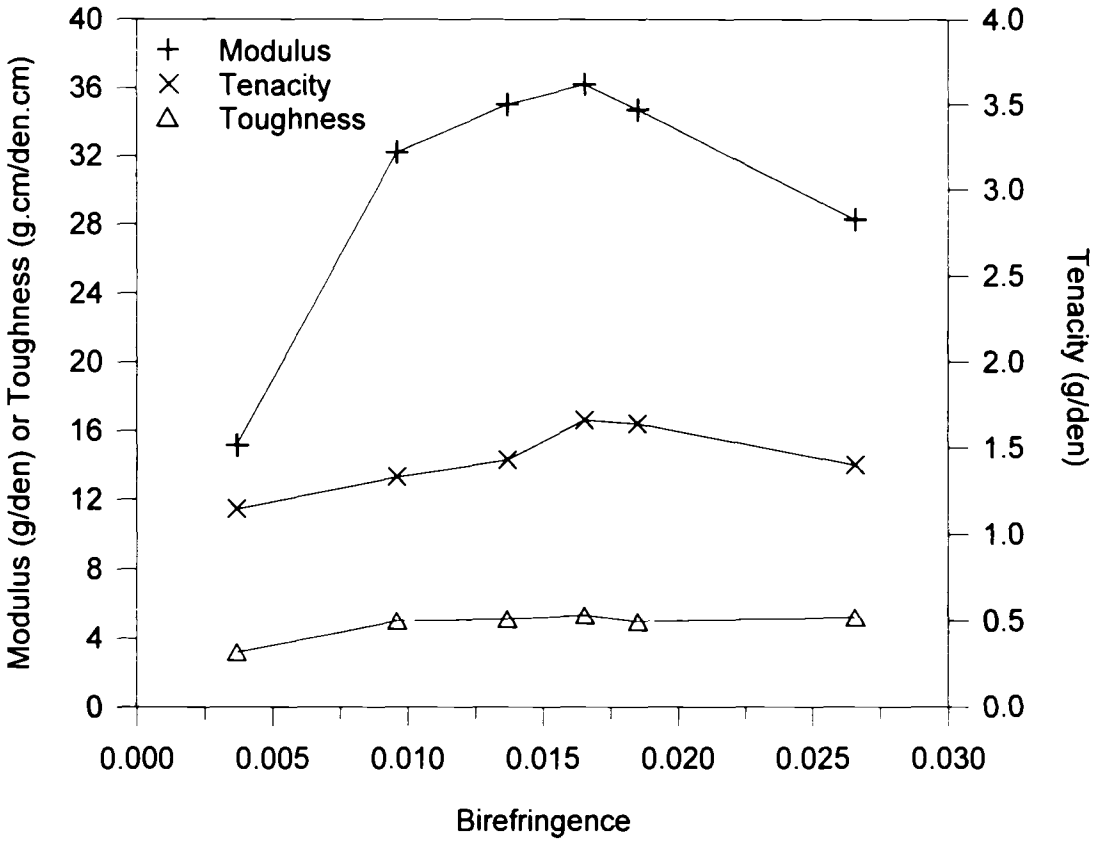

Figure 5.7: Modulus, toughness, and tenacity versus birefringence for fibers with a constant outer diameter of 40 microns.

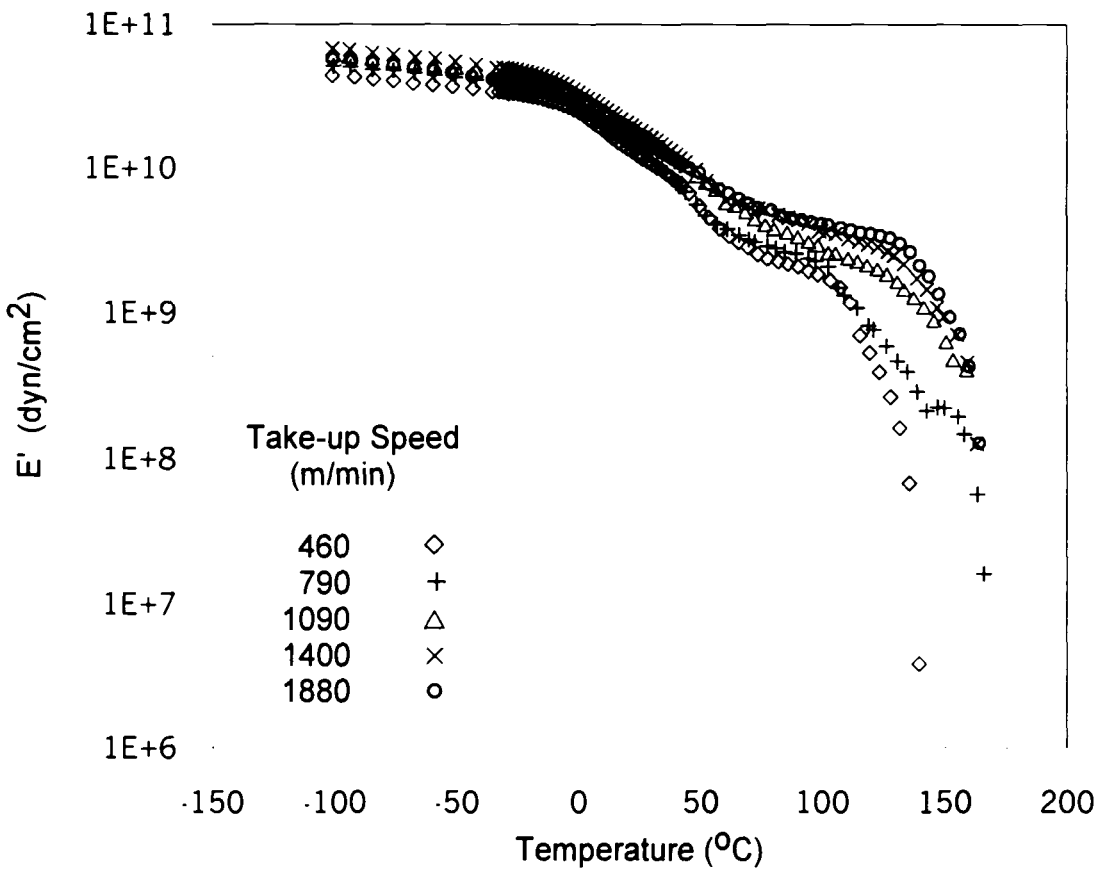

Figure 5.8: Elastic modulus E` versus temperature for various take-up speeds.
Polymer throughput = 2.33 g/min;
Nitrogen flowrate = 1.7 ml/min.

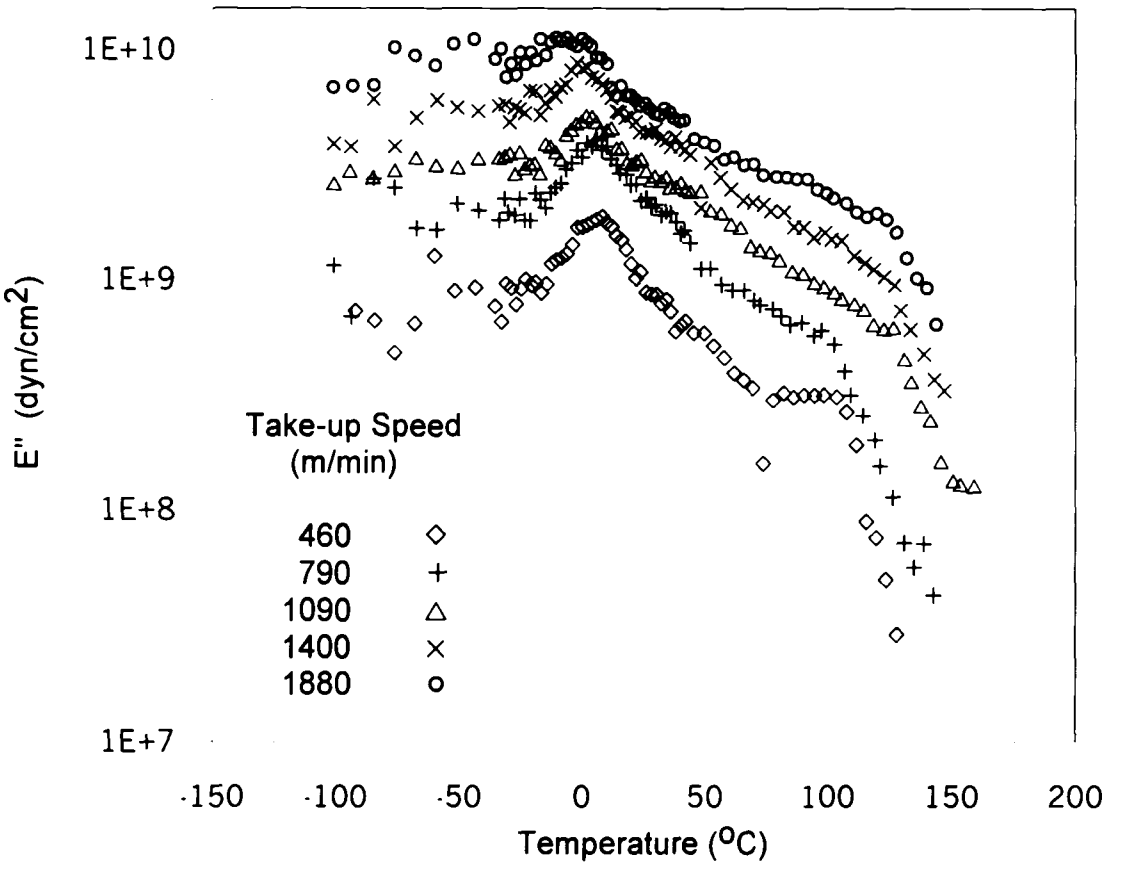

Figure 5.9: Complex modulus E" versus temperature for various take-up speeds.
Polymer throughput = 2.33 g/min;
Nitrogen flowrate = 1.7 ml/min.

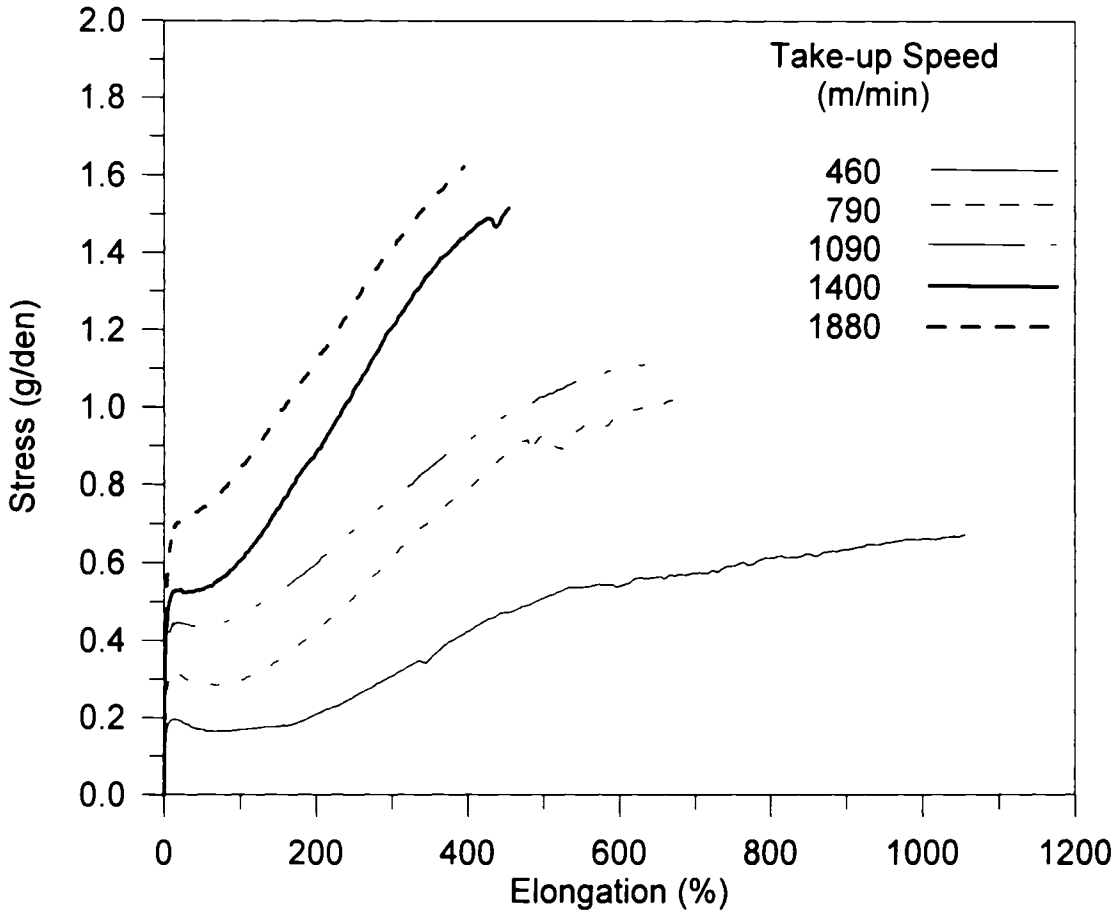

Figure 5.10: Stress-strain curve for different processing take-up speeds on hollow fibers.
Polymer throughput = 2.33 g/min;
Nitrogen flowrate = 1.7 ml/min.

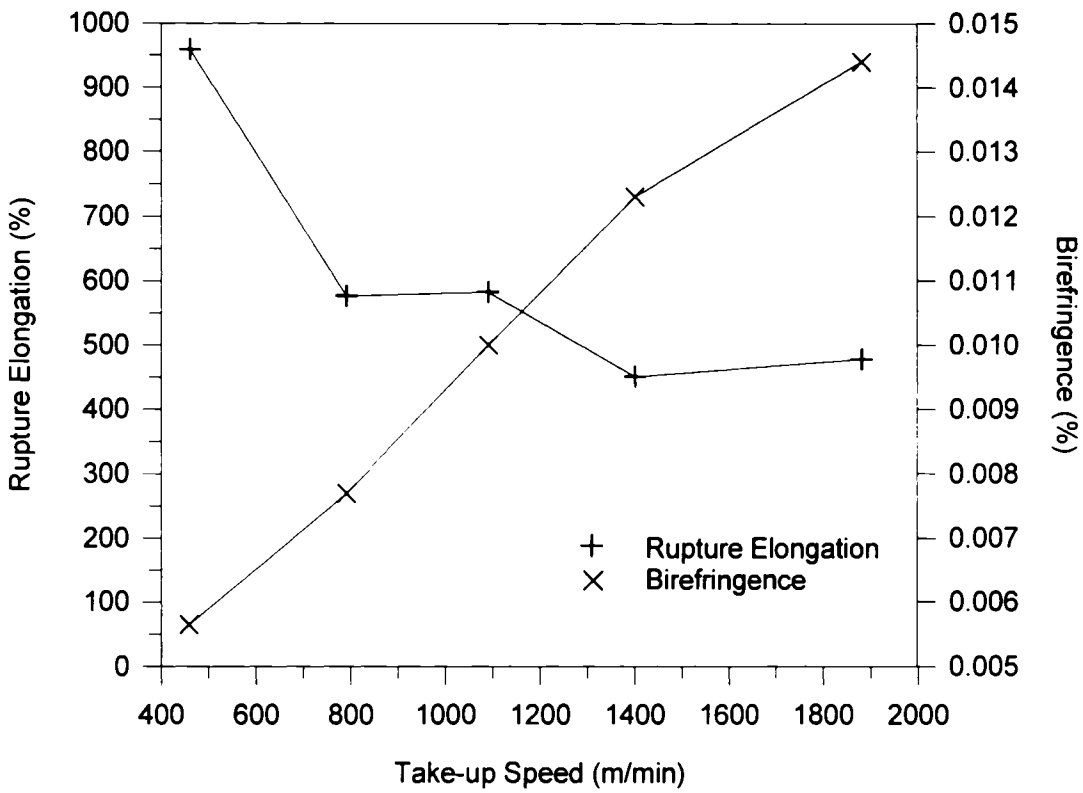

Figure 5.11: Effect of take-up speed on rupture elongation and birefringence for hollow fibers.
Polymer throughput = 2.33 g/min;
Nitrogen flowrate = 1.7 ml/min.

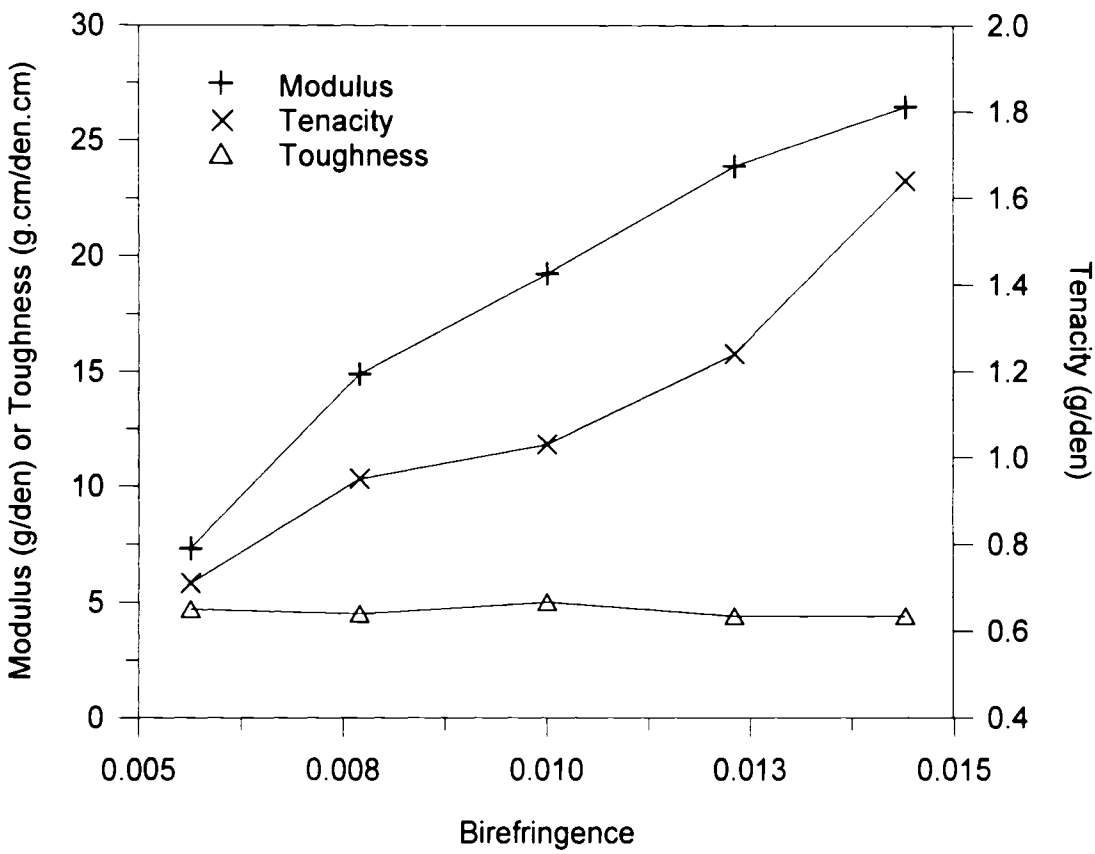

Figure 5.12: Effect of take-up speed on modulus, toughness and tenacity for hollow fibers.
Polymer throughput = 2.33 g/min;
Nitrogen flowrate = 1.7 ml/min.

CHAPTER 6

CONCLUSIONS

For many nonwoven uses, hollow polypropylene fibers can be substituted for solid polypropylene fibers. When this substitution is made, the polymer cost savings can be substantial. For the purpose of replacing solid fibers by hollow fibers in nonwoven webs, polypropylene hollow fibers were produced via melt spinning. The properties of both webs and individual fibers were studied off-line.

The compression-recovery and opacity behaviors of polypropylene hollow fiber webs were quite similar to that of solid polypropylene fiber webs. At constant outer diameter, individual hollow fibers exhibited stronger properties (than solid filaments) in terms of crystallinity, orientation, modulus, and tenacity. However, hollow fiber properties started to decrease for hollowness higher than 50%.

The process of hollow fiber spinning was measured on-line. Combination of on-line measurement techniques with polymer and nitrogen continuity equations allowed us to follow on-line density of hollow fibers. High degrees of orientation were obtained for large windup speeds, large nitrogen rates (large inner diameters), and low polymer throughputs. In conventional melt spinning (solid filaments),

windup speed is known as an important factor influencing stress-induced crystallization. In hollow fiber spinning, we showed that nitrogen flowrate (inner diameter size) also plays an important role in on-line stress.

A mathematical model was developed to predict on-line hollow fiber spinning. Newtonian and Phan-Thien constitutive equations were used. In the melt spinning of hollow fibers, the effects of heat transfer (cooling) on the threadline are more important than the choice of constitutive equation. Hence, the Newtonian model fitted the data quite well. However, more complex constitutive equations are useful for stress predictions along the threadline.

Melt spinning applied to hollow fiber production was found to improve fiber properties (in comparison to solid fibers). Since melt blown solid fibers are known as weal fibers, it would be very interesting to see if melt blowing applied to hollow fibers also produces fibers with improved properties.

APPENDICES

APPENDIX A

COMPUTER PROGRAM FOR HOLLOW FIBER MELT SPINNING

GLOSSARY OF VARIABLES

a(4):	Gill constant array
aj:	temporary storage variable
alpha1:	dimensionless relaxation time
alpha2:	dimensionless relaxation time
aux(6):	help array for intermediate storage of numbers
b(4):	Gill constant array
beta:	proportionality constant in the Matsui correlation
bj:	temporary storage variable
c(4):	Gill constant array
cj:	temporary storage variable
cpfib:	heat capacity of polymer melt
denair:	air density
denfib:	fiber density
denitro:	nitrogen density
denitro0:	initial nitrogen density
dery (1):	derivative of the dimensionless fiber velocity
dery(2):	derivative of the first component of the axial rheological stress (t_1)
dery(3):	derivative of the first component of the radial rheological stress (p_1)
dery(4):	derivative of the second component of the axial rheological stress (t_2)
dery(5):	derivative of the second component of the radial rheological stress (p_2)
dery(6):	derivative of the dimensionless filament temperature
dstrdz:	derivative of the total axial rheological stress inside the fiber
dtdz:	fiber temperature gradient
dvdz:	fiber velocity gradient
e:	Phan-Thien parameter related to stress saturation at high extension rates
eps1, epslon:	dimensionless reciprocal initial rheological force inside the fiber
fluid:	selection of a polymer (fluid = 1 : polypropylene)
f0:	initial force
ftmp:	fiber temperature

fvel:	fiber velocity
g1:	shear modulus of the polymer melt, first relaxation time
g2:	shear modulus of the polymer melt, second relaxation time
gamma:	proportionality factor in the Kase-Matsuo correlation for the Nusselt number
h:	reciprocal of the number of steps used to traverse the analysis region
i:	integer counter in subroutine RKGS
ID:	fiber inside diameter
ID0:	fiber initial inside diameter
j:	integer counter in subroutine RKGS
k1, k2, k3:	simplifying group
ka:	Phan-Thien parameter K1
kb:	Phan-Thien parameter K2
kfair:	thermal conductivity of the air stream
kfib:	thermal conductivity of he polymer melt
l:	length of the analysis region (threadline)
le:	position along the spinline
m:	exponent in the Kase-Matsuo correlation for the Nusselt number
model:	selection of constitutive equations (model = 1 : Newtonian model; model = 2 : Phan-Thien Model)
n:	exponent in the Matsui correlation
next1:	selection of the type of display (next1 = 0: results are not displayed; next1 = 1: results are displayed)
OD:	fiber outside diameter
OD0:	fiber initial outside diameter
pr:	Prandtl number
r1:	temporary storage variable
r2:	temporary storage variable
rair:	modified Reynolds number for the air side
rt1:	first relaxation time
rt2:	second relaxation time
ta:	air stream temperature
tamax:	initial air temperature
tfor:	total axial rheological force inside the filament
thetaa:	dimensionless air temperature
tm:	initial fiber temperature
tstr:	total axial rheological stress inside the filament
v0:	fiber initial velocity
vamax:	air velocity
visfib:	zero shear rate viscosity of the polymer melt
x:	dimensionless position along the threadline
xdiv:	dimensionless position along the threadline to display results
xi:	Phan-Thien parameter related to viscous shear thinning
y(1):	dimensionless fiber velocity

y(2): first component of the axial rheological stress (t_1)
y(3): first component of the radial rheological stress (p_1)
y(4): second component of the axial rheological stress (t_2)
y(5): second component of the radial rheological stress (p_2)
y(6): dimensionless filament temperature
z: position along the threadline

```
c       The main program is set up for Newtonian
c       and Phan-Thien calculations of the melt spinning
c       of hollow filaments
c       ------------------------
c       specification statements
c       ------------------------
        integer fluid,model,next1
        real dery(6),y(6)
        real dstrdz,dtdz,dvdz,f0,ftmp,fvel,h,l,tamax,tfor,
     *       tm,tstr,v0,vamax,OD,ID,OD0,ID0,denitro0
        OPEN(UNIT=2,FILE='output.dat',STATUS='UNKNOWN')
        OPEN(UNIT=4,FILE='outderiv.dat',STATUS='UNKNOWN')
        OPEN(UNIT=3,FILE='input.dat',STATUS='UNKNOWN')
C       -------------
c       initialization
c       --------------
        fluid=1
        model=2
        next1=1
        write(*,*)'enter the initial outer diameter'
        read(3,*)OD0
        write(*,*)'enter the initial inner diameter'
        read(3,*)ID0
        write(*,*)'enter the initial speed'
        read(3,*)v0
        write(*,*)'enter the initial temperature'
        read(3,*)tm
        write(*,*)'enter the length of the spinline'
        read(3,*)l
        vamax=0.00
        tamax=298.15
        write(*,*) 'Enter the initial rheological force'
        read(*,*) f0
        denitro0=0.339/tm**1.001
        h=0.00005
        y(1)=1.0
        y(2)=1.0
        y(3)=0.0
        y(4)=0.0
        y(5)=0.0
        y(6)=1.0
        dery(1)=0.0
        dery(2)=0.0
        dery(3)=0.0
```

```
      dery(4)=0.0
      dery(5)=0.0
      dery(6)=0.0
      call rkgs(OD0,ID0,dery,OD,ID,dstrdz,dtdz,dvdz,f0,fluid,
     *          ftmp,fvel,h,l,model,next1,tamax,tfor,tm,tstr,
     *          v0,vamax,y)
      stop
      end
c     ------------------------------------------------------------
c     ------------------------------------------------------------
      subroutine rkgs(OD0,ID0,dery,OD,ID,dstrdz,dtdz,dvdz,f0,
     *                fluid,ftmp,fvel,h,l,model,next1,tamax,
     *                tfor,tm,tstr,v0,vamax,y)
c     ------------------------
c     specification statements
c     ------------------------
      integer fluid,i,j,model,next1
      real aux(6),a(4),b(4),c(4),dery(6),y(6)
      real aj,bj,cj,cpfib,OD0,ID0,denair,denfib,OD,ID,
     *dstrdz,dtdz,dvdz,e,f0,ftmp,fvel,g1,g2,h,kfair,
     *kfib,l,le,r1,r2,rair,rt1,rt2,ta,tamax,tfor,tm,
     *tstr,v0,vair,vamax,visfib,x,xdiv,xi,z,visair
c     --------------------
c     start of computations
c     --------------------
c
c     calculation of all the properties at the initial point
c
  1   x=0.0
      xdiv=0.005
      le=0.0
      call air(OD0,ID0,denair,kfair,rair,ta,tamax,v0,vair,
     *         vamax,0.0,visair)
      if (fluid.eq.1) then
          call pprop(cpfib,denfib,e,g1,g2,kfib,model,rt1,rt2,tm,
     *               visfib,xi,y,dery,v0,l)
       write(*,*)' test 1'
          go to 10
      endif
      if (fluid.eq.2) then
         call pethyl(cpfib,denfib,e,g1,g2,kfib,model,rt1,rt2,tm,
     *               visfib,xi,y)
         go to 10
      end if
      if (fluid.eq.3) then
         call pet(cpfib,denfib,e,g1,g2,kfib,model,rt1,rt2,tm,
     *            visfib,xi,y)
         go to 10
      end if
c     ------------------------------------------------------------
c     ------------------------------------------------------------
  10  call fct(cpfib,OD0,ID0,denair,denfib,dery,OD,ID,
     *         dstrdz,dtdz,dvdz,e,f0,ftmp,fvel,g1,g2,
     *         kfair,kfib,l,model,rair,rt1,rt2,ta,tfor,
```

```
     *            tm,tstr,v0,vair,visfib,xi,y,visair)
c
c        test printing
c        -------------
         If (next1.eq.1) then
           write(6,100) le,OD*(10.0**6.0),ID*(10.0**6.0),
     *                  fvel*60,ftmp-273.15
           write(2,100) le,OD*(10.0**6.0),ID*(10.0**6.0),
     *                  fvel*60,ftmp-273.15,tstr
           write(4,200) dvdz,dtdz,dstrdz
         endif
  100    format(f6.2,1x,f6.1,1x,f6.1,1x,f10.4,1x,f5.1,1x,e9.3)
  200    format(e9.3,1x,e9.3,1x,e9.3)
c        end test
c        ------------------------------
c        calculation of Gill constants
c        ------------------------------
  11     a(1)=0.5
         a(2)=1-2**(-0.5)
         a(3)=1+2**(-0.5)
         a(4)=1/6
         b(1)=2.0
         b(2)=1.0
         b(3)=1.0
         b(4)=2.0
         c(1)=0.5
         c(2)=1-2**(-0.5)
         c(3)=1+2**(-0.5)
         c(4)=0.5
c        ----------------------------------
c        start of innermost Runge-Kutta loop
c        ----------------------------------
  12     do 13 i=1,6
            aux(i)=0.0
  13     continue
         j=1
  14     aj=a(j)
         bj=b(j)
         cj=c(j)
         do 15 i=1,6
            r1=h*dery(i)
            r2=aj*(r1-( bj*aux(i) ))
            y(i)=y(i)+r2
            r2=r2+r2+r2
            aux(i)=aux(i)+r2-(cj*r1)
  15     continue
         if (j-4) 16,26,26
  16     j=j+1
         if (j-3) 17,18,17
  17     x=x+(0.5*h)
  18     if (fluid.eq.1) then
           call pprop(cpfib,denfib,e,g1,g2,kfib,model,rt1,
     *                rt2,tm,visfib,xi,y,dery,v0,1)
                go to 25
```

```
          end if
          if (fluid.eq.2) then
                  call
pethyl(cpfib,denfib,e,g1,g2,kfib,model,rt1,rt2,
     *                         tm,visfib,xi,y)
                  go to 25
          end if
          if (fluid.eq.3) then
                  call
pet(cpfib,denfib,e,g1,g2,kfib,model,rt1,rt2,tm,
     *                       visfib,xi,y)
               go to 25
          endif
  25      z=x*l
          call air(OD0,ID0,denair,kfair,rair,ta,tamax,v0,
     *             vair,vamax,z,visair)
          call fct(cpfib,OD0,ID0,denair,denfib,dery,OD,ID,dstrdz,
     *             dtdz,dvdz,e,f0,ftmp,fvel,g1,g2,kfair,kfib,
     *             l,model,rair,rt1,rt2,ta,tfor,tm,tstr,v0,
     *             vair,visfib,xi,y,visair)
          go to 14
c         ---------------------------------
c         end of innermost Runge-Kutta loop
c         ---------------------------------
c
c         ------------------------------------------------------
c         calculation of derivatives and properties in new point
c         ------------------------------------------------------
  26      if (fluid.eq.1) then
              call pprop(cpfib,denfib,e,g1,g2,kfib,model,rt1,
     *                   rt2,tm,visfib,xi,y,dery,v0,1)
              go to 35
          end if
          if (fluid.eq.2) then
              call pethyl(cpfib,denfib,e,g1,g2,kfib,model,rt1,rt2,tm,
     *                   visfib,xi,y)
              go to 35
          end if
          if (fluid.eq.3) then
              call pet(cpfib,denfib,e,g1,g2,kfib,model,rt1,rt2,tm,
     *                visfib,xi,y)
              go to 35
          end if
  35      z=x*l
          call air(OD0,ID0,denair,kfair,rair,ta,tamax,v0,
     *             vair,vamax,z,visair)
          call fct(cpfib,OD0,ID0,denair,denfib,dery,OD,ID,dstrdz,
     *             dtdz,dvdz,e,f0,ftmp,fvel,g1,g2,kfair,kfib,
     *            l,model,rair,rt1,rt2,ta,tfor,tm,tstr,v0,
     *             vair,visfib,xi,y,visair)
c         -------------
c         test printing
c         -------------
  36      If (next1.ne.1) go to 37
```

```
          If(x.ge.(xdiv-10**(-6.0))) then
            le=l*x*100.0
            write(6,100) le,OD*(10.0**6.0),ID*(10.0**6.0),
     *                   fvel*60,ftmp-273.15
            write(2,100) le,OD*(10.0**6.0),ID*(10.0**6.0),
     *                   fvel*60,ftmp-273.15,tstr
            write(4,200) dvdz,dtdz,dstrdz
            xdiv=xdiv+0.01
          endif
c         --------
c         end test
c         --------
c
c         ---------------
c         final point test
c         ---------------
  37      if(x.lt.(1.0-10.0**(-6.0)))go to 12
c         close (90)
          return
          end
c
c         ---------------------------------------------------------------
c         ---------------------------------------------------------------
c
          subroutine fct(cpfib,OD0,ID0,denair,denfib,dery,OD,ID
     *     ,dstrdz,dtdz,dvdz,e,f0,ftmp,fvel,g1,g2,kfair,kfib,l,
     *          model,rair,rt1,rt2,ta,tfor,tm,tstr,v0,vair,
     *          visfib,xi,y,visair)
c
c         specification statements
c         ------------------------
          integer model
          real dery(6),y(6)
          real alph1,alph2,beta,cpfib,OD0,ID0,denair,denfib,OD,ID,
     *    dstrdz,dtdz,dvdz,e,eps1,eps2,epslon,f0,ftmp,fvel,g1,g2,
     *    gamma,j,k1,k2,k3,ka,kb,kfair,kfib,l,m,n,pr,rair,rfib,
     *    rt1,rt2,ta,tfor,thetaa,tm,tstr,v0,vair,visfib,xi,
     *    denitro,denitro0,reynolds,visair
c         ------------
c         calculations
c         ------------
   1      if ((y(1)*v0).eq.vair)j=0.0
          if ((y(1)*v0).lt.vair)j=-1.0
          if ((y(1)*v0).gt.vair)j=1.0
             gamma=0.420
             beta=0.78
             m=0.334
             n=0.61
             denitro0=0.339/tm**1.001
             denitro=0.339/(y(6)*tm)**1.001
             ID=(ID0**2*denitro0/(denitro*y(1)))**0.5
             OD=(ID**2+((OD0**2-ID0**2)/y(1)))**0.5
             k1=l*3.14159*(OD**(1-n))*beta*(denair**(1-n))*
     *          visair**n*(v0**(2-n))/(2*f0)
```

```
            k2=denfib*v0**2*0.78539*(OD0**2-ID0**2)/
     *         (f0)
            k3=1*0.78539*(OD**2-ID**2)*denfib*9.81/(f0)
            thetaa=ta/tm
            rfib=(denfib*OD0*v0)/visfib
            pr=(cpfib*visfib)/kfib
            reynolds=(denair*OD*v0*y(1))/visair
            if (model.eq.1) then
                go to 2
              else
                go to 3
            end if
c           ------------------------------------
c           calculations for the Newtonian model
c           ------------------------------------
    2       epslon=(visfib*0.7853982*(OD0**2.0-ID0**2.0)*v0)/(1*f0)
            y(3)=(-0.5)*y(2)
            y(4)=0.0
            y(5)=0.0
            dery(1)=y(2)/(2.0*epslon)
            dery(2)=(2/3)*k1*(y(1))**(3-n)+(2/3)*k2*y(1)*dery(1)
     *            -(2/3)*k3*y(1)+y(2)*dery(1)/y(1)
            dery(3)=(-0.5)*dery(2)
            dery(4)=0.0
            dery(5)=0.0
            dery(6)=(-4.0/(pr*rfib))*(OD0/(OD0**2-ID0**2))*
     *            (kfair/kfib)*gamma*(rair**m)*(y(6)-thetaa)*
     *             (y(1)**(0.5*m))
c           dery(6)=-4*1*kfair*gamma*(reynolds**m)*
c    *            (y(6)-thetaa)/(denfib*v0*(OD0**2-ID0**2))
            go to 4
c           ------------------------------------------------
c           calculations for the Phan-Thien and Tanner model
c           ------------------------------------------------
    3       alph1=(rt1*v0)/1
            eps1=(rt1*g1*(0.7853982)*(OD0**2.0-ID0**2.0)*
     *         v0)/(1*f0)
            ka=exp((e*f0*(y(2)+2.0*y(3)))/
     *          (g1*0.7853982*(OD0**2-ID0**2)))
c           ------------------------------------------------
c           Phan Thien and Tanner model with 1 relaxation time
c           ------------------------------------------------
            if (model.eq.2) then
c            y(4)=0.0
c            y(5)=0.0
             dery(1)=((ka*(y(3)-y(2))/alph1)-k1*(y(1)**(4-n))
     *              +k3*y(1)**2)/(k2*y(1)**2+y(2)-y(3)
     *              -3.0*(eps1/alph1)-(1-xi)*(2*y(2)-y(3)))
             dery(2)=(2.0*eps1*dery(1)+2.0*(1-xi)*alph1*y(2)
     *              *dery(1)-y(2)*ka)/(alph1*y(1))
             dery(3)=(eps1*(-1.0)*dery(1)-(1-xi)*alph1*y(3)
     *              *dery(1)-y(3)*ka)/(alph1*y(1))
             dery(4)=0.0
             dery(5)=0.0
```

```
          dery(6)=(-4.0/(pr*rfib))*(OD0/(OD0**2.0-ID0**2.0))*
     *             (kfair/kfib)*gamma*(rair**m)*(y(6)-thetaa)*
     *             ((y(1)**0.5)**m)
          end if
c         ------------------------------------------------
c         calculations of properties of interest to the user
c         ------------------------------------------------
   4      denitro=0.339/(tm*y(6))**1.001
          fvel=y(1)*v0
          ID=((ID0**2)*denitro0/(denitro*y(1)))**0.5
          OD=(ID**2+(OD0**2-ID0**2)/y(1))**0.5
          ftmp=y(6)*tm
          tstr=((y(2)-y(3)+y(4)-y(5))*f0)/(0.7853982*
     *          (OD0**2.0-ID0**2))
          tfor=tstr*(0.7853982*(OD0**2.0-ID0**2))/y(1)
          dvdz=dery(1)*(v0/l)
          dtdz=dery(6)*(tm/l)
          dstrdz=(f0/(l*0.7853982*(OD0**2.0-ID0**2)))*
     *           (dery(2)+dery(4)-dery(3)-dery(5))
          return
          end
c
c       ---------------------------------------------------------------
c       ---------------------------------------------------------------
c
          subroutine pprop(cpfib,denfib,e,g1,g2,kfib,model,
     *                     rt1,rt2,tm,visfib,xi,y,dery,v0,l)
c         ------------------------
c         specification statements
c         ------------------------
          integer model
          real y(6),dery(6)
          real cpfib,denfib,e,g1,g2,kfib,rt1,rt2,tm,visfib,xi,
     *         v0,l,visfib1
c         ------------
c         calculations
c         ------------
   1      cpfib=2570.0
          denfib=800.0
          kfib=0.1735
          visfib=0.00376*exp(5754.71/(y(6)*tm))
c         visfib=5000000*exp(-0.017*y(6)*tm)
c         visfib=350*exp((101008*(503-y(6)*tm)/
c    *           (1.987*503*y(6)*tm)))
          if (model.eq.1) then
             e=0.0
             xi=0.0
             rt1=0.0
             rt2=0.0
             g1=0.0
             g2=0.0
             go to 3
          end if
c         ------------------------------------------------------
```

```
c        additional properties for the Phan-Thien & Tanner model
c        ------------------------------------------------------
   2     e=0.015
         xi=0.1
         g1=28000.0
         rt1=visfib/g1
         if (model.eq.2) then
            rt2=0.0
            g2=0.0
            go to 3
         end if

   3     return
         end
c        ------------------------------------------------------------
c        ------------------------------------------------------------
         subroutine air(OD0,ID0,denair,kfair,rair,ta,tamax,v0,
     *                  vair,vamax,z,visair)
c        ------------------------
c        specification statements
c        ------------------------
         real OD0,ID0,denair,kfair,rair,ta,tamax,v0,vair,
     *        vamax,visair,z
c        --------
c        Velocity
c        --------
   1     if(z.le.0.0091914)then
            vair=0.00
            go to 2
         end if
         vair=0.00
c        -----------
c        Temperature
c        -----------
   2     if(z.le.0.007738)then
            ta=298.15
            go to 3
         end if
         ta=298.15
         if(z.ge.0.1759512)then
            ta=298.15
         end if
c        ---------------------
c        Density air (Kg/m**3)
c        ---------------------
   3     denair=363.06/(ta**1.005)
c        --------------------------------
c        Thermal conductivity (watts/m*K)
c        --------------------------------
         kfair=0.000336826*(ta**0.761272)
c        ---------
c        Viscosity
c        ---------
         visair=(10.0**(-5.0))*(0.147117+0.00689716*ta
```

```
     *           -4.44916*(10.0**(-6.0))*(ta**2.0)
     *           +1.61408*(10.0**(-9.0))*(ta**3.0))
C         ------------------------
C         Modified Reynolds Number
C         ------------------------
          rair=(denair*OD0*v0)/visair
          return
          end
```